The Hong Kong Polytechnic University

Department of Applied Biology and Chemical Technology

Discovery of Novel Inhibitors of the Bacterial Cell Division Protein FtsZ by Computational Drug Screening Coupled with Bioassays

CHAN FUNG YI

A thesis submitted

in partial fulfillment of the requirements for the degree of

Doctor of Philosophy

August 2010

Certificate of Originality

I hereby declare that this thesis is my own work and that, to the best of my knowledge and belief, it reproduces no material previously published or written, nor material that has been accepted for the award of any other degree or diploma, except where due acknowledgement has been made in the text.

Chan Fung Yi

August 2010

Abstract

The problem of antibiotic resistance is worsening worldwide because of the overuse of existing antibiotics. In order to overcome the crisis of antibiotic resistance, there is an urgent need for alternative antibacterial agents that have novel mechanisms of action. FtsZ is an unexploited and attractive target for antibacterial drug discovery because of its widespread conservation in the bacterial kingdom, its absence in the mitochondria of higher eukaryotes and its known biochemical activity and molecular structure. FtsZ plays an essential role in prokaryotic cell division machinery in which undergoes GTP-dependent polymerization at midcell and assembles into the dynamic Z-ring at the site of division. The Z-ring acts on a framework for the recruitment of other cell division proteins to initiate Z-ring contraction to form bacterial daughter cells. Although FtsZ shares structural and functional similarity with eukaryotic tubulin, most of the tubulin/microtubule targeting agents, paclitaxel and colchicines, do not affect the dynamic assembly of FtsZ, indicating that FtsZ can be a selective antibacterial target. Although several compounds that block bacterial cell division and/or inhibit the biochemical activity of FtsZ *in vitro* have been reported, so far none has demonstrated efficacy in models of infection or has entered clinical evaluation.

In this thesis, a computer-aided drug screening method was employed to identify potential FtsZ inhibitors. After *in silico* screening of several natural product libraries, 16 potential FtsZ inhibitors were subjected to bacterial growth inhibitory tests and *in*

vitro assays. The compound 4-(((2*R*,4*S*,5*R*)-5-(2-Methyl-6-(thiophen-2-yl)pyrimidin-4-yl)-quinuclidin-2-yl)methylcarbamoyl)butanoic acid (**5**) was found to exhibit modest antibacterial activity against a number of Gram-positive and -negative bacteria. Compound **5** perturbed the Z-ring assembly in living *E. coli* cells and caused the elongation of *B. subtilis* and *E. coli* cells *in vivo*. It also perturbed the assembly and bundling of FtsZ protofilaments by inhibiting the GTPase activity of FtsZ. The ligand-induced destabilization of FtsZ protofilaments would hamper the functioning and formation of Z-ring to cause an inhibition of bacterial cytokinesis without affecting DNA replication or nucleotide segregation. Compound **5** was also found to show no inhibition on tubulin assembly into microtubules *in vitro*.

In order to obtain the optimal model for predicting the binding mode of compound **5** in the GTP binding site of FtsZ and for subsequent virtual screening of compound **5** derivatives, SCan Alanines and REfine (SCARE) and homology modeling techniques were applied. As a result, several best docking models were successfully built to predict the optimal binding mode of compound **5**. These models were then used to screen a library of compound **5** analogues. Sixty-nine top-scoring compounds were selected and tested experimentally. Finally, compound **5-706** was identified as the most potent derivative against FtsZ, which also exhibited high antibacterial activity against a broad range of bacteria with enhanced inhibitory effect on the GTP hydrolysis of FtsZ. The combination of docking simulation and experimental bioassays leads to study the early structure-activity relationship (SAR) of compound **5** derivatives, which can facilitate the subsequent lead optimization

process.

To assess the potential of compound **5** and its derivatives for combination therapy in treating bacterial infections, the synergistic effects in combination with a conventionally used β-lactam antibiotic (ampicillin) or H7 helix inhibitor of FtsZ (3-MBA) were investigated. Combination of compound **5** or **5-316** with ampicillin demonstrated synergistic effects against drug-resistant *S. auerus* strain. For a drug-sensitive *S. auerus* strain, compound **5** with ampicillin or 3-MBA showed partial synergistic effect.

Acknowledgements

I would like to thank my chief supervisor Professor K. Y. Wong for his enthusiastic supervision and his unwavering support during my postgraduate study. Prof. Wong provided me a meaningful and challenging project to work on and taught me to think critically about the problems. I am grateful for his allowing me the freedom to pursue my interests and his many valuable suggestions and ideas about my project. In addition, I would like to especially thank my co-supervisor Dr. K. W. Mok for his guidance and valuable support.

I would like to express my appreciation to Prof. Y. C. Leung for his valuable comments about my project. Moreover, Professor R. Abagyan is especially thanked for giving me a wonderful attachment opportunity to study at the Scripps Research Institute, University of California, San Diego and Molsoft LLC in 2009. I owe a great deal to Professor R. Abagyan and Dr. P. C. Lam for their guidance and computing support at the critical stage of my project. Prof. Abagyan and Dr. Lam gave many precious comments on the design of docking models of the cell division protein FtsZ. Besides, I am truly thankful for Dr. M. C. Chow who gave me constructive suggestions about the susceptibility test, Dr. L. K. Wong for her assistance and expertise with the cytotoxicity experiment, and Dr. P. K. So for his assistance in mass spectrometry.

From the bottom of my heart, I express my special thanks to all my postgraduate

colleagues and friends in the Department of Applied Biology and Chemical Technology for their help, encouragement and friendships. I am greatly indebted to Dr. K. C. Cheung, Dr. W. H. Chung, Dr. M. W. Tsang, Mr. N. Sun and other colleagues in Y606 for their assistance and fruitful discussions in my study.

I give utmost thanks to my parents and family for supporting me with continued love and encouragement and teaching me never to give up. I also thank my best friends for their love and support through those hard times of writing a dissertation.

Last, but not the least, I would like to express my gratitude to the members of the examination committee for spending their precious time on my thesis. I would additionally like to thank the Research Committee of the Hong Kong Polytechnic University for offering me a studentship and a travelling grant in 2006-2010.

Table of Contents

List of Abbreviations

ATCC	American Type Culture Collection
BLAST	Basic Local Alignment Search Tool
BPMC	Biased probability Monte Carlo
B. subtilis	*Bacillus subtilis*
BSA	Bovine serum albumin
CH_3CN	Acetonitrile
$CaCl_2$	Calcium chloride
DAPI	4’,6-diamidino-2-phenylindole
DNA	Deoxyribonucleic acid
DMEM	Dulbecco's Modified Eagle's Medium
DMSO	Dimethyl sulfoxide
E. coli	*Escherichia coli*
E. faecium	*Enterococcus faecium*
E. faecalis	*Enterococcus faecalis*
FBS	Fetal serum albumin
FICI	Fractional inhibitory concentration index
FITC	Fluorescein isothiocyanate
FtsZ/ *ftsZ*	Filamenting temperature sensitive strain Z
GDP	Guanosine diphosphate
GFP	Green fluorescent protein
GTP	Guanosine triphosphate

HTS	High-throughput screening
ICM	Internal Coordinate Mechanics
KCl	Potassium chloride
kDa	Kilodaltons
LB medium	Luria–Bertani medium
$MgCl_2$	Magnesium chloride
MeOH	Methanol
MOPS	4-morpholinepropanesulfonic acid
MIC	Minimum inhibitory concentration
M. catarrhalis	*Moraxella catarrhalis*
MTS	3-(4,5-dimethylthiazol-2-yl)-5-(3-carboxy-methoxyphenyl)-2-(4-sulfophenyl)-2H-tetrazolium
min	Minute(s)
MMFF	Merck Molecular Force Field
NCBI	National Center for Biotechnology Information
PBS	Phosphate-buffered saline
P. aeruginosa	*Pseudomonas aeruginosa*
OD_x	Optical density at wavelength of x nm
PDB	Protein Data Bank
PCR	Polymerase chain reaction
Phe	Phenylalanine
PMS	Phenazine methosulfate
Res.	Resolution

RMSD	Root mean standard derivation
rpm	Revolution per min
SCARE	SCan Alanines and REfine
S. auerus	*Staphylococcus aureus*
S. epidermidis	*Staphylococcus epidermidis*
SARs	Structure-activity relationship study
SDS	Sodium dodecyl sulphate
SDS-PAGE	Sodium dodecyl sulphate- polyacrylamide gel electrophoresis
VLS	Virtual ligand screening
3-MBA	3- Methoxybenzamide

Chapter 1

Introduction

1.1 Bacterial infection

The treatment of bacterial infections has become a major challenge all over the world because of the rapid increase in antibiotic-resistant pathogenic bacteria strains, constantly emerging new pathogens and emerging biothreat organisms, which cause almost all antibiotics less effective. Thus, there is an urgent need to develop antibacterial agents with new mechanisms of action against antibiotic-resistant strains. The causes for the development of resistant mechanisms against clinically used antibiotics include 1) overuse or inappropriate use of antibiotics; 2) rapid development of mutation in bacteria; 3) exchange of genetic material among bacteria which causes resistance; 4) formation of surface aggregates called biofilms; 5) activity of efflux pump systems, membrane-associated proteins or protein complexes that reduce the intracellular concentration of inhibitory compounds by actively pumping them out of the cell [1]. There are six generic categories of action for antibacterial agents, namely, inhibition of cell division, cell wall synthesis, cell membrane function, protein synthesis, nucleic acid synthesis and intermediary metabolism [2]. There are clinically efficacious antibiotics in use against some of these targets based on the knowledge of their biochemical pathways. But many commonly used antibiotics have become ineffective against antibiotic-resistant bacterial strains. In order to overcome this problem, extensive modification of the structure of existing antibiotics was used in an attempt to maintain activity against their targets. One typical example is β-lactam antibiotics which target at the bacterial cell wall synthesis enzyme transpeptidase. The bacteria deverlop the resistance against the β-lactam by secreting the enzyme β-lactamase which hydrolyse the

β-lactam antibiotics. New generations of β-lactams which are resistant to the β-lactamases have to be developed. But efficacious modification is becoming increasingly difficult. Thus, the development of new antibiotics with novel mechanisms of action is needed to tackle the emerging resistance problem. Cell division is a crucial process in every organism because it must be coordinated with other cellular events such as chromosome replication and nucleoid segregation. Nevertheless, bacterial cell division is not yet targeted by clinically approved antibiotics. Therefore, discovery of inhibitors of FtsZ, a protein that is essential in bacterial cell division, is an attractive approach in the search for new antibacterial agents.

1.2 Bacterial cell division

1.2.1 Bacterial cell division pathway

In the last few years, substantial progress has been made in several aspects of research on cell division. For example, the molecular basis for regulation control of cell division by the Min system, to inhibit Z-ring assembly at the cell poles, is now better understood. The crystal structures of most division proteins are now available, their catalytic activities and their interactions with other proteins have been well characterized and studied.

The cell division of two rod-shaped bacteria, *B. subtilis* and *E. coli*, have been extensively studied over the past two decades [3-6]. Many essential cell division

proteins were identified in these model organisms by screening temperature-sensitive mutants that normally grow and divide at the permissive temperature. But bacterial cells continue to elongate without cell division at restrictive temperature. These long cells without cell division are called filaments that contain multiple chromosomes. Mutagenesis and genetic experiments in the Gram-negative *E. coli* have shown that a null mutation in the *ftsZ* gene (filamenting temperature sensitive strain Z) results in disassembly of the cytokinetic Z-rings and formation of filamentous cells that are able to divide at nonpermissive temperature [7, 8]. During the cell division, invagination of cell envelope layers (the cell membrane and cell wall) are involved to form a septum between two newly replicated chromosomes (the midcell) (Figure 1.1). Two newborn cells are then separated by hydrolyzing the peptidoglycan in the division septum. At least 12 cell division proteins have been confirmed to involve in the septation process at the division site of midcell [9, 10]. These proteins are recruited to the division site to form the division ring, commonly known as the divisome.

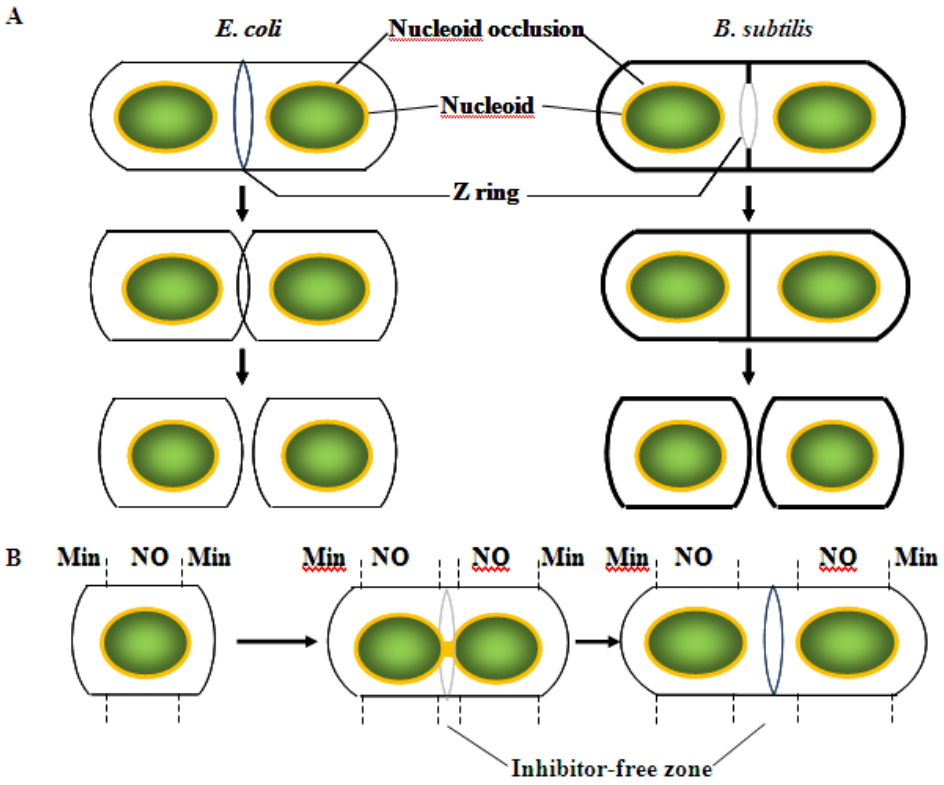

Figure 1.1 Bacterial cell division in rod-shaped bacteria. (A) Two different modes of division. FtsZ proteins form a Z-ring at midcell after chromosome replication and segregation into nucleoids. The membrane-bound cell-division proteins are recruited to initiate the invagination of the cell wall and membrane to form a division septum. Cell wall synthesis follows the ring inwards. In *E. coli*, synthesis of the division septum and constriction of the outer membrane are undertaken at the same time. In *B. subtilis*, a cross wall of peptidoglycan firstly divides the cell before it is degraded and remodeled to form the new cell poles. (B) The position of Z-ring formation. Nucleoid occlusion (NO), which is activated by Noc (in *B. subtilis*) or SlmA (in *E. coli*), inhibits Z-ring assembly close to the nucleoid. The function of Min system is to prevent Z-ring assembly at the cell poles. From left to right: in 'newborn' cells, both systems firstly inhibit Z-ring assembly throughout the cell; following cell elongation and chromosome replication, NO prevent Z-ring formation in the cylindrical part of the cell; and finally, the progression of chromosome segregation shows an inhibitor-free region at mid-cell, allowing the Z-ring to assemble [11].

1.2.2 The role of FtsZ in cell division

In *E. coli*, *ftsZ* was identified as the first cell division gene to initiate the cell division process [12, 13]. The cell division protein FtsZ, encoded by the gene *ftsZ*, is conserved in virtually all eubacteria, archeae and chloroplasts [10]. FtsZ performs a variety of roles in cell division. It is the first protein to move to the division site. Then, FtsZ assembles into a dynamic Z-ring via GTP-dependent polymerization [14-16]. The Z-ring acts as a framework for the recruitment of other proteins to form a divisome complex, which causes the constriction of membrane. Finally, a septum is formed at midcell to mediate the cell division process [14].

1.2.3 The position of FtsZ ring formation

In *E. coli*, the position of Z-ring at midcell is controlled by various regulatory factors which ensure that Z-ring assembly is taken part at the correct spatial position within the cell and at the correct time in the bacterial cell cycle. FtsZ polymerization is closely linked to the Min family of proteins (Figure 1.1B). In the Min system, three proteins, MinC, MinD and MinE, are responsible for preventing a cell division at the poles [17]. MinC and MinD are responsible for a negative regulator of FtsZ ring assembly. MinE is present at the centre of the cell to oscillate and then repel MinCD to allow FtsZ ring assembly [18, 19]. MinCD has been found to inhibit FtsZ polymerization and facilitate the correct interaction of FtsA with the FtsZ ring *in vivo* [20]. Another regulation system is the nucleoid occlusion model [21]. In this model, cell division cannot proceed in the vicinity of the nucleoid because the assembly of

the FtsZ ring is inhibited. Thus, FtsZ assembles before nucleoid separation in the cell division process, and the Min system cooperates with the nucleoid occlusion system to control the level of Z-ring formation at the appropriate place and time [10].

1.2.4 Corporation with other cell division proteins

The other proteins that comprise the septal ring fall into several functional classes: (i) modulating the assembly state of FtsZ (FtsA, ZipA, ZapA), (ii) connecting the Z-ring to the cytoplasmic membrane (FtsA, ZipA), (iii) coordinating septation with chromosome segregation (FtsK), (iv) synthesis of peptidoglycan cell wall (FtsI, FtsW) and (v) hydrolysis of peptidoglycan to separate daughter cells (AmiC, EnvC). The septal ring also contains many proteins of essentially unknown function [FtsEX, FtsQ, FtsL, FtsB (formerly called YgbQ) and FtsN]. These proteins work together during cytokinesis. Several proteins such as ZipA, FtsA and ZapA have been shown to bind directly to FtsZ [22-24]. Figure 1.2 illustrates all cell division proteins localized at the division site after Z-ring formation. The function of these cell division proteins are summarized in Table 1.1.

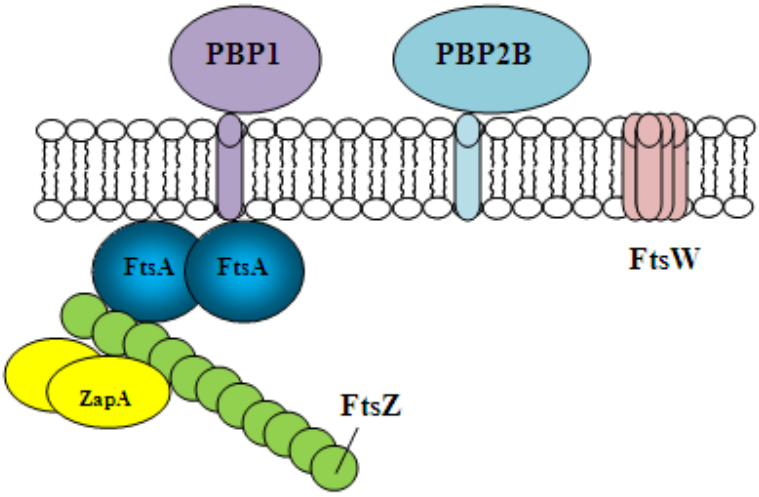

Figure 1.2 Model of a cross section of the cell at the division site. The FtsZ ring is tethered to the cytoplasmic membrane via ZipA while FtsA is responsible for the localization of other division proteins [11].

Table 1.1 Functions of the cell division proteins

Cell division protein	Function	Localization
FtsZ	Firstly initiates the Z-ring formation at midcell in cell division and serves as a platform to recruit all downstream division proteins to midcell	Cytoplasm
FtsA	Tethers FtsZ to membrane for Z-ring assembly, organizes FtsZ polymers and recruits downstream division proteins	Cytoplasm
ZipA	Stabilizes Z-rings at membrane	Cytoplasm, anchored to cytoplasmic membrane
ZapA	Promotes FtsZ polymerization and protofilament bundling	Cytoplasm
FtsK	DNA translocase (ATPase); chromosome segregation and septum formation	Cytoplasmic membrane
FtsW	Septal peptidoglycan synthesis; signal transduction and stabilization of FtsZ ring	Cytoplasmic membrane
FtsL	Unknown function; possible for regulation of division site assembly	Periplasm, anchored to cytoplasmic membrane
FtsI	Transpeptidase forms cross-links into septal peptidoglycan	Periplasm, anchored to cytoplasmic membrane

1.3 Functional and structural similarities between eukaryotic tubulin and prokaryotic FtsZ

FtsZ shares several structural and functional features and thus is a distant homologue of the eukaryotic cytoskeleton protein tubulin. FtsZ is a 40 kDa protein present in almost all bacteria, many archaea, some chloroplasts and a few primitive mitochondria. It is the main component of the Z-ring that initiates bacterial cell division [25]. Tubulin is the key component of eukaryotic microtubules, which is responsible for various cellular functions such as intracellular trafficking, maintenance of cell shape and structure, and cell division. FtsZ and tubulin are shown to play crucial roles in living cells [26]. FtsZ is the first protein to form Z-ring and recruits all other downstream proteins to initiate cell division in prokaryotes. Like tubulin, FtsZ is a nucleotide-binding protein that binds GTP and has GTPase activity to hydrolyze its nucleotide following self-assembly into filaments. Although FtsZ shares limited sequence identity with tubulin (< 20%), the tertiary structure of FtsZ is similar to that of tubulin signature motif GGGTGS/TG [27, 28]. These two proteins are a distinct class of GTPase and adopt very similar folds [29], especially in the vicinity of the GTP binding site. This can be seen in the three-dimensional structures of *M. jannaschii* FtsZ (PDB code: 1FSZ) [26] and eukaryotic α/β tubulin (PDB code: 1TUB) [30]. The crystal structures of FtsZ and β-tubulin are shown in Figures 1.3 and 1.4 respectively. However, it has been demonstrated that FtsZ and tubulin have significant differences in the binding ability of nucleotides, C-terminus sequence and content of α-helices [28, 31, 32]. Both proteins are made of two domains formed by a

β-sheet surrounded by α-helices and they were connected via a long "core" helix H7. Nucleotide binding involves many regions in the N-terminal domain. The guanine base and the phosphates interact with the T1-loop, while the T2-loop is in contact with the β- and γ-phosphates and have conserved Asn and Asp residues. The Asp residue may be responsible for coordinating with the Mg^{2+} ion at the nucleotide-binding site. Loop T3 is in contact with γ-phosphate in α-tubulin. Loop T4 contains the tubulin signature motif GGGTGS/TG, which is conserved in both proteins to interact with the α- and β-phosphates. Loop T5 contains important residues participating in ribose binding in both protein, but there is no homology in this loop between tubulin and FtsZ. For loop T6, a conserved Asn occurs in both tubulin and FtsZ which interacts with the guanine base by forming a hydrogen bond. Both FtsZ and tubulin involve amino acid residues to bind with GTP in the assembly into protofilaments. The crystal structures of the α/β tubulin dimer and FtsZ showed that the GTP nucleotide is located at the interface between subunits in protofilament, which may stimulate the GTP hydrolysis. For the α/β tubulin dimer, the GTP pocket on the top of one subunit (the plus-end of a microtubule) is in contact with the opposite face of the next subunit to bind GTP at the interface of two subunits (Figure 1.4) [31]. In the case of FtsZ, it consists of an N-terminal GTP binding domain and a C-terminal GTPase-activating domain [30]. During filament formation, the T7 loop of the C-domain from the upper subunit contacts the top of H7 of N-domain at the lower subunit to form the GTPase site. GTP firstly binds at one end of the GTP binding domain of the FtsZ monomer, designated the 'plus' end by convention. Addition of C-terminal domain of another monomer acts synergistically by providing

the co-catalytic aspartate residues for GTP binding/hydrolysis and FtsZ polymerization [31, 33]. But the structure of the FtsZ polymer is different from microtubule. Microtubules consist of heterodimers of α and β tubulin and have distinct polarity, while FtsZ polymers consist of only one form of FtsZ monomers [26, 31]. While FtsZ protofilaments can assemble either alone or in association with other filaments to form multistranded structures, the microtubule only consists of tubulin filaments.

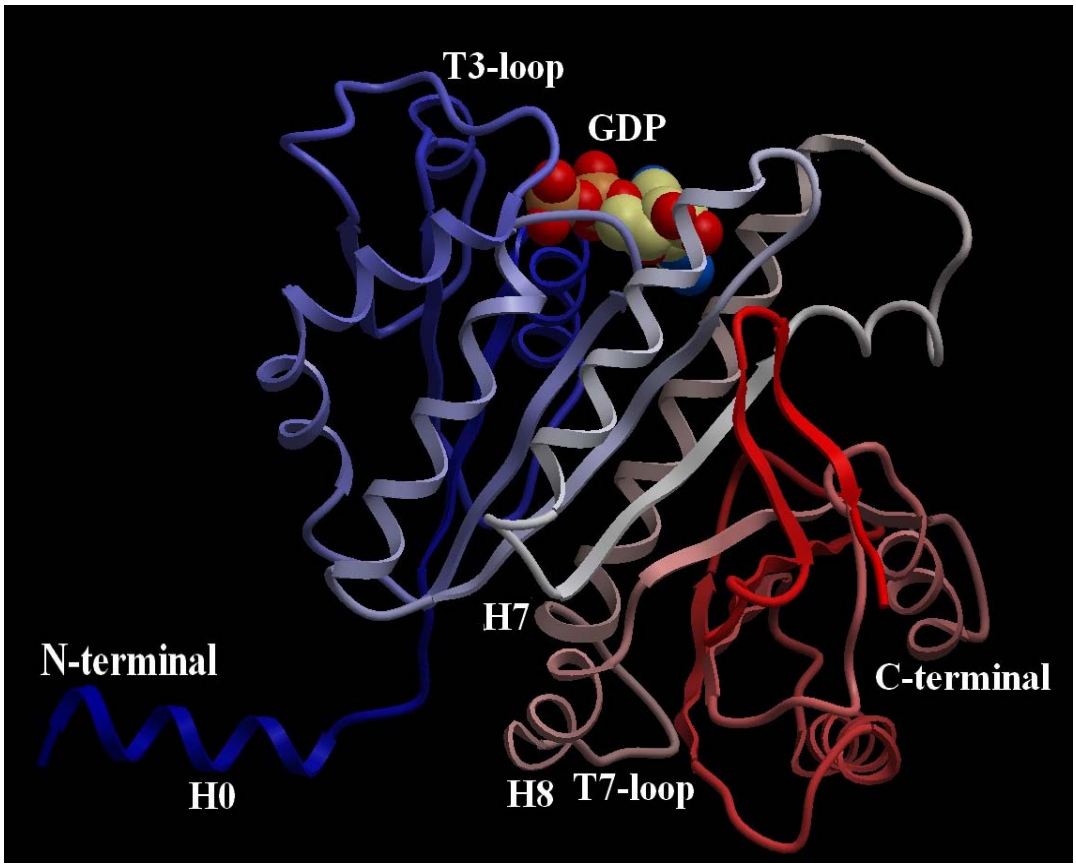

Figure 1.3 Crystal structure of *M. jannaschii* FtsZ bound to GDP (PDB code: 1FSZ) (prepared by Molsoft [34])

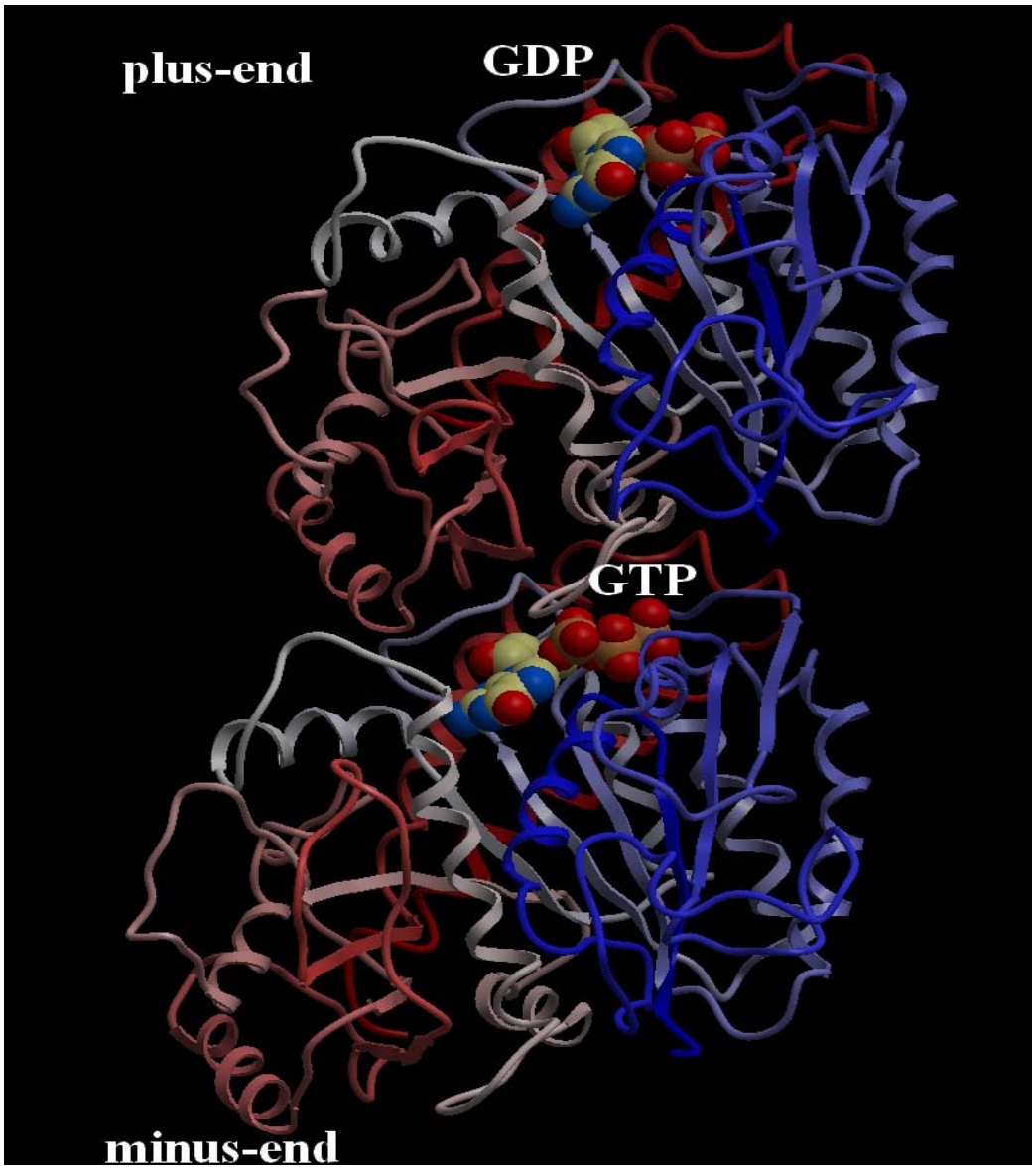

Figure 1.4 Crystal structure of α/β-tubulin bound to GDP (PDB code: 1TUB) (prepared by Molsoft [34]).

1.4 Dynamics of FtsZ

1.4.1 The dynamic structure of Z-ring

The first step in bacterial cytokinesis is the assembly of FtsZ into protofilaments to form a contractile Z-ring on the inner face of the cytoplasmic membrane at the site of division [14, 35]. The Z-ring acts on a framework for the recruitment of other cell division proteins. Among all bacterial cell division proteins, FtsZ is the most abundant and plays an important role in the cell division process [36]. About 15,000 FtsZ monomers are present in the cytoplasm of *E. coli* cells [37] and the concentration of FtsZ is kept constant during the whole cytokinesis process [38]. In the early stage of cytokinesis, the Z-ring is assembled at the midcell after the termination of DNA replication but before the segregation of nucleoids [38, 39]. FtsZ-GFP fusion protein has been used to track the behavior and nature of the Z-ring in bacterial cells [35]. This study revealed that Z-ring is a highly dynamic structure. About 30% of the total amount of FtsZ move in and out the Z-ring at a given time [40]. A fluorescence recovery after photobleaching (FRAP) experiment using FtsZ-GFP fusion protein showed a rapid turnover of FtsZ and a continuous exchange of monomers between the cytoplasm and the protofilaments in the Z-ring [41]. At the later stage of cell division, the Z-ring undergoes constriction to form daughter cells [42, 43]. The Z-ring disassembles at the end of cytokinesis and assembles again in the daughter cells. These phenomena indicated that the Z-ring is a highly dynamic structure. The regulation and stability of the Z-ring at midcell are controlled by a number of proteins mentioned previously. When the assembly of FtsZ cannot occur

properly, the formation of Z-ring also disappears. Even if DNA replication and nucleoid segregation function as normal, the bacterial cell only elongates without any cell division. Finally, it leads to cell lethality. Polymerization and GTP hydrolysis have been found to be at the root of the dynamics of the Z-ring. Therefore, it is important to understand the mechanism of FtsZ dynamics and how it influences the Z-ring assembly and disassembly in bacterial cells in order to develop new antibacterial agents through the inhibition of FtsZ activity.

1.4.2 Contribution to the dynamicity of Z-ring by polymerization and GTP hydrolysis of FtsZ

Analyzing the mechanism of polymerization and GTP hydrolysis of FtsZ are very useful to understand the basis of dynamic behavior of Z-ring in bacterial cells. In an early report, the basis of the dynamicity of Z-ring was believed to be caused by reversible polymerization and depolymerization of FtsZ monomers [44]. It was found that FtsZ has a GTPase activity, but the GTP-binding amino acid sequence of FtsZ is slightly different from other GTP-binding proteins [29, 45]. In addition, the GTPase activity of FtsZ is strongly dependent on protein concentration, i.e. a sufficient protein concentration is required to activate GTPase activity, indicating that FtsZ is a self-activating GTPase [46]. The binding of GTP to FtsZ has been demonstrated to assist the assembly of FtsZ monomers into protofilaments [47]. FtsZ monomers are assembled into a straight protofilament in a head-to-tail longitudinal manner. Different polymer morphologies and higher-ordered structures of FtsZ such as sheets,

mini-rings [48], tubes [46], asters and polymeric networks [49] have been observed by transmission electron microscopy. Apart from longitudinal interaction between FtsZ monomers to form a straight protofilament, FtsZ bundles can be formed through lateral interactions of several protofilaments. The formation of FtsZ bundles is affected by calcium [49, 50], glutamate [51], pH, ionic strength [52] and the presence of stabilizing proteins like SepF [53] and ZipA [54]. Although the actual mechanism on how the FtsZ protofilaments are associated into Z-ring is still unclear, six to seven protofilaments are reported to constitute a Z-ring *in vivo* [37]. Based on *in vitro* studies, the dynamicity of Z-ring is caused by GTP hydrolysis in the FtsZ polymer [55, 56]. The GTP-bound state in the FtsZ polymers can be maintained by rapidly exchanging the bound nucleotide [57] and subunit exchange [55]. When GTP is exhausted, disassembly of the Z-ring occurs which is promoted by the GDP-bound FtsZ. FtsZ facilitates the formation of dynamic Z-ring through the transition of polymerized FtsZ from straight protofilaments in the presence of GTP to curved form in the presence of GDP [58]. When the FtsZ protein undergoes oligomerization, its GTPase function is activated to hydrolyze GTP. The GDP content in the Z-ring then increases to lead the transformation of linear protofilaments to curved protofilaments. Finally, constriction of the Z-ring proceeds as the FtsZ polymers disassemble.

1.5 FtsZ as a novel antibacterial drug target

Although nearly all of the proteins locating at the cell division site have been identified [9, 59], the actual function of most of these proteins are still elusive. The best characterized protein is FtsZ, which plays an essential role in the cell division process. In the earliest known step in bacterial cytokinesis in *E. coli* and *B. subtilis*, FtsZ assembles into the Z-ring at the division site. The Z-ring as a platform recruits other proteins to initiate cytokinesis. Thus, other cell division proteins are dependent on FtsZ for their localization to form the Z-ring. In addition, the dynamics of FtsZ assembly to form the Z-ring was found to generate the contractile force for cell constriction and cell division. Thus FtsZ is a potential target for the development of new antibacterial agents. An important consideration is that FtsZ is conserved in almost all prokaryotes so that antibiotics targeting at FtsZ are able to exhibit a broad-spectrum activity combating infection by different bacterial populations, which will be useful in the management of polymicrobial infections and before determination of the nature of the infectious agent. The significant conservation of FtsZ protein also makes the bacteria difficult to develop resistance against FtsZ-targeting drugs. Moreover, FtsZ is absent in the mitochondria of higher eukaryotes and shares a limited sequence identity with tubulin. Another important point is that the biochemical activity and X-ray crystal structures of FtsZ are known, which highly facilitates the high-throughput virtual screening and structural modification of lead compounds. Inhibition of FtsZ to prevent bacterial growth is a promising approach to treat bacterial infection because FtsZ inhibitors act by a mechanism which is different from any clinically used antibiotics. Previous findings

showed that some FtsZ inhibitors not only kill the wild type bacteria, but also have the same effectiveness on antibiotic-resistant bacterial strains [60-62]. Up to now, no antibiotic(s) based on the inhibition of FtsZ has reached the clinical trial phase. All these make FtsZ an attractive target for the development of novel antimicrobial agents.

Discovery of novel antibacterials via targeting the GTP binding site in FtsZ is preferred over other domains such as the T7 loop and H7 helix. Several FtsZ inhibitors such as cinnamaldehyde [63], curcumin [64] and PC190723 [60] were found to bind the T7 loop or H7 helix at the C-terminus domain of FtsZ. However, they only inhibited the Gram-positive bacterial strains. One possible reason is that they bind to the less conserved domain at the C-terminus of FtsZ. Indeed, the alignment of the C-terminal region of the FtsZ proteins are most variable amongst bacterial species (Gram-positive and -negative bacterial strains) [28]. Thus, targeting at the GTP binding site of FtsZ has a better chance of developing broad spectrum antibacterial agents because the GTPase binding site is located at the highly conserved N-terminal part with recognizable sequence identity.

1.6 FtsZ inhibitors

1.6.1 Natural compounds as FtsZ inhibitors

Natural products are very popular in the pharmaceutical research and many antibacterials were obtained from natural sources like plants and microbial fermentations. Natural products not only provide a diverse range of chemical structures, they also have bioactive substructures and potentially lower toxicity profiles [65]. The advancement in technology in isolation, screening and profiling of natural molecules also make them more attractive for the discovery of antibacterials. A number of natural products were found to inhibit FtsZ (Table 1.2). Viriditoxin was firstly identified as an FtsZ inhibitor from a high-throughput screening of several thousand microbial fermentation broths and plant extracts [62]. It was found to inhibit FtsZ GTPase activity and polymerization with IC_{50} of 7 μg/mL and 8.2 μg/mL respectively. Viriditoxin has a broad spectrum activity against sensitive and drug-resistant Gram-positive strains with MICs between 2 and 16 μg/mL. Sanguinarine, a benzophenanthridine alkaloid derived from the plant *Sanguinaria canadensis*, has been shown to exhibit an inhibitory effect on a broad range of pathogenic bacteria without influencing DNA replication or nucleoid segregation [66]. It strongly induced bacterial filamentations and perturbed Z-ring formation by inhibiting cytokinesis. Sanguinarine also caused FtsZ filamentation *in vitro* by inducing a conformation change in FtsZ and then weakening the lateral interactions among the protofilaments. However, sanguinarine is toxic to mammalian cells as it inhibits tubulin assembly into microtubules. Totarol, a diterpenoid phenol, was

reported to induce the filamentation of *B. subtilis* cells and cause bacterial cytokinesis *in vivo* [67]. Totarol also inhibits the assembly dynamic of *M. tuberculosis* FtsZ (MtbFtsZ) *in vitro* but does not affect the mammalian cells. Some polyphenols, [(±)-Dichamanetin and (±)-2‴-Hydroxy-5″-benzylisouvarinol-B)], isolated from natural sources [68], were also reported as potent anti-FtsZ agents. (±)-Dichamanetin was found to kill Gram-positive pathogenic species such as *S. auerus* and *B. subilitis* only. On the other hand, (±)-2‴-Hydroxy-5″-benzylisouvarinol-B exhibited a broad spectrum of activity, which effectively killed both Gram-positive and Gram-negative bacteria. Cinnamaldehyde, a phenylpropanoid compound, is a natural product to be found in spices [63]. Using saturation transfer difference-NMR and *in silico* docking techniques, it has been demonstrated that cinnamaldehyde binds to the T7 loop of FtsZ resulting in inhibition of GTP hydrolysis and perturbation of the Z-ring morphology. Berberine is another natural plant alkaloid to be extracted from various species of *Berberis*, which is also a FtsZ inhibitor [69]. It was found to inhibit the assembly of the Z-ring and perturb cytokinesis by binding to the hydrophobic core of GTP binding site. It was also shown to destabilize FtsZ protofilaments and inhibit the FtsZ GTPase activity in *E. coli* with an IC_{50} of 16 μM. Although berberine has weak activity against Gram-negative bacteria, it can inhibit antibiotic-resistant pathogens such as methicillin-resistant *S. aureus* (MRSA). Curcumin, a dietary polyphenolic compound, was demonstrated to perturb FtsZ assembly and induce filamentation in *B. subtilis* 168 by binding to the T7 loop of FtsZ [70]. It has a totally different mechanism from the other known FtsZ inhibitors because it was also found to perturb the assembly dynamic of FtsZ by increasing the GTPase activity of FtsZ. An increase

of 35 % GTPase activity was found in the presence of 30 μM curcumin. This compound reduced the formation of Z-ring, but did not affect the nucleoid segregation. However, the main limitations of curcumin are poor bioavailability and its inhibition of eukaryotic tubulin polymerization [70]. Recently, Chrysophaentins A-H, a series of antimicrobial natural products, were found to inhibit the GTPase activity of FtsZ in clinically relevant Gram-positive bacteria. Among them, Chrysophaentin A, the most potent inhibitor, was found by saturation transfer difference-NMR and *in silico* docking to bind to the GTP binding site of FtsZ [61].

Table 1.2 FtsZ inhibitors from natural sources

Compound	Source of compound	Mode of action on FtsZ	Anti-FtsZ activity
Berberine	*Berberis aquifolium*, *Berberis aristata*	Binds to hydrophobic core of GTP binding site; Inhibits *Ec*FtsZ GTPase activity (IC_{50} = 16 ± 5 μM) and assembly	*B. subtilis* (MIC = 100 μg/mL) and *E. coli* (MIC > 400 μg/mL)
Chrysophaentin A	Yellow aglae *Chrysophaeum taylori*	Binds to GTP binding site; Inhibits *Ec*FtsZ GTPase activity (IC_{50} = 6.7 ± 1.7 μg/mL) and assembly	Broad-spectrum activities against Gram-positives bacteria; (MIC_{50} = 1.3 ± 0.4 μg/mL)
Cinnamaldehyde	*Cinnamomum cassia*	Binds to T7 loop binding site; Inhibits *Ec*FtsZ GTPase activity (IC_{50} = 5.8 ± 2.2 μM) and FtsZ polymerization	*B. subtilis* (MIC = 4 μg/mL) and *E. coli* (MIC = 1000 μg/mL)
Curcumin	*Curcuma longa*	Unknown about targeting binding site; Increases GTPase activity	*B. subtilis* (MIC = 37 μg/mL)
Dicharnanetin	*Uvaria chamae*	Binds to GTP binding site; Inhibits *Ec*FtsZ GTPase activity (IC_{50} = 12.5 ± 0.5 μM)	*B. subtilis* (MIC = 1.7 μM)
Sanguinarine	Rhizomes of *Sanguinaria canadensis*	Unknown about targeting binding site; Inhibits *Ec*FtsZ assembly and protofilament bundling	*B. subtilis* (MIC = 10 μM) and *E. coli* (MIC = 70 μM)
Totarol	*Podocarpus totara*	Unknown about targeting binding site; Inhibits *Mt*FtsZ GTPase activity (IC_{50} = 40 μM) and assembly	*B. subtilis* (MIC = 2 μM)

Continue……

Compound	Source of compound	Mode of action on FtsZ	Anti-FtsZ activity
Viriditoxin	*Aspergillus viridinutans*	Unknown about targeting binding site; Inhibits GTPase activity (IC_{50} = 7 μg/mL) and polymerization	Broad-spectrum activities against Gram-positive bacteria; (MIC = 2-6 μg/mL)

1.6.2 Synthetic and semi-synthetic compounds as FtsZ inhibitors

With the development of computer-aided drug design, synthetic chemistry plays a crucial role in the discovery and modification of antibiotics. Nowadays, synthetic drugs are mainly developed from the scaffolds of natural molecules and knowledge on the binding pockets of the target. There are several synthetic compounds targeting at FtsZ (Table 1.3). 3-Methoxybenzamide (3-MBA) was found to exhibit weak antibacterial activity with FtsZ as the drug target [60, 71, 72]. The chemical structure of 3-MBA was modified to optimize its effectiveness against FtsZ. In a structure-activity relationship study of more than 500 analogues, PC190723 has been identified to have a potent anti-staphylococcal activity. The potency of PC190723 against *S. auerus* was 2000 times greater than that of 3-MBA. According to the results of the mutagenesis and *in silico* docking studies, PC190723 apparently binds to the core helix (H7) of FtsZ, which is equivalent to the binding site of the antitumor drug taxol in tubulin [60, 72, 73]. Another synthetic compound 2-carbamoyl-pteridine was found to inhibit the polymerization of *M. tuberculosis* FtsZ *in vitro* [74]. Despite the easy and inexpensive synthetic pathway of this molecule, it is less effective than its lead compound **1** from natural source [74]. After screening over 200 synthetic alkoxycarbonylpyridines SRI-7614 and SRI-3072 were identified to inhibit FtsZ polymerization and GTPase activity [75]. They were found to effectively inhibit the wild type and resistant *M. tuberculosis* strains, indicating that drug-resistant strains are vulnerable towards these FtsZ inhibitors. SRI-3072 was also shown to be specific for FtsZ and did not inhibit tubulin polymerization [75]. C-8 bromine substituted GTP, a GTP derivative, was identified to be a competitive inhibitor to inhibit FtsZ

polymerization and GTPase activity. It can serve as an excellent pre-lead molecule to synthesize effective antibacterial agents against FtsZ [76, 77]. After screening 95,000 synthetic compounds, A189 was identified to possess potent antibacterial activity. It could inhibit FtsZ assembly *in vitro* and Z-ring formation *in vivo* without influencing chromsome segregation [78]. Using solid-phase parallel synthesis approach, a series of GTP analogues was prepared. Some of these derivatives were shown to effectively inhibit *S. auerus in vivo* [79]. Using a high-throughput protein-based chemical screening approach, small molecules such as Zantrins (Z1-Z5), which are dissimilar to GTP analogues, were found to inhibit FtsZ GTPase activity and polymerization. Z1, Z2 and Z4 were demonstrated to destabilize FtsZ assembly while Z3 and Z5 stabilized FtsZ bundles [80]. PC58538 was found to inhibit FtsZ GTPase activity after screening 105,000 synthetic compounds in a cell-based antibiotic screening assay [81]. Mutation experiment showed that PC58538 may bind to the GTP-binding pocket. Although it was found to inhibit the GTPase activity of FtsZ, it only exhibited weak antimicrobial activity. In order to enhance its potency and broaden the spectrum of activity, a number of PC58538 analogues were synthesized. The most potent compound, PC170942, was active against a broad spectrum of antibiotic-sensitive and antibiotic-resistant Gram-positive species [81]. There are several examples of using structure-guided synthesis to optimize the properties of the lead molecules. For example, *N*-Benzyl-3-sulfonamido-pyrrolidine (543F6), was found to show a weak GTPase inhibition activity. Using structure-activity relationship data, the antibacterial activity of this molecule was improved. But the modified molecule did not affect the GTPase activity of FtsZ,

indicating that the more potent derivative exhibited a different mode of inhibition from the parent molecule [82]. Taxanes are known potent inhibitors of tubulin assembly, which were screened to identify lead compounds against FtsZ using the microdilution broth assay [83]. The most potent lead compound, TRA 2a, was found to effectively inhibit drug-sensitive and drug-resistant *M. tuberculosis* (MTB) strains and did not bind to microtubulin. Optimization of lead molecules showed that a series of TRA 10 compounds, also called C-seco-taxane-multidrug-resistance (MDR) reversal agents, possessed potent anti-TB activity (MIC = 1.25-2.5 μM) against drug-sensitive and drug-resistant MTB strains without appreciable cytotoxicity (IC_{50} > 80 μM). These FtsZ specific taxanes were also found to be non-cytotoxic to human host cells at the concentration required for their antibacterial activity [83]. This example demonstrated that some molecules can differentate between FtsZ and tubulin and are non-cytotoxic to the host. Amikacin, a potent semi-synthetic aminoglycoside derived from kanamycin, is a commonly used antibiotic to treat bacterial infections. It is interesting to find that amikacin can cause cell elongation and perturb FtsZ assembly *in vivo* [84]. Recently, after screening 81 compounds of different structural scaffolds, OTBA (3-{5-[4-oxo-2-thioxo-3-(3-trifluoro-methylphenyl)thiazolidin-5-ylidenemethyl]-furan-2-yl}-benzoic acid) was found to promote FtsZ assembly *in vitro* [85]. OTBA was found to exhibit a different antibacterial mechanism from other known FtsZ inhibitors. It was shown to increase the bundling of FtsZ protofilaments by promoting FtsZ assembly *in vitro*, cause filamentation and inhibit the formation of cytokinetic Z-rings in bacteria, but did not influence the proliferation of mammalian cells [85].

Table 1.3 FtsZ inhibitors from synthetic and semi-synthetic approaches

Compound	Source of compound	Mode of action on FtsZ	Anti-FtsZ activity
2-carbamoyl pteridine	-	Unknown about targeting binding site; Inhibits GTPase activity and polymerization	*M. tuberculosis*
534F6 derivatives	-	Unknown about targeting binding site; Inhibits of cell division but not the GTPase activity	*E. coli*
A-189	4-aminofurazan derivative	Unknown about targeting binding site; Inhibits GTPase activity (IC_{50} = 80 μg/ml) and Z-ring assembly	*E. coli* (MIC = 128 μg/mL) and *S. auerus* (MIC = 16 μg/mL)
Amikacin	Semi-synthetic aminoglycoside derived from kanamycin	Unknown about targeting binding site; Perturbs Z-ring formation	*E. coli*
BrGTP	GTP analogues	Binds to GTP binding site; Inhibits *Ec*GTPase activity (IC_{50} = 27 μM)	*E. coli* and *S. auerus*
OTBA	-	Unknown about targeting binding site; Inhibits *Bs*FtsZ and *Ec*FtsZ GTPase activity, but promotes assembly of FtsZ	*B. subtilis* (MIC = 2 μM)
PC 170942	-	Binds to GTP binding site; Inhibits *Ec*GTPase activity (IC_{50} of lead and derivative = 136 and 24 μg/mL respectively)	*S. auerus* (MIC = 64 μg/mL) and *E. coli* (MIC > 256 μg/mL)

Continue……

Compound	Source of compound	Mode of action on FtsZ	Anti-FtsZ activity
PC 190723	-	Binds to H8 helix binding site; Inhibits *Sa*FtsZ GTPase activity (IC_{50} =55 ng/mL) and perturbs Z- ring formation	*S. auerus* (MICs = 1 μg/mL), *E. coli* (MIC > 64 μg/mL)
SRI-3072	2-alkoxycarbonylaminopyridine	Unknown about targeting binding site; Inhibits *Mtb*GTPase activity and polymerization	*B. subtilis* (MIC = 0.28 μM)
TRA 10 series	Taxane derivatives	Unknown about targeting binding site; Stabilizes *Mtb*FtsZ against depolymerization	*B. subtilis* (MIC = 2.5 μM)
Z1-Z3	Zantrins (polyphenols)	Unknown about targeting binding site; Z1, Z2 and Z4 destabilize FtsZ assembly, Z3 and Z5 hyperstabilize FtsZ assembly, inhibit *Ec*FtsZ and *Mt*FtsZ GTPase activity (IC_{50} = 2-15 μg/mL)	Broad -spectrum activity (MICs of Z1 on *S. auerus* and *E. coli* = 1 μg/mL and 8 μg/mL)

1.7 The use of computer-aided drug screening in drug discovery and development

1.7.1 Introduction

Development of lead compounds into new drugs for a particular disease is an extremely difficult process and it usually takes 10 to 15 years to develop a new prescription drug to the market. The major difficulty is the extremely high research and development cost. On the contrary, the average number of new drugs released has been decreasing over the last decade because regulatory authorities become much more restrictive and demanding for highly effective and safe drugs [86, 87]. It means that any new drugs should show substantial benefits over existing ones used in the market [88]. Over the last several decades, drug discovery and development process has changed dramatically. The use of computer science within the traditional drug design campaigns is an alternative method to improve the successful rate of drug discovery process [89, 90]. Nowadays, computer techniques are used in all stages of drug screening, design and development from the early identification of disease related genes to the interpretation of clinical trial data at the later stage. At the early stage of drug discovery, virtual screening is an important tool to identify small molecules that are complementary with the active site of biological targets. The biological activities of potential compounds are then measured and based on the results of a series of related compounds, computational techniques can be applied to build statistical models. Computer-aided drug design (CADD) not only facilitates the understanding of the chemical and physical properties of a compound that are

significant for target interaction, it also provides information to guide future synthesis in lead optimization. In addition, CADD is useful for understanding and predicting the pharmacokinetic and toxicological properties of compounds, which can optimize the potential compounds into efficacious drugs (Figure 1.5) [91]. There are many successful examples of rational computer-aided drug design including dorzolamide (Trusopt® from Merck, a carbonic anhydrase inhibitor for glaucoma treatment) [92], zanamivir (Relenza® from GlaxoSmithKline, a neuraminidase inhibitor for influenza virus treatment) [93], lopinavir (Kaletra® from Abbott, a protease inhibitor for HIV treatment) [94] and imatinib (Gleevec® from Novartis, a tyrosine kinase inhibitor for the treatment of chronic myeloid leukemia) [95].

Figure 1.5 Workflow of drug discovery and development. Computer-aided drug design is used in lead discovery, lead optimization and pre-clinical phases.

1.7.2 The basic principles of computer-aided drug design

CADD, also called structural-based drug design, involves computational chemistry in the discovery, screening, design and optimization of biologically active compounds. The basic goal of CADD is to estimate whether a given molecule will bind to a particular target and how strong the binding interaction is. Additionally, the biochemical information of ligand-receptor interaction is used for the subsequent ligand refinement. For example, if information about the steric complementarity of the ligand inside the binding site is available, the affinity of ligand can be improved for its receptor.

There are three different situations to be faced in computer-aided drug design of new lead compounds: 1) the structure of the receptor is known but the bioactive conformation of the ligand is unknown, 2) only the bioactive conformation of the ligand is available and 3) the structure of target and the bioactive conformation of the ligand are unknown. Various computational methods in computer-aided drug design can be used in these three situations, which will be described in section 1.7.2.4.

1.7.2.1 Structural optimization

Before describing how to use computational techniques to discover new active molecules, it is necessary to understand the basic theory of the approaches to compute the energy of a molecule (target and ligand) because the low energy conformation of a ligand plays an important role in its activity. For example, when a ligand binds to a

specific receptor, a low energy conformation of ligand is adopted in order to be complementary to the binding pocket. This protein-ligand bound conformation is called the bioactive conformation. Molecular mechanics (MM) and quantum mechanics (QM) are used to calculate the energy of a particular arrangement of atoms (conformation), optimize a compound's energy and calculate properties such as charge, dipole moment and heat of formation, which are very useful for structure optimization.

1.7.2.1.1 Principle of molecular mechanics

Molecular mechanics (MM) is the classic mechanics to describe the behavior of a biomolecular system. This mathematical model takes the nuclei of atoms in a molecule as spheres connected by springs without consideration of the electron. Changes in energy (force field) due to bond stretching, angle bending, torsional energies and non-bonded interactions (electrostatic and van der Waals interactions) are calculated using parameters such as bond lengths (l), angles (θ), torsions (ω), charges (q) and Lennard-Jones parameters (the collision parameter σ and the well depth ε), which together with a set of equations are referred to as a force field (Figure 1.6) [96]. A molecular mechanics program is usually used in the energy minimization process. Energy calculations using a MM force field measure how much the bond lengths, angles and torsion of a molecule deviate from the "ideal" values. The bond lengths, angles and torsions in the energy minimization process are varied in order to obtain improved ligand conformations [97]. In each step, the energy of the new conformation is measured and the lower energy conformation is retained for further

optimization until no additional improvement can be achieved. After achieving the energy minimum of a system, the ligand tends to stop in a local minimum conformation rather than overcoming an energy saddle to the global minimum as shown in Figure 1.7. As a result, the lowest energy conformation at the global minimum cannot be achieved. In order to overcome this energy barrier, another computational tool, conformational search, can be used to generate different starting conformations by stepwise bond rotation followed by energy minimization of each of these. Molecular dynamics is another useful computational tool to perform conformational analysis, which generates different conformations by simulating the time-dependent movement of the compound [98, 99]. Monte Carlo simulations are also commonly used to generate random conformations of the compound to sample all possibilities. But this method requires longer computer running time.

Although the energies calculated by molecular mechanics have no meaning as absolute quantities, they are useful in comparing different conformations of the same molecule. Molecular mechanics calculation is fast and is less computer time demanding than quantum mechanics. Consequently, it is commonly used to optimize initial geometries into realistic compound structures. Some force fields such as AMBER [100], GROMOS [101] and CHARMM [102] were designed for the study of proteins. The Molecular Merck Force Field (MMFF) is commonly used for describing force field of small molecules [103].

$$V = \sum_{bonds} \frac{k_i}{2}(l_i - l_{i,0})^2 + \sum_{angles} \frac{k_i}{2}(\theta_i - \theta_{i,0})^2 + \sum_{torsions} \frac{V_\Omega}{2}[1 + \cos(n\omega - \gamma)]$$
$$+ \sum_{electrostatic} \frac{q_i q_j}{4\pi\varepsilon_0 r_{ij}} + \sum_{van\ der\ Waals} 4\,\varepsilon_{ij}\left[\left(\frac{\sigma_{ij}}{r_{ij}}\right)^{12} - \left(\frac{\sigma_{ij}}{r_{ij}}\right)^{6}\right]$$

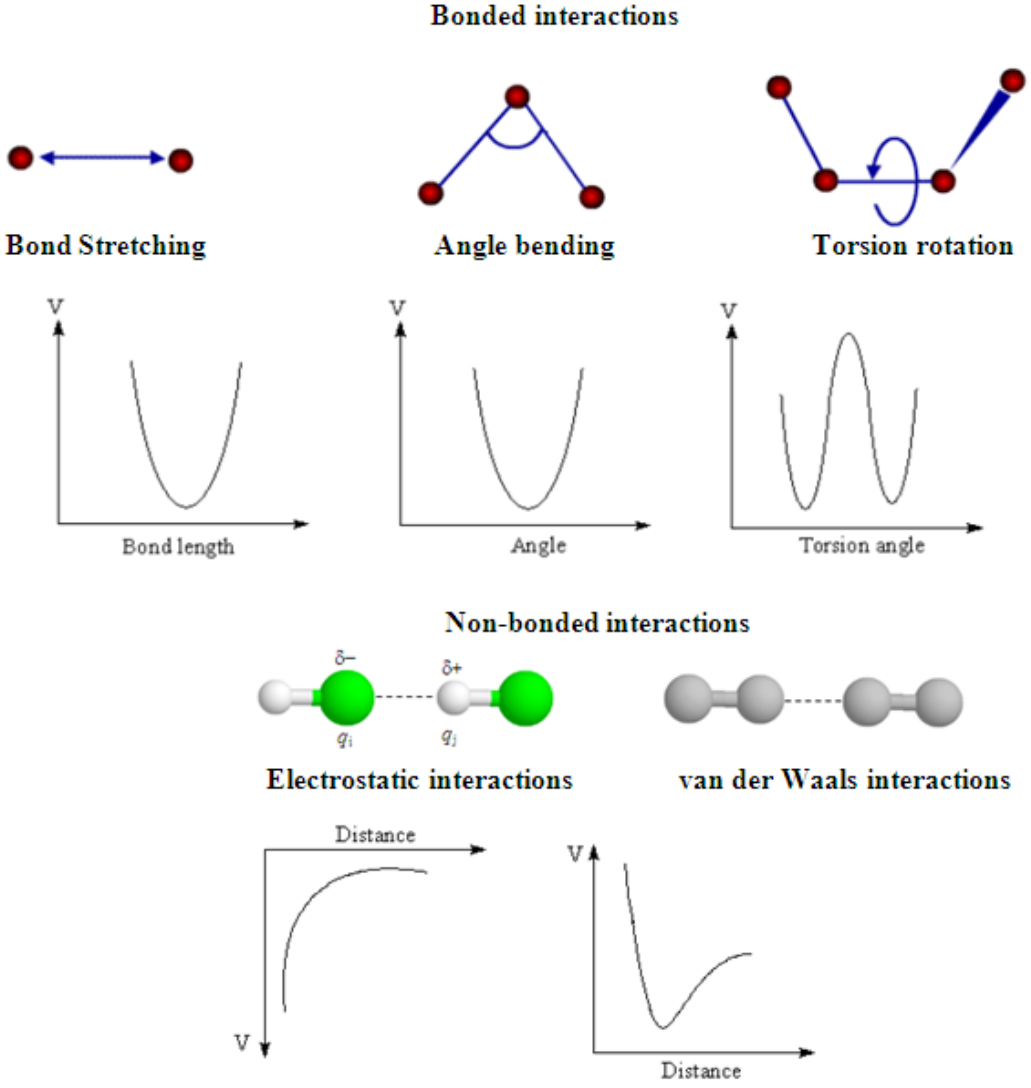

Figure 1.6 Schematic representations of the main energy contributions to a molecular mechanics force field. Various potential energy are illustrated. This figure was adopted from reference [96].

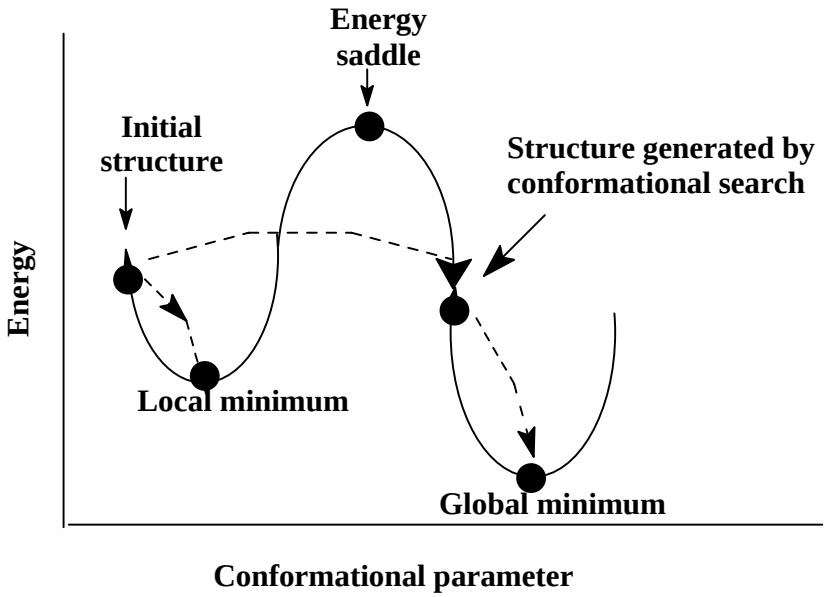

Figure 1.7 Schematic diagram of a one-dimensional energy surface. Molecular dynamics can be used to search different conformations by crossing of energy barriers, eventually leading to the most stable molecular conformation. This figure was adopted from reference [97].

1.7.2.1.2 Principle of quantum mechanics

Quantum mechanics (QM) uses quantum physics to calculate the properties of a molecule by considering the interaction between the electrons and nuclei of the molecule. Unlike molecular mechanics, atoms are not treated as solid spheres. The use of quantum mechanics is more accurate to calculate the ligand conformations [104]. QM techniques can be divided into two broad categories including *ab initio* and semi-empirical calculations. *Ab initio* technique is more rigorous which does not require pre-defined parameters, and is only dependent on the selection of basis set. However, the required computer time is much more intensive and is only applied to small molecule. On the other hand, semi-empirical methods are quicker though less accurate because only the valence electrons are considered. This method can be applicable to higher molecular weight compounds [105].

1.7.2.2 Molecular dynamics

Molecular dynamics (MD) is a computational technique which integrates Newton's law of motion to generate successive configurations of a system. This method can be used to trace how the positions and velocities of particles in the system vary with time and provide atomic detail on the internal motions of biological macromolecules [99]. MD simulations are commonly used for drug design applications such as estimation of free energies of binding, prediction of target selectivity, generation of multiple conformations for flexible docking, development of dynamic protein-based pharmacophores, metabolism prediction and refinement of

protein homology models.

1.7.2.3 Homology modeling

Generally, the 3D structures of macromolecular targets are determined experimentally by nuclear magnetic resonance (NMR) spectroscopy and/or X-ray crystallography. NMR spectroscopy solves the structure of macromolecules in solution. The main limitation of NMR spectroscopy is that it only applies to small proteins. Thus, X-ray crystallography plays an important role to determine the protein structures for structure-based drug design [106]. In the absence of experimentally derived protein structures, molecular modeling is an alternative method to build up theoretical models. The binding sites of a target protein can be constructed if the primary amino acid sequence is known and the X-ray structure of a related protein-ligand complex has been determined. Usually about 30% of sequence similarity of two proteins can share the same 3D structure [107]. In homology modeling, the sequence of model is firstly compared against the sequences of available crystal structures. Structures with high degree of sequence similarity are defined as templates. The next step is to align the sequence of the template protein with that of the protein to be modeled. It is followed by the generation of the backbone of the protein and modeling of the side-chains, often using rotamer libraries. The model is then optimized using an MM force field and validated by statistical comparison of physicochemical properties of the resulting structure, to averaged values found in high-quality structures [108]. For the FtsZ protein, the structure of *E. coli* FtsZ is unknown. Hence, a homology modeling technique is commonly used to

construct a three-dimensional (3D) structure of FtsZ for *E. coli* from *B. substilis* FtsZ (PDB code: 2VXY), *P. aeruginosa* FtsZ (PDB code: 1OFU) and *M. jannaschii* FtsZ (PDB code: 1FSZ) [60, 61, 69].

1.7.2.4 Virtual screening in drug discovery

1.7.2.4.1 Introduction

Various computational methodologies are available to complement experimental high-throughput screening. Among these, virtual screening (VS) is one of the popular approaches because it can evaluate almost unlimited number of chemical structures *in silico* for subsequent high-throughput screening experiment. VS refers to the screening of large number of compounds (10^5 to 10^7) *in silico* before selecting a limited number of candidate molecules for testing and identification of possible drug candidates [109]. Virtual screening is a knowledge-driven technology because it depends on the available information regarding either a 3D structure of the target (structural-based virtual screening) or known compounds that bind to the corresponding target (ligand-based virtual screening), or both [110]. Virtual screening includes a variety of computational screens and can effectively exploit different types of information describing the receptor. For example, given the 3D structure of a target protein is available, molecular docking or combinatorial drug design can be used to perform a target-based virtual screening [111]. Even if the structure of the binding site of the receptor is unknown, various computational methods can be used to predict its 3D structure by comparing the chemical and physical properties of known drugs that

bind to the specific site of the target [112].

1.7.2.4.2 Virtual screening based on molecular docking

Molecular docking is the process of predicting the protein-ligand interactions. The structural information from the theoretic model or the crystal structure of ligand-protein complex may clarify the putative binding modes (search algorithm), and provide guidance to discover new drug-like candidates according to the estimated binding affinities between receptor and ligands (scoring function). There are a large number of docking algorithms available for use in virtual screening (Table 1.4). Their differences are the sampling algorithm, scoring functions, the flexibility of ligand and receptor and the CPU time required to dock a molecule to a given target. In the past several years, virtual screening based on molecular docking in drug design is a successful application in pharmaceutical industry (Table 1.5). For example, ICM software was used to screen ACD database resulting in the discovery of several new antagonists of Retinoic acid receptor [113]. Inhibitors of AmpC β-lactamase were discovered using the DOCK program [114].

In earlier docking approaches, both the protein and the ligand were treated as rigid bodies, compounds were docked by rotation and translation into the binding pocket of the target. Then, semi-flexible docking was used in which the ligand was treated flexibly by allowing bonds to rotate. Nowadays, flexible protein docking methods become much more important because it incorporates receptor flexibility. But the treatment of receptor flexibility remains a major challenge because of the

long computing time [111]. Among various flexible docking algorithms, the Internal Coordinate Mechanics (ICM) method adopts on the global optimization of entire flexible ligand in the receptor field in the docking process [115]. It combines large-scale random moves of several types with gradient local minimization [116], which include pseudo-Brownian moves [117], optimally biased moves of groups of torsions [118] and single torsion changes. The optimized docking functions in ICM program can successfully predict the binding pose of 26 protein-ligand complexes with better than 2 Å RMSD in comparing with their crystallographic poses.

The reliability of molecular docking is significantly dependent on precise scoring functions. Although the scoring functions are not always accurately ranking all compounds in terms of their binding affinity, they are able to separate the most promising compounds from non-binders of the macromolecular target [119]. A large number of scoring functions are available to estimate the free energies of binding for small molecules (Table 1.4). They have different accuracy and required different computing time. Amongst these, force field functions such as DOCK [120] and GOLD [121] use the van der Waals grids and coulombic potentials to produce docking scoring function. Empirical scoring functions such as FlexX [122] and ICM [123] predict the binding energy of a ligand conformation in terms of physicochemical interactions [124]. Knowledge-based functions use structural information obtained from high-quality X-ray structures of protein-ligand complexes [125].

Table 1.4 Docking programs for virtual screening

Method	Sampling method	Scoring function	Speed	Ref.
DOCK	Incremental build	Force field	Fast	[120]
EUDOC	Exhaustive search	Force field	Fast	[126]
FlexX	Incremental build	Empirical score	Fast	[122]
ICM	Stochastic global optimization	Empirical score	Fast	[123]
LigandFit	Monte Carlo	Empirical score	Fast	[127]
FlexiDock	Genetic algorithm	Force field	Slow	[128]
Slide	Conformational ensembles	Empirical score	Fast	[129]
Affinity	Monte Carlo	Force field	Slow	[130]
AutoDock	Genetic algorithm	Empirical score	Slow	[131]
Glide	Exhaustive search	Empirical score	Slow	[132]
Gold	Genetic algorithm	Empirical score	Fast	[121]

Table 1.5 Examples of discovering bioactive molecules using docking-based virtual screening

Target	Activity	Method	Protocol	Ref.
AmpC β-lactamase	K_i = 26 μM	DOCK	Rigid docking	[114]
Aldose reductase (ALR2)	IC_{50} = 0.1 μM	DOCK	Rigid docking	[133]
Human carbonic anhydrase	IC_{50} < 0.5 μM	FlexX	Flexible docking	[134]
tRNA-guanine tranglycosylase	K_i < 10 μM	FlexX	Flexible docking	[135]
HIV-1 TAR	CD_{50} = 1	ICM-Dock	Flexible docking	[136]
Retinoic acid receptor	ED_{50} = 2	ICM-Dock	Flexible docking	[113]
Farnesyltransferease	IC_{50} = 25 μM	EUDOCK	Rigid docking	[137]

1.7.2.4.3 Virtual screening based on pharmacophore model

Pharmacophore perception method is commonly used to identify new bioactive compounds in ligand-based virtual screening. A pharmacophore consists of steric and electronic features that are significant to interact with a specific biological target [138]. The typical functional groups in a pharmacophore model include hydrogen bond donors and acceptors, ionizable groups and hydrophobic regions. The new molecules are generally studied in 3D so that the pharmacophore model can feature both the nature of the functional groups and good orientation to avoid steric clashes in the active site of the biological target [139]. Pharmacophore models can be used to quickly screen databases of hundreds of thousands of compounds to discover new leads.

1.8 Drug synergy effect

For several decades, many studies on the effectiveness of drug combinations have been reported which include antibiotics, analgesics, insecticides, fungicides, plant and animal hormones and cellular poisons. There are three possibilities of drug combination: synergism, zero-interaction and antagonism [140, 141]. Two approaches are commonly used in a combination therapy [142]. The first approach is to use multiple drugs to target multiple targets at the same time. The second approach is to use multiple drugs with different mechanisms or modes of action that may affect a single target or a disease so as to treat it more effectively. A combination drug regime would be most advantageous in the development of novel antibacterial therapies, as it may increase the efficacy of the therapeutic effect, reduce the dosage to minimize toxicity without compromising the efficacy, and minimize the development of drug resistance [143]. Even a compound with only weak interaction with the target may be significant for its mechanistic implications in the design and development of new agents. Drug combinations have been widely used to treat dreadful diseases such as cancer and infectious diseases, including AIDS and methicillin-resistant *Staphylococcus aureus* (MRSA) [144] .

In antibacterial treatment, synergism is defined as the ability of two or more antimicrobial drugs acting together to enhance the rate of early bactericidal action in comparison to the rate with either drug alone. A combination of drugs can kill greater numbers of bacteria or cure clinical infections more effectively than a single drug. The degree of synergy between antibacterial drugs is expressed in terms of the

Fractional Inhibitory Concentration index (FICI) [145].

1.9 Aims and objectives

Since many multidrug-resistant bacteria have emerged to cause most existing antibiotics less effective, discovery of new antibacterial agents against antibiotic-resistant strains is of utmost importance to the health of human beings. As discussed in the previous sections, FtsZ protein is a promising target for the development of new antibacterial agents because it is conserved among the prokaryotes, absent in the mammalian cells and plays an important role in bacterial cell division. The main objective of this project is to develop new inhibitors for FtsZ as novel antibacterial agents through computer-aided drug design and bioassays.

The identification of hit compounds from chemical databases and libraries by virtual screening of X-ray structure of FtsZ and study of their antibacterial activities will be discussed in chapter 2. In order to increase the accurary of the docking simulation and identify more potent FtsZ inhibitors, optimization of the GTP binding pocket in FtsZ with a hit compound and building a model of the GTP binding site of *S. auerus* FtsZ will be presented in chapter 3. Lastly, the validation of top-scoring derivatives by various biochemical assays will be reported in chapter 4 of this thesis.

Chapter 2

In silico hit identification and biochemical validation

2.2 Introduction

In the past several years, physical high-throughput screening (HTS) methods have been utilized to discover antibacterials that inhibit the GTPase activity or assembly of FtsZ. For example, PC58538 was identified after screening of 105,000 synthetic compounds using a cell-based antibiotic screening assay [81]. Zantrins were discovered by a high-throughput protein-based chemical screening method [80]. Viriditoxin was identified by *in vitro* high-throughput screening of more than 100,000 extracts of microbial fermentation broths and plants [62]. Although physical HTS significantly supports the drug discovery process, it is time-consuming and needs expensive experimental set up. In the early 2000s, studies showed that computational docking hit rates were 10-fold to 1000-fold higher than those obtained by a physical HTS against the same drug target [146-149]. Computer-based docking has therefore been extensively applied to the discovery and early optimization of leads in a drug design process. Additionally, computer-aided rational drug design can facilitate and complement chemical synthesis and biological assays [150]. In a structural-based virtual screening, molecular docking is utilized to screen commercially available databases or virtual compounds on three-dimenional target models *in silico* [151]. The docking scoring function is then used to evaluate ligands complementing the active site of target and high-ranking compounds will be tested experimentally [152]. Typically, a virtual HTS process consists of three stages. First, the large compound database is divided into clusters according to structural similarity which ensure compounds with same or similar scaffolds will be in the same group. Then, representative compounds of each cluster are selected and

flexibly docked into the target binding site in the crystal structure and top-ranked compounds are selected. After that, all members of identified hits in the cluster are subjected to a docking process incorporating protein flexibility again to obtain the top scoring hits. There are two common approaches in computer-aided drug design to discover novel ligands *in silico*. One approach is structure-based virtual screening that can identify hit or lead compounds by screening available commercial and in house libraries based on the crystal structure of a particular target [153]. The other approach is ligand-based virtual screening in which a novel inhibitor is discovered based on the vast information on strong inhibitors published in the literature [154]. In the past several years, only a few FtsZ inhibitors were found to bind the GTP binding site which include berberine [69], GTP analogues [79], PC170942 [60] and Chrysohaentins A-H [61]. Therefore, it is difficult to predict the important physicochemical features which can guide us to design new FtsZ inhibitors using a ligand-based virtual screening approach. On the contrary, much effort has been made to determine the structure of FtsZ proteins by X-ray crystallography [60, 77, 155-158], which faciliates us to search for novel inhibitors by a rational structure-based virtual screening of compounds from vendor or in-house databases and libraries. To our best knowledge, no attempt has ever been made to identify and optimize the potency of lead compounds towards FtsZ using a molecular docking of structural-based virtual screening. It also motivates us to use the structural-based virtual screening approach to identify new FtsZ inhibitors. Even if the crystal structure of FtsZ of a particular bacterium is not solved by crystallography, a homology model can be built based on available X-ray crystal structures in the

protein databank.

Over the last two decades, many approved drugs were discovered from natural products and their derivatives [159]. Natural products possess the advantages of high molecular diversity, bioactive substructures and potentially lower toxicity profiles compared to synthetic compounds [160, 161]. With regard to the importance of natural products in the drug discovery process, it would be advantageous to identify novel FtsZ inhibitors using high-throughput virtual screening of natural product databases.

In this study, one of the most popular docking algorithms, Internal Coordinate Mechanics (ICM) [123], was used in hit identification and hit-lead optimization. ICM performs fast and accurate docking of fully continuously flexible small molecule ligands to a protein represented by grid interaction potentials. In this chapter, using molecular docking of ICM software [123] to screen libraries of natural products containing over 20,000 compounds will be reported. Potential FtsZ inhibitors were identified by *in silico* screening. Various *in vivo* and *in vitro* assays were used to test the inhibitory effect of the hit compounds on FtsZ. The minimal inhibitory concentration (MIC) of each hit compound was measured against a range of bacterial strains. On-target activity of the compounds was also studied by morphometric analysis. *In vitro* assays were employed to measure the inhibitory ability of each compound on FtsZ. The most biologically active compound was also tested for its effect on the polymerization of tubulin, the eukaryotic homologue of

FtsZ.

2.2 Experimental

2.2.1 Materials

2.2.1.1 Bacterial strains and cell lines

E. coli XL-1 Blue was used as a recipient of recombinant plasmids and for plasmids amplification. *S. auerus* FtsZ was over-expressed in a host of *E. coli* BL21 (DE3). The bacterial strains used in minimum inhibitory concentration (MIC) determination are: *S. aureus* ATCC 29213, *S. aureus* ATCC 29247, *S. epidermidis* ATCC 12228, *E. faecalis* ATCC 29212, *E. faecium* ATCC 49624, *M. catarrhalis* ATCC 25240 and *P. aeruginosa* ATCC 27853 which were purchased from American Type Culture Collection (USA). *B. subtilis* 168 and *E. coli* ATCC 25922 are our laboratory collections. Three mammalian cell lines (L929: mouse fibroblast cells, MKCKII: Madan-Darby canine kidney cells and HEK293/pcDNA3.1: human embryonic kidney cells containing a pcDNA3.1 vector) were used in the cytotoxicity test.

2.2.1.2 Plasmids

pRSET-A-S FtsZ was cloned from the *S. auerus* (ATCC 29213) *ftsZ* gene which was employed for the over-expression of the FtsZ protein in a *E. coli* expression system. The plasmid map is shown at Figure 2.1.

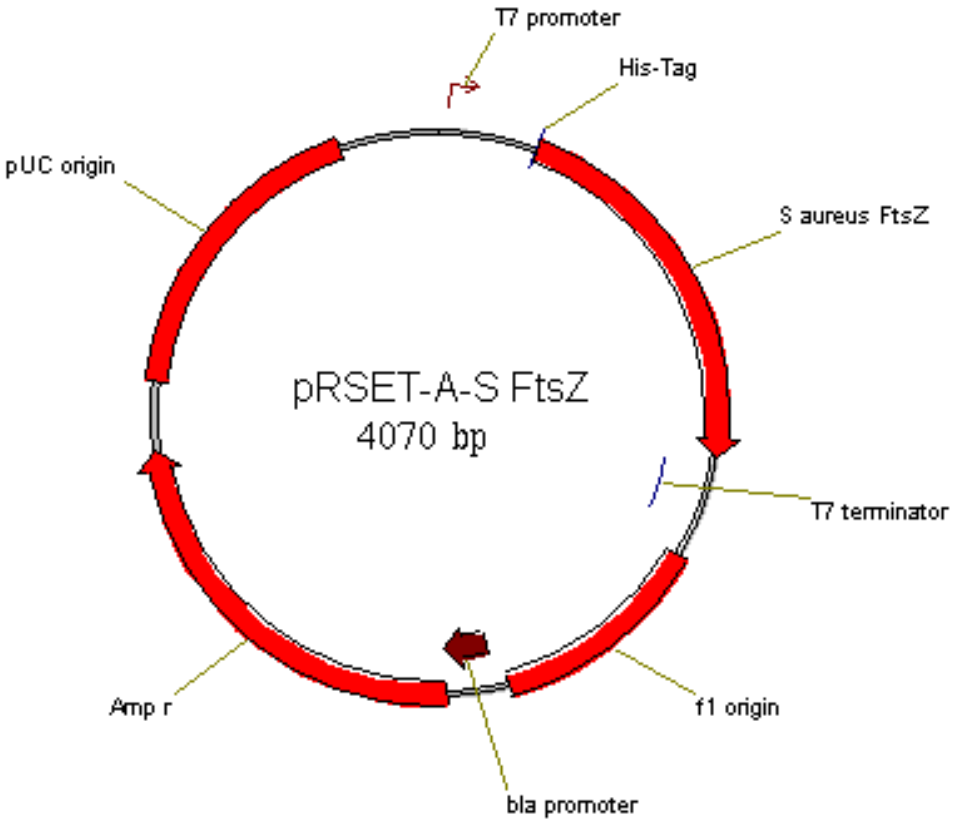

Figure 2.1 Plasmid map of pRSET-A-S FtsZ with ampicillin resistant marker (Amp r). *S. auerus* FtsZ was cloned between NdeI and XhoI located in the multi-cloning site (MCS).

2.2.1.3 DNA manipulation reagents

PCR and site-directed mutagenesis were performed by PfuUltra High-Fidelity DNA Polymerase (Stratagene). Primers used in PCR were purchased from Sigma-Proligo. Restriction digestion enzymes (NdeI and XhoI) and dNTPs were purchased from Promega. The PCR purification kit was purchased from Roche.

2.2.1.4 Media

Nutrient agar, tryptone and yeast extract were obtained from Oxoid Ltd. (Nepean, Ontario, Canada). Luria-Bertani (LB) medium was purchased from USB Corporation and used for preparation and transformation of *E. coli* competent cells and *in vivo* assays. 2 × TY medium for the over-expression of FtsZ protein was prepared by the addition of 16 g tryptone, 10 g yeast extract and 5 g sodium chloride into 1 L deionized water and sterilized. Müller-Hinton broth (MHB), cation-adjusted Müller-Hinton broth (CA-MHB) and trypticase soy broth (TSB) for Minimum Inhibitory Concentration (MIC) determination were purchased from Becton, Dickinson and Company (New Jersey, USA). All nutrient agar plates containing 50 μg/mL ampicillin were prepared by the addition of 0.5 mL ampicillin (10 mg/mL) into 100 mL sterilized molten agar at about 50 ^{o}C.

2.2.1.5 Chemicals

Ampicillin, chloramphenicol, cinnamaldehyde, totarol, 4-morpholinepropane sulfonic acid (MOPS), Tris-HCl, calcium chloride, magnesium chloride, potassium

chloride, EDTA, 4', 6-diamidino-2-phenylindole (DAPI), guanosine 5'-triphosphate (GTP) and phosphotungstic acid (PTA) were purchased from Sigma-Aldrich. Sodium chloride, potassium hydroxide, potassium dihydrogenphosphate and isopropyl β-D-1-thiogalactopyranoside (IPTG) were obtained from USB Corporation. FM 4-64 and SlowFade Antifade kit were purchased from Invitrogen (Eugene, Oregon). Polyclonal anti-FtsZ rabbit antibody was developed in rabbit against *E. coli* FtsZ by Agrisera (Sweden). FITP-conjugated goat anti-rabbit secondary antibody was obtained from Acris Antibodies GmbH (Germany). All natural products and semi-synthetic natural derivatives were purchased from AnalytiCon Discovery (Potsdam, Germany). The chemical structures of hit compounds were verified by using high-resolution mass spectrometry (Micomass Q-Tof-2) to determine the molecular weight $(M+H)^+$. For example, the mass spectral analysis on the sample of compound **5** indicated an observed mass of $[(M+H)^+ = 429.13]$, which in agreement with the calculated mass (428.19) based upon the chemical structure. All other chemicals used were of analytical grade.

2.2.1.3 Proteins

BSA and lysozyme were obtained from Sigma-Aldrich. Restriction enzymes for cloning were purchased from Promega. *E. coli* FtsZ protein was obtained from Cytoskeleton (USA).

2.2.2 Computational techniques

2.2.2.1 Receptor preparation

The X-ray structure of the co-crystallized FtsZ dimer with GTP from *M. jannaschii* (PDB code: 1W5B) [157] was used as our initial docking template. All atom types, hydrogen and missing heavy atoms were added to the structure after the protein had been converted into an ICM object. The position of asparagine and glutamine side chains were also optimized to improve the hydrogen bond pattern. Unless involved in at least three specific and conserved contacts with non-water atoms, water molecules in the ICM object were removed. Metal ions and the original ligand from the X-ray structure were deleted before starting a docking simulation process. The residues were renumbered based on the protein sequence retrieved from UniProt [162].

2.2.2.2 Ligand preparation

Merck Molecular Force Field (MMFF) atom assignment and force field optimization were used to convert ligands from two-dimensional to three-dimensional chemical structure and the three-dimenional structure was then optimized for a docking simulation. Charges and hydrogen atoms of each ligand were added in the optimization process.

2.2.2.3 Determination of binding pocket

The IcmPocketFinder [163] tool as implemented in ICM 3.6 was used to identify putative binding sites on the entire structure of the *M. jannaschii* FtsZ dimer. The tolerance value was set to be 4.6. IcmPocketFinder used the marco to provide a mesh associated to every detected pocket.

2.2.2.4 High-throughput screening of natural product databases

The ICM-Pro 3.6-1c software (Molsoft) [164] was used to screen natural product and semi-synthetic natural product derivative libraries containing more than 20,000 compounds based on more than 60 highly diverse chemotypes [165]. The molecular conformation was represented by the internal coordinate variables. The adopted force field was a modified version of the ECEPP/3 force field [166] with a distance-dependent dielectric function. The initial structure was converted into an ICM object by adding polar hydrogen, assigning atom type and charges from residues. Then, a grid map was calculated with grid spacing of 0.5 Å. Docking was performed with a global optimization algorithm to find the global minimum of the energy function. This algorithm consists of five grid potentials describing interactions between the flexible ligand with the receptor and internal conformational energy of the ligand. Then, a series of five grid potential representations of the rigid receptor were generated and superimposed to give rise to the hydrogen-bonding profile, hydrophobicity, carbon-based and hydrogen-based van der Waals boundaries, and electronstatic potential of the predefined ligand

binding site of FtsZ [163]. It means that all the residues with at least one side chain non-hydrogen atom in the range of 3.0 Å from the selected mesh were considered part of the pocket. The reduced receptor representation can greatly minimize the calculation time. A biased probability Monte Carlo (BPMC) global stochastic optimizer implemented in the ICM program was used for global energy optimization. In the BPMC method, a flexible ligand from a chemical library of natural product and semi-synthetic natural product derivatives was docked into the grid representation of the pocket. During the docking, either one of the torsional or roto-translational variables of the ligand was randomly changed or a pseudo-Brownian move was performed. Then, the ICM global optimization algorithm was used to optimize the resulting conformation of the complex between small molecule and the FtsZ dimer to calculate the complete energy such as the solvation energy and those of the conformational entropy. A total energy of new conformation after each run was accepted or rejected based on the Metropolis criterion [167]. A new random change is introduced and the whole procedure was repeated until the lowest energy conformation of complex was obtained. The free energy of binding of each conformation was assessed by means of the standard ICM empirical scoring function [168]. Each compound was docked three times and the best score of each compound was then retained. The ICM binding score was used to reflect its fit with receptor. The reasonable approximation of the free binding energy of binding between the compound and FtsZ were evaluated with a full-atom ICM binding score [34] from a multi-receptor screening benchmark. The score was calculated using the following formula:

$Score = E_{int} + T\Delta S_{Tor} + E_{vw} + \alpha_1 E_{el} + \alpha_2 E_{hb} + \alpha_3 E_{hp} + \alpha_4 E_{sf}$

where E_{vw}, E_{el}, E_{hb}, E_{hp}, and E_{sf} are van der Waals, electrostatic, hydrogen bonding, and nonpolar and polar atom desolvation energy differences between bound and unbound states respectively. E_{int} is the internal strain of ligand calculated as a difference between its internal force-field energy in the bound state and its ground state energy, ΔS_{Tor} is the ligand conformational entropy loss upon binding, and T = 300 K, and the α coefficients are empirical weights introduced to balance the different contributions.

2.2.3 *In vivo* assays

2.2.3.1 Antimicrobial testing

Minimum inhibitory concentration (MIC) value was determined by a broth microdilution method according to the National Committee for Clinical Laboratory Standards (CLSI) guidelines [169]. The experiments were conducted in 96-well microtiter plates (IWAKI, Japan) using 2-fold serial dilutions in cation-adjusted Müller-Hinton (CA-MH) (*S. auerus* ATCC 29213 and ATCC 29247) and Müller-Hinton (MH) broths (other bacterial strains). Compounds were dissolved in DMSO and then diluted in serial two-fold manner. The final DMSO concentration in the medium was 1% and should have no effect on the growth of the panel of organisms. Exponentially growing cells were diluted to approximately 5×10^5 CFU/mL (final optical density) in MH broth. In this susceptibility test, ampicillin, totarol and cinnamaldehye were used as positive controls. After 18 h incubation at

37 ^{o}C, absorbance (A_{600}) readings were recorded to calculate the percentage inhibition in cell growth with respect to control (BioRad 680). MIC was defined as the lowest concentration of the tested compound that inhibited pathogen visible growth and reproduction. Data were collected and analyzed using Microsoft Excel. The A_{600} of respective blanks having only tested compounds was subtracted to give the final A_{600}. The percentage inhibition of bacterial growth was calculated by the equation:

% Inhibition = [1 − (final A_{600}/ A_{600} of the control culture)] × 100

The percentage inhibition of bacterial growth was determined 18 h after the addition of tested compound to the bacterial culture. Inhibition is defined as the reduction of absorbance of ≥ 90% relative to the control without any inhibitor. The experiment was set up in triplicates.

2.2.3.2 Visualization of bacterial morphology

B. subtilis 168, *E. coli* (ATCC 25922) and *S. auerus* (ATCC 29213) cells were grown in LB medium. The cultures were inoculated at an OD_{600} of 0.01 from an overnight culture in the same medium containing 1% DMSO or different concentrations of compounds and grown at 37 ^{o}C. After 4 h, the bacteria cells were harvested and resuspended in 100 μL of PBS buffer containing 0.25% agarose. Then, a total of 10 μL suspension mixture was placed on the microscopic slide which had been pretreated with 0.1% (w/v) poly-L-lysine and the morphology of the bacterial cells was observed under a light phase-contrast microscope (Leica) at ×40 magnification. The images were captured using a Nikon camera. The length of a

bacterial cell was measured using a software installed in the Nikon camera. 200 cells were analyzed to determine the bacterial average cell length.

2.2.3.3 Membrane staining

FM4-64, a red fluorescent dye, was used to stain the membrane of bacterial strains [66]. In this study, *B. subtilis* 168 and *E. coli* cells from overnight culture in 10 mL of LB were diluted to OD 0.01 and were further grown in the absence or presence of various concentrations of compound **5** for 4 h at 37 ^{o}C. FM4-64 was added to 1 mL of the growing *B. subtilis* 168 and *E. coli* cultures to a final concentration of 1.6 μM and incubated at 30 ^{o}C. After 15 min, the bacteria cells were harvested and resuspended in 100 μL of PBS buffer containing 0.25% agarose. 10 μL of sample mixture was placed on a pretreated microscopic slide with 0.1% (w/v) poly-L-lysine and observed under a fluorescence microscope (Leica) by a ×100 oil immersion objective.

2.2.3.4 Visualization of Z-ring in the bacteria

A culture of *E. coli* JM109 WM647 (a gift from Dr. W. Margolin) containing an IPTG-inducible plasmid for the production of GFP-tagged FtsZ was grown in LB medium supplemented with chloramphenicol (30 μg/mL). After overnight incubation, a sample of the culture was diluted to 1% in the LB medium containing different concentrations of compounds and 40 μM IPTG [16]. After 4 h incubation at 37 ^{o}C, the *E. coli* cells were fixed, harvested and resuspended in PBS buffer containing

0.25% of agarose. 10 μL sample of these were pipetted onto the pretreated microscopy slide with 0.1% (w/v) poly-L-lysine and visualized by a fluorescence microscope (Leica) at ×100 oil immersion with a standard fluorescein isothiocyanate filter set for GFP. 100 cells were analyzed to calculate the frequency of FtsZ rings.

2.2.3.5 Immunofluorescence microscopy

Immunofluorescence microscopy was applied to visualize the Z rings of *B. subtilis* 168 cells. *B. subtilis* 168 cells were immunostained with procedures described in the literature [170]. Briefly, a colony of *B. subtilis* strain 168 was resuspended in LB medium and grown exponentially at 37 ^{o}C until A_{600} reached ~ 0.3-0.4. Then, samples of the culture were treated with different concentrations of the compound or 1% DMSO (control). After 90 min incubation at 37 ^{o}C, samples of the culture were fixed with 2.5% formaldehyde and 0.04% glutaraldehyde in PBS buffer at pH 7.4. After 10 min incubation at room temperature, cells were collected and washed three times with PBS buffer. To quench auto-fluorescence and enhance antigenicity, the cells were incubated with 1 mg/mL of sodium borohydride ($NaBH_4$) in PBS buffer for 5 min on a rotator and then washed twice with PBS buffer. The cells were resuspended in PBS containing 0.05% Titron X-100 for 45 min. After washing the cells three times with PBS buffer, the washed cells were resuspended in GTE buffer (20 mM Tris, pH 7.5, 50 mM glucose and 10 mM EDTA) containing freshly prepared 20 μg/mL of lysozyme incubated at room temperature for 30 min and washed again with PBS. The cells were immediately transferred to the microscope slide that had been pretreated with 0.1% (w/v) poly-L-lysine. After 5

min, loosely adherent bacterial cells were aspirated. A blocking solution (2% [w/v] bovine serum albumin in PBS) was added and the cells were incubated for 30 min. After removing the blocking solution, cellular FtsZ was stained with a polyclonal anti-FtsZ rabbit antibody and the cells were incubated overnight at 4 ^{o}C. A FITC-conjugated goat anti-rabbit secondary antibody was added to further stain the cellular FtsZ for 2 h. After that, the slides were washed 10 times with PBS containing 0.05% Tween 20. Nucleoids were visualized by staining the bacterial cells with 1 μg/mL 4',6-diamidino-2-phenylindole (DAPI) and the cells were then incubated for 1 min at 25 ^{o}C. The cells were washed twice with distilled water and then 2 drops of the SlowFade equilibration buffer were added to pre-equilibrate the bacterial specimens for 5 min before being mounted in 5 μL of SlowFade and 5 μL of PBS buffer containing 0.25% (w/v) agarose. Finally, the bacterial specimens were visualized under a fluorescence microscope (Leica).

2.2.4 *In vitro* assays

2.2.4.1 Cloning and DNA manipulation

2.2.4.1.1 Preparation of *E. coli* competent cells

E. coli BL21 (DE3) strain was cultured in 5 mL sterilized LB medium for 14-16 h at 37 ^{o}C with shaking at 280 rpm. Overnight culture (200 μL) was added into 100 ml sterilized LB medium and incubated at 37 ^{o}C with shaking at 280 rpm. When the optical density (OD_{600}) of the bacterial culture reached 0.3 - 0.4, cells were harvested and centrifuged at 4000 rpm for 20 min at 4 ^{o}C. Then, the cell pellet was

resuspended in 10 mL sterilized ice-cold 100 mM $CaCl_2$ and kept in ice. After 25 min, the cells were pelleted again by centrifugation at 4000 rpm for 20 min at 4 ^oC and then the pellet was resuspended in 700 μL ice-cold $CaCl_2$. 300 μL of 50% sterilized glycerol was added to make up a final glycerol concentration of 15%, and the mixture was aliquoted into eppendorf. These competent cells were frozen quickly by liquid nitrogen and stored at – 80 ^oC.

2.2.4.1.2 Transformation of competent cells

Plasmid DNA or ligation product was added and mixed thoroughly with 50 mL competent cells. After being incubated on ice for 25 min, the competent cells were heat shocked at 42 ^oC for 2 min. Then, 200 mL sterilized LB medium was added to the eppendorf containing the competent cells which were incubated at 37 ^oC for 1 hour. These competent cells were streaked on nutrient agar plate containing 50 μg/mL kanamycin and incubated at 37 ^oC overnight.

2.2.4.1.3 Extraction and purification of genomic DNA from *S. aureus* strain

Genomic DNA from *S. aureus* strain (ATCC 29213) was extracted according to the protocol of the illustra bacteria genomicPrep Mini Spin Kit (GE healthcare).

2.2.4.1.4 Subcloning of *S. auerus* FtsZ gene into expression vector

Genomic DNA (template) was isolated from *S. auerus* strain (ATCC 29213) by the illustra bacteria genomicPrep Mini Spin Kit (GE healthcare). The *ftsZ* gene was

amplified by PCR using oligonucleotides *Sa* Ftz-F (CTATGTCATATGTTAGAAT-TTGAACAAGGATTTAATC) and *Sa* Ftz-R (CATTGACTCGAGTTAACGTCTT-GTTCTTCTTGAAC) flanked by NdeI and XhoI restriction site respectively. The PCR profile was set as follows: pre-denaturation at 95 ^{o}C for 5 min, 30 cycles amplification at 94 ^{o}C for 1 min, 55 ^{o}C for 1 min, 72 ^{o}C for 1 min 10 s and final elongation at 72 ^{o}C for 10 min. The PCR product was purified and digested with NdeI and XhoI restriction enzymes. Digested *ftsZ* gene was ligated into pRSET-A-S which had been previously digested by NdeI and XhoI restriction enzymes. Histidine tag was added to the N-terminal of FtsZ protein by inserting 6 codons (CATCACCATCACCATCAC) between the translation start and the second codon by the QuickChange® II Site-Directed Mutagenesis Kits (Stratagene) according to the manufacturer's instructions. The insertion was preformed by using two primers, FtsZ-F (GGAGTATACATATGCATCACCATCACCATCACTTAGAAT-TTGAACAAGGA) and FtsZ-R (TCCTTGTTCAAATTCTAAGTGATGGTGATG-GTGATGCATATGTATACTCC) under the following PCR cycling condition: pre-denaturation at 95 ^{o}C for 2 min, 18 cycles at 95 ^{o}C for 30 s, 57 ^{o}C for 1 min, and 68 ^{o}C for 4 min. FtsZ, 6His-tagged at its N-terminus, was expressed from pRSET-A-S FtsZ in *E. coli* BL21(DE3) cells under control of the T7-promoter. The expressed protein contains 396 residues and has a molecular weight of 41.8 kDa.

2.2.4.2 Preparation of *S. auerus* His-tagged FtsZ

2.2.4.2.1 Expression of *S. auerus* His-tagged FtsZ in *E. coli*

In this study, His_6-FtsZ was overexpressed in *E. coli* BL21(λDE3) cells. *E. coli* cells containing the *ftsZ* gene was streaked on a nutrient agar plate with 50 μg/mL ampicillin and incubated at 37 ^{o}C overnight. A few single colonies were inoculated into 5 mL LB medium, incubated at 37 ^{o}C and shaked at 250 rpm for 14-16 h. This pre-culture was transferred to a flask containing fresh 2 × TY medium in 1:100 dilution and 50 μg/mL ampicillin was added, followed by incubation at 37 ^{o}C with shaking at 280 rpm. Cell growth was monitored by measuring the optical density at 600 nm (OD_{600}). When OD_{600} reached 0.8, His-tagged FtsZ was induced with 0.4 mM filtered isopropyl-β-D-thiogalactopyranoside (IPTG) for 4 h at 37 ^{o}C with shaking at 250 rpm. Cells were harvested by centrifugation at 4 ^{o}C, 9000 rpm for 20 min. Before subsequent purification steps, the cell pellet was stored at – 80 ^{o}C.

2.2.4.2.2 Purification of intracellular His-tagged *S. auerus* FtsZ

Before the purification step, the 6his-tagged FtsZ in the cell pellet was extracted by homogenization. First, the cell pellet was resuspended in 20 mL of solubilization buffer (50 mM Tris-HCl, 150 mM NaCl, 1 mM PMSF and 1 mM EDTA, pH 7.4) and incubated with 75 μg/mL lysozyme for 1 h at 30 ^{o}C, followed by a 30 s-sonication for 5 times with a Soniprep 150 ultrasonic disintegrator (MSE Scientific Instrument, England) to obtain cell extracts. Soluble and particulate fractions were separated by centrifuging cell extracts at 13,000 rpm for 1 h at 4^{o}C. Most His-tagged

FtsZ protein was obtained in the soluble fraction.

In order to purify the soluble protein (His_6-FtsZ), metal affinity chromatography was performed using an Amersham-Pharmacia ÄKTA FPLC system (Amersham-Pharmacia Biotech Inc., Piscataway, NJ). The supernatant was passed through a 0.22 μm filter before loaded on a 5-mL nickel (II) sulfate charged 5-mL HiTrap chelating column (Amersham-Pharmacia Biotech Inc.) that had been pre-equilibrated with a pH 7.4 starting buffer made up of 20 mM sodium phosphate and 150 mM KCl. The column was then washed with 8 column volumes of the starting buffer and the His_6-FtsZ was eluted by a linear imidazole gradient from 0.1 to 0.2 M. Eluates with the UV absorbance peak were pooled and dialyzed extensively against a 50 mM MOPs buffer, pH 6.5 or other bioassay buffers such as 50 mM Tris.HCl (pH 7.4). The protein was aliquoted and stored at –70 ^{o}C. His-tagged FtsZ was purified to more then 95% homogeneity by this chromatographic procedure. For long-term storage, the purified enzyme was buffer-exchanged with 20 mM ammomium bicarbonate, lyophilized and stored at –20 ^{o}C.

2.2.4.3 SDS-polyacrylamide gel electrophoresis (SDS-PAGE)

Protein samples were analyzed on 12% SDS-PAGE in a Mini-PROTEAN III dual slab cell (Bio-Rad Laboratories). The sample was mixed with reducing agent *β*-mercaptoethanol and SDS. The SDS-PAGE gel comprised of 5% stacking gel (pH 6.8) and 12% separating gel (pH 8.8) and was subjected to electrophoresis in 1× running buffer at 200 V for 60 min. After electrophoresis, the gel was stained with

Coomassie blue for 5 min. Then the gel was immersed into the destain solution with shaking; and the destain solution was replaced until a clear background of the gel was obtained. Afterwards, the gel was air-dried and finally mounted with gel drying film (Promega).

2.2.4.4 Determination of protein concentration

The total FtsZ concentration of the samples was determined by Bradford assay. In this assay, 200 μL of Bradford Reagent Dye (Bio-Rad) was mixed with 800 μL of sample and then incubated for 10 min at room temperature. The absorbance of the sample was measured spectrophotometrically at 595 nm. The protein concentration of the sample was determined by comparison against a protein standard curve, which was constructed by different concentrations of BSA standards.

2.2.4.5 Electrospray ionization-mass spectrometry (ESI-MS)

A VG Platform single quadrupole or quadrupole-time of flight (Q-TOF2) mass spectrometer (Micromass, Altrincham, Cheshire, UK) equipped with an electrospray interface was used to obtain ESI-mass spectra. Protein samples were dissolved in H_2O/CH_3CN (1:1 v/v) or H_2O/MeOH (1:1 v/v) containing 0.2% formic acid (v/v) and injected into the electrospray source via a 20 μL-loop injector (Rheodyne 5717) at a flow rate of 10 μL/min. The mass spectrometer was scanned over the m/z 570 – 1600 range. The instrument was calibrated with myoglobin (10 ρmol/μL, average molecular mass 16,951.5).

2.2.4.6 Light scattering assay

The polymerization and depolymerization of *S. auerus* FtsZ was followed by 90^{o} light scattering in a thermostatically (37 ^{o}C) controlled Pekin Elmer LS-50B spectrofluorometer using a 0.5 mL quartz curvet (10 mm, Hellma). Both excitation and emission wavelengths were set at 600 nm with a slit width of 2.5 nm. *S. auerus* FtsZ (12.5 μM) in 50 mM MOPS buffer (pH 6.5) was incubated with 1% DMSO or different concentrations of compounds for 10 min at 25 ^{o}C. Then, 50 mM KCl and 10 mM $MgCl_2$ were added to establish a baseline. After 8 min, a final concentration of 1 mM GTP was added at the last fraction and the increase in light scattering was measured for an additional 25 - 30 min. The rate and extent of polymerization were determined. The appropriate blank was subtracted from all experimental data. Each light scattering assay was repeated three times to obtain the average result.

2.2.4.7 GTPase activity

The conversion of GTP to GDP by *E. coli* and *S. auerus* FtsZ proteins was measured by monitoring the release of inorganic phosphate in an end point enzyme assay using CytoPhos™ phosphate assay Biochem Kit™ (Cytoskeleton, USA). In this assay, 2 μM *E. coli* FtsZ or 7.5 μM *S. auerus* FtsZ was preincubated with a serial dilution of compounds in a 15 μL buffer containing 50 mM Tris at pH 7.4 (*E. coli* FtsZ protein) or 50 mM 4-morpholinepropanesulfonic acid (*S. auerus* FtsZ protein) for 10 min at 25 ^{o}C. The control tube contained 1% DMSO alone. Then, 5 mM of $MgCl_2$ and 200 mM KCl were added. The reaction was started by the addition of 500 μM GTP followed by incubation at 37 ^{o}C. 100 μL of Cytophos reagent was added into each sample containing *E. coli* FtsZ and *S. auerus* FtsZ after 5 min or 30 min respectively. After 10 min incubation, the absorbance (A_{650}) was taken in a 96-well microplate reader (BioRad 680). The IC_{50} (50 % inhibitory concentration) value of hit compound was determined from the relative slopes of GTP hydrolysis at different concentrations of compounds compared to the control with DMSO only.

2.2.4.8 Transmission electron microscopy

S. auerus FtsZ (12 μM) was incubated in the absence and presence of different concentrations of hit compound in 50 mM MOPS buffer at pH 6.5 for 10 min at 25 ^{o}C. Then, 50 mM KCl, 5 mM $MgCl_2$ and 1 mM GTP were added to the reaction mixtures which were then incubated at 37 ^{o}C for 15 min. Subsequently, 10 μL

aliquots were applied to a glow-discharged Formvar carbon-coated copper grid (400 mesh) and blotted dry. 10 μL of distilled water was added to wash away any excess sample solution on the grids for 30 s. The grid was subsequently subjected to negative staining using 10 μL of 0.5 % phosphotungstic acid (PTA) for 30 s, air-dried and digital images of the specimen were observed with a JEOL model JEM 2010 transmission electron microscope operated at 200 kV and equipped with a Gatan MSC 794 CCD camera.

2.2.4.9 Tubulin polymerization assay

A hit compound was tested for inhibition of bovine brain (mammalian) tubulin polymerization using the Tubulin Polymerization Assay Kit (Cytoskeleton, Inc.). Polymerization was monitored by measuring the fluorescence enhancement from a fluorescent reporter [4',6-diamidino-2-phenylindole (DAPI)] incorporated into the microtubules. The final concentration of bovine brain tubulin was 2 μg/mL. Paclitaxel (20 μM) and vinblastine (30 μM) which are known tubulin polyermization enhancer and inhibitor respectively, were also included as reference compounds as compared to the control (1% DMSO). Compound **5** was tested in the assay at a final concentration of 384 μg/mL (890 μM in 1% DMSO final). Fluorescence was measured using a PolarStar Optima (BMG) microplate reader at wavelength settings of 360 nm (excitation) and 450 nm (emission). Data were collected using Microsoft Excel and treated by Origin.

2.3 Results and discussion

2.3.1 Identification of potential FtsZ inhibitors by the structure-based virtual screening method

Computer-aided drug screening was conducted to identify potential FtsZ inhibitors that bind to the GTP binding pocket. ICM-Pro (version 3.6-1c) [123] was used to dock the libraries of natural products and semi-synthetic natural products containing more than 20,000 compounds against the X-ray structure of *M. jannaschii* FtsZ (PDB code: 1W5B). More than one druggable binding sites of the FtsZ dimer were identified (Figure 2.2). Since the GTP binding site (pocket 2) has been shown to be highly conserved with recognizable sequence identity, it is likely to be a good target site for new inhibitors with a broad spectrum activity of bacteria. In the first round virtual screening, each continuously flexible compound of the natural product databases was docked to the rigid pocket of the receptor using the biased probability Monte Carlo (BPMC) global energy minimization procedure. Each compound was docked three times. The best scoring pose of each compound from different clusters were inspected manually and evaluated. Some hit compounds which were not necessarily those with the best final scores were chosen because they showed the best characteristic interaction with the GTP binding site of *M. jannaschii* FtsZ. The hit compounds were selected for subsequent biochemical tests based on criteria such as formation of specific hydrogen bonds with significant residues to bind GTP substrate, contact with most parts of GTP pocket and compounds with

best scoring from each cluster were selected for further biochemical validation. The chemical structures of the hit compounds are summarized in Table 2.1.

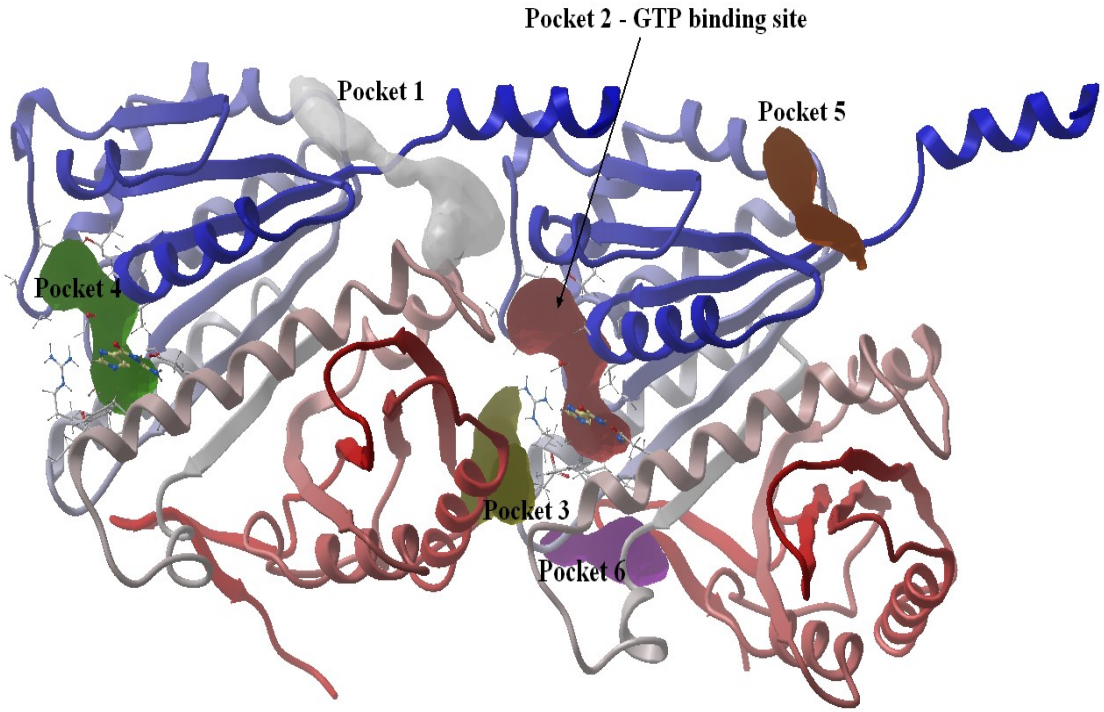

Figure 2.2 X-ray structure of the FtsZ dimer (PDB code: 1W5B) are shown in ribbon form. The GTP substrate is depicted as ball-and-stick models displaying carbon (yellow), hydrogen (grey), oxygen (red) and nitrogen (blue) atoms. The favorable binding pockets of the FtsZ dimer are represented as grey (pocket 1), red (pocket 2 – GTP binding site in subunit B), yellow-brownish (pocket 3 near T7 loop at C-terminus), green (pocket 4 – nucleotid binding site in subunit A), brown (pocket 5), purple (pocket 6- unknown function).

Table 2.1 Chemical structure of hit compounds

Hit	Score	Structure	Hit	Score	Structure
1	-30.05	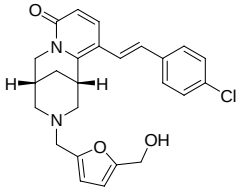	**7**	-20.50	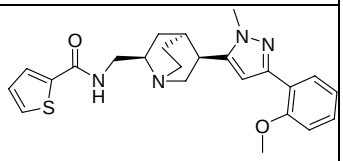
2	-29.04	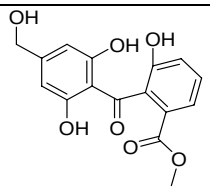	**8**	-29.84	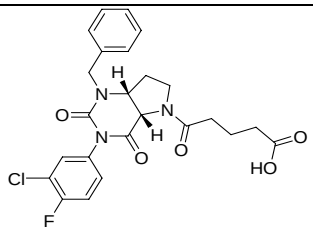
3	-20.30	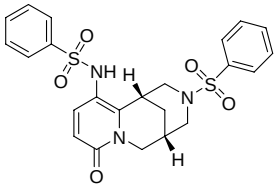	**9**	-25.72	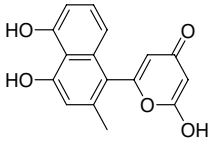
4	-26.58	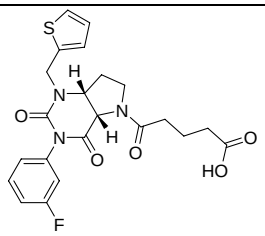	**10**	-26.95	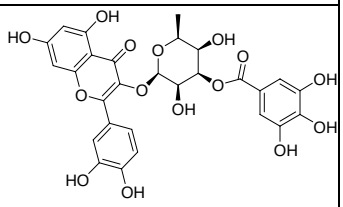
5	-20.53	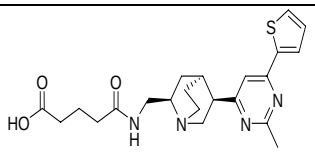	**11**	-30.49	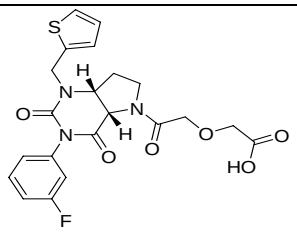
6	-38.69	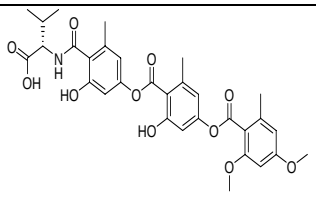	**12**	-28.89	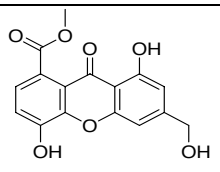

Continuous ……

Hit	Score	Structure	Hit	Score	Structure
13	-30.03	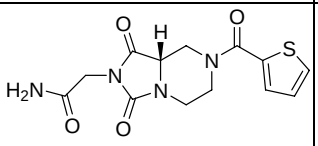	**15**	-30.89	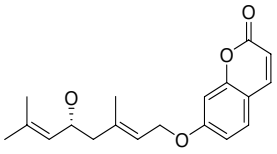
14	-32.67	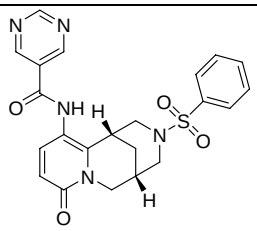	**16**	-27.80	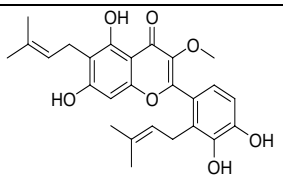

2.3.2 Antimicrobial testing

Since FtsZ is an intracellular protein in bacteria, it is important to identify cell-permeable small-molecule inhibitors that are able to penetrate into bacterial cell wall. Hence, the minimal inhibitory concentration (MIC) of each hit compound was measured against a range of Gram-positive and -negative bacterial strains at 384 μg/mL. Five hit compounds demonstrated the ability to inhibit the bacterial growth; the MIC values are summarized in Table 2.2. The remaining compounds did not show antibacterial activity. Gram-positive organisms were significantly more sensitive to compounds **1**, **2**, **6** and **16** than Gram-negative bacteria. These four compounds failed to kill Gram-negative bacteria strains. The MICs of compound **1** against three of the tested strains were at 96 μg/mL. Compound **2** only inhibited Gram-positive sensitive and resistant *S. aureus* strains at 192 μg/ml. Compound **16** strikingly caused the cell death of *B. subtilis* 168 at 24 μg/mL. The MICs of compounds **6** and **16** for the opportunistic food-born pathogen *B. cereus* were found to be the same (96 μg/mL). Although 4-(((2*R*,4*S*,5*R*)-5-(2-methyl-6-(thiophen-2-yl)-pyrimidin-4-yl)quinuclidin-2-yl)methylcarbamoyl)butanoic acid (**5**) (Table 2.1) showed relatively weak antibacterial activity against Gram-positive and -negative bacterial strains contrasting to ampicillin, it was found to be more potent against *B. subtilis* and *S. auerus* than some literature reported FtsZ inhibitors such as cinnamaldehyde and 3-MBA (Table 2.3). Compound **5** was also found to be more effective than totarol, cinnamaldehyde and 3-MBA to inhibit *E. coli*. In order to eliminate false positives in susceptibility tests, the five possible FtsZ inhibitors were inspected for inhibition of cell division in vegetative growing *B. subtilis*, *E. coli* and

S. aureus under a phase-contrast microscope.

Table 2.2 MICs of hits against gram-positive and gram-negative bacteria

Strain	MIC (μg/mL)				
	1	**2**	**5**	**6**	**16**
B. subtilis 168	>384	>384	96	192	24
B. cereus	96	>384	96	96	96
E. faecalis ATCC 29212	>384	>384	384	>384	>384
E. faecium ATCC 49624	>384	>384	192	>384	>384
E. coli ATCC 25922	>384	>384	192	>384	>384
M. catarrhalis ATCC 25240	n.d.	n.d.	96	n.d.	n.d.
P. aeruginosa ATCC 27853	>384	>384	>384	>384	>384
S. epidermidis ATCC 12228	>384	>384	48	>384	>384
S. aureus ATCC 29213	96	192	384	>384	>384
S. aureus ATCC 29247	96	192	384	>384	>384

n.d. - not determined

Table 2.3 MICs of positive controls against gram-positive and gram-negative bacteria

Strain	MIC (μg/mL)			
	Ampicillin	Totarol	Cinnamaldehdye	3-MBA
B. subtilis 168	0.09	1.5	250	1250
B. cereus	n.d.	n.d.	n.d.	n.d.
E. faecalis ATCC 29212	6	n.d.	n.d.	n.d.
E. faecium ATCC 49624	3	n.d.	n.d.	n.d.
E. coli ATCC 25922	6	400	500	>2500
M. catarrhalis ATCC 25240	1.5	n.d.	500	n.d.
P. aeruginosa ATCC 27853	n.d.	n.d.	n.d.	n.d.
S. epidermidis ATCC 12228	3	1.5	250	n.d.
S. aureus ATCC 29213	1.5	1.5	250	2500
S. aureus ATCC 29247	24	n.d.	n.d.	n.d.

n.d. - not determined

2.3.3 Visualization of bacterial morphology

The effects of the five possible hit compounds and positive controls on bacterial morphology are shown in Figures 2.3-2.5. Untreated *B. subtilis* cells have typical short rod morphology (Figure 2.4A). After treatment with compound **6** or **16** (Figure 2.3C or 2.3E), the cell morphology of *B. subtilis* were found to be short rod shaped. Regarding compounds **1** and **2** (Figures 2.3D and 2.3F), they didn't influence the cell morphology of spherical-shaped *S. aureus*. Figure 2.4A-D showed the effect of compound **5** on the cell morphology of various bacterial strains. It induced filamentation in *B. subtilis* and *E. coli* cells (Figures 2.4B and 2.4D). The average cell length of untreated *B. subtilis* and *E. coli* cells were about 3.1 ± 1 μm and 2 ± 1 μm respectively. After 4 h of incubation, the average cell length of *B. subtilis* was increased by 8 folds from 3.1 ± 1 μm to 24 ± 20 μm in the presence of 48 μg/mL (112 μM) of **5**. The average cell length of *E. coli* was increased by 2.6 folds from 2 ± 1 μm to 5.2 ± 1.9 μm. Thus, **5** showed a stronger inhibitory effect on the proliferation of *B. subtilis* cells than *E. coli* cells. The results indicated that depletion of FtsZ in *S. aureus* caused a different effect on morphology than in rod-shaped *B. subtilis* and *E. coli*. Some *S. aureus* cells treated with 96 μg/mL (450 μM) of compound **5** (Figure 2.4F) became enlarged but still remained a spherical shape. But some depleted cells of *S. aureus* were burst. Although **5** could effectively inhibit the cell divisions of *B. subtilis*, *E. coli* and *S. aureus*, at least seven known proteins in *B. subtilis* and *E. coli* cells are responsible for efficient cell division [3]. Anyone or more of these proteins might be the targets for compound **5**. Additional assays were

therefore needed to identify the specific target for compound **5**.

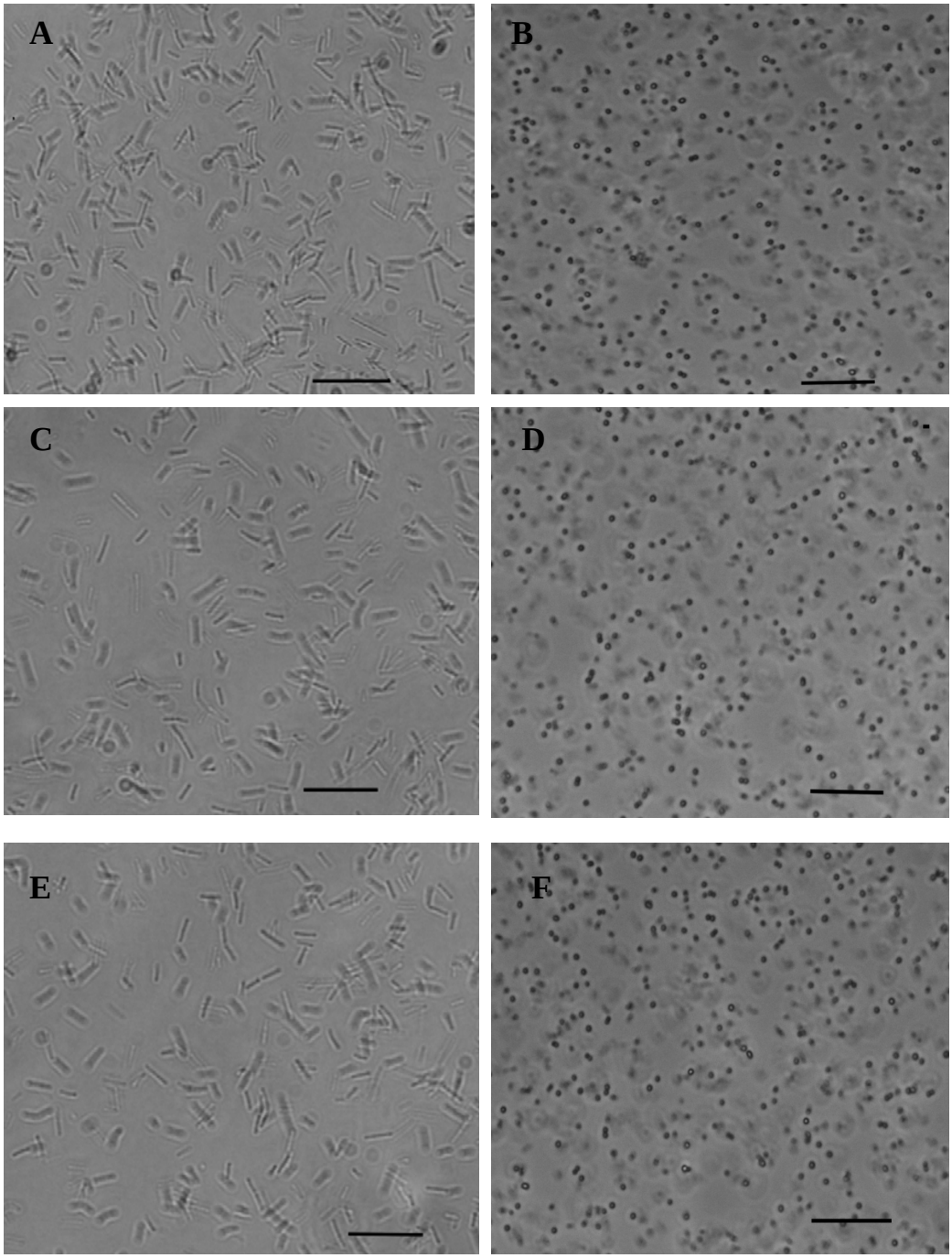

Figure 2.3 Effect of **1**, **2**, **6** and **16** on cell division and cell morphology. Cells of *B. subtilis* 168 (A, C and E) were grown for 4 h in the absence (A) or presence of 96 μg/mL (160 μM) of **6** (C) or 12 μg/mL (53 μM) of **16** (E). Cells of *S. aureus* ATCC 29213 (B, D and F) were grown for 4 h in the absence (B) or presence of 48 μg/mL (110 μM) of **1** (D) or 96 μg/mL (300 μM) of **2** (F). The cells were visualized using a phase contrast microscope. The scale bar is 10 μm. The experiment was repeated 3 times.

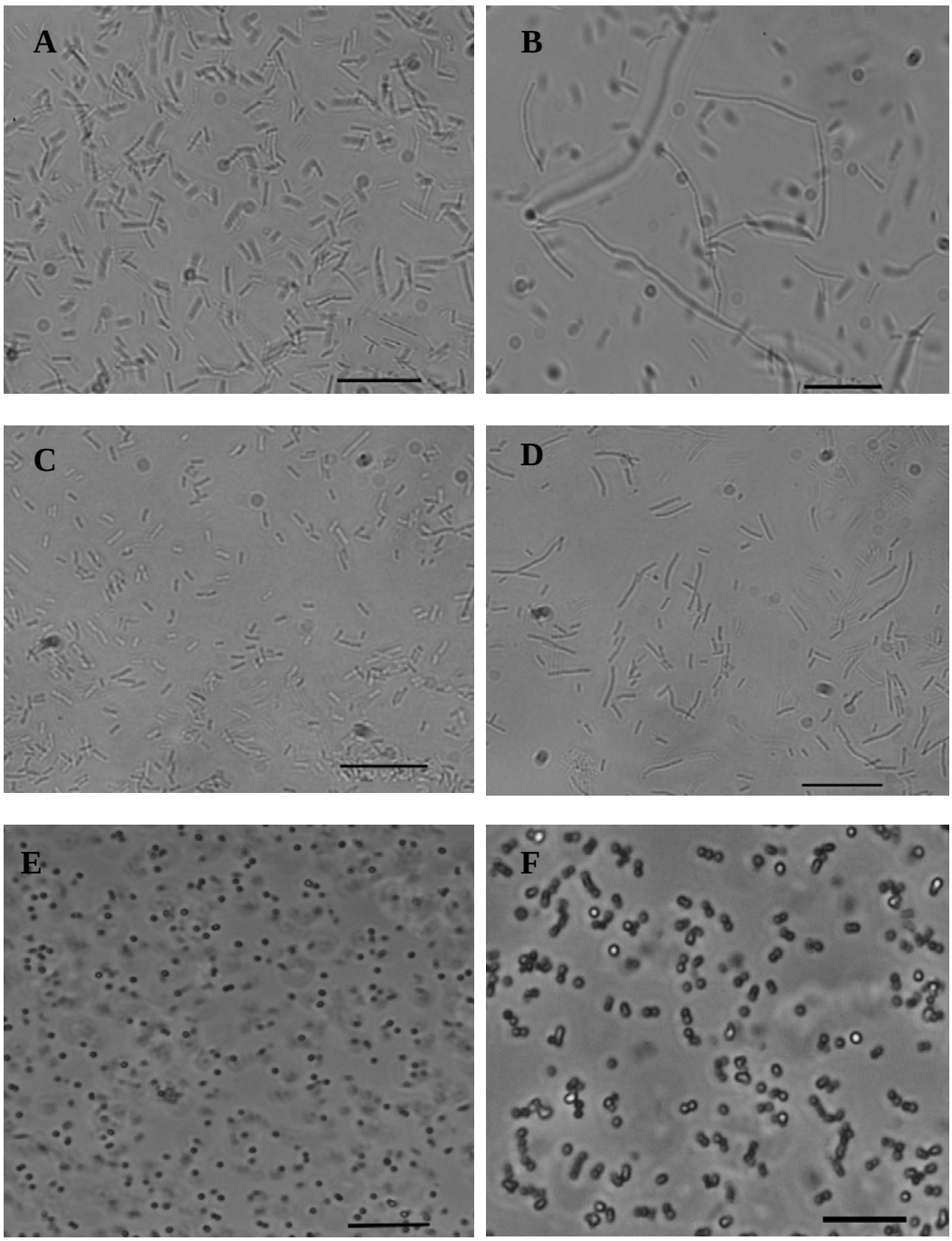

Figure 2.4 Effect of **5** on cell division and cell morphology. Cells of *B. subtilis* 168 (A and B) or *E. coli* ATCC 25922 (C and D) or *S. aureus* ATCC 29213 (E and F) were grown for 4 h in the absence (A, C and E) or presence of 48 μg/mL (112 μM) of **5** (B) or 96 μg/mL (450 μM) of **5** (D and F). The cells were visualized using a phase contrast microscope. The scale bar is 10 μm. The experiment was repeated 3 times.

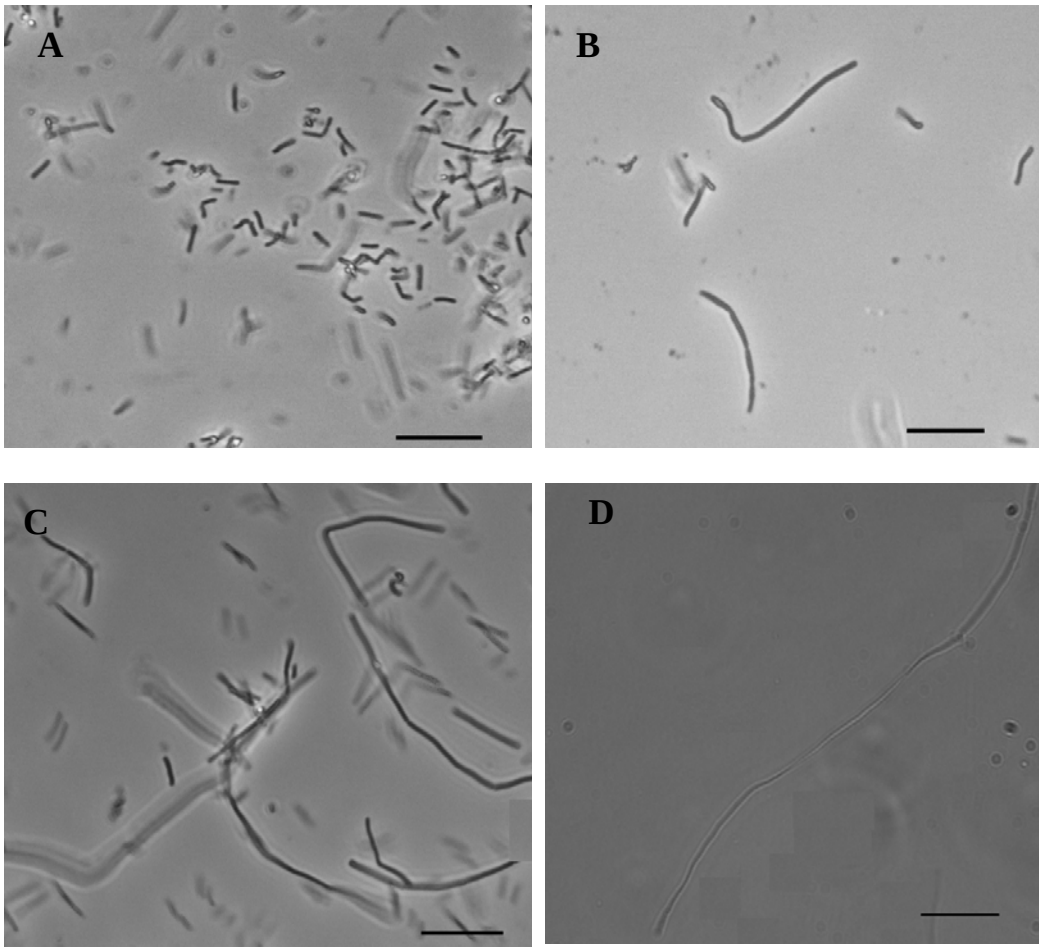

Figure 2.5 Effect of cinnamaldehyde, totarol and 3-MBA on cell division and cell morphology. Cells of *B. subtilis* 168 were grown for 4 h in the absence (A) or presence of 1.89 mM (250 μg/mL) of cinnamaldehyde (B), 2 μM of totarol (C), 8.28 mM (1250 μg/mL) of 3-MBA (D). The cells were visualized using a phase contrast microscope. The scale bar is 10 μm. The experiment was repeated 3 times.

2.3.4 Membrane staining

Perturbation of the membrane structure also induced cell lysis and death. Therefore, the effects of **5** on the membrane structure of *B. subtilis* and *E. coli* cells were examined. The results of membrane staining with FM 4-64 demonstrated that compound **5** did not perturb the membrane structures of *B. subtilis* (Figures 2.6A and C) and *E. coli* (Figures 2.6B and D). The formation of integral septa at the division sites of *B. subtilis* and *E. coli* cells were observed after treatment with **5**.

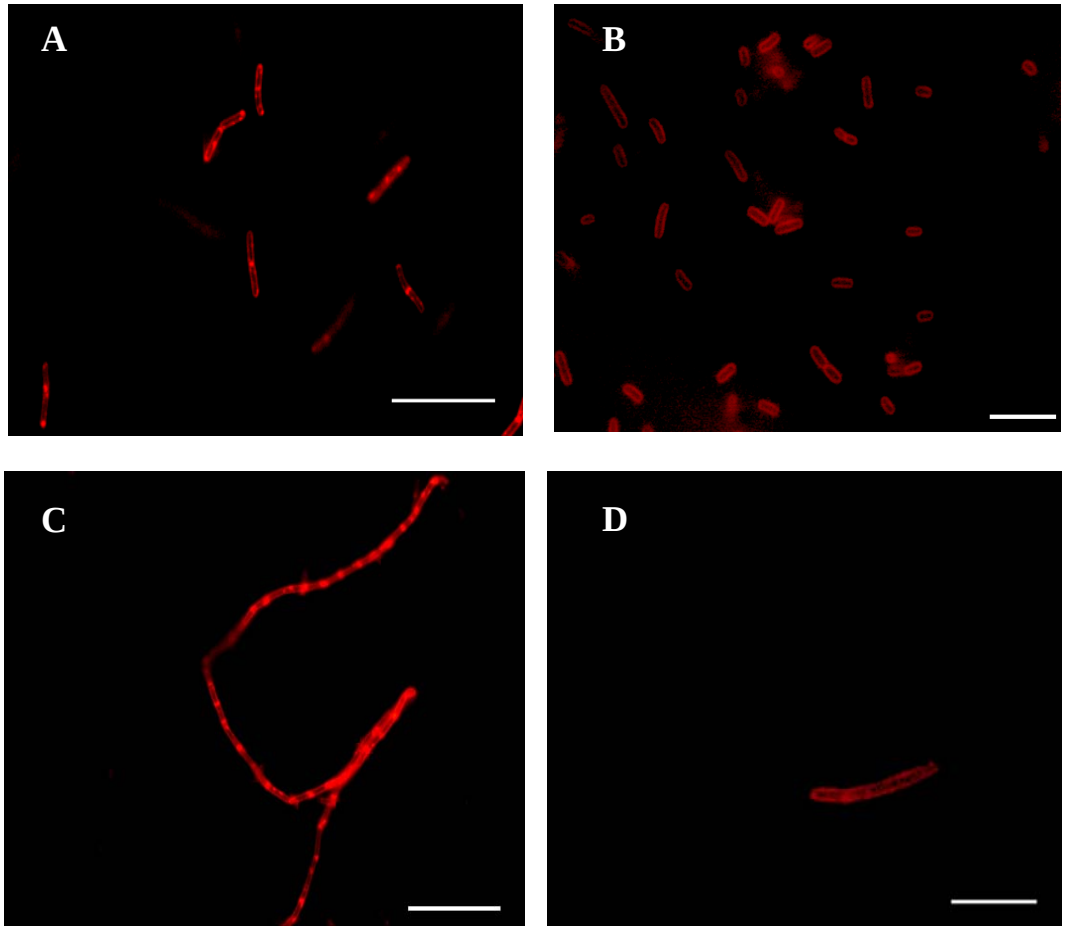

Figure 2.6 Effects of **5** on the bacterial cell membrane. Cells of *B. subtilis* 168 were grown for 4 h in the absence (A) or presence of 88 μM of **5** (C). *E. coli* ATCC 25922 cells were grown for 4 h without (B) or with 450 μM of **5** (D). The cells were stained with the membrane stain FM 4-64 for 30 min and visualized using a fluorescence microscope. The scale bar is 10 μm. The experiment was repeated 3 times.

2.3.5 Visualization of Z-ring in the bacteria

As another approach to confirm that FtsZ is the target for compound **5**, we tired to observe the formation of the dynamic Z-ring in the bacteria. In rod-shaped *E. coli*, septum formation during cell division is initialized by the dynamic Z-ring. When the Z-ring is perturbed, the bacterial cell division is then inhibited to induce the increase of bacterial cell length [171, 172]. In the absence of **5**, a fluorescent band at the cell midpoint was appearently observed in a high percentage of *E. coli* cells as assisted by the GFP-tagged FtsZ (Figure 2.7A). These fluorescent bands represented the septation-competent localized Z-rings (cytoskeletal structures). Upon the exposure to 96 μg/mL (224 μM) compound **5**, GFP-FtsZ dispensed as discrete foci throughout the most elongated cells, indicating that **5** perturbed the Z-ring assembly and integrity significantly due to FtsZ mislocalization. Besides, compound **5** did not change the frequency of occurance of nucleoids per micrometer of cell length, suggesting that it did not influence the DNA replication and nucleoid segregation in the elongated *E. coli* cells. The effect of **5** on dynamic Z-ring formation was similar to the PC190723 inhibitor of FtsZ [60]. But our results were different from other FtsZ inhibitors, which cause the dissipation of FtsZ assembly [80, 81].

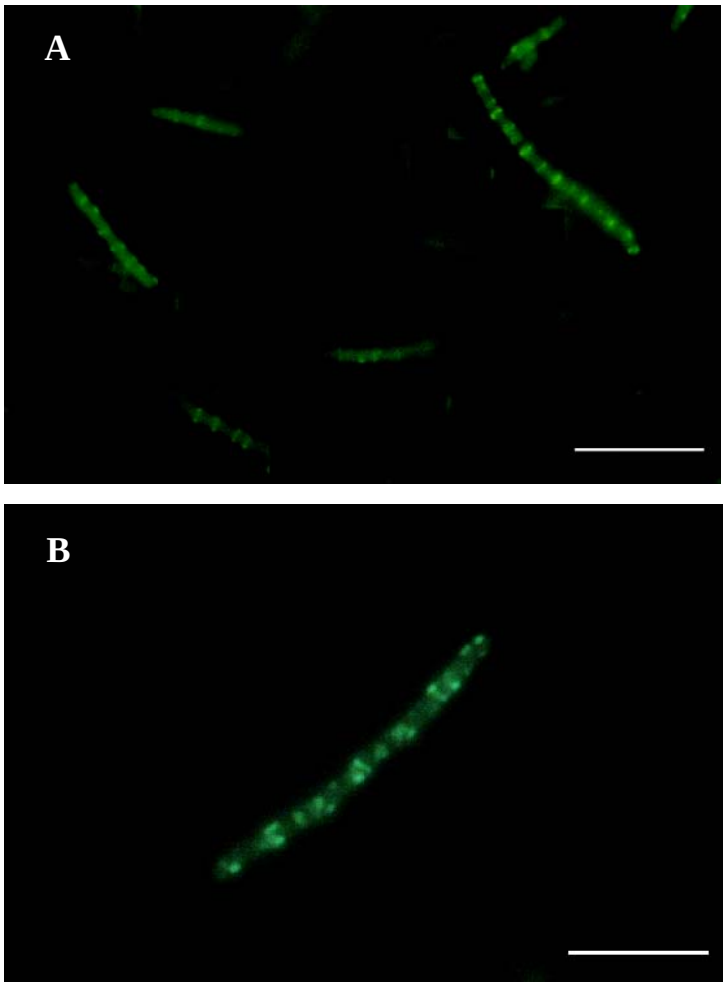

Figure 2.7 Perturbation of cytokinetic Z-ring in *E. coli*. *E. coli* (JM109 WM647) cells were grown in the absence (A) or presence of 96 μg/mL (224 μM) of **5** (B). The scale bar is 10 μm. The experiment was repeated 3 times.

2.3.6 Immunofluorescence microscopy

Compound **5** did not display any background fluorescence. The electron microscopy results showed that the *B. subtilis* cells treated with compound **5** caused the formation of filamentous cells. Together with the disruption of Z-ring formation in *E. coli* cells, these observations implied that **5** may perturb cytokinesis by influencing the function of FtsZ. The effects of **5** on the Z-ring formation and nucleoid in *B. subtilis* 168 were studied by staining the cells with anti-FtsZ antibodies and DAPI fluorescence (Figure 2.8). It was found that most untreated *B. subtilis* cells showed an integral Z-ring. In the presence of 112 μM compound **5**, only very few cells were found to assemble a well-defined Z-ring. Figure 2.9B showed that the immunostained FtsZ proteins were found throughout the filamentous cell. However, the number of nucleoids per micrometer of cell length in the absence (0.48 ± 0.01) and presence of compound **5** (0.46 ± 0.01) are almost the same. These findings showed that compound **5** influenced the Z-ring formation rather than nucleoid segregation.

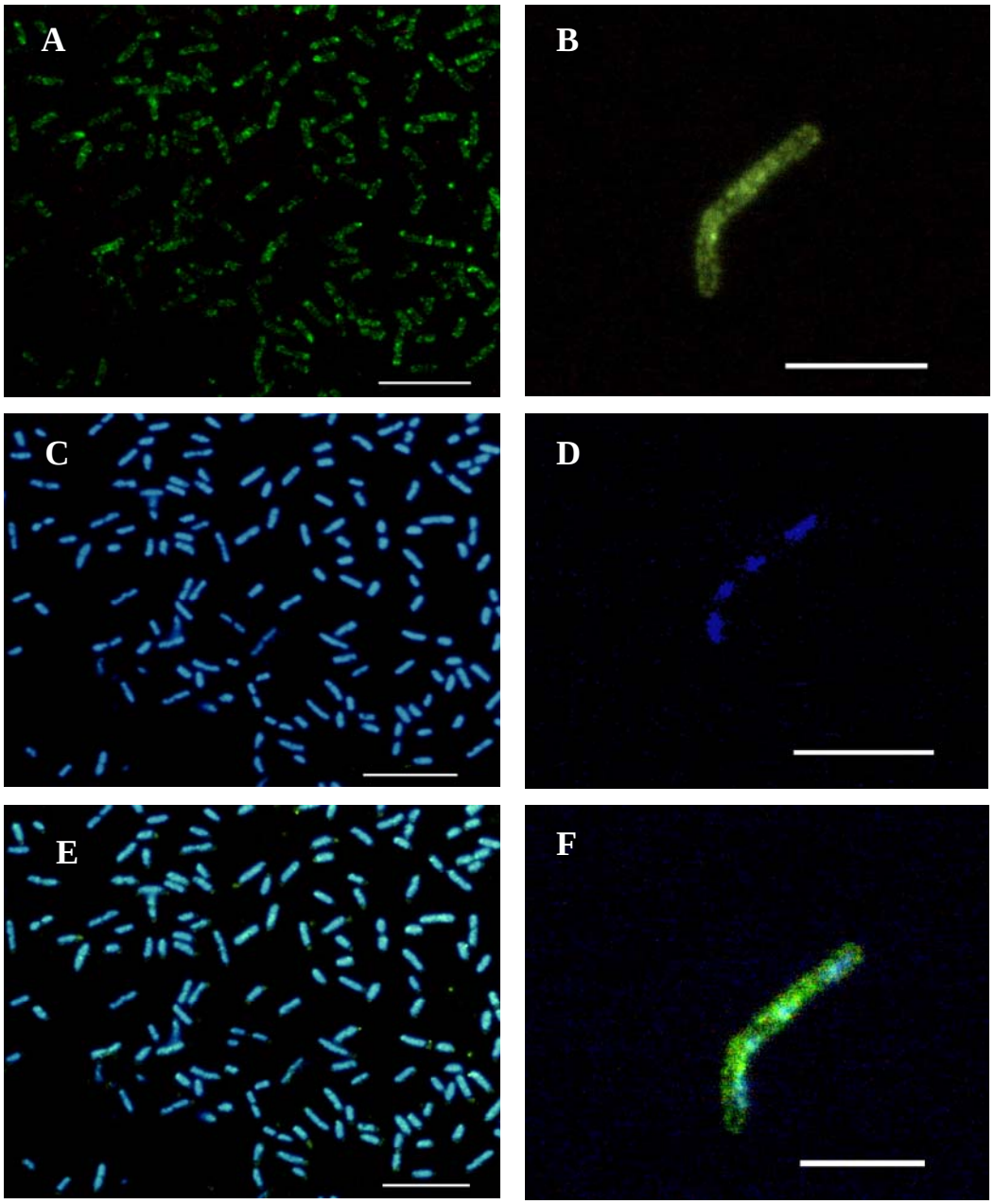

Figure 2.8 Effects of **5** on the Z-ring and nucleoid segregation in *B. subtilis* 168. Cells were immunostained with polyclonal anti-FtsZ rabbit antibody followed by FITC-conjugated goat anti-rabbit secondary antibody for the observation of Z-ring and stained with 1 μg/mL DAPI to observe the nucleotides. The cells in A and C and overlay (E) were in the absence of **5**. The cells in B and D and overlay (F) were treated by 112 μM (48 μg/mL) of **5.** The Z-rings and nucleotide are shown in green and blue respectively and were visualized under a fluorescence microscope with 100× oil immersion len. The scale bar is 10 μm. The experiment was repeated 3 times.

2.3.7 Expression and purification of *S. auerus* His-tagged FtsZ

S. auerus His-tagged FtsZ was successfully expressed and purified by a HiTrap chelating column. The chromatogram and 12% SDS-PAGE are shown in Figure 2.9. The purity was analyzed by 12% SDS-PAGE. In general a single peak of His-tagged FtsZ was found in the chromatogram with typically 85-90 % purity and the protein yield was about 20 mg per 1g of cell paste. The purity of *S. auerus* FtsZ was further confirmed by ESI-mass spectrometry (Figure 2.10). A mass spectrum showed that the measured mass of *S. auerus* FtsZ was consistent with the calculated value. The purified *S. auerus* FtsZ protein was then used for subsequent *in vitro* experiments to validate the action mode of compound **5** on FtsZ.

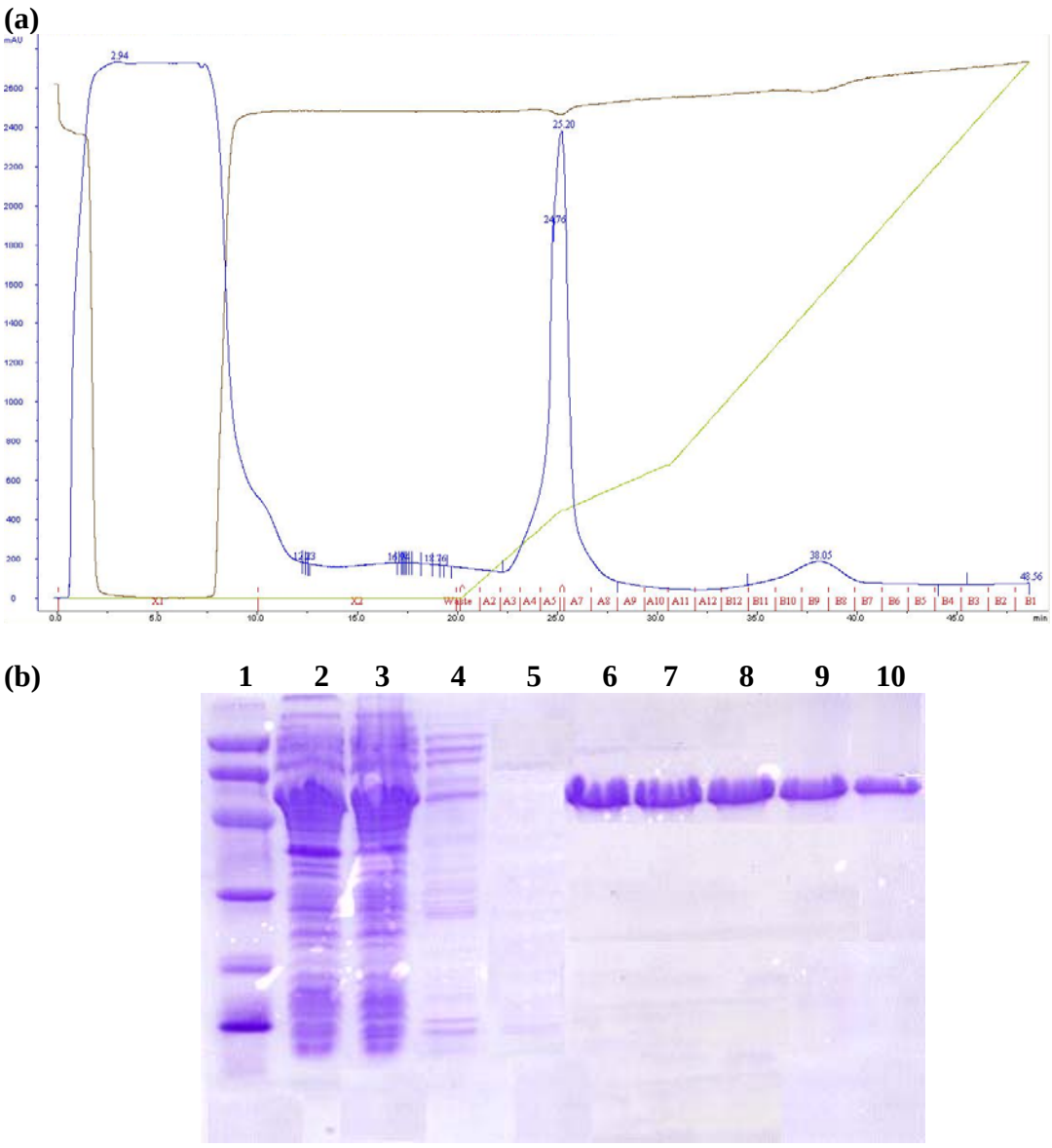

Figure 2.9 Purification of *S. auerus* His_6-FtsZ (a) Elution profile of the enzyme from cell lysate obtained from 400 mL culture (b) 12 % SDS-PAGE. Lane 1, low range molecular marker: rabbit muscle phosphorylase b (97400 Da), BSA (66200 Da), hen egg white ovalbumin (45000 Da), bovine carbonic anhydrolase (31000 Da), soybean trypsin inhibitor (21500 Da), hen egg white lysozyme (14400 Da); lane 2, crude cell lysate; lane 3, soluble fraction of cell lysate; lane 4, insoluble fraction of cell lysate; lane 5, soluble fraction after passing through nickel-affinity column; lanes 6-10, elution of *S. auerus* His_6-FtsZ by elution buffer.

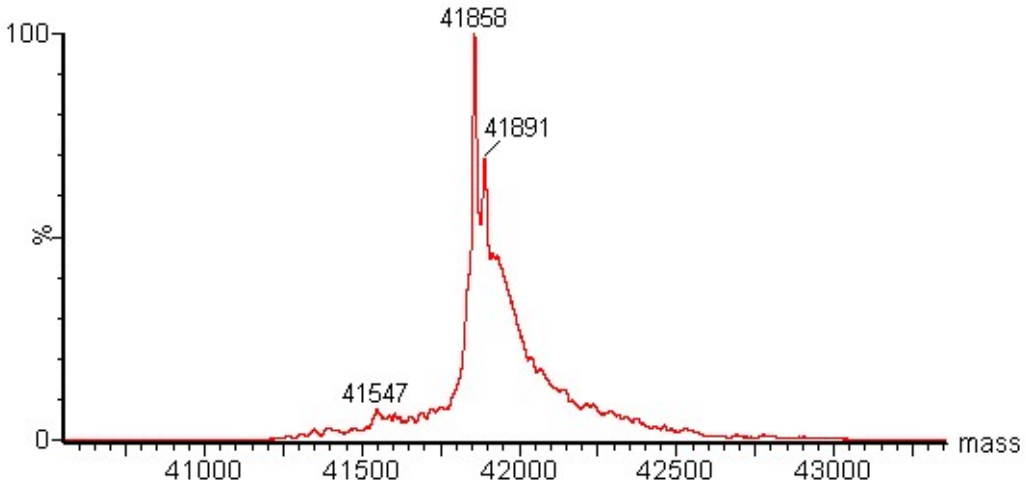

Figure 2.10 ESI-mass spectrum of *S. auerus* 6HisFtsZ

2.3.8 Light scattering assay

Since **5** significantly induced the cell filamentation in *B. subtilis* and *E. coli* and perturbed the formation of Z-ring in living *E. coli* cells, the effect of compound **5** on *S. auerus* FtsZ polymerization and depolymerization was monitored using light scattering assay. This assay can be used to trace the dynamics of FtsZ assembly into protofilaments *in vitro* because light scattering signal at 600 nm is directly proportional to the polymer mass of FtsZ [173]. The results showed that the assembly of FtsZ monomers in the absence of compound **5** occurred at a much higher rate than in the presence of that compound (Figure 2.11). Compound **5** inhibited the light-scattering signal of the FtsZ assembly in a dose-dependent manner. Compared with the control, the FtsZ polymerization was inhibited by ~ 20% and 40% in the presence of 90 μM and 240 μM compound **5** respectively.

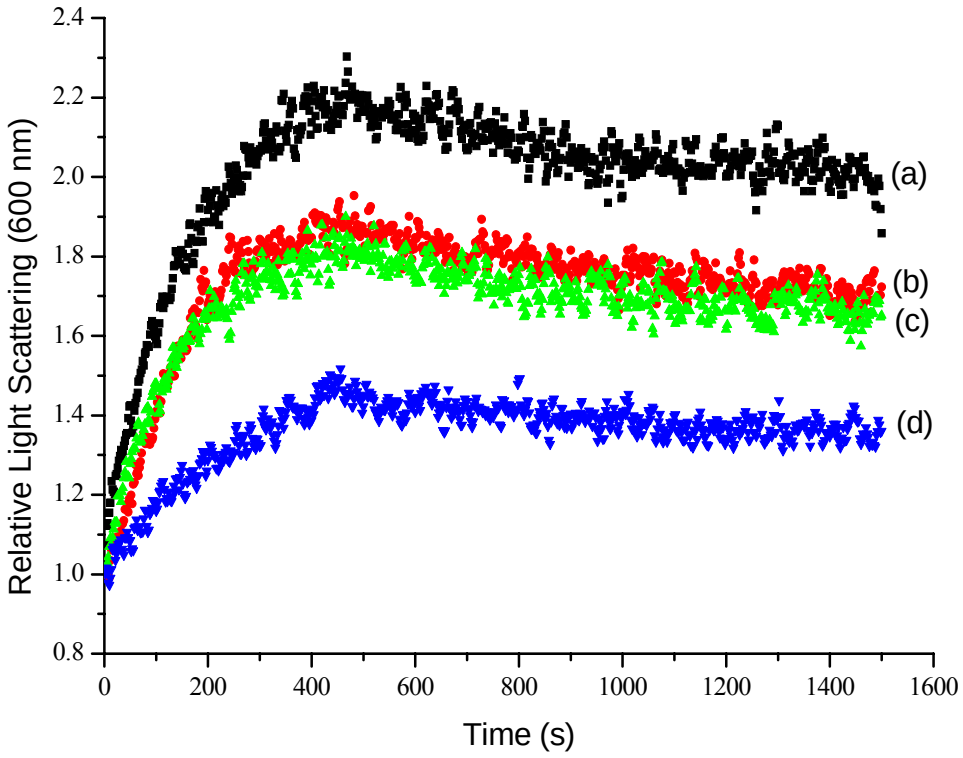

Figure 2.11 Effect of **5** on FtsZ assembly *in vitro*. *S. auerus* FtsZ (12 μM) was polymerized in 50 mM MOPS, pH 6.5, 50 mM KCl, 10 mM $MgCl_2$ and 1 mM GTP in the absence of **5** (a), in the presence of 90 μM (b), 120 μM (c) and 240 μM (d) of **5**. Appropriate blanks were subtracted from all the traces. The experiment was performed three times.

2.3.9 GTPase activity

The dynamic assembly of FtsZ was regulated by the GTPase activity of FtsZ [174, 175]. The effect of **5** on the GTPase activity of *E. coli* FtsZ and *S. auerus* FtsZ were measured from the half-maximal inhibitory concentration (IC_{50}). The concentration-response curve for compound **5** is shown in Figure 2.12. Compound **5** was found to moderately reduce the GTPase activities of *E .coli* FtsZ and *S. auerus* FtsZ in a concentration-dependent manner with IC_{50} values of 221.5 ± 19.7 μg/mL (572.3 ± 50.9 μM) and 145.0 ± 37.2 μg/mL (387.6 ± 96.1 μM) respectively. The results showed that compound **5** suppressed the GTPase activity of *S. auerus* FtsZ more effectively than *E. coli* FtsZ. Many biochemical data strongly suggest that nucleotide hydrolysis is driven by oligormerization of FtsZ [45, 46, 175, 176]. On the basis of measuring GTPase activity, compound **5** might inhibit the GTP hydrolysis rate of both FtsZ assembly either by modulating assembly dynamics of FtsZ protofilaments or by inhibiting the binding of GTP to FtsZ. Together the above light scattering study, **5** may perturb the assembly of dynamic FtsZ by inhibiting the GTPase activity of FtsZ.

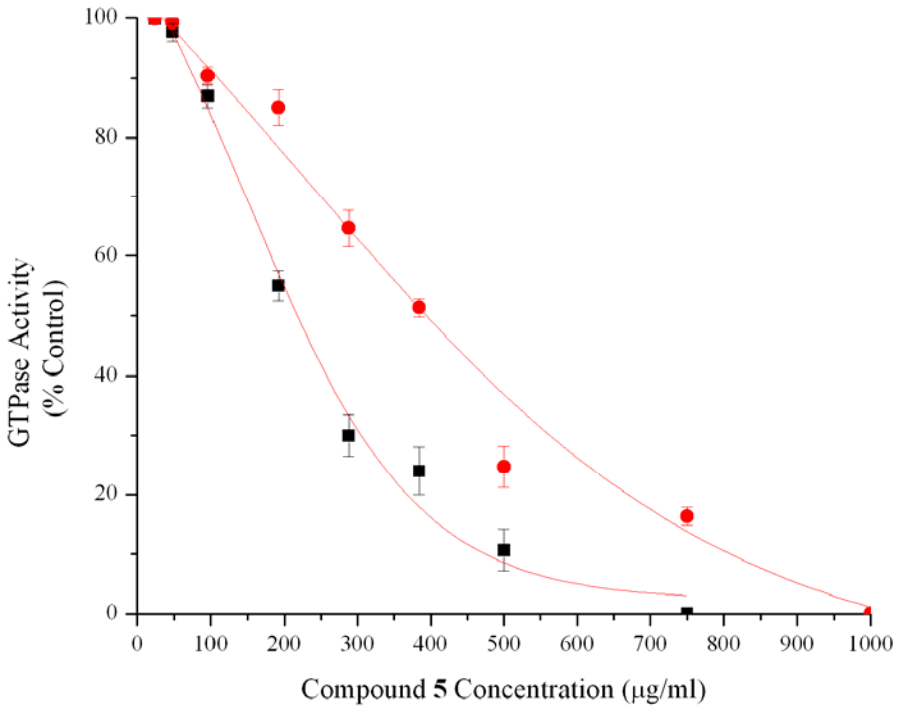

Figure 2.12 Concentration-response curve of **5** as tested against *S. auerus* FtsZ (■) and *E. coli* FtsZ (●). Each point represents the mean of three assays and the vertical bars show the standard error of the mean. The data were plotted and IC_{50} was calculated by nonlinear regression using a sigmoidal concentration-response curve (Original Software).

2.3.10 Transmission electron microscopy

The effect of compound **5** on the assembly of *S. auerus* FtsZ protofilament was examined by transmission electron microscopy. The electron microscopic images are shown in Figure 2.13. In the absence of compound **5**, a dense network of bundles of FtsZ polymers with an average width of 110 ± 22 nm was observed. The number and thickness of FtsZ polymers were significantly reduced with increasing the concentration of compound **5**. For example, the average thickness of the Ftsz bundles was 88 ± 10 nm and 31 ± 24 nm in the presence of 50 μM and 120 μM **5** respectively. In the presence of 120 μM compound **5**, FtsZ formed short bundles with a mean length of 2000 ± 1000 nm as compared with the FtsZ protofilaments formed in the absence of compound **5**. The high concentration of compound **5** not only inhibited the assembly of FtsZ protofilament by weakening its self-association process, but also induced aggregation of FtsZ monomers. The findings of this experiment can explain the moderate effect of **5** on the polymerization of FtsZ *in vitro* as determined by the light-scattering experiment and GTPase activity analysis. In accord with these experimental results, the effect of **5** on the GTPase activity of both FtsZ proteins may be caused by the disruption of FtsZ assembly in an organized and regulated fashion. As a result, a balanced FtsZ polymer stability may not be achieved for the assembly and positional regulation of the Z-ring in the cytokinesis.

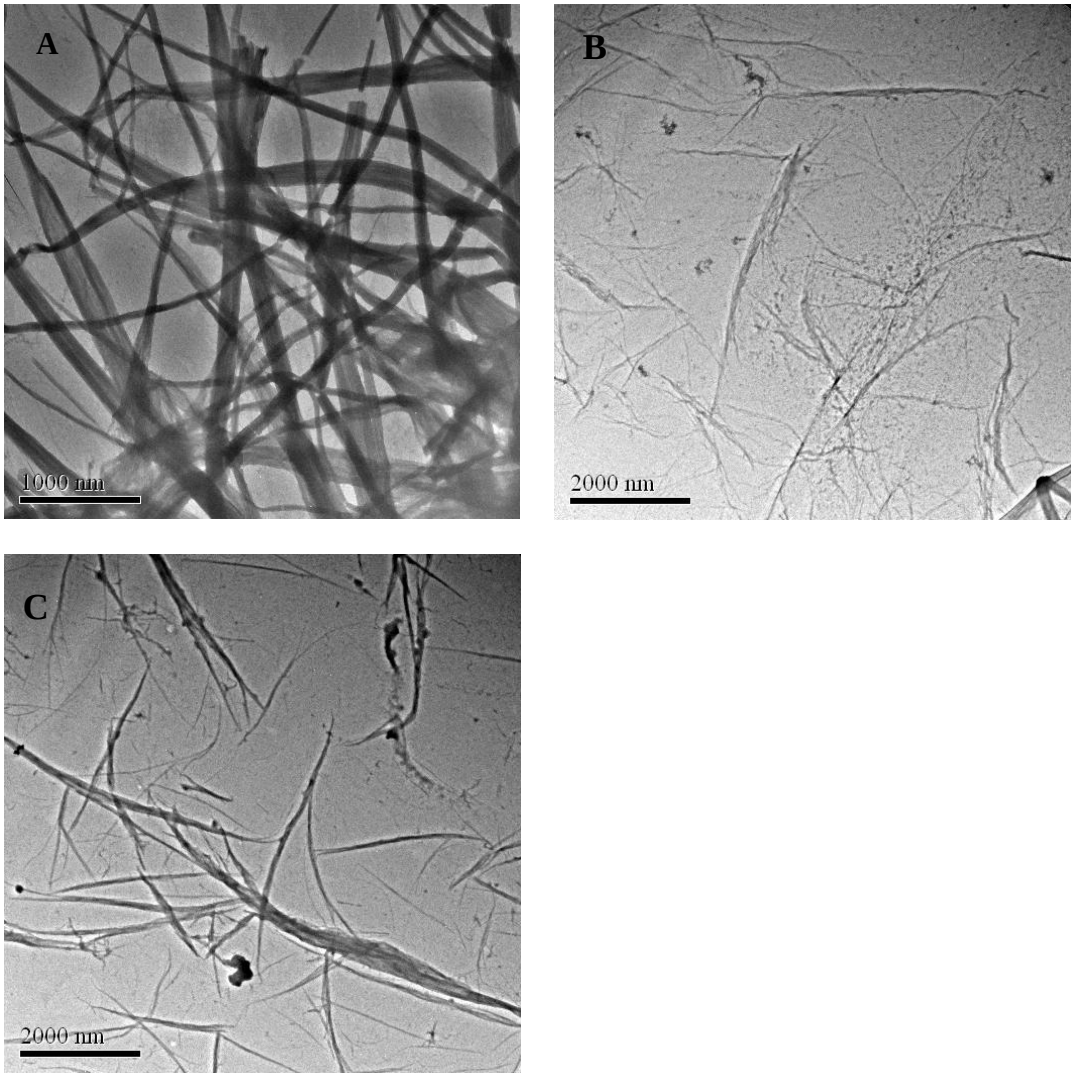

Figure 2.13 Electron micrographs of FtsZ polymers. *S. auerus* FtsZ (12 μM) was polymerized in 50 mM MOPS buffer, pH 6.5, containing 50 mM KCl, 5 mM $MgCl_2$, and 1 mM GTP in the absence and presence of **5** for 15 min at 37 ^{o}C. Shown are the electron micrographs of FtsZ polymers formed in the absence (A) and presence of 120 μM (B) and 50 μM (C) of **5**. The scale bar of A = 1000 nm. The scale bar of B and C = 2000 nm.

2.3.11 Tubulin polymerization assay

The effect of compound **5**, paclitaxel (an enhancer of tubulin polymerization as positive control) and vinblastine (a microtubule destabilizing drug as negative control) on mammalian tubulin polymerization were evaluated using *in vitro* tubulin polymerization assay. The results are shown in Figure 2.14. The fluorescent reporter inside microtubules allowed a simple and rigorous quantification of the extent of the tubulin polymerization. The curves in Figure 2.14 demonstrated that the polymerization of tubulin consisted of three phases: nucleation, growth and steady state equilibrium. The fluorescence intensity was significantly increased in the presence of paclitaxel because paclitaxel eliminated the nucleation phase and greatly enhanced the rate of polymerization of mammalian tubulin (curve a). On the other hand, vinblastine completely inhibited the polymerization of mammalian tubulin (curve d). In the case of compound **5**, it did not affect the polymerization of mammalian tubulin. The increase of fluorescence intensity in the presence of compound **5** (curve c) was similar to one in the blank control (curve b). These results implied that compound **5** is highly selectivity against FtsZ rather than the eukaryotic cytoskeletal protein tubulin.

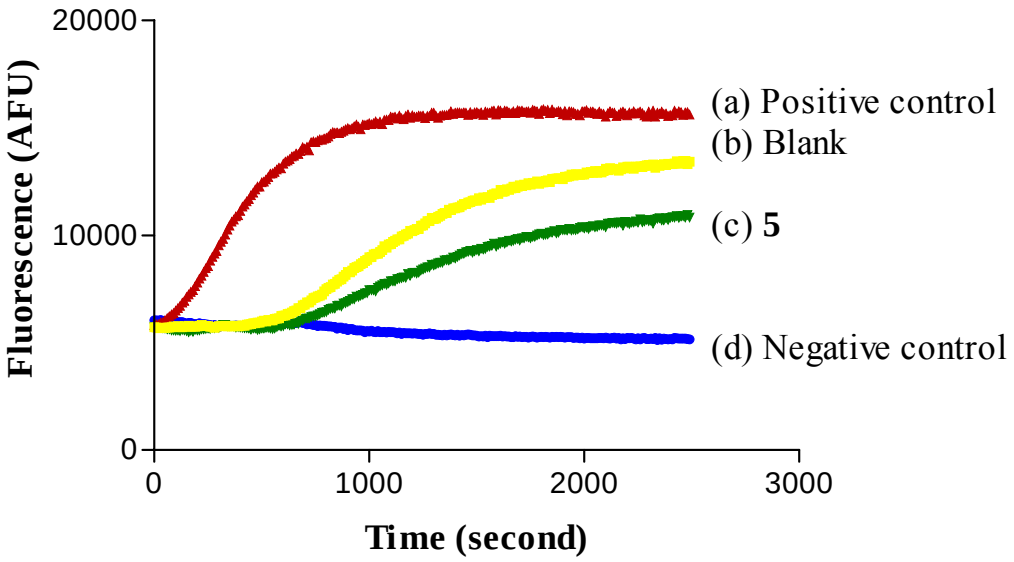

Figure 2.14 Effect of **5** on the polymerization of mammalian tubulin. A tubulin polymerization assay was performed under the presence of 20 μM paclitaxel (an enhancer of tubulin polymerization (a), 384 μg/mL of **5** (c), 3 μM vinblastine (an inhibitor of tubulin polymerization (d) or 1% DMSO only (b). The polymerization of mammalian tubulin was monitored by the increase in the Absolute Fluorescence Units (AFU) for 30 minutes.

2.4 Concluding remarks

In summary, a structure-based virtual screening approach has been successfully employed to identify an FtsZ antibacterial agent after screening natural product libraries containing 20,000 compounds *in silico*. Among the 16 hit compounds, only compound **5** showed the inhibitory effect on the growth of bacterial strains and the GTPase activity of FtsZ. Although **5** had moderate antibacterial activity on the bacterial strains, it effectively perturbed bacterial cytokinesis as shown by the elongation of *B. subtilis* and *E. coli* cells and the disruption of Z-ring formation at mid cells. Compound **5** also sustained the membrane integrity of bacterial cells, indicating that it is specifically targeting against FtsZ rather than other targets in the bacterial cell membrane. Despite the low inhibitory effect of compound **5** on the GTPase activity of FtsZ proteins, it can inhibit the bundling and size of FtsZ protofilements *in vitro*. Compound **5** was found to disrupt the assembly of FtsZ protofilements. But it did not inhibit the polymerization of mammalian tubulin. These results motivate us to use *in silico* screening method to identify more potent FtsZ inhibitors. But, the major problem encountered in this study is that sufficiently high scoring pose(s) of **5** were not achieved in the first round high-throughput virtual screening due to protein flexibility and induced fit effect. Thus, a more thorough approach was employed in the subsequent docking studies to determine the optimal binding pose(s) of compound **5**. The results will be reported at chapter 3.

Chapter 3

In silico optimization of the binding pocket structure

3.1 Introduction

In the drug discovery process, initial hits are explored by screening vendor or in-house databases covering as many structural analogues as possible. After hit identification, the potency, physiochemical and metabolic properties of validated hits are optimized to increase the likelihood for success in subsequent clinic trials. The main aim of *in silico* hit optimization is to identify more potent derivatives based on the absolute binding free energies predicted from the docking simulation. Hit optimization involves docking a series of hit analogues to the X-ray crystal structure of the target to calculate more accurate binding free energy and obtain consistent and optimal binding pose of the hit(s). Finally, a structure-activity relationship (SAR) study is used for hit-lead optimization process. However, the rigid-receptor high-throughput docking method is often inadequate for hit identification and hit optimization because subtle energy changes of protein are not involved in docking calculation. Incorporating flexible docking and induced fit algorithms into ligand-receptor docking were found to significantly improve the accuracy of docking results [119, 177-180].

In the previous chapter, virtual screening using the crystal structure of *M. jannaschii* FtsZ resulted in the discovery of an inhibitor, 4-(((2*R*,4*S*,5*R*)-5-(2-methyl-6-(thiophen-2-yl)pyrimidin-4-yl)-quinuclidin-2-yl)methyl -carbmoyl)butanoic acid (**5**), which is dissimilar from known natural product FtsZ inhibitors and provides a novel scaffold for further optimization. Despite exhibiting only weak antibacterial activity against bacteria, it can penetrate the bacterial cell

wall, which is always a barrier in antibacterial discovery. These experimental results encouraged us to find more potent FtsZ inhibitors based on the scaffold of **5**. However, the success of hit optimization significantly depends on the accuracy of docking score and pose of a hit compound. In the study reported in the previous chapter, the binding scores were found not to rank compounds accurately and could not differentiate between active and inactive compounds. In addition, the docking pose of **5** could not fit very well in the GTP binding site, and the docking result of compound **5** was found not to directly correlate with the measured activity in biochemical assays. One possible reason is that **5** may induce a pocket rearrangement upon binding to the GTP binding site and hence the conformation of **5** is incompatible with the initial pocket geometry. In addition, the protein flexibility of FtsZ was not incorporated in the initial screening. As a result, high scoring binding pose of **5** could not be achieved. The current study is to incorporate a novel computational technique, SCARE (Scan Alanines and Refine), to improve the accuracy of docking protocol and score functions implemented in the ICM docking program. SCARE algorithm has been developed that takes into account full protein flexilibility and an induced fit into a docking simulation. Compound **5** was firstly docked into an ensemble of protein conformations extracted from the crystal structures of FtsZ rather than docking it into a static protein receptor. The docking pose of **5** at each conformation was ranked according to ICM scoring function [34] to identify the optimal binding poses.

Many available FtsZ crystallographic structures, in complex with substrate (GTP)

or substrate product (GDP) or GTP analogue inhibitor, provided new alternative templates to build a homology model of other FtsZ proteins. Modeling of small compound-FtsZ complexes is useful to understand the molecular mechanisms of inhibition and to provide a basis for structure-based drug design and virtual ligand screening. In the past few years, homology modeling techniques have widely been used for the prediction of binding pose of FtsZ inhibitors, highlighting their favorable binding sites and guiding the design of new potent compounds such as berberine [181] and PC190723 [60]. In order to obtain more accurate docking results to explain our experimental findings, a homology model of *S. auerus* FtsZ was constructed based on the crystal structure of *A. aeolicus* FtsZ (PDB code: 2R6R). The amino acid sequence identity between the target *S. auerus* FtsZ and the template *A. aeolicus* FtsZ determined from NCBI protein BLAST tool is 44%. The high sequence identity between the target and template proteins has facilitated us to accurately construct a homology model of FtsZ for *S. auerus* based on the template structure of *A. aeolicus* FtsZ with compound **5** using the ICM/Homology program [123].

A library of compound **5** derivatives were then docked against several refined models prepared by SCARE and homology modeling methodologies. Based on the results of high-throughput virtual screening, top-scoring compounds were selected for subsequent *in vitro* and *in vivo* assays.

3.2 Methods

3.2.1 Structural preparation

3.2.1.1 Benchmark selection

All atomic coordinates of FtsZ were retrieved from the Protein Data Bank (PDB) [182]. Before starting a docking simulation, all available FtsZ crystal structures were aligned, superimposed and clustered into different subgroups according to the conformational changes of GTP binding site. There are two important rules to select crystal structures representing the protein flexibility of FtsZ. Firstly, no more than two structures of the same protein were used in order to increase the diversity of the X-ray crystal structures from different bacterial strains. Secondly, holo crystal structures (co-crystallized with ligands) were preferred over apo structures (without ligand) because the side chains in the pocket of apo-crystal structure may not be in the correct conformation: some side chains always stick out and hinder ligand binding in the docking process. Based on these criteria, eight crystal structures were selected to represent different conformations of the GTP binding site in FtsZ (PDB codes: 1OFU, 1RLU, 1W5B, 1W5F, 2R6R, 2R75, 2VXY and 2VAP). The detailed information of the eight crystal structures are summarized in Table 3.1. The sequence alignment of the eight crystal structures of FtsZ are shown in Figure 3.1.

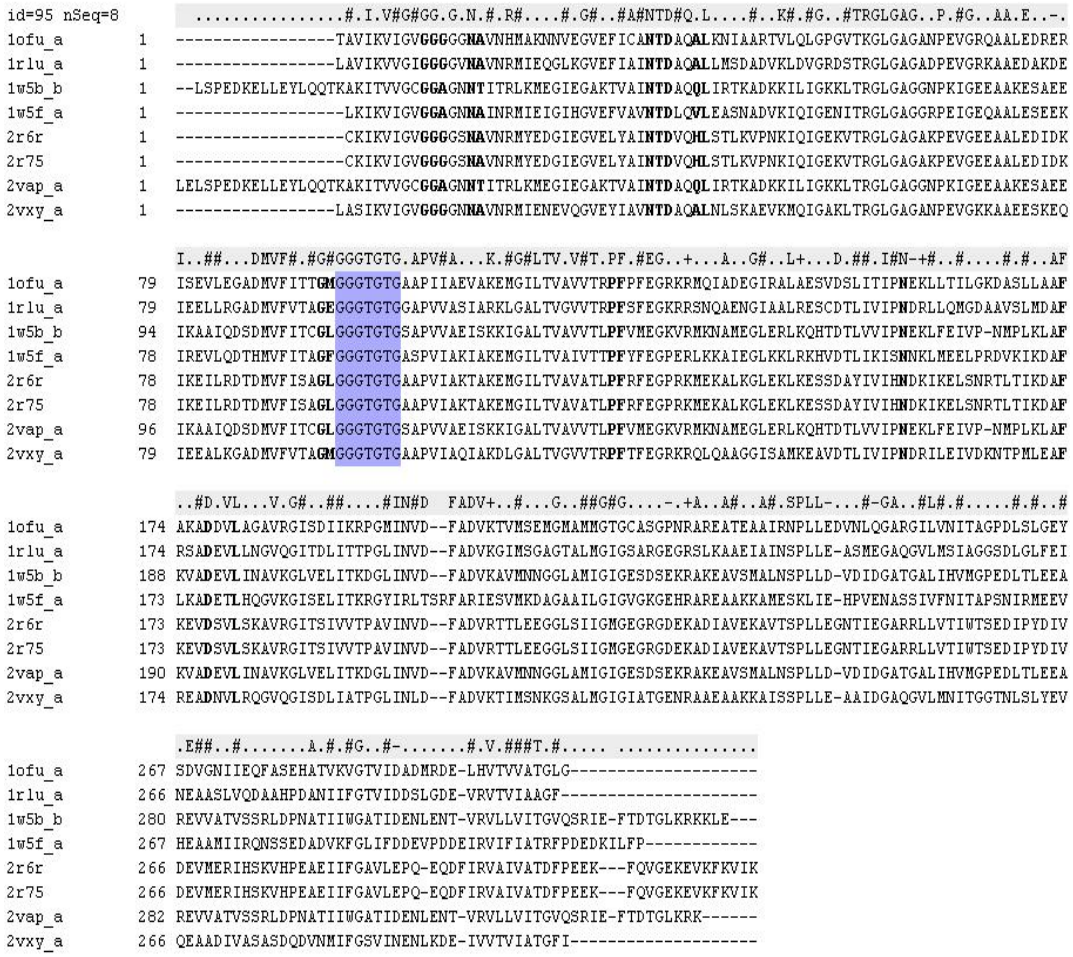

Figure 3.1 Sequence alignment of eight crystal structures of FtsZ which represent different conformations of the GTP binding site. The unique GTP-binding motif is highlighted in gray. The residues of the GTP binding site are in bold form. The eight crystal structures are *P. aeruginosa* FtsZ (PDB code: 1OFU), *M. tuberculosis* FtsZ (PDB code: 1RLU), *M. Jannaschii* FtsZ (PDB codes: 1W5B and 2VAP), *T. maritime* FtsZ (PDB code: 1W5F), *A. aeolicus* FtsZ (PDB codes: 2R6R and 2R75) and *B. substilis* FtsZ (PDB code: 2VXY).

Table 3.1 X-ray crystal structures of FtsZ used in the SCARE docking

PDB	Res. (Å)	Bacterial strain	Ligand name[a]	Ligand function
1OFU	2.1	*P. aeruginosa*	GDP	FtsZ substrate product
1RLU	2.08	*M. tuberculosis*	GSP	GTP analogue
1W5B	2.2	*M. jannaschii*	GTP	FtsZ substrate
1W5F	2.0	*T. maritima*	G2P	GTP analogue
2R6R	1.7	*A. aeolicus*	GDP	FtsZ substrate product
2R75	1.4	*A. aeolicus*	8-morpholino-GTP	FtsZ inhibitor
2VAP	1.7	*M. jannaschii*	GDP	FtsZ substrate product
2VXY	1.7	*B. substilis*	Apo structure	-

[a] GDP = Guanosine diphosphate, GTP = Guanosine triphosphate, GSP = 5'-Guanosine- diphosphate-monothiophosphate, G2P = Phosphomethylphosphonic acid guanylate ester and 8-morpholino-GTP = 8-morpholin-4-ylguanosine 5'-(tetrahydrogen triphosphate)

3.2.1.2 Receptor preparation

When more than one copies of a crystal structure were included in the asymmetric unit, the best solved one was chosen. Other detailed procedures of receptor preparation for subsequent SCARE docking and virtual screening of hit derivatives have been described in sections 3.2.3 and 3.2.5.

3.2.1.3 Preparation of a virtual library of compound 5 analogs

Based on the scaffold of **5**, a collection of 720 derivatives were extracted from the commercially available libraries by the substructure search function implemented in ICM MolCart. Before starting virtual screening, each compound of the virtual library of 720 derivatives was processed using the same procedure as described in section 2.2.2.2.

3.2.2 Single grid docking simulation of compound 5

In the single grid docking simulation of **5**, eight FtsZ crystal structures were used as our docking models. The procedure of the single grid docking has been described in section 2.2.2.4. Briefly, the GTP binding site was firstly identified by means of IcmPocketFinder tool implemented in ICM 3.6. The GTP binding site at each FtsZ receptor was represented by pre-calculated potential grid maps. A flexible ligand (compound **5**) was then placed to the GTP binding site. The top scoring poses of compound **5** at different receptor representations were selected to undergo the

refinement process of the receptor pocket around the ligand. The refinement procedure was based on the BPMC global energy optimization. During the entire refinement process, the temperature was set at 600 K. The side chain variables of residues within 5 Å from the ligand were sampled. In this refinement step, the backbone and side chain variables of receptor with the free variables of the ligand could be effectively optimized by means of Monte Carlo sampling. After the refinement process, the energy of each conformation was re-assessed. The most energetically favorable ligand-receptor pairs were re-docked and rescored.

3.2.3 SCan Alanines and REfine (SCARE) docking of compound 5

In order to obtain the optimal docking poses of compound **5**, an SCARE algorithm was used [183]. The application and function of this algorithm has been described previously. In the SCARE docking, multiple receptor variants of FtsZ (X-ray crystal structures of FtsZ selected from different bacterial strains) were used. The conformational change of residues at each receptor was scanned upon the binding of compound **5** to the GTP binding site. No more than three hampering residues of each variant were mutated into alanine. The mutation process did not change the backbone conformation. The mutated residue of each variant are listed in Table 3.2. A refinement procedure was used to optimize the tethered ligand. During the refinement, both the side-chain and backbone of the pocket residues surrounding the ligand (compound **5**) were actively optimized followed by generating stack comformations of the ligand/receptor complex. The lowest energy stack of the ligand/receptor complex was then selected to redock compound **5**. Subsequently, the

mutated residues of the lowest energy conformation were changed back to their original residues. The side chains were refined again. Compound **5** was re-docked to the refined model again. The SCARE procedure was repeated on the multiple receptors of FtsZ (different PDB codes). Finally, the receptor conformation with the lowest score assigned to compound **5** was saved and selected as a docking template for further virtual library screening of compound **5** derivatives.

Table 3.2 List of mutated residues of eight crystal structures.

PDB	
1OFU	N25A, R143A and D187A
1RLU	N22A and R140A
1W5B	N51A, R169A and D212A
1W5F	N35A, R153A and D197A
2R6R	N21A, K139A and D183A
2R75	N21A, K139A and D183A
2VAP	R169A and D212A
2VXY	N25A, R143A and D187A

3.2.4 Homology model of FtsZ for *S. auerus*

Until now, the crystal structure of *S. auerus* FtsZ (Swiss-Prot accession numbe: B5LV58) used in this study is unknown. Therefore, the refined model from SCARE algorithm of *A. aeolicus* FtsZ (PDB code: 2R6R) with compound **5** was used as a template to build the model of *S. auerus* FtsZ using the ICM-Homology modeling algorithm [168, 184-186]. Deriving the homology model required several steps. Firstly, the sequence of *S. auerus* FtsZ (ATCC 29213) was aligned and superimposed to a single homologue template of *A. aeolicus* (PDB code: 2R6R) (Figure 3.2). Subsequently, a homology model was built by inheriting the backbone conformation of the template and replacing the non-identical side chains of the GTP binding site at N-terminal domain to prevent changing as many torsion variables from the template as possible. The conformation of the *A. aeolicus* FtsZ was left unchanged, whereas the GTP binding site at N-terminal domain of *A. aeolicus* FtsZ (K139, K70, L101, L130 and V182) was mutated into the corresponding residues of *S. auerus* FtsZ (ATCC 29213) (R143, N74, M105, R134, A186) respectively. The superimposed structures between template (PDB code: 2R6R) and model of *S. auerus* FtsZ (ATCC 29213) are shown in Figure 3.3. The homology model of *S. auerus* FtsZ with compound **5** was refined using the ICM global optimization algorithm. After structural refinement, flexible compound **5** was docked to the GTP binding site again.

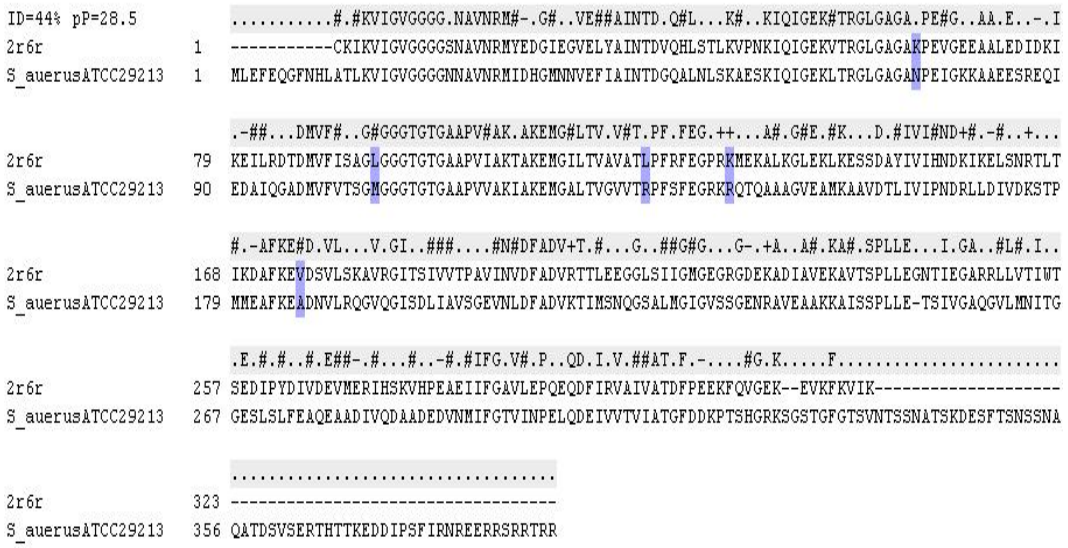

Figure 3.2 Alignment of *A. aeolicus* (PBD code: 2R6R) FtsZ and *S. auerus* ATCC 29213 (Swiss-Prot accession number: B5LV58) FtsZ was performed by the alignment algorithm implemented in ICM. Amino acid changes are highlighted in gray with corresponding positions in the *A. aeolicus* FtsZ sequence at the top.

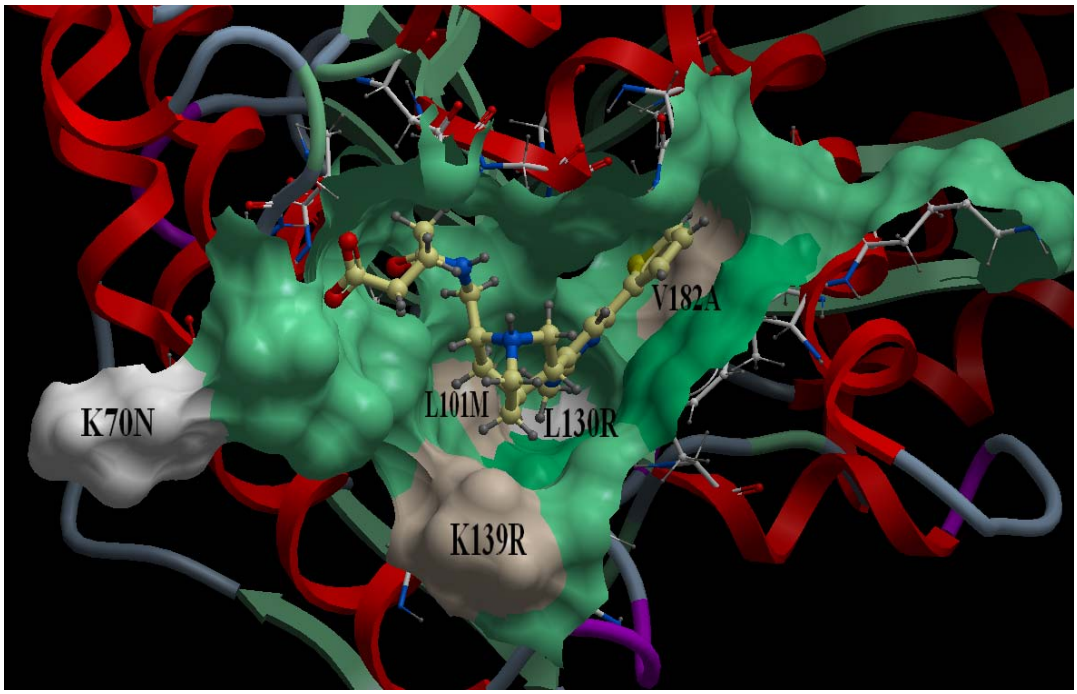

Figure 3.3 Homology model of the GTP binding site of *S. auerus* FtsZ (Swiss-Prot: B5LV58) built based on the template of *A. aeolicus* FtsZ (PDB code: 2R6R) with compound **5** obtained from the SCARE algorithm. Residues K139, K70, L101, L130 and V182 of *A. aeolicus* FtsZ are the equivalents of R143, N74, M105, R134, A186 respectively in *S. auerus* FtsZ (Swiss-Prot accession number: B5LV58). These five residues of *A. aeolicus* FtsZ were mutated into the corresponding residues of *S. auerus* FtsZ to prepare the model.

3.2.5 Virtual screening

ICM virtual library screening (VLS) module was used to screen the library of compound **5** derivatives against a panel of five refined models of FtsZ that were prepared by the SCARE algorithm (section 3.2.3) and homology modeling (section 3.2.4). The detailed procedure of VLS has been described in section 2.2.2.4 of the previous chapter. The 1% top-scoring ligand-protein complexes were manually inspected: parameters taken into account included hydrogen bond network, shape complementarity and docking pose similarity with the hit compound **5**. Based on these requirements, selected compounds were then validated by *in vitro* and *in vivo* assays.

3.3 Results

3.3.1 Benchmark selection

28 crystal structures of FtsZ from different organisms were clustered and then evaluated. Some FtsZ crystal structures were found to adopt quite different conformations in the presence of different bound ligands. Finally, eight FtsZ crystal structures were selected to represent different conformations of the GTP binding site of FtsZ. In the ensemble of protein conformations extracted from FtsZ crystal structures, seven structures are bound with different nucleotides or GTP-analogue inhibitors (PDB codes: 1OFU, 1RLU, 1W5B, 1W5F, 2R6R, 2R75 and 2VAP). One is an apo crystal structure without ligand (PDB code: 2VXY).

3.3.2 Single rigid receptor docking of compound 5

The experimental results in the previous chapter showed that **5** (Figure 3.4) has a moderate antibacterial activity against FtsZ protein *in vitro* and *in vivo* assays. Here, we tried to address why the best scoring docking pose of compound **5**-FtsZ could not be attained in the first round of molecular docking. Docking simulation with a full atom representation of each FtsZ receptor was done to determine the binding pose of **5** by Monte Carlo energy minimization of the complex with both flexible ligand and receptor side chains. In a docking experiment, compound **5** was docked into an ensemble of protein conformations rather than a static protein receptor. Since the docking experiment had eight conformations to represent FtsZ flexibility, molecular

docking was repeated eight times for each conformation. The binding scores are summarized in Table 3.3. In the context of putative binding pose of **5** at the GTP binding site of the eight FtsZ conformations, we noted that the docking poses were greatly different from each other. Based on these observations, we could not attain an optimal binding pose of compound **5** with FtsZ. In these eight FtsZ crystal structures, the highest binding scores were -22.7 and -22.6 obtained from *A. aeolicus* FtsZ (PDB codes: 2R6R and 2R75). The schematic diagram of compound **5** interacting with the GTP binding site of *A. aeolicus* FtsZ (PDB code: 2R6R) is shown in Figure 3.5. With a docking analysis, it was observed that three hydrogen bonds were formed between compound **5** and important active site residues, including a carbonyl oxygen of **5** interacting with Gly106 (2 Å), another carbonyl oxygen atom and hydroxyl groups of carboxyl group of **5** interacting with Thr105 (1.8 Å) and Ala67 (1.7 Å) respectively. These three residues all play an important role in substrate binding for GTP hydrolysis activity of FtsZ [157]. In addition, hydrophobic interactions with many residues of the binding site including Gly18, Thr129, Pro131, Pro135, Lys139, Phe179, Val182, Leu186 and Lys193, were also observed. Regarding other seven conformations (docking templates), the docking results indicated that neither the binding pose nor meaningful binding score of compound **5** could be achieved. The possible reason is that compound **5** induces a pocket rearrangement resulting in incompatibility with the initial pocket geometry. Therefore, SCARE algorithm was ultilized to validate the effect of the protein flexibility and induced fit of compound **5** to the FtsZ receptors.

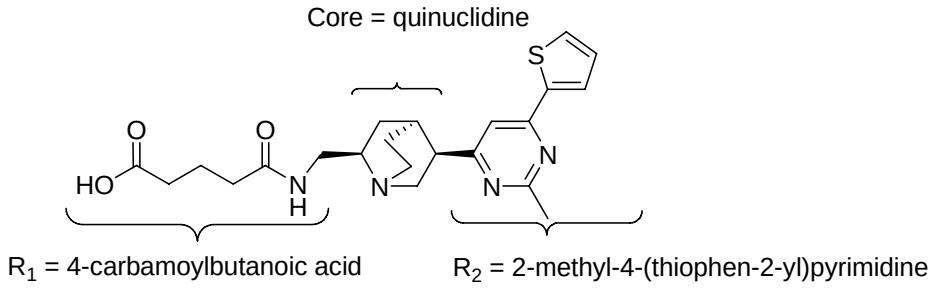

Figure 3.4 Chemical structure of compound **5**

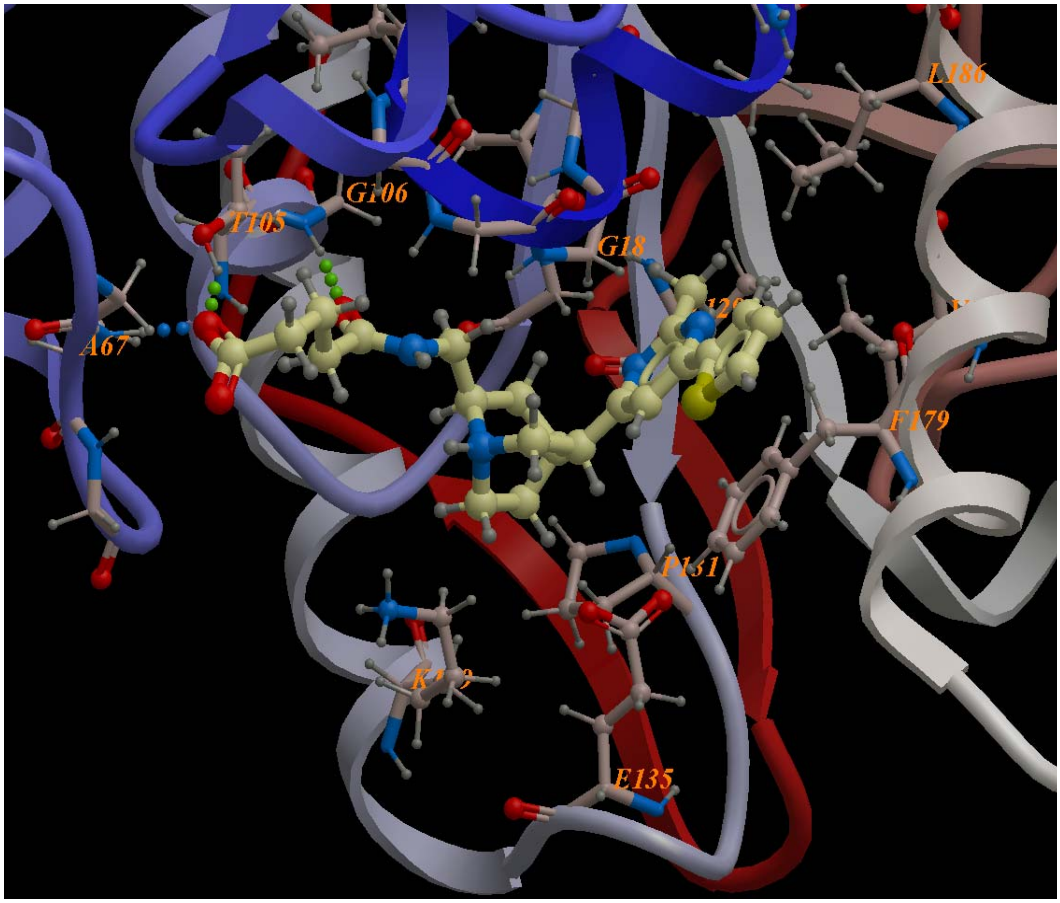

Figure 3.5 Docking pose of **5** in the GTP binding site of FtsZ (PDB code: 2R6R). The subunit of the FtsZ monomer is depicted in ribbon form. Compound **5** is depicted as a ball-and-stick model showing carbon (yellow), hydrogen (grey), oxygen (red) and nitrogen (blue) atoms. Three hydrogen bonds are depicted as dotted lines.

Table 3.3 Results of single grid docking of compound **5** on eight crystal structures of FtsZ

PDB	Score
1OFU (*P. aeruginosa*)	-11.1
1RLU (*M. tuberculosis*)	-14.3
1W5B (*M. jannaschii*)	-20.5
1W5F (*T. maritima*)	-12.6
2R6R (*A. aeolicus*)	-22.7
2R75 (*A. aeolicus*)	-22.6
2VAP (*M. jannaschii*)	5.6
2VXY (*B. subtilis*)	-4.9

3.3.3 SCan Alanines and Refine (SCARE) docking of compound 5

In order to find the optimal docking pose of compound **5**, the SCARE algorithm was used. The results of using SCARE algorithm on the eight FtsZ receptors are summarized in Table 3.4. To compare with the results from section 3.3.2 (single rigid receptor docking of compound **5**), the scores of compound **5** on the eight receptor templates were found to be improved significantly by mutating not more than three flexible residues into alanines to remove the bulky residues, then re-mutating these residues into original one. The docking poses of **5** on four receptors (PDB codes: 1W5B, 1W5F, 2VAP and 2VXY) are not shown because the scores are not good enough to predict the possible binding poses of compound **5**. The best scoring poses of compound **5** obtained from *P. aeruginosa* FtsZ (PDB code: 1OFU), *M. tuberculosis* FtsZ (PDB code: 1RLU) and *A. aeolicus* FtsZ (PDB codes: 2R6R and 2R75) were described in detail. Figures 3.6-3.9 show the binding poses of **5** to be determined from a SCARE docking. Interestingly, the scores and binding poses of compound **5** after the mutation to alanine and back mutation to original one are similar. In the case of *P. aeruginosa* FtsZ (PDB code: 1OFU), the score of compound **5** being docked to the native crystal structure was -11.1 (Table 3.4). Only one H-bond was found to form between Gly108 (2 Å) and the carbonyl oxygen of **5** (Figure 3.6A). The result showed that the docking pose of **5** was clashed by the bulky side chains of Asn25, Asp187 and Arg143. These clashing effects may cause the methyl group of the pyrimidine moiety of compound **5** to point inward and a sulphur atom of thiophene ring was forced to point outward. When the hampering residues were mutated into alanine to modify the pocket shape, more hydrophobic region of GTP

pocket was available for docking the ligand. As a result, the binding score of **5** was greatly improved from -11.1 to -30.7. Three H-bonds were formed between a carboxyl group of compound **5** and the main chains of Gly108 and Thr109. Figure 3.6B shows that a methyl group on the pyrimidine moiety of compound **5** is pointing outward and the sulphur atom of thiophene ring is pointing inward. The binding pose of compound **5** changed a lot after the mutation of residues into alanine especially for the direction of the quinuclidine core. The final step of SCARE method was to change the mutated residues back into original one and the binding pocket was then refined with compound **5**. The score of compound **5** was further improved from -30.7 to -36.0 (Table 3.4). For the *M. tuberculosis* FtsZ receptor structure (PDB code: 1RLU), compound **5** was shown to interact with two critical residues for GTP substrate binding, Gly19 (2.2 Å) and Ala70 (1.8 Å) (Figure 3.7A). The binding pose of the pyrimidine moiety and thiophene ring of compound **5** are similar to those in the *P. aeruginosa* FtsZ receptor (Figure 3.6A). The Asn22, Arg140 and Asp184 residues of *M. tuberculosis* FtsZ receptor structure (PDB code: 1RLU) also contributed to the steric hindrance, which influenced the binding geometry of **5**. After the removal of these bulky effects on compound **5** by mutating these three residues into alanines, the conformation of the R_1 group of compound **5** (Figure 3.4) was changed. The conformation change is important to improve the binding score with compound **5** (Table 3.4). Stronger H-bonds were formed between the carbonyl oxygen of amide group and that on the R_1 moiety with Gly107 (2 Å) and Ala70 (1.7 Å) respectively (Figure 3.7B). After mutating these alanines back to their original residues, the score of compound **5** was similar to that with the FtsZ receptor mutated into alanines and

their docking poses were almost the same (Figures 3.6B and 3.6C and Table 3.4). The scores of compound **5** docking to the native crystal structures of *A. aeolicus* FtsZ (PDB codes: 2R6R and 2R75) were similar with three H-bonds observed (Figures 3.8A and 3.9A). Figure 3.8 showed that three H-bonds were formed at Ala67 (1.7 Å), Thr105 (1.8 Å) and Gly106 (2 Å). The methyl group on the pyrimidine moiety of **5** was found to point inward at the upper hydrophobic region of GTP binding site. But changing Asn21, Lys139 and Asp183 into alanines led to the replacement of H-bond with Thr105 by Gly104 (2.3 Å). Another two H-bonds with Ala67 (1.9 Å) and Thr105 (2.4 Å) became weaker because the whole molecule of compound **5** moved slightly toward the hydrophobic region of GTP binding site to form the fourth new H-bond (2 Å) between Thr192 and the nitrogen atom of the pyrimidine ring (Figure 3.8B). After mutating the three residues into original ones, the best binding score and docking pose of compound **5** were still retained (Figures 3.8C and 3.9C).

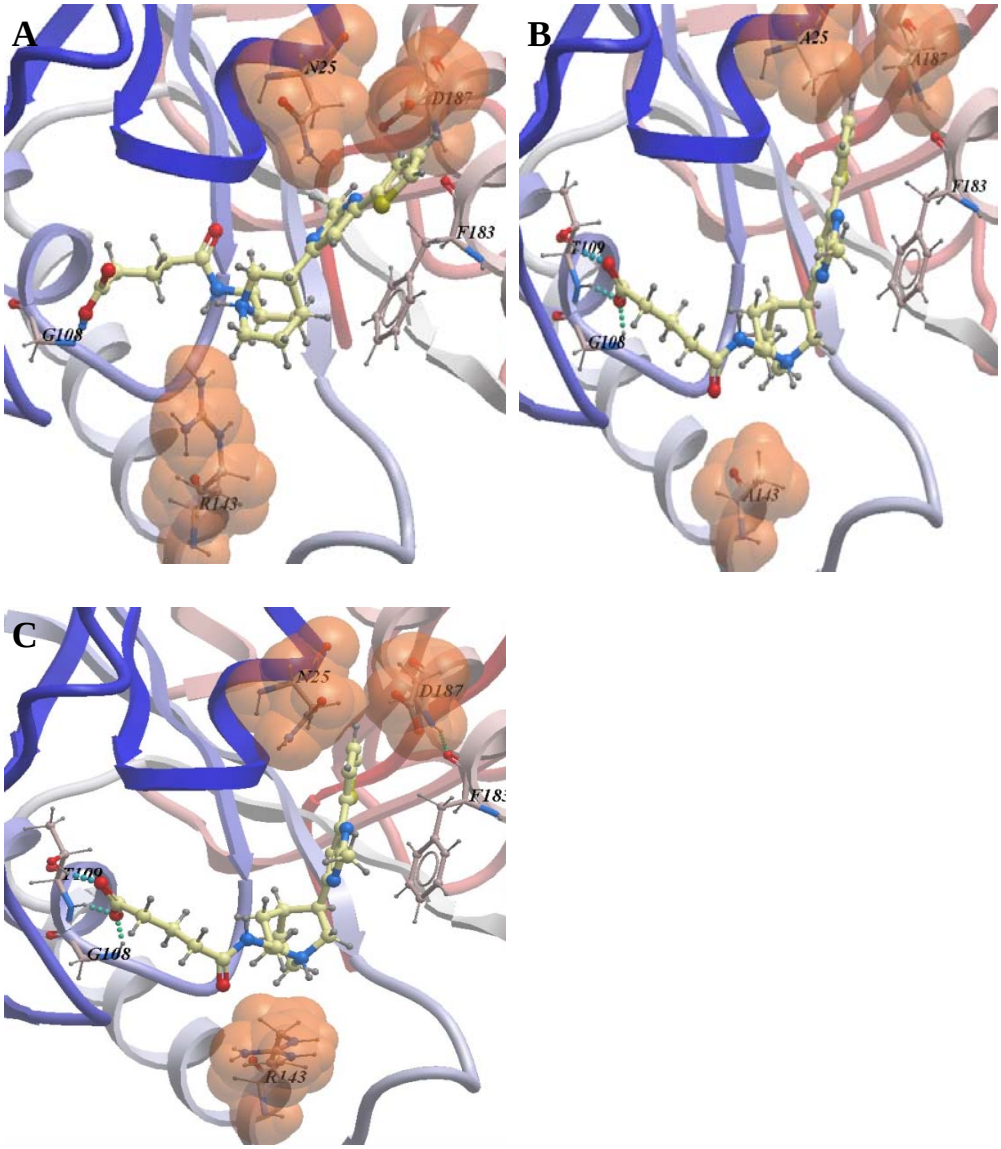

Figure 3.6 Predicted binding poses of compound **5** in the GTP binding site of *P. aeruginosa* FtsZ (PDB code: 1OFU) using the SCARE algorithm. (A) Before the alanine mutation. (B) After the triple mutation into alanine. (C) These three alanines were mutated into original residues. Compound **5** was depicted as a ball-and-stick model and coloured by atom types.

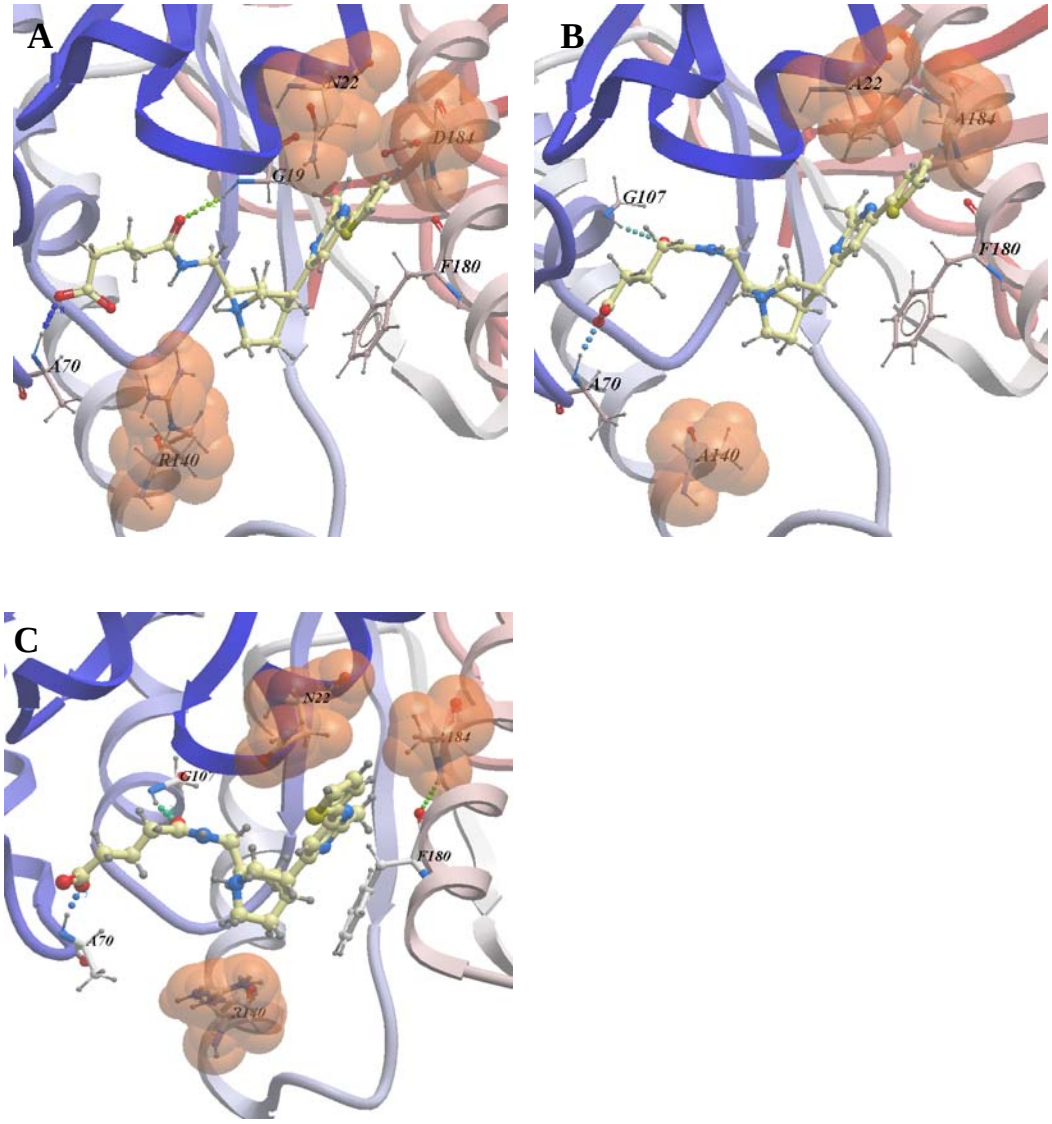

Figure 3.7 Predicted binding poses of compound **5** in the GTP binding site of *M. tuberculosis* FtsZ (PDB code: 1RLU) using the SCARE algorithm. (A) Before the alanine mutation. (B) After the triple mutation into alanine. (C) These three alanines were mutated into original residues. Compound **5** was depicted as a ball-and-stick model and coloured by atom types.

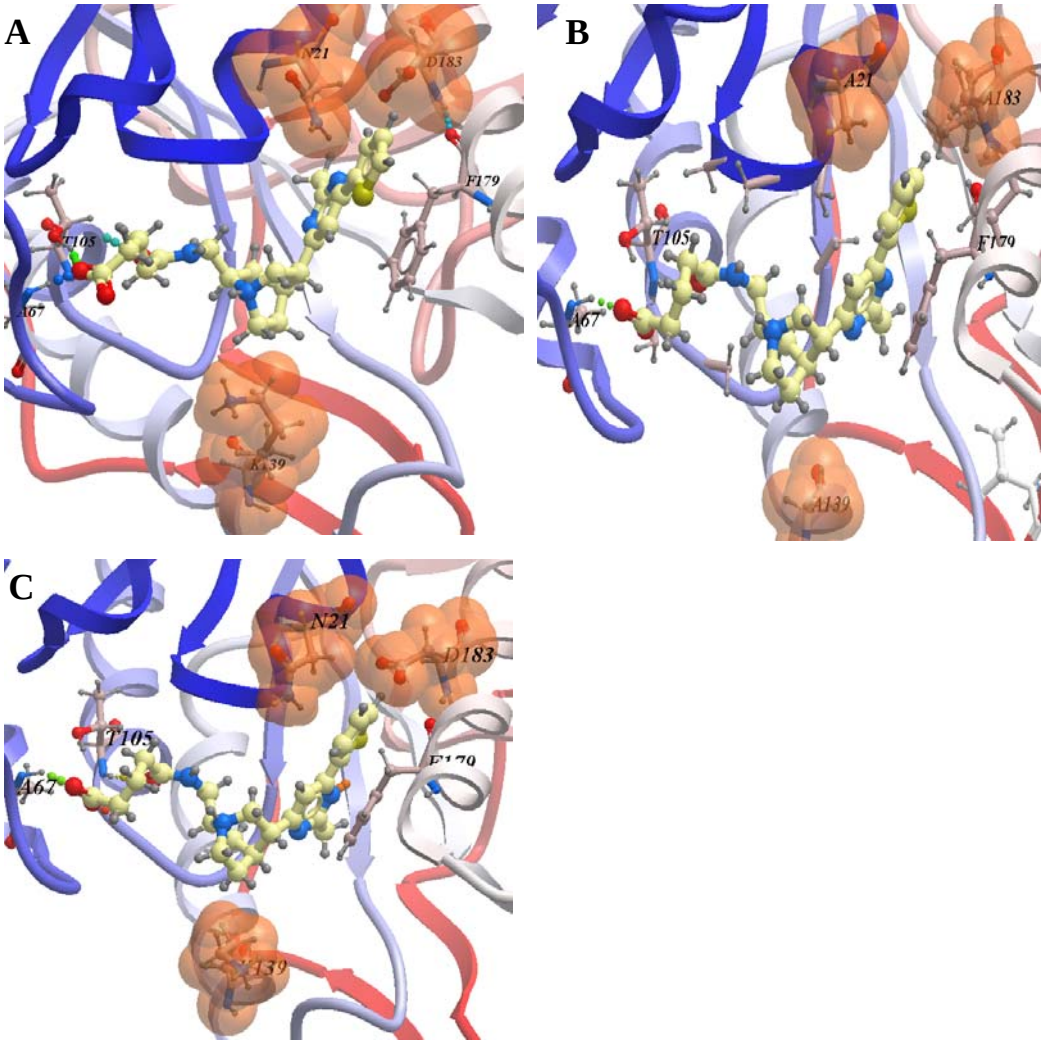

Figure 3.8 Predicted binding poses of compound **5** in the GTP binding site of *A. aeolicus* FtsZ (PDB code: 2R6R) using the SCARE algorithm. (A) Before the alanine mutation. (B) After the triple mutation into alanine. (C) These three alanines were mutated into original residues. Compound **5** was depicted as a ball-and-stick model and coloured by atom types.

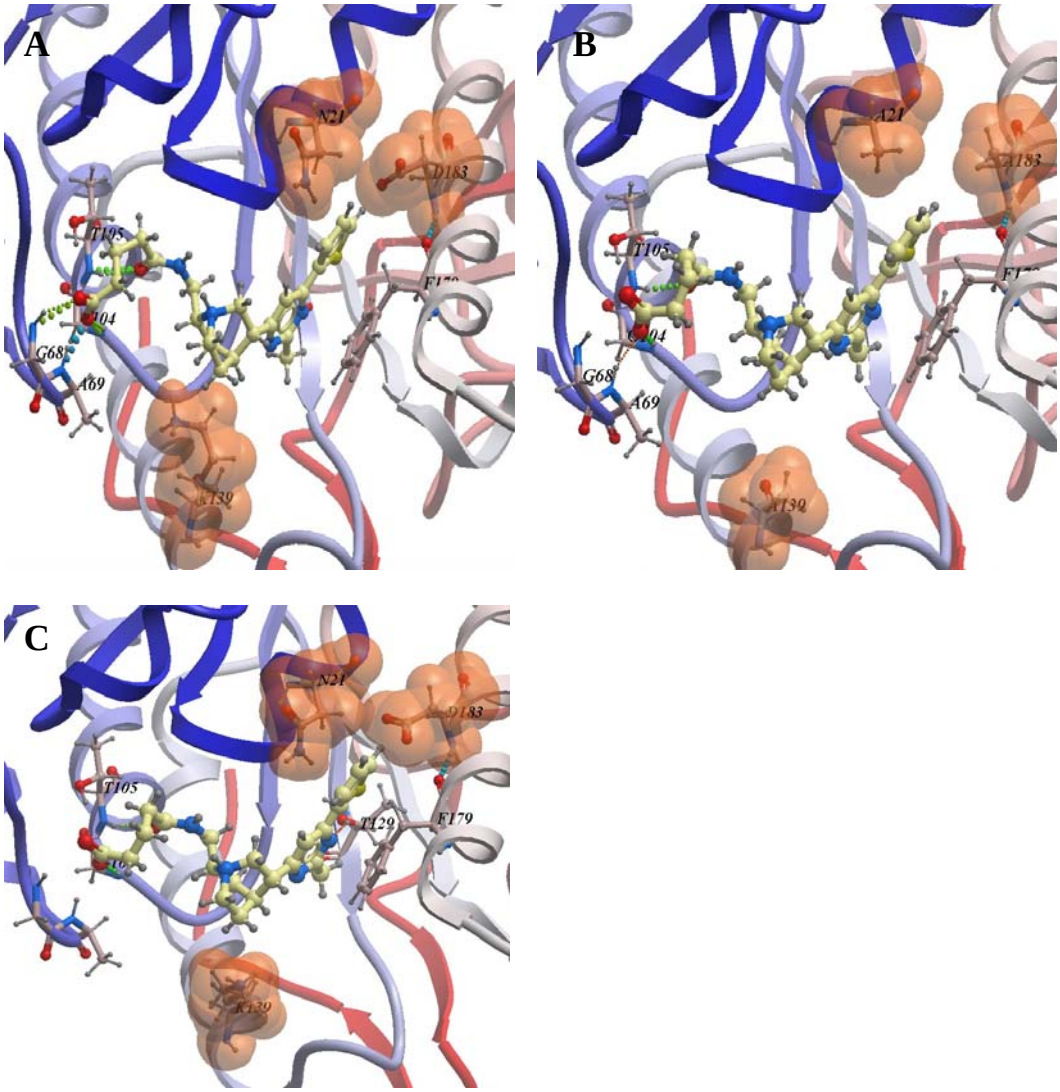

Figure 3.9 Predicted binding poses of compound **5** in the GTP binding site of *A. aeolicus* FtsZ (PDB code: 2R75) using the SCARE algorithm. (A) Before the alanine mutation. (B) After the triple mutation into alanine. (C) These three alanines were mutated into original residues. Compound **5** was depicted as a ball-and-stick model and coloured by atom types.

Table 3.4 Results of the SCARE docking

	Score		
PDB code (strain)	**Before alanine mutation**	**After alanine mutation**	**Mutation into original residues**
1OFU (*P. aeruginosa*)	-11.1	-30.7	-36.0
1RLU (*M. tuberculosis*)	-14.3	-30.6	-31.5
1W5B (*M. jannaschii*)	-20.5	-26.5	-28.6
1W5F (*T. maritima*)	-12.6	-25.1	-15.2
2R6R (*A. aeolicus*)	-22.7	-33.7	-41.3
2R75 (*A. aeolicus*)	-22.6	-33.7	-41.1
2VAP (*M. jannaschii*)	5.6	-21.4	-25.4
2VXY (*B. subtilis*)	-4.9	-22.0	-22.7

3.3.4 Homology modeling of *S. auerus* FtsZ

The high-resolution X-ray crystal structure of *A. aeolicus* FtsZ (PDB code: 2R6R) was used as a template for homology modeling the GTP binding site of *S. auerus* FtsZ [155]. *S. auerus* FtsZ and *A. aeolicus* FtsZ shared a high degree of homology in their amino acid sequences (44% identify) and most residues of both GTP binding sites are the same according to the sequence alignment. When a sequence identity of more than 30% exists between the target protein (*S. auerus* FtsZ) and the template protein (*A. aeolicus* FtsZ), a computational homology modeling method can provide an accurate 3D structure for the target protein [107]. Therefore, ICM homology modeling algorithm was employed to build and refine the model of *S. auerus* FtsZ (Figure 3.10B) on the basis of the template obtained by using SCARE algorithm of *A. aeolicus* FtsZ with compound **5** (Figure 3.10A). In homology modeling, all non-identical residues within the GTP binding pocket of the template structure were mutated into the corresponding residues of *S. auerus* FtsZ. Next, the modeled 3D complex structure bound with compound **5** was constructed through molecular dynamic simulation to refine the side chain conformation (Figure 3.10C). Comparison of a model of *S. auerus* FtsZ with the template *A. aeolicus* FtsZ showed that the conformations of the GTP binding site are essentially the same. The RMSD of main-chain between the optimized *S. auerus* FtsZ model and the template structure was within 1 Å. Finally, compound **5** was docked to the optimized model of *S. auerus* FtsZ. The best binding score and pose of **5** were obtained. The binding score is -37.51 and the docking pose of **5** on the homology model (Figure 3.11) was as same as the template (Figure 3.10D).

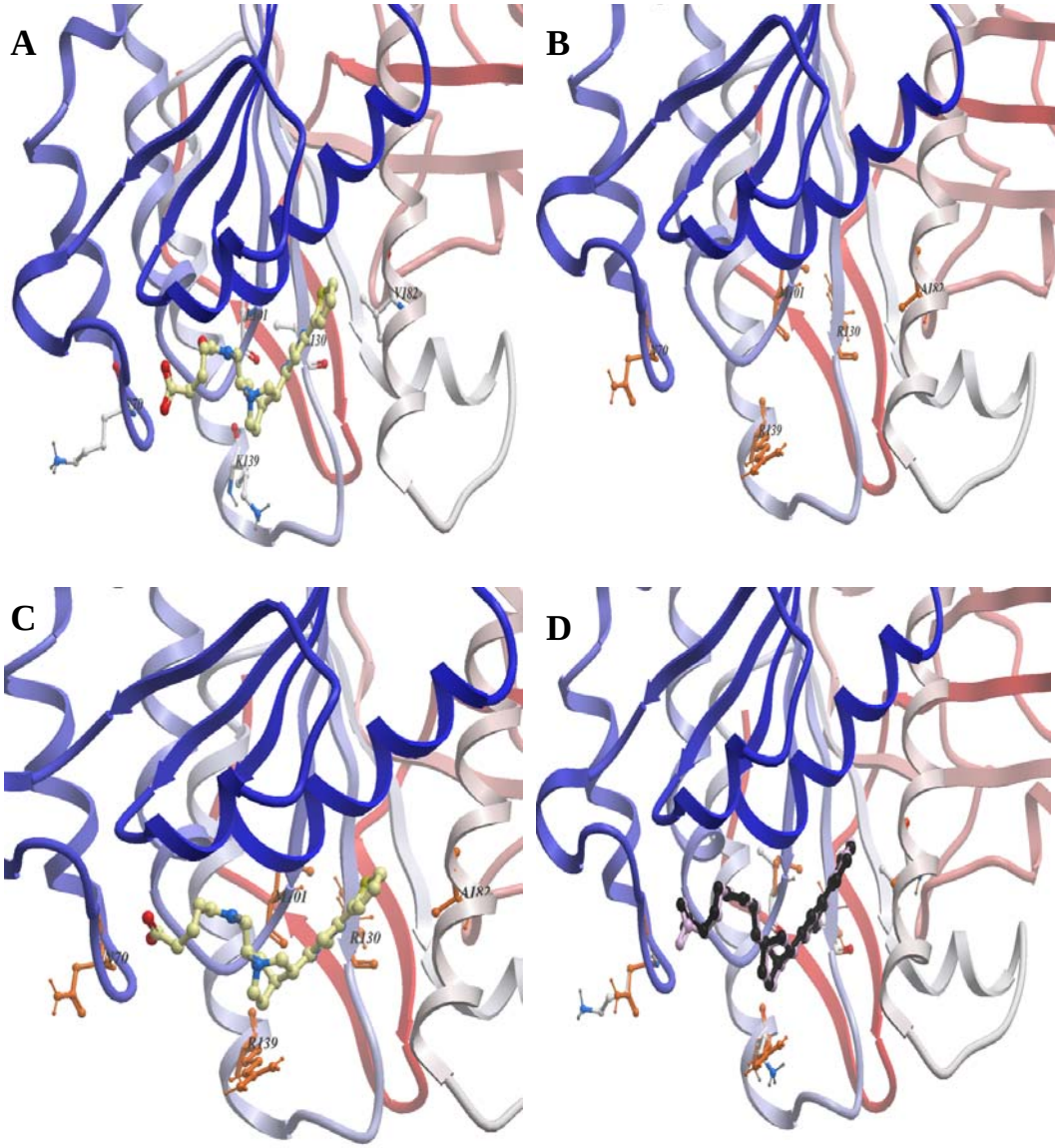

Figure 3.10 (A) The GTP binding site of *A. aeolicus* FtsZ (PDB code: 2R6R) in the presence of compound **5** obtained from the SCARE docking. (B) The homology model of GTP binding site of FtsZ for *S. auerus*. (C) The homology model of GTP binding site of FtsZ for *S. auerus* with compound **5** was refined using a molecular dynamic simulation with compound **5**. Compound **5** was depicted as a ball-and-stick model and coloured by atom types. (D) The predicted docking pose of compound **5** on the refined homology model of *S. auerus* FtsZ. The docking pose of compound **5** on *S. auerus* FtsZ and *A.aeolicus* FtsZ were represented in black and pink respectively.

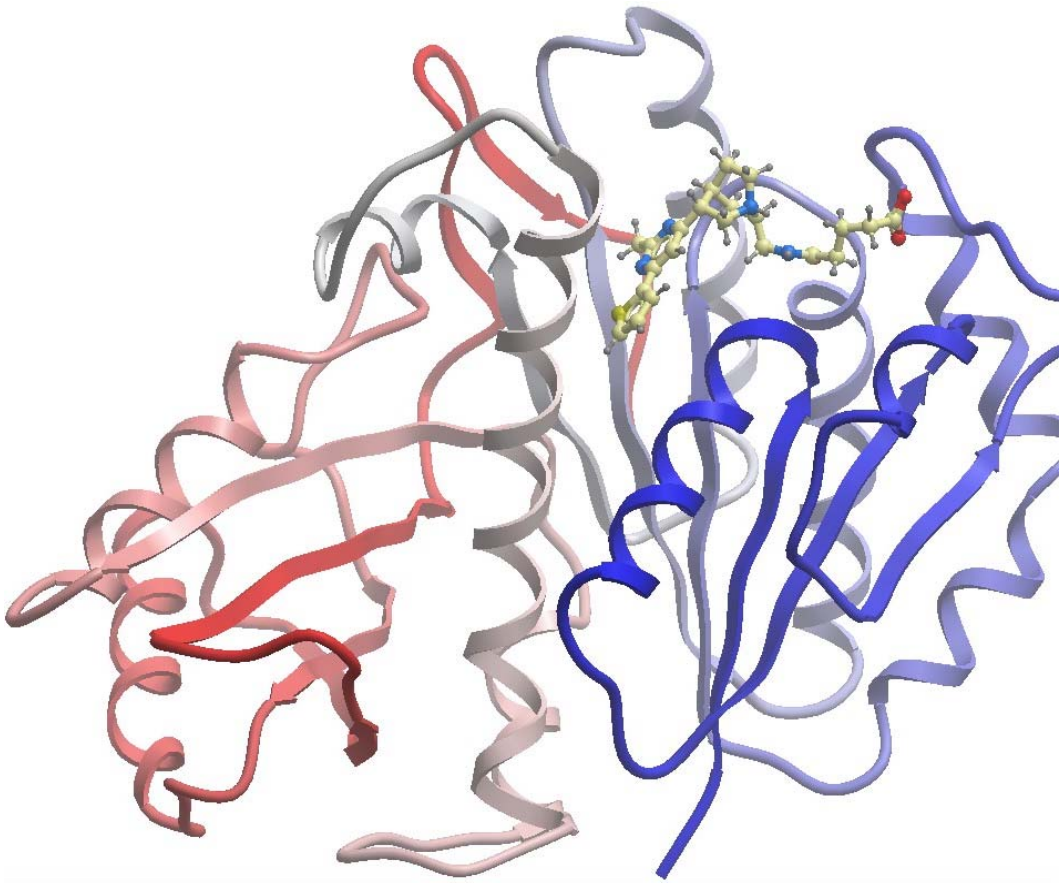

Figure 3.11 Ribbon diagram showing compound **5** in the GTP binding site of the homology model of *S. auerus* FtsZ. Compound **5** was depicted as a ball-and-stick model and coloured by atom types.

3.3.5 Virtual screening of compound 5 derivatives

Five best scoring refined models of FtsZ were attained by SCARE and homology modeling techniques including *P. aeruginosa* FtsZ (PDB code: 1OFU), *M. tuberculosis* FtsZ (PDB code: 1RLU), *A. aeolicus* FtsZ (PDB codes: 2R6R and 2R75) and the optimized *S. auerus* FtsZ model. These five docking models of FtsZ were employed in the present study as receptors for virtual screening of a small library of compound **5** analogues. After the compounds had been virtually screened and scored, 15 best scoring derivatives at each FtsZ receptor structure were selected. A total of 69 compounds were tested experimentally to validate the accuracy and quality of the five selected conformations of FtsZ. The chemical structures of the 69 compounds are shown in Tables 3.5-6. They are divided into two main groups bearing the pyrimidine-linked (Tables 3.5) or pyrazole-linked quinuclidine core (Table 3.6).

Table 3.5 Chemical structures of compound **5** derivatives

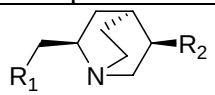

Cpd	R_1	R_2	Cpd	R_1	R_2
5	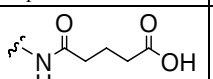	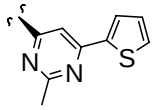	**5-293**	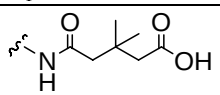	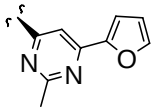
5-11	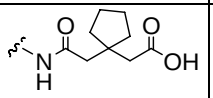	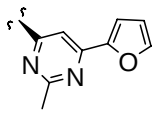	**5-294**	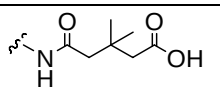	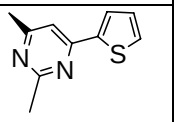
5-13	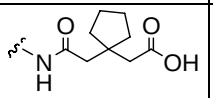	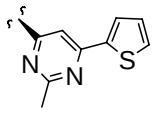	**5-296**	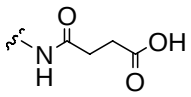	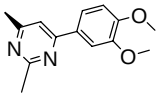
5-31	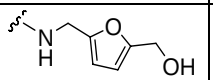	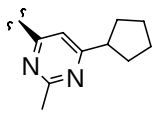	**5-297**	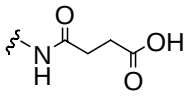	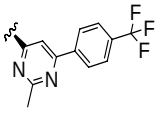
5-120	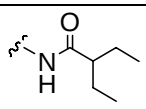	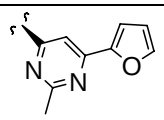	**5-298**	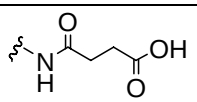	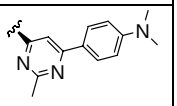
5-133	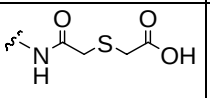	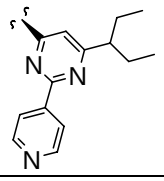	**5-299**	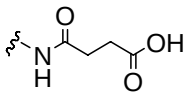	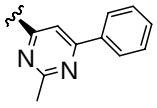
5-254	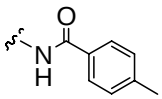	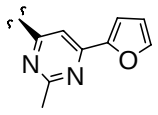	**5-300**	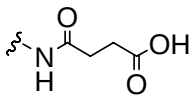	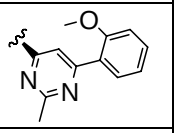
5-256	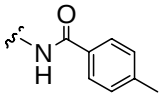	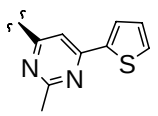	**5-301**	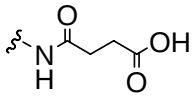	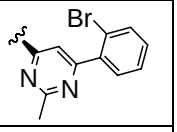
5-285	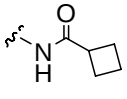	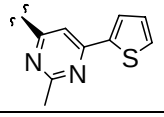	**5-302**	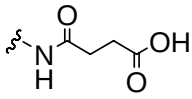	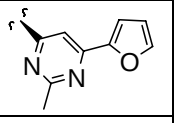
5-288	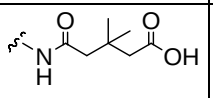	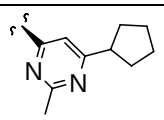	**5-304**	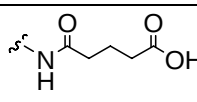	
5-289			**5-305**		

Continue……

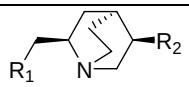

Cpd	R_1	R_2	Cpd	R_1	R_2
5-306	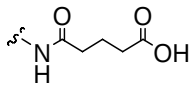	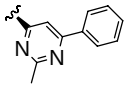	**5-336**	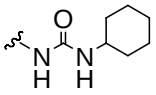	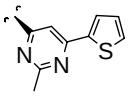
5-307	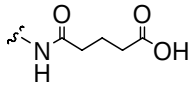	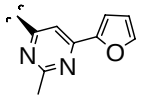	**5-341**	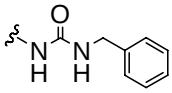	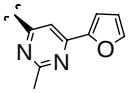
5-312	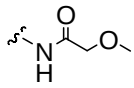	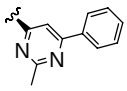	**5-353**	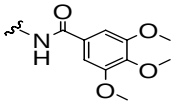	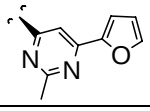
5-315	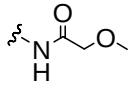	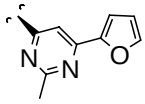	**5-359**	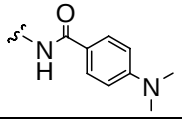	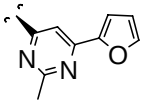
5-316	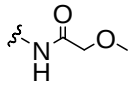	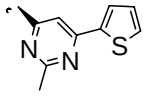	**5-360**	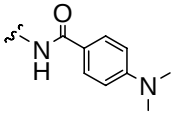	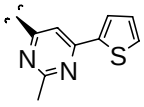
5-319	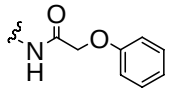	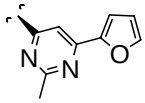	**5-379**	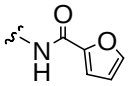	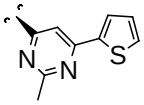
5-320	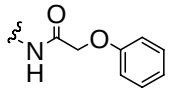	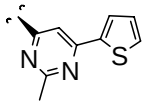	**5-387**	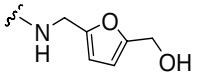	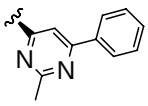
5-321	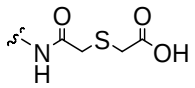	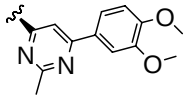	**5-701**	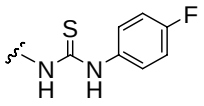	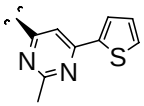
5-323	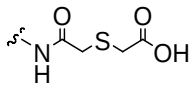	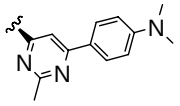	**5-702**	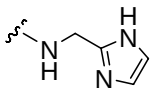	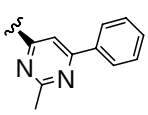
5-324	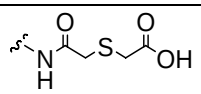	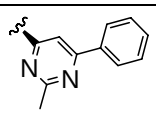	**5-703**	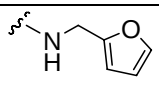	
5-325			**5-704**		
5-326			**5-705**		

Continue……

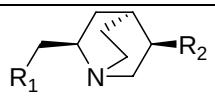

Cpd	R_1	R_2	Cpd	R_1	R_2
5-706	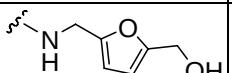	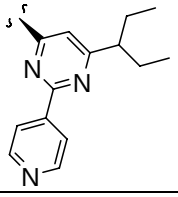	**5-708**	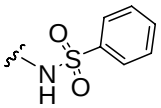	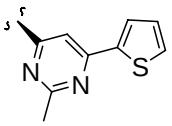
5-707	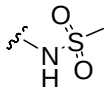	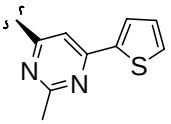			

Table 3.6 Chemical structures of compound **5** derivatives

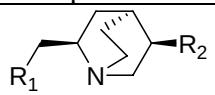

Cpd	R_1	R_2	Cpd	R_1	R_2
5-9	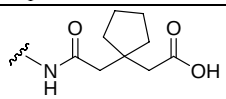	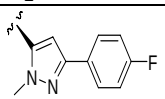	**5-507**	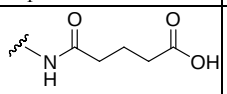	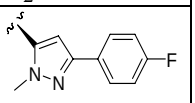
5-12	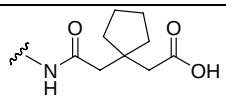	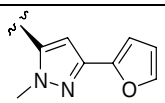	**5-609**	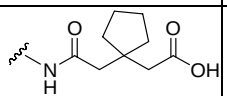	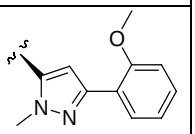
5-14	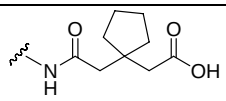	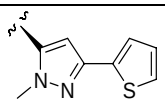	**5-614**	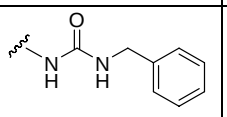	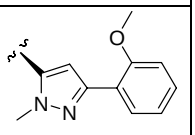
5-42	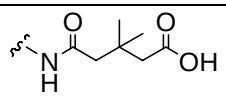	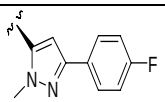	**5-617**	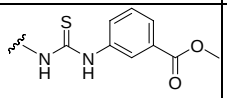	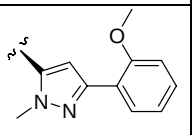
5-43	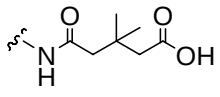	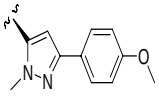	**5-623**	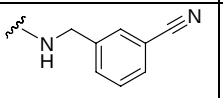	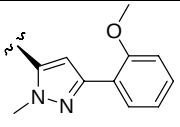
5-44	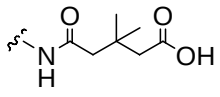	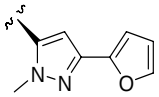	**5-633**	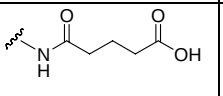	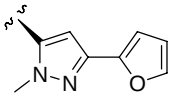
5-45	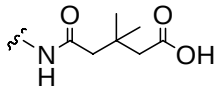	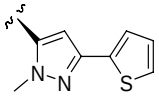	**5-641**	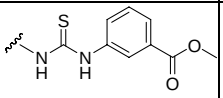	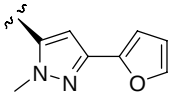
5-216	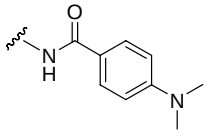	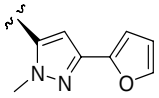	**5-655**	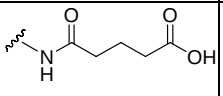	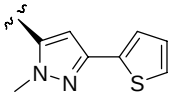
5-433	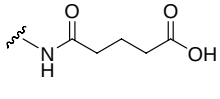	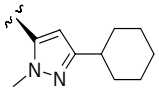			

3.4 Discussion

3.4.1 Determination of optimal docking pose of compound 5

Although the theoretical and technical aspect of virtual high-throughput screening have been significantly improved [187], this screening method still has some unsatisfactory performance and is not able to accurately predict the correct binding mode of a ligand due to the lack of receptor flexibility [180]. This phenomenon has occurred in a large region of low structural stability of many active sites because binding a ligand into an enclosed binding site necessitates that part of the receptor to be flexible in order to allow access [188, 189]. Although incorporating the protein flexibility in molecular docking remains challenging because a large conformational space will be involved, the rank-order performance was found to be greatly improved [190]. Nowadays, many diverse attempts were made to incorporate protein flexibility into the molecular docking. One of the commonly used methods to account for receptor flexibility is an ensemble docking [191]. Several crystal structures can be employed to calculate the average potential grids for molecular docking. This approach can greatly shorten the calculation time. But the large repulsive energy associated with steric clashes with the binding site would heavily bias the mean after combining possible conformations into an average structure. In addition, less space will be available for docking, which greatly decreases the size of the binding site and the conformational space accessible to the ligand [180]. Another approach is an induced fit with multiple receptor conformations [192-195]. In this approach, different rigid protein conformations obtained from the crystal structure of

target or being generated by molecular dynamics simulations (MD) [196, 197] are used as initial docking templates in VLS.

Since compound **5** was found not to fit into the GTP binding site of FtsZ, receptor flexibility has been incorporated into the subsequent docking calculation to find the optimal binding pose. Eight of twenty-three available crystal structures were selected to represent possible conformations of FtsZ. Although using more receptor conformations can reflect the dynamic nature of receptor structure, it may increase the "false-positive" rate in virtual screening studies and the computing time. In order to accomplish a compromise between the computing time and performance in predicting an optimal docking pose of **5** in our study, attempts were made to combine the SCARE approach with a multiple-receptor conformation docking method. Notably, the optimal docking pose of compound **5** could be attained. For example, the binding score of compound **5** on most selected FtsZ crystal structures were less than -30. The more negative scores represent more energetically favorable binding to the active site. In chapter 2, the optimal binding mode of **5** may not be correctly predicted because some bulky side chains may hinder the access of ligand to the GTP binding site. After superimposing the sequence of eight models, we found that the orientation of some flexible side chains were totally different from each other. It may cause the different docking poses of compound **5** as shown in Figures 3.6-9A. Thus, not more than three flexible residues were mutated into alanine to dock a ligand again in the SCARE study. In light of the SCARE results, mutating several residues into alanine significantly improved the docking poses of compound **5** on all FtsZ crystal structures.

After eliminating the steric hindrance effect of several bulky side chains in the GTP binding site, the R_2 substituent group of compound **5** (Figures 3.6-3.9B) was found to interact better with the residues at the hydrophobic region. Changing these mutated residues into their original one did not cause deterioration of the binding score of compound **5** except for one docking template (PDB code: 1W5F). Although the SCARE approach can improve the binding score of compound **5** on all crystal structures, only the scores on four crystal structures are less than -30. Based on the above docked results, the optimal binding modes of compound **5** could be predicted by the best scoring pose determined from four crystal structures (PDB codes: 1OFU, 1RLU, 2R6R and 2R75). This technique is particularly important for selecting appropriate receptor structures for *in silico* hit optimization.

3.4.2 Homology modeling

Knowledge on the three dimensional structure of *S. auerus* FtsZ is important to understand its mechanism of action and inhibition by the ligand. Unique information can be obtained from the atomic detail of the GTP binding site which was then used to identify key interactions between FtsZ protein and compound **5**. The structures of many FtsZ proteins from different bacterial strains have already been reported. Despite the low sequence identity of C-terminus between members of different FtsZ families, they all share the same overall topology [155]. In addition, the GTP binding pocket cavity shows a high degree of sequence identity (Figure 3.1). According to the result of the SCARE docking, the best scoring pose of compound **5** was *A. aeolicus* FtsZ (PDB code: 2R6R) with a score of -41.254. Therefore, we used the structure of

A. aeolicus FtsZ (PDB code: 2R6R) with compound **5** as a template to construct a model of GTP binding site for *S. aureus* FtsZ and further refined the side chain conformations through molecular dynamics simulation. Comparison of our modeled *S. aureus* FtsZ structure with the *A. aeolicus* FtsZ showed both the overall fold and binding site conformation are almost the same with similar docking poses and scores for compound **5**.

3.4.3 High-throughput virtual screening of library of compound 5 derivatives

To optimize the ligand interactions with the GTP binding site, the four best scoring models of FtsZ obtained from a SCARE protocol and the homology model of *S. auerus* FtsZ were used for *in silico* virtual screening of a small library of compound **5** derivatives. Based on the binding score and the docking pose, 69 top-scoring derivatives were selected for the subsequent biochemical assays. The experimental results can then be used to validate the accuracy of docking calculations in this chapter.

3.5 Conclusing remark

Eight different receptor conformations were selected to represent a protein flexibility of FtsZ and were used as the initial docking templates. Compound **5** was docked to each conformation. It was found that the best scoring and the optimal docking pose of **5** on these eight receptors could not be attained. Hence, the 3D structures of these eight receptors were superimposed. It was found that several residues inside the GTP binding site of FtsZ have different orientations and bulky side chains that might hinder ligand entering that pocket. In order to investigate the effect of protein flexibility and induced effect of ligand, a novel docking algorithm, SCARE, was used. As a result, the highest-scoring pose of **5** could be found on four docking templates, which is attributed to the incorporation of an induced fit effect upon ligand binding to the GTP binding pocket and protein flexibility in a docking simulation. In these docked models, **5** was found to interact with several residues that are critical for interacting with nucleotides in the GTP binding site to form several hydrogen bonds, charged and hydrophobic interactions. Good shape complementarity of **5** with the active site was shown in these docked models. However, the optimal binding pose of **5** on four docked models might not be used directly to correlate with the experimental results of *S. auerus* FtsZ protein in chapter 2 because no X-ray crystallographic structure of *S. auerus* FtsZ is available. Herein a homology modeling of FtsZ for *S. auerus* was successfully constructed based on the optimized model of *A. aeolicus* FtsZ (PDB code: 2R6R) with compound **5** obtained from SCARE. Compound **5** was docked to this optimized homology model. The result revealed that a highest scoring pose of **5** was obtained. Homology model of *S. aureus* FtsZ gave

results in good agreement with the experimental results shown in chapter 2. After obtaining several optimal docking models from SCARE and homology techniques, a series of compound **5** derivatives were screened *in silico* for hit optimization. 69 top-ranking derivatives were then selected for validation of the potency and the results will be reported in chapter 4.

Chapter 4

Biochemical studies on the anti-FtsZ activity of hit derivatives

4.1 Introduction

4.1.1 Biochemical assays of the anti-FtsZ activity of hit derivatives

Once the optimal binding pose of compound **5** at the GTP binding site has been determined, hundreds of its analogs can be docked via structure-based virtual screening and this pharmacophore class can be examined in details to improve its antibacterial activity and inhibitory affinity towards FtsZ. Based on the docking poses and binding scores of the hit derivatives, sixty-nine compounds were selected. The antibacterial activities of these compounds were firstly tested experimentally to determine their MICs against a panel of bacterial isolates and to determine their on-target activity as indicated by the cell filamentation of *B. subtilis* and *E. coli* using the morphometric analysis. Derivatives with higher antibacterial activity were then tested to determine their inhibitory effects of GTPase activity and assembly of FtsZ *in vitro*. According to the experimental results and binding conformations from molecular docking through SCARE and homology models of FtsZ, a structure-activity relationship (SAR) of compound **5** derivatives can be obtained to determine which functional groups of the molecule are important to biological activity. The cytotoxicity effect of more potent derivatives on mammalian cell lines was also studied. Studying the toxicity effect of new drugs at an early phase is very crucial because it is possible to establish a relationship between the molecular structure of a compound and its toxic effects. Even if a compound is found to be toxic, it can be chemically modified to eliminate its toxicity and retain its potency.

There are three ways to cause cytotoxicity which are pharmacophore-induced, structure-related or metabolism-induced [198]. Pharmacophore-induced toxicity was led by the pharmacology of the compound. At elevated doses (excess of the therapeutic dose), the original selectivity of the compound for the target is lost because the compound affects structures that are closely related to the original target. In the case of a structural-related toxicity, it is triggered by structural features or physicochemical properties of the compound. For example, the presence of iodine in the amiodarone molecule causes hypothyroidism and hyperthyroidism in patients [199]. When the drug is a highly lipophilic base, it can easily accumulate in some tissues to cause side effects after a long-term therapy [200]. The third cause of cytotoxicity is metabolism-induced, which is not caused by the parent compound itself but by reactive metabolites formed *in situ* inside the cells. A key functional group of the compound can be altered by oxidation, reduction or conjugation to become a reactive electrophile group. Then, the electrophile group reacts with nucleophiles in proteins, nucleic acids and small peptides in the body. Finally, this reaction causes cell disorders and toxic effects. The reactive electrophile group can be attributed by compounds containing epoxides, quinines, imines, nitrenium ions, iminium ions, hydroxylamines, thiophene rings, thioureas or chloroquinolines [198]. In this study, *in vitro* cytotoxicity test was undertaken to evaluate the toxicity effect of selected derivatives on three mammalian cell lines namely L929: mouse fibroblast, MKCKII: Madan-Darby Canine Kidney Cell and HEK293/pcDNA3.1: human embryonic kidney cell containing a pcDNA3.1 vector.

4.1.2 Exploring the synergistic effect of compound 5 and its derivatives with other antibacterial agents

The emergence of resistant bacteria is considered to be one of the most prevalent health hazards all over the world. Most clinically used antibiotics to treat infections from bacteria have become less effective. To overcome this problem, several strategies could be used to combat resistant strains: one is to identify compounds against novel bacterial targets; the other approach is to investigate the synergistic effect of two or more compounds on the treatment of bacterial infections. In the earlier studies in chapter 2, compound **5** was identified to inhibit the GTPase and assembly activities of FtsZ. But the antibacterial potency of **5** and its derivatives were found to be only moderate. In order to improve the antibacterial efficiency and better understand the mode of action of compound **5** and its derivatives on the bacterial strains, 3-methoxybenzamide (3-MBA) and ampicillin were tested in combination with compound **5** (or its derivatives) against the Gram-positive and -negative bacterial strains in this study. 3-MBA is known to be a T7 loop inhibitor of FtsZ that inhibited bacterial cell division in the Gram-positive bacterium *B. substilis*. But it only exhibits a weak antibacterial potency against the Gram-positive bacteria, and is not potent against Gram-negative bacteria [60, 201]. Ampicillin is one commonly used beta-lactam antibiotic that treats bacterial infections by inhibiting bacterial cell wall synthesis. But ampicillin has become less effective in clinical treatment because many ampicillin-resistant strains have been identified. Therefore, the main aim of this study was to compare the activities of compound **5** and its

derivatives in combination with 3-MBA or ampicillin with the activity of individual compounds and to examine their synergistic effects on antibiotic-susceptible or -resistant bacterial strains.

4.2 Methods

4.2.1 *In vivo* and *in vitro* assays

The biological activities of compound **5** derivatives were tested experimentally according to the detailed procedures of *in vivo* and *in vitro* assays described in section 2.2. The chemical structures of compounds **5-316**, **5-326**, **5-387**, **5-701**, **5-702**, **5-705** and **5-706** were verified by using high-resolution mass spectrometry (Micomass Q-Tof-2) to determine the molecular weight $(M+H)^+$. The detail procedures had been described in section 2.2.1.5.

4.2.2 Cytotoxicity

4.2.2.1 Cell Culture

L929 cells and MDCKII cells were maintained in a DMEM medium supplemented with 10% (v/v) heat-inactivated FBS and 100 units/mL penicillin and 100 μg/mL streptomycin. HEK293/pcDNA cells were maintained in a RPMI1640 medium supplemented with 10% (v/v) heat-inactivated FBS and 100 units/mL penicillin and 100 μg/mL streptomycin. Cells were cultured at 37^{o}C in a humidified atmosphere with 5% CO_2. When the cells had reached confluence, they were detached by 0.05% trypsin-EDTA.

4.2.2.2 Cytotoxicity Assay

50,000 cells of L929 or MDCKII or HEK293/pcDNA3.1 were mixed with

compound **5** derivatives of different concentrations and adjusted to a final volume of 100 μL in each well of a 96-well plate. DMSO was used as vehicle control at a final concentration of 2%. The microplates were then incubated for 3 days at 37 ^{o}C. The half-maximal inhibition (IC_{50}) of the compounds was determined using the CellTiter 96 AQ_{ueous} Assay (Promega). MTS (3-(4,5-dimethylthiazol-2-yl)-5-(3-carboxy-methoxyphenyl)-2-(4-sulfophenyl)-2H-tetrazolium, 2 mg/mL) and PMS, (phenazine methosulfate, 0.92 mg/mL), were mixed in a ratio of 20:1. An aliquot (10 μL) of the freshly prepared MTS/PMS mixture was added into each well, and the plate was incubated for 2 hours at 37 ^{o}C. Optical absorbance at 490 nm was then recorded with a microplate absorbance reader (Bio-Rad). IC_{50} values were calculated from the dose-response curves of MTS assays (Prism 4.0). All experiments were performed in triplicates and the results were represented as the average of the three independent measurements.

4.2.3 Synergistic effect of compound 5 and its derivatives with 3-MBA or ampicillin

In synergistic study, combinations of compound **5** or its derivatives with 3-MBA or ampicillin were tested against four bacterial strains. Three Gram-positive bacteria strains (drug-susceptible *S. auerus*, ampicillin-resistant *S. auerus* and drug-susceptible *B. subtilis*) and one Gram-negative bacteria strain (drug-susceptible *E. coli*) were evaluated. The MIC of each compound was determined individually and in combination at a fixed ratio of 1:1. The MICs of the compounds were determined by a broth microdilution method according to the National Committee for Clinical Laboratory Standards guidelines [169]. The effects of interaction between the antibacterial agents and the test organisms were evaluated using the fractional inhibitory concentration index (FICI). FICI was calculated as follows: FICI = ($MIC_{a\ combination}/MIC_{a\ alone}$) + ($MIC_{b\ combination}/MIC_{b\ alone}$). The detailed procedures of MIC value determination were the same as those described in section 2.2.3.1. The MIC values were determined by three independent experiments and FICI was calculated from both the FICI of compound **5** or its derivatives and 3-MBA or ampicillin. The FIC indexes at values of ≤0.5, 0.5 - 0.75, 0.76 - 1, 1 - 4, and >4 were defined as synergy, partial synergy, additive effect, indifference, and antagonism, respectively [202].

4.3 Results and Discussion

4.3.1 *In vivo* assays

4.3.1.1 Antimicrobial testing

After manual inspection of 100 top-scoring derivatives, 69 compounds were selected and separated into two groups bearing the pyrimidine-linked or pyrazole-linked quinuclidine core. They were firstly tested for potency and spectrum of activity against *S. auerus* ATCC 29213 and *E. coli* ATCC 25922, and the MICs were determined by the CLSI method [169]. The results for the selected compounds are summerized in Table 4.1. The results revealed that several compound **5** derivatives bearing the pyrimidine-linked quinuclidine core not only caused lethality on *E. coli* and *S. auerus* cells, but also appeared to possess higher potency and exhibited a broader spectrum of activity than compound **5**, whereas the series of pyrazole-linked quinuclidine core derivatives showed little antibacterial activity against *S. auerus* and *E. coli*. Table 4.1 shows that replacing the thiophene ring in compound **5** with a phenyl or furan ring would diminish the antimicrobial activity against *S. auerus* and *E. coli*, the MICs of **5-306** or **5-307** were >384 μg/ml. The addition of more bulky substituent groups such as methylbenzyl group (**5-256**) or benzyl amine group (**5-360**) to the amide moiety enhanced the antibacterial activity. But the replacement of the butyric acid group of **5** with either a 1-ethyl-propyl group (**5-120**) or a phenylether group (compound **5-320**) or a furan ring (compound **5-379**) was deleterious to the activity. On the contrary, replacing the butyric acid group with either a methoxy group (compound **5-316**) or a thioether group (compound **5-326**) or

a (trifluoromethyl)benzyl group (compound **5-705**) could improve the activity. Replacement of the thiophene ring of **5-256**, **5-316** or **5-326** by a phenyl ring (compound **5-312**) or a furan ring (compound **5-254** or **5-315** or **5-324**) also affected the inhibitory activity. The antibacterial activity was significantly improved when the amide substituent at R_1 group was changed into a thiourea group (compound **5-701**). Interestingly, when the amide substituent at R_1 group (compound **5-379**) was replaced with an amine group (compound **5-387**), a greater antibacterial activity against *S. auerus* and *E. coli* was observed. Replacement of the furfuryl alcohol group (compound **5-379**) with an imidazole (compound **5-702**) still retained the antibacterial activity. Strikingly, adding more bulky and hydrophobic group at R_2 group (compound **5-706**) could greatly enhance the antibacterial activity in comparison to compound **5-387**.

After screening the 69 compounds in the susceptibility test, several derivatives such as **5-705** and **5-706** were found to exhibit a greater antibacterial activity and possess a higher potency than the hit compound **5** (Table 4.2). Although the antibacterial activity of **5-316** was weaker than **5-705** and **5-706**, it was more active than the hit against certain Gram-positive bacterial strains. For example, **5-316** showed an 4-fold and 8-fold improvement in potency over **5** against *S. auerus* ATCC 29213 and *E. faecalis* ATCC 29212 respectively. **5-705** showed an 16-fold improvement in potency over **5** in tests on *B. subtilis* and *S. auerus*, and 6-fold improvement on *E. coli* respectively. Regarding **5-706**, the potency against *B. subtilis* and *E. coli* were the same as **5-705**. Both ampicillin-sensitive and -resistant *S.*

auerus strains were more sensitive to **5-706** than other derivatives with the MIC of 24 μg/mL. The results revealed that the antibacterial activities of compounds **5-705** and **5-706** against ampicillin-resistant *S. auerus* ATCC 29247 were the same as a conventionally used β-lactam antibiotic, ampicillin (MIC = 24 μg/mL, Table 2.3). The MICs of compounds **5-387**, **5-701** and **5-702** (48 μg/mL) against the ampicillin-resistant *S. auerus* ATCC 29247 were found to be comparable to that of ampicillin. We also tested the compound **5** derivatives on Gram-negative strain *P. aeruginosa* ATCC 27853. Among the derivatives tested, only **5-702** and **5-705** were found to inhibit *P. aeruginosa* ATCC 27853 at 192 μg/mL. Other derivatives showed no activity against *P. aeruginosa*. The low susceptibility towards antibiotic and our derivatives are attributable to an action of multidrug efflux pumps with chromosomally-encoded antibiotic resistance genes and the low permeability of the bacterial cellular envelopes. Although only a small number of strains were tested against compounds **5-387**, **-701**, **-702**, **-705** and **-706**, they were found to exert greater potency and broader spectrum of activity than the parent compound **5**.

Table 4.1 Antimicrobial activities of selected analogues of compound **5**

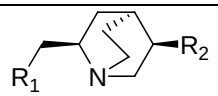

MIC (μg/mL)				
Compound	R_1	R_2	*S. auerus* ATCC 29213	*E. coli* ATCC 25922
5	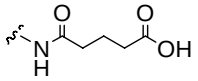	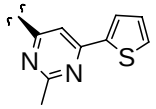	384	192
5-13	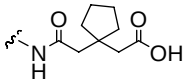	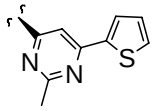	192	96
5-31	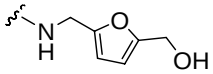	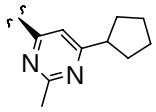	>384	>384
5-120	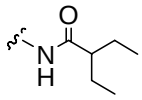	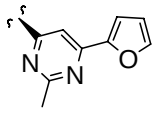	>384	>384
5-254	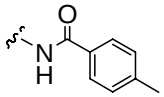	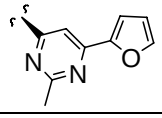	>384	>384
5-256	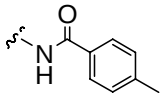	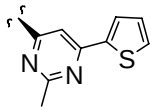	192	96
5-306	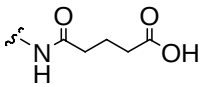	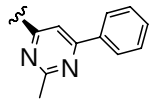	>384	>384
5-307	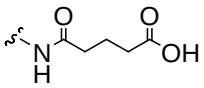	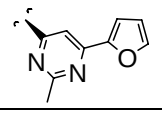	>384	>384
5-312	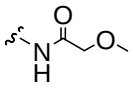	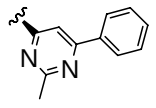	192	192
5-315	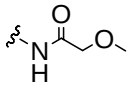	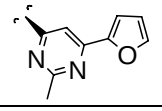	>384	>384

Table 4.1 continued…..

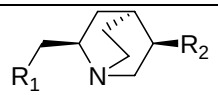

Compound	R_1	R_2	MIC (μg/mL) *S. auerus* ATCC 29213	MIC (μg/mL) *E. coli* ATCC 25922
5-316	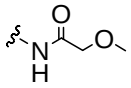	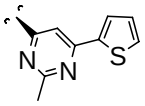	96	96
5-320	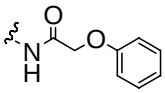	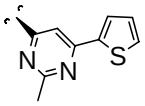	>384	192
5-324	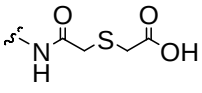	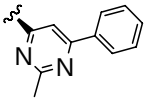	>384	>384
5-326	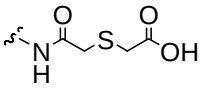	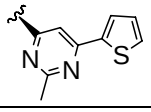	96	192
5-360	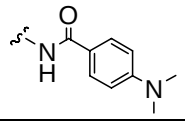	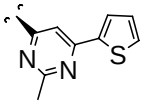	192	192
5-379	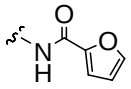	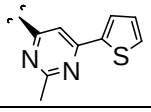	>384	>384
5-387	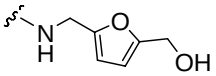	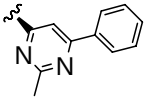	48	96
5-655	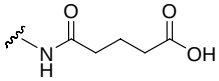	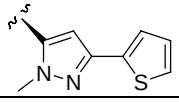	>384	>384
5-701	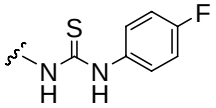	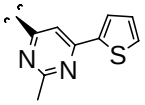	48	96
5-702	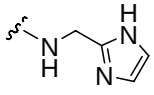	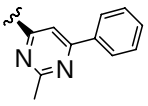	48	96
5-705	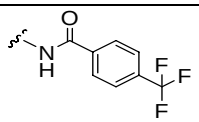	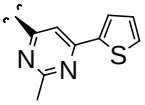	24	36
5-706	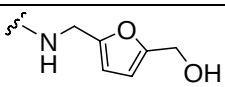	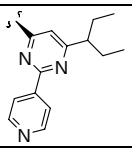	24	36

Table 4.2 MICs of a selection of more potent derivatives against gram-positive and gram-negative bacteria

Strains	MIC (μg/mL)								
	5-13	**5-256**	**5-316**	**5-326**	**5-387**	**5-701**	**5-702**	**5-705**	**5-706**
S. aureus ATCC 29213	192	192	96	96	48	48	48	24	24
S. aureus ATCC 29247	192	192	96	96	48	48	48	24	24
B. subtilis 168	96	96	24	48	48	24	24	24	24
S. epidermidis ATCC 12228	48	48	48	48	n.d.	n.d.	n.d.	24	12
E. faecium ATCC 49624	48	48	48	96	n.d.	n.d.	n.d.	24	24
E. faecalis ATCC 29212	384	384	48	96	n.d.	n.d.	n.d.	36	24
M. catarrhalis ATCC 25240	96	96	48	96	n.d.	n.d.	n.d.	n.d.	n.d.
E. coli ATCC 25922	96	96	96	192	96	96	96	36	36
P. aeruginosa ATCC 27853	>384	>384	>384	>384	>384	>384	192	192	>384

n.d. is not determined

4.3.1.2 Effect of compounds on bacterial morphology

To determine whether **5-316**, **5-387**, **5-705** and **5-706** possess *in vivo* on-target activity, they were tested against two bacterial strains by observing the change in the bacterial cell morphology (Figures 4.1 and 4.2). Log-phase cultures of *B. substilis* and *E. coli* were treated with 1% DMSO or the four compounds (the final concentration was 0.5 × MIC). The microscopic results indicated that the four derivatives had the ability to inhibit bacterial cell division, causing filamentation of *B. subtilis* and *E. coli* cells. The results obtained were similar to compound **5** in section 2.3.3. The average cell length of untreated *B. subtilis* and *E. coli* cells were about 3.1 ± 1 μm and 2 ± 1 μm respectively. These four compound **5** derivatives (12 μg/mL) were found to cause lengthening in cell size of *B. subtilis* from 6-fold to 8-fold (Figures 4.1B-D). For example, **5-316** extended the cell length of *B. subtilis* from 3.1 ± 1 μm to 18 ± 10 μm. As shown in Figure 4.1E, **5-706** showed a great effect on the elongation of *B. subtilis* cells (Figure 4.1B-D). About 90% of **5-706**-treated *B. subtilis* cells exhibited cell length (22 ± 12 μm) 8 times longer than non-treated cells (3.1 ± 1 μm) after a 4 h incubation. Concerning the cell morphology of *E. coli*, different derivatives led to different extent of cell elongation (Figures 4.2A-E). The average cell length of *E. coli* was increased by 2.9-fold from 2.2 ± 1.3 μm to 6.3 ± 1.9 μm in the presence of **5-316**. Comparing to compound **5**, **5-705** and **5-706** showed a stronger inhibitory effect on the proliferation of *E. coli* cells. The average cell length of *E. coli* was increased by 4-fold, which was correlated with the antibacterial activity of these two compounds in Table 4.2 (MICs

= 36 μg/mL). The effects of **5** and **5-706** on the length of *B. subtilis* 168 and *E. coli* ATCC 25922 cells are shown in Figure 4.3. In the absence of compound **5** or **5-706**, the length of the *B. subtilis* 168 cells were found to be within 2-4 μm (80%) and 4-6 μm (20%) respectively. When the *B. subtilis* 168 cells were treated with **5** (88 μM), only 10% and 15% cells were found to be within 2-4 and 4-6 μm respectively. 75% of the cells were longer than 6 μm length. **5-706** produced a similar distribution of the *B. subtilis* cell length. The length of 65%, 34% and 1% of the *E. coli* cells were measured to be within 2-4, 4-6 and 6-8 μm respectively in the absence of compound **5** or **5-706**. The percentage of *E. coli* cells longer than 6 μm in the presence of **5-706** (50 μM) was higher than that in the presence of compound **5** (450 μM). The results showed that compounds **5** and **5-706** may inhibit bacterial proliferation by blocking cytokinesis.

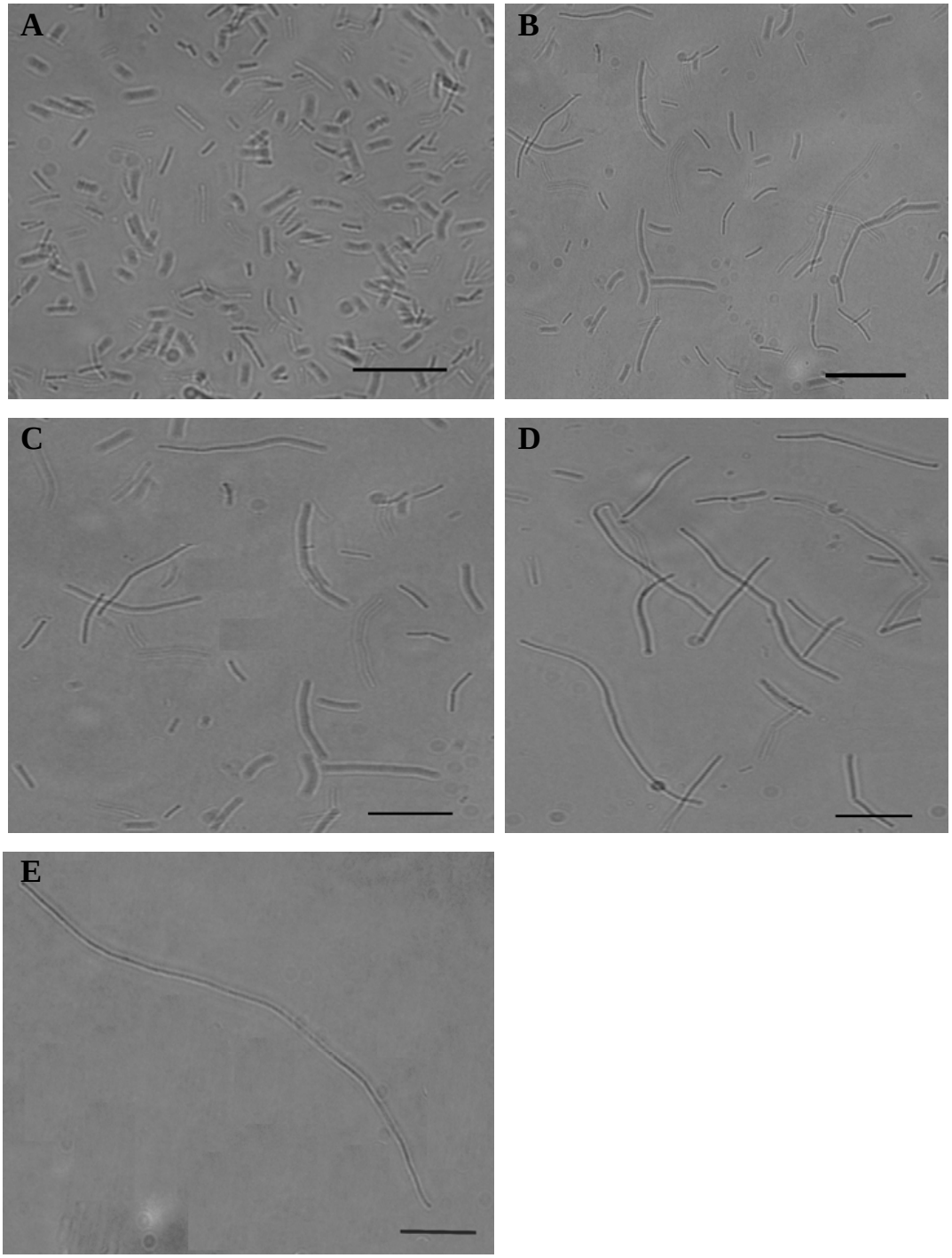

Figure 4.1 Effects of compound **5** derivatives on cell division and cell morphology. Cells of *B. subtilis* 168 was grown for 4 h in the absence (A) or presence of 31 μM of **5-316** (B), 29 μM of **5-387** (C), 25 μM of **5-705** (D) or 25 μM of **5-706** (E). The cells were visualized using a phase contrast microscope. The scale bar is 10 μm. The experiment was repeated 3 times.

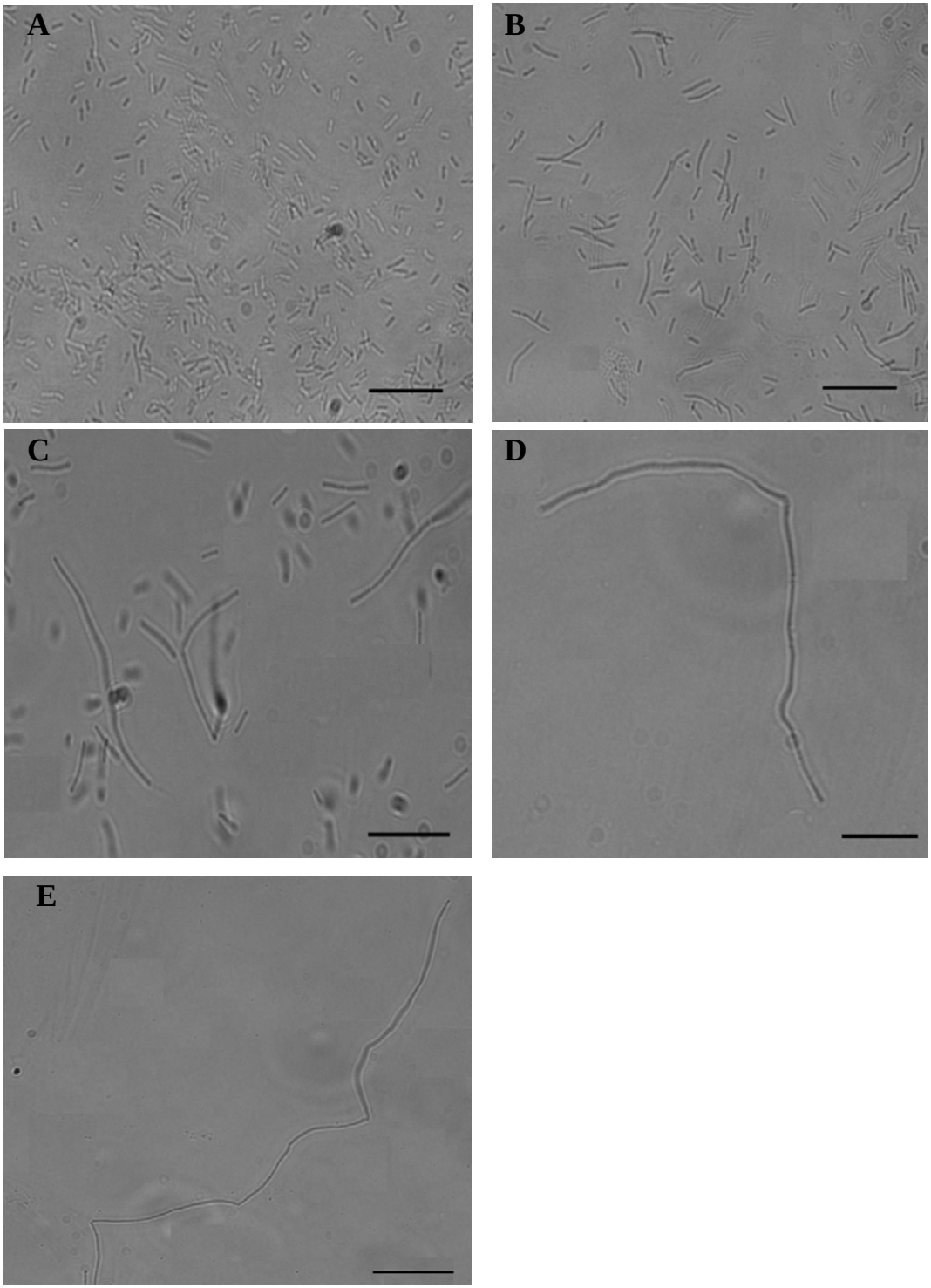

Figure 4.2 Effect of compound **5** derivatives on cell division and cell morphology. Cell of *E. coli* ATCC 25922 was grown for 4 h in the absence (A) or presence of 124 μM of **5-316** (B), 124 μM of **5-387** (C), 50 μM of **5-705** (D) or 50 μM of **5-706** (E). The cells were visualized using a phase contrast microscope. The scale bar is 10 μm. The experiment was repeated 3 times.

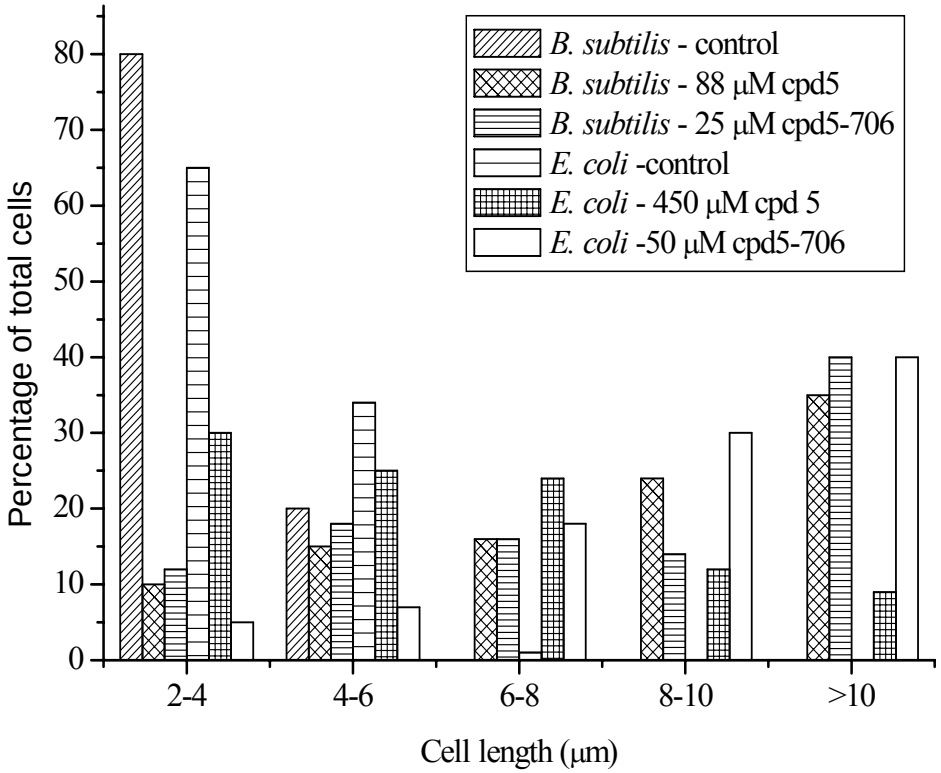

Figure 4.3 Compounds **5** and **5-706** induced cell elongation in *B. subtilis* 168 and *E. coli* ATCC 25922.

4.3.1.3 Membrane staining

That compound **5** does not perturb the membrane structures of *B. subtilis* and *E. coli* cells has been reported in section 2.3.4. The effects of the four derivatives, **5-316**, **5-387**, **5-705** and **5-706** on the membrane of both bacterial cells were also examined using the membrane-staining dye FM4-64. The results are shown in Figures 4.4-4.5. The fluorescence intensities across the membrane were found to be similar in the absence and presence of compounds. In spite of an increase in the average length of *B. subtilis* and *E. coli* cells, they were found not to induce detectable perturbation of cell membrane, demonstrating that they performed the antibacterial activity by targeting FtsZ rather than other cell membrane targets.

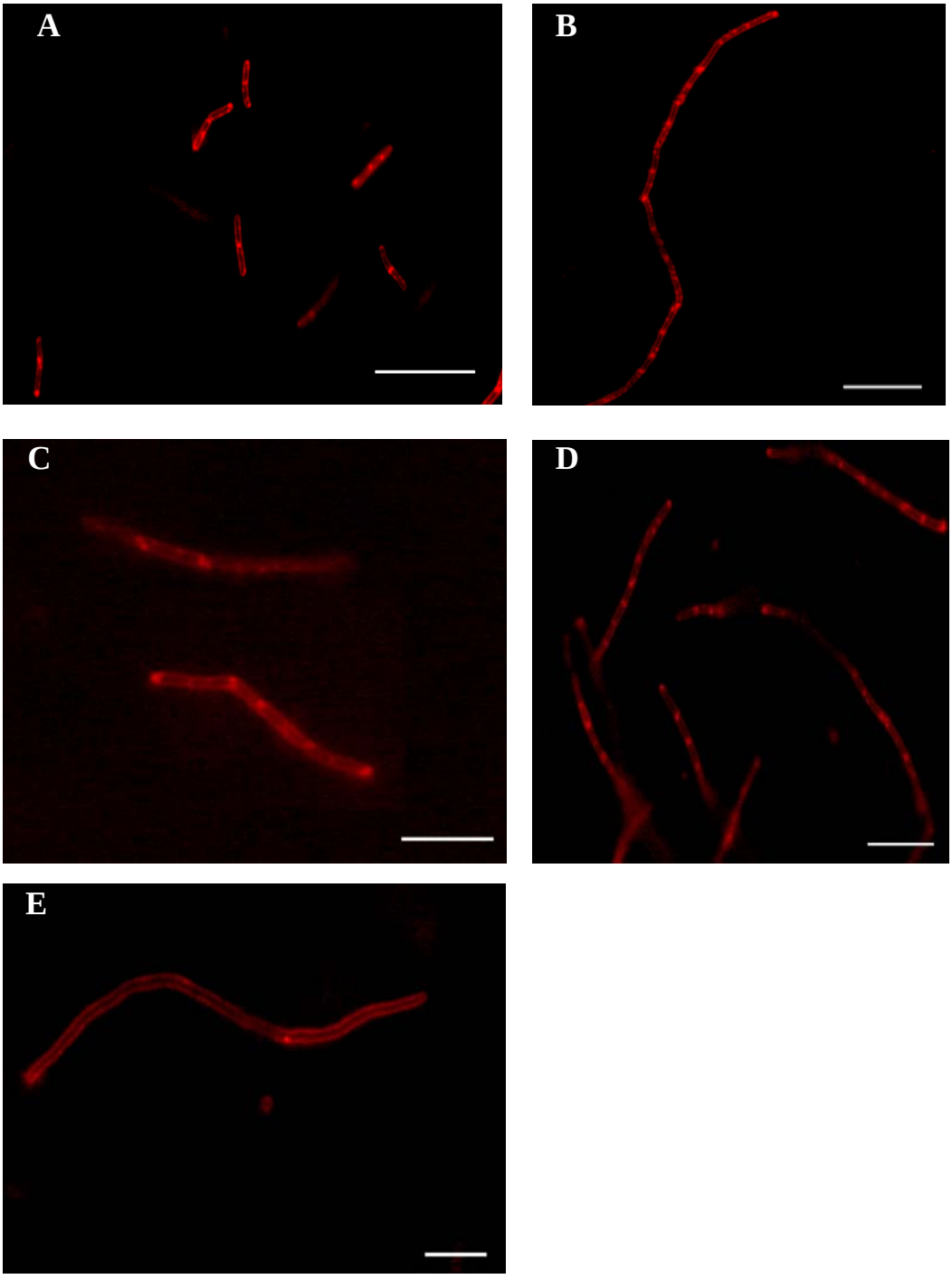

Figure 4.4 Effect of derivatives on the bacterial cell membrane. Cells of *B. subtilis* 168 were grown for 4 h in the absence (A) or presence of 31 μM of **5-316** (B), 29 μM of **5-387** (C), 49 μM of **5-705** (D) or presence of 51 μM of **5-706** (E). The cells were stained with the membrane stain FM4-64 for 30 min and visualized using a fluorescence microscope. The scale bar is 10 μm. The experiment was repeated 3 times.

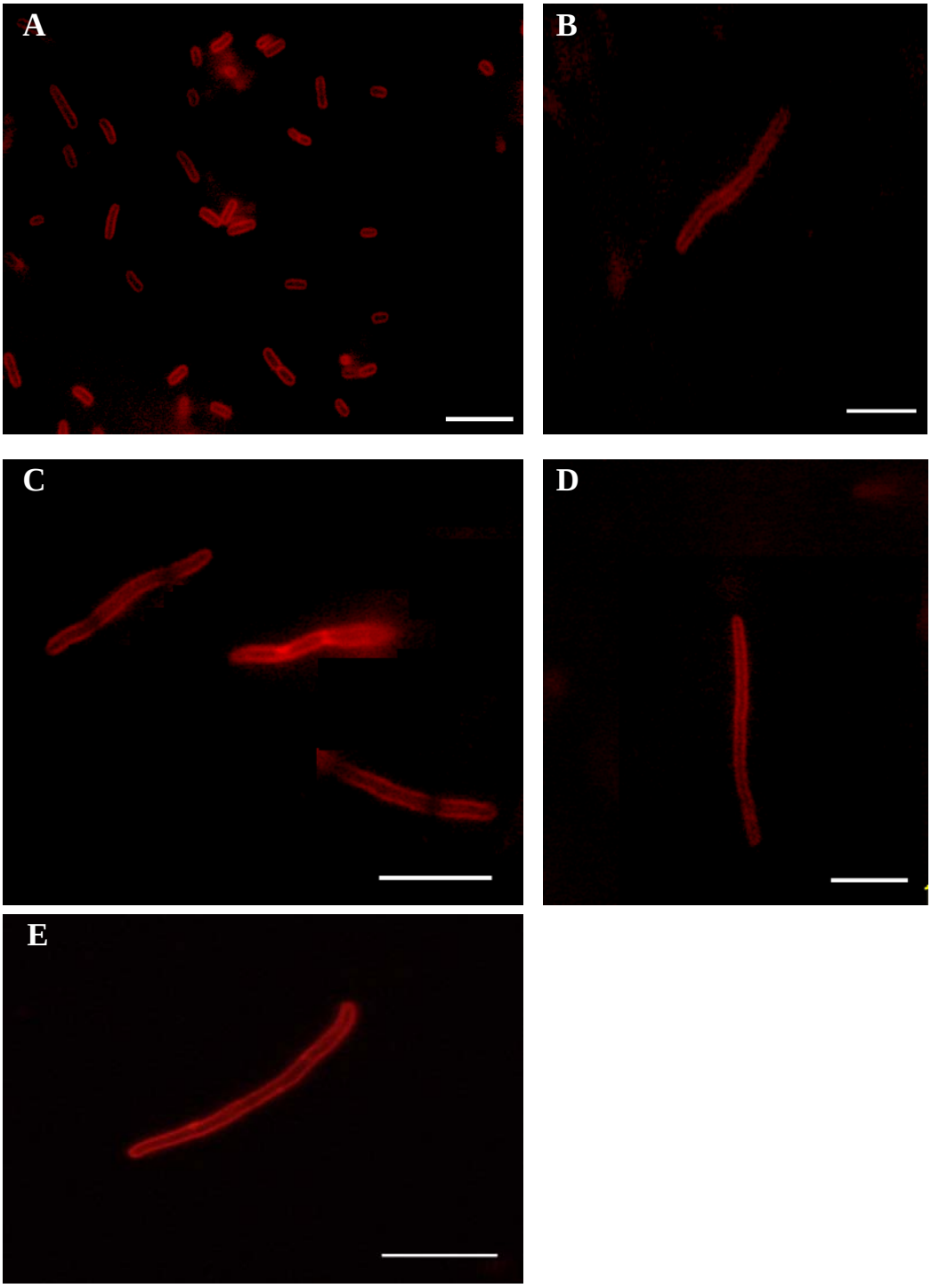

Figure 4.5 Effect of derivatives on the bacterial cell membrane. *E. coli* ATCC 25922 cells were grown for 4 h without (A) or with 124 μM of **5-316** (B) or in the presence of 115 μM of **5-387** (C), 49 μM of **5-705** (D) or 51 μM of **5-706** (E). The cells were stained with FM4-64 for 30 min and visualized using a fluorescence microscope. The scale bar is 10 μm. The experiment was repeated 3 times.

4.3.1.4 Visualization of Z-ring in the bacteria

The green fluorescence protein (GFP) FtsZ was used to trace the dynamic of FtsZ movement in *E. coli* JM109 (WM647) and to investigate the effect of derivatives on the Z-ring formation. In the absence of compound **5** derivatives, fluorescence microscopic observation showed integral Z-rings at the mid-cells (Figure 4.6A). On the contrary, GFP-FtsZ proteins were found to dispense randomly throughout the elongated *E. coli* cells in the presence of compound **5** derivatives (Figures 4.6B-E). Furthermore, compound **5** derivatives induced the cell elongation of *E .coli*. The average cell length of treated *E. coli* cells was increased by 2-fold in the presence of compound **5** or **5-316** and 3-fold in the presence of compound **5-706** (Table 4.3). The average of cell length of untreated cells was 3.9 ± 1.1 μm while those under the treatment of compounds **5**, **5-316** and **5-706** were found to possess average cell lengths of 7.6 ± 1.5, 8.5 ± 1.8 and 13.2 ± 1.4 μm, respectively. The percentage of derivative-treated cells possessing intact Z-rings was significantly reduced. For instance, the addition of compound **5-706** resulted in decreasing the percentage of cells having Z-rings from 93 % (0 μM) to 24 % (51 μM), indicating that **5-706** inhibited the septation process. Further, the frequency of Z-ring occurrence per unit cell length of *E. coli* cells were found to be 0.38 ± 0.01, 0.12 ± 0.01, 0.07 ± 0.02, and 0.05 ± 0.01 in the absence (control) and presence of compounds **5**, **5-316** and **5-706**, respectively (Table 4.3). These four selected derivatives, **5-316**, **5-387**, **5-705** and **5-706**, are similar to other known FtsZ inhibitors targeting the dynamic assembly of FtsZ [66, 67, 76, 78, 80, 81, 203]. For

example, sanguinarine induced filamentation in bacteria and perturbed dynamic Z-ring formation in *B. subtilis* 168 [66]. In this study, **5-316**, **5-387**, **5-705** and **5-706** were found to strongly inhibit the formation of the cytokinetic Z-ring.

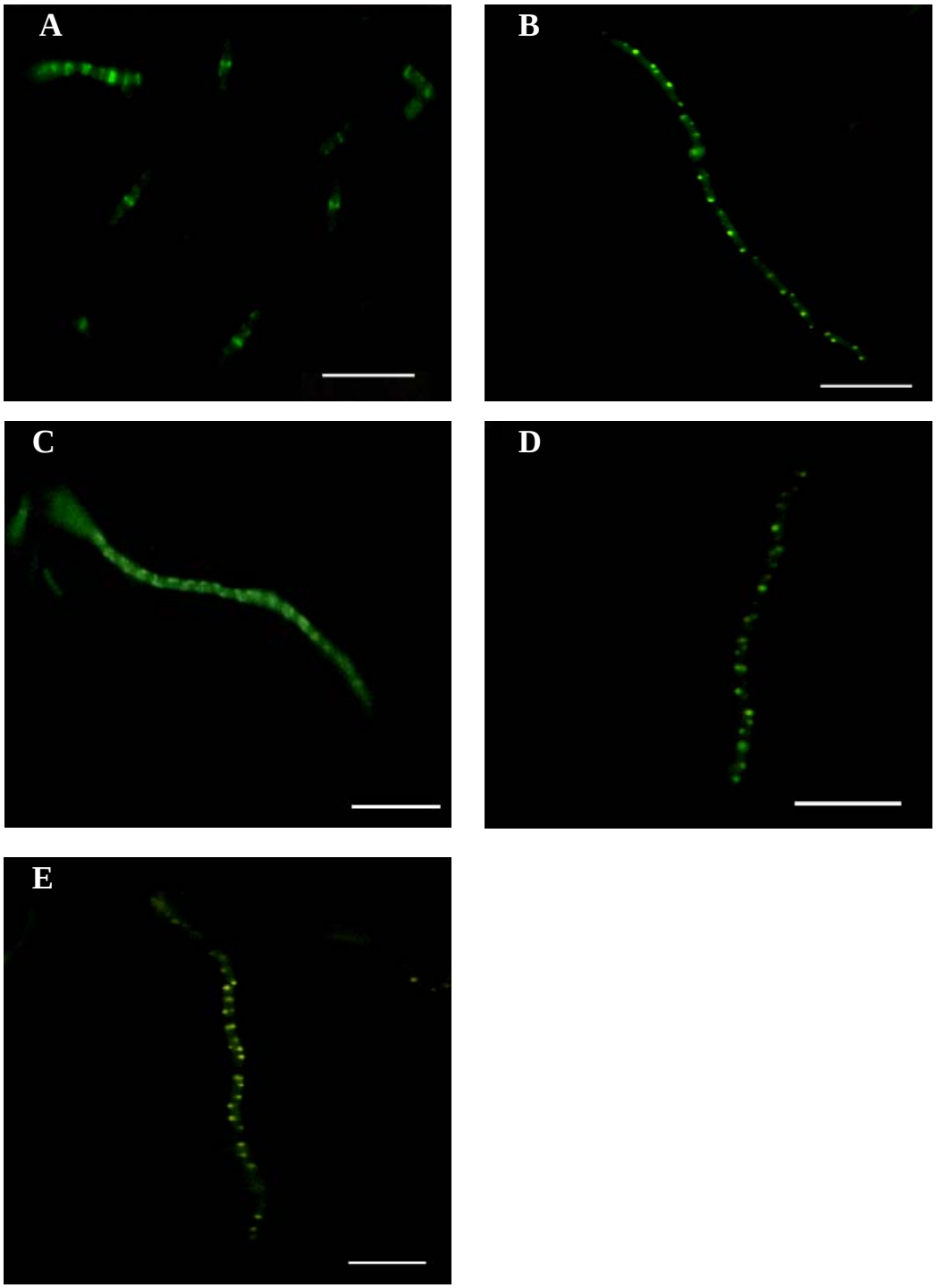

Figure 4.6 Perturbation of cytokinetic Z-ring in *E. coli*. *E. coli* (JM109 WM647) cells were grown in the absence (A) or presence of 62 μM **5-316** (B), 56 μM of **5-387** (C), 49 μM of **5-705** (D) or 51 μM of **5-706** (E). The scale bar is 10 μm. The experiment was repeated 3 times.

Table 4.3 Effects of compound **5** and derivatives on the Z-rings of *E. coli* cells

Description	Control	**5** (224 μM)	**5-316** (62 μM)	**5-706** (51 μM)
Cell length	3.9 ± 1.1 μm	7.6 ± 1.5 μm	8.5 ± 1.8 μm	13.2 ± 1.4 μm
% of cells having a Z-ring[a]	93	30	45	24
Frequency of Z-rings per μm	0.38 ± 0.01	0.12 ± 0.01	0.07 ± 0.02	0.05 ± 0.01

[a] 100 cells were counted to calculate the frequency of occurrence of Z-rings

4.3.1.5 Immunofluorescence microscopy

The effect of derivatives on the cytokinetic Z-ring and DNA organization in *B. subtilis* 168 were investigated using anti-FtsZ antibodies and DAPI fluorescent stain (Figures 4.7 and 4.8). The findings showed that the four selected derivatives not only decreased the frequency of Z-ring occurrence per micrometer of cell length, they also inhibited the morphology of the remaining Z-rings (Figures 4.7C, F, I and 5.8C and F). But they were found not to perturb the DNA condensation and nucleoid segregation (Figures 4.7B, E, H and 4.8 B, E). Among the derivatives, **5-706** was found to be the most potent FtsZ inhibitor. Thus, the effect of **5-706** on the cytokinetic Z-ring and chromosome organization was further investigated and the results are summarized in Table 4.4. It was shown that most of the control cells contained two nucleotides. For example, the percentage of control cells containing one, two and more than four nucleotides were 8%, 80% and 12%, respectively. A total of 72% of the control cells was found to contain two well-defined nucleotides (Table 4.4). On the contrary, only 25% of the cells had two well-defined nucleotides in the presence of **5-706** (Table 4.4). Interestingly, the percentage of cells containing two nucleoids was greatly decreased in the presence of **5-706**. The cells treated by **5-706** containing one, two and more than four nucleotides were found to be 0%, 15% and 85%, respectively. The number of nucleoids per micrometer of the cell length in the absence and presence of **5-706** (Table 4.4) were found to be similar. For example, the number of nucleoids per micrometer of the cell length were determined to be 0.51 ± 0.01 in the control and 0.49 ± 0.01 in the presence 51 μM **5-706**. The results together implied that **5-706** inhibited the formation of the Z-ring without influencing the nucleoid segregation.

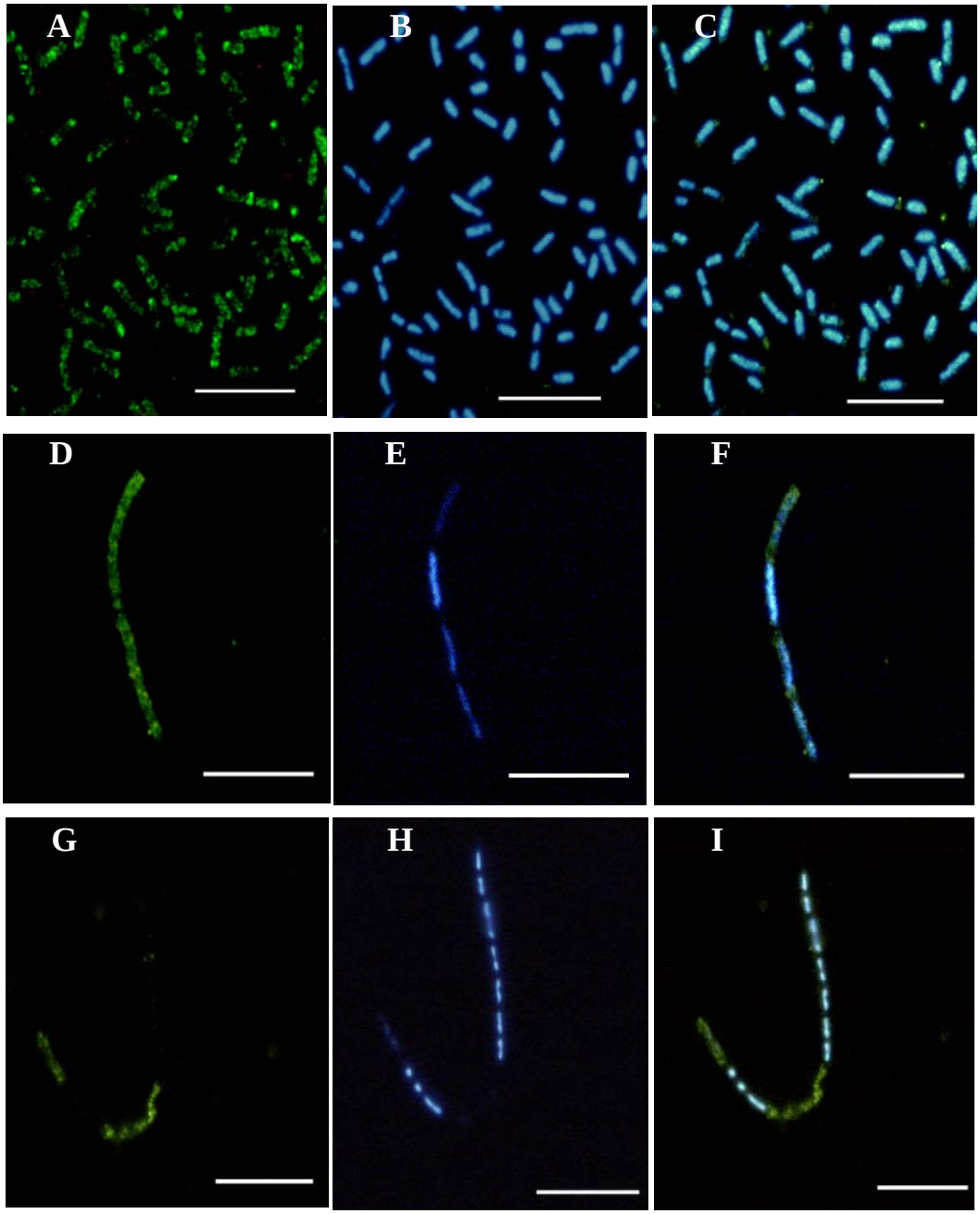

Figure 4.7 Effects of derivatives on the Z-ring and nucleoid segregation in *B. subtilis* 168. Cells were immunostained with polyclonal anti-FtsZ rabbit antibody followed by FITC-conjugated goat anti-rabbit secondary antibody for the observation of Z-ring and stained with 1 μg/ml DAPI to observe the nucleotides. The cells (A and B) and overlay (C) were in the absence of derivative. The cells (D and E) and overlay (F) were treated with 12 μg/mL **5-316**. The cells (G and H) and overlay (I) were treated with 12 μg/mL **5-387.** The Z-rings and nucleotide are shown in green and blue respectively. They were visualized under a fluorescence microscope with 100× oil immersion len. The scale bar is 10 μm. The experiment was repeated 3 times.

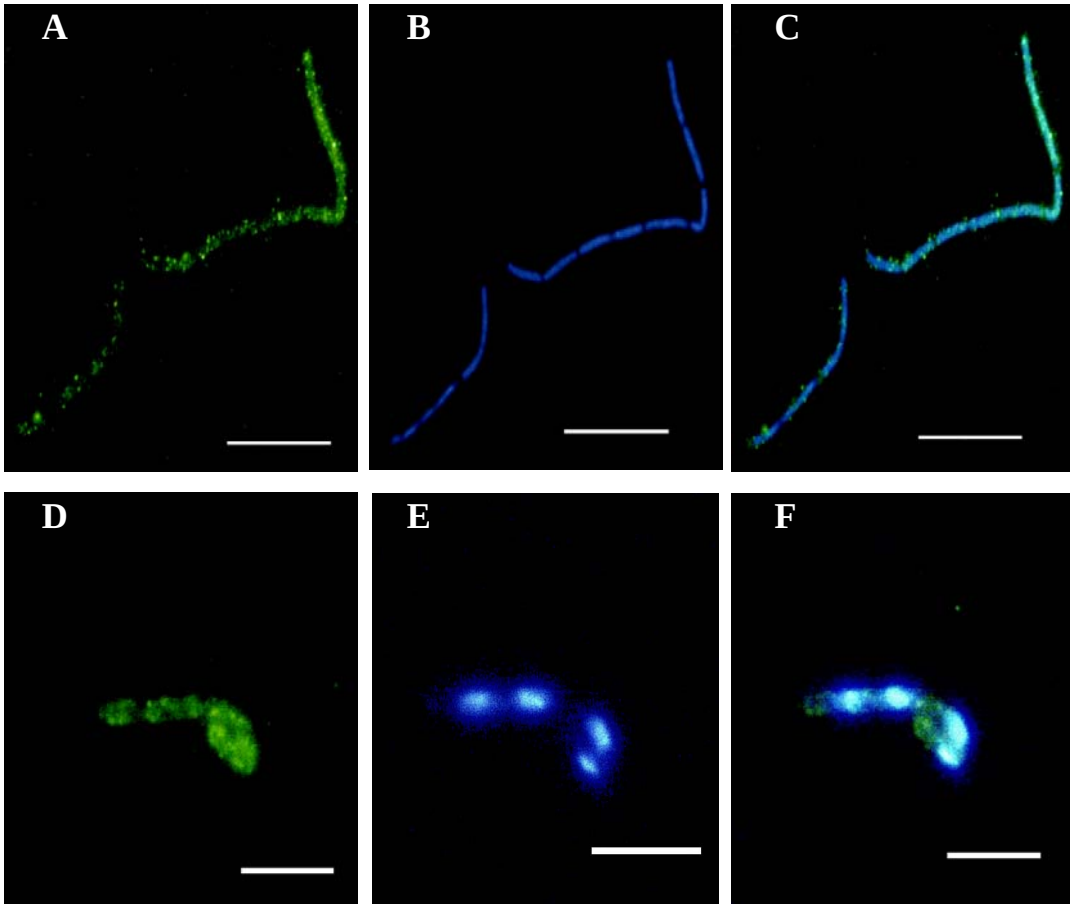

Figure 4.8 Effects of derivatives on the Z-ring and nucleoid segregation in *B. subtilis* 168. Cells were immunostained with polyclonal anti-FtsZ rabbit antibody followed by FITC-conjugated goat anti-rabbit secondary antibody for the observation of Z-ring and stained with 1 μg/mL DAPI to observe the nucleotides. The cells (A and B) and overlay (C) were treated with 49 μM (12 μg/mL) **5-705.** The cells (D and E) and overlay (F) were in the presence of 51 μM (12 μg/mL) **5-706**. The Z-rings and nucleotide are shown in green and blue respectively. They were visualized under a fluorescence microscope with 100× oil immersion len. The scale bar is 10 μm. The experiment was repeated 3 times.

Table 4.4 Effects of compound **5-706** on the Z-ring and nucleotides of *B. subtilis* 168 [a]

Description	Control	**5-706** (51 μM)
Cell length	3.9 ± 1.1 mm	13.2 ± 1.4 mm
% of cells having a Z-ring	72	25
frequency of Z-rings/μm of the cell length	0.27 ± 0.01	0.02 ± 0.01
frequency of nucleoids/μm of the cell length	0.51 ± 0.01	0.49 ± 0.01
% of cells containing two nucleoids	79	40
% of cells containing two nucleoids having a Z-ring	85	20
frequency of Z-ring/ μm of the cells containing two nucleoids	0.22 ± 0.01	0.04 ± 0.01

[a] 200 cells were counted in both cases.

4.3.2 *In vitro* assays

4.3.2.1 Light scattering assay

The effects of **5-316**, **5-705** and **5-706** on FtsZ assembly were studied by measuring the change of light scattering signal at 600 nm. The results are shown in Figures 4.9-4.11. The observations were similar to that obtained with compound **5** (Figure 2.12). The addition of compound **5-316** or **5-705** or **5-706** decreased the magnitude of light scattering signal, suggesting that they inhibited the assembly and bundling of FtsZ protofilaments *in vitro*.

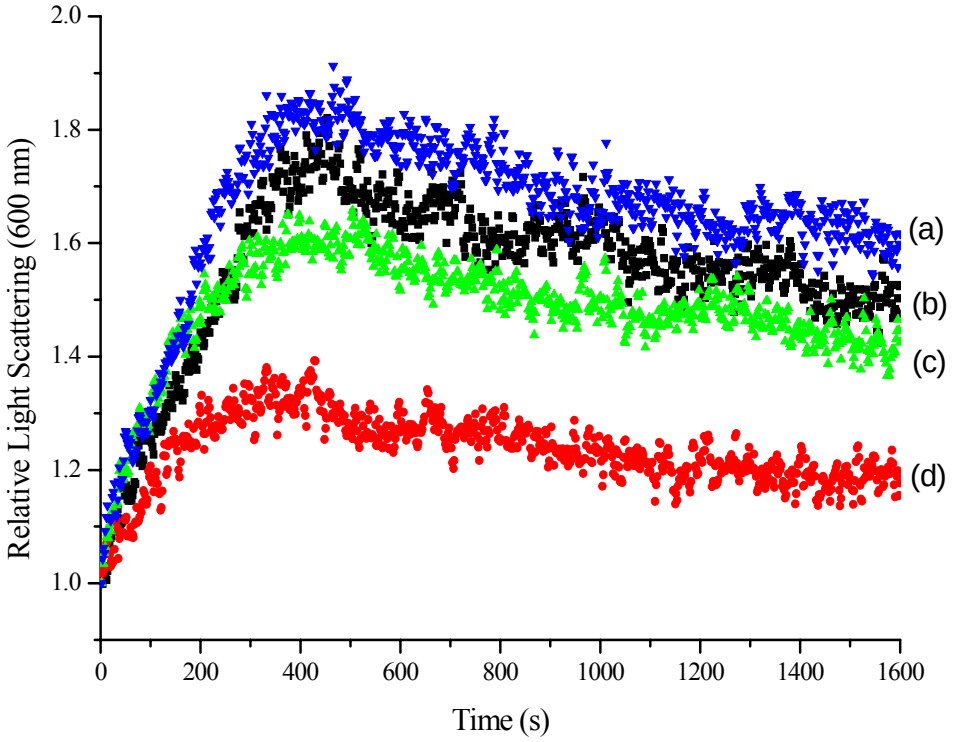

Figure 4.9 Effect of **5-316** on FtsZ assembly *in vitro*. *Sa*FtsZ (12 μM) was polymerized in 50 mM MOPS, pH 6.5, 50 mM KCl, 10 mM $MgCl_2$ and 1 mM GTP in the absence of (a), and the presence of 30 μM (b), 50 μM (c) and 70 μM (d) of **5-316**. Appropriate blanks were subtracted from all the traces. The experiment was repeated three times.

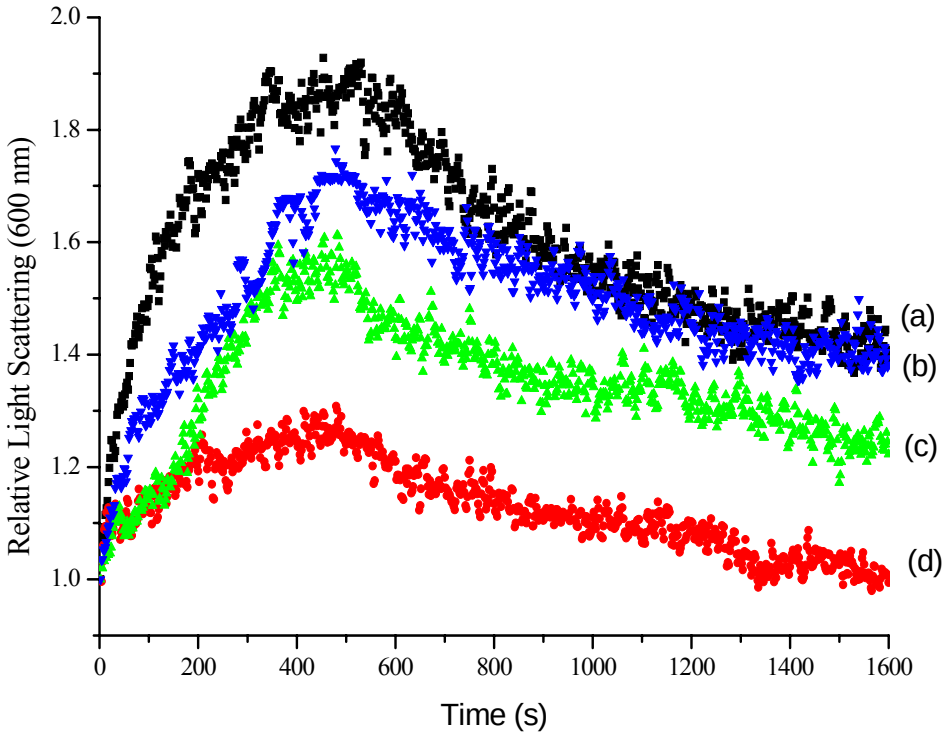

Figure 4.10 Effect of **5-705** on FtsZ assembly *in vitro*. *Sa*FtsZ (12 μM) was polymerized in 50 mM MOPS, pH 6.5, 50 mM KCl, 10 mM $MgCl_2$ and 1 mM GTP in the absence of (a), and the presence of 50 μM (b), 70 μM (c) and 100 μM (d) of compound **5-705**. Appropriate blanks were subtracted from all the traces. The experiment was repeated three times.

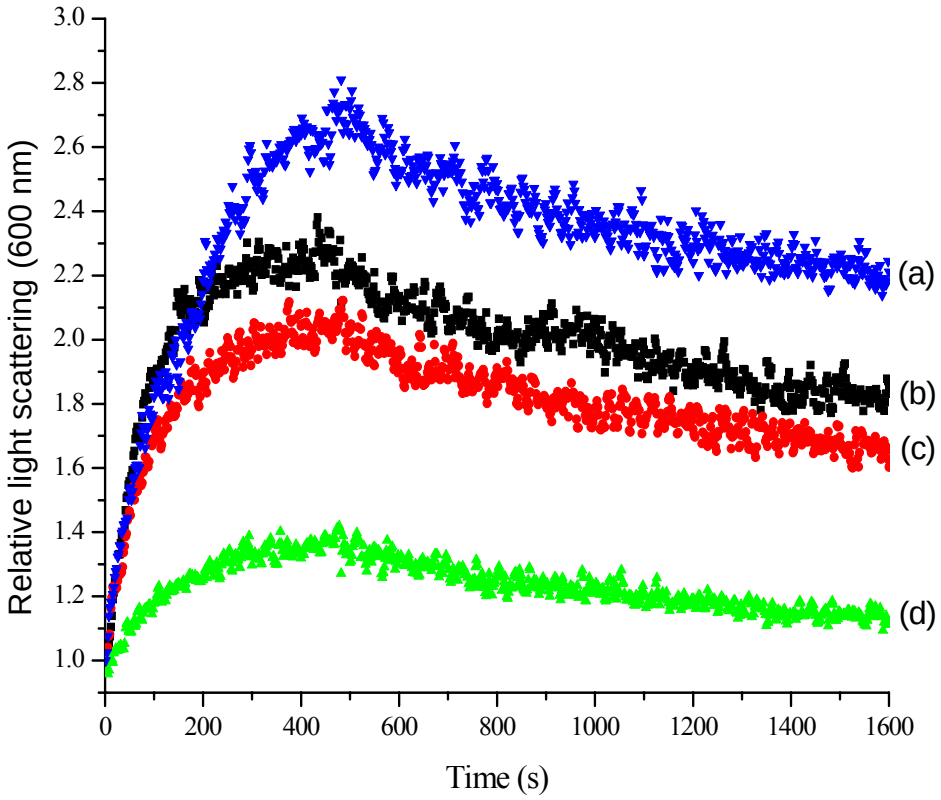

Figure 4.11 Effect of **5-706** on FtsZ assembly *in vitro*. *Sa*FtsZ (12 μM) was polymerized in 50 mM MOPS, pH 6.5, 50 mM KCl, 10 mM $MgCl_2$ and 1 mM GTP in the absence of (a), and the presence of 50 μM (b), 70 μM (c) and 100 μM (d) of **5-706**. Appropriate blanks were subtracted from all the traces. The experiment was repeated three times.

4.3.2.2 GTPase activity

The antibacterial activities of the compound **5** derivatives were determined by measuring the MIC values. To verify the mechanism of inhibition of several derivatives that were found to effectively inhibit the bacterial growth *in vivo*, the inhibition ability of these compounds were tested against the GTPase activities of *Sa*FtsZ and *Ec*FtsZ *in vitro*. The IC_{50} values of these compounds are summerized in Table 4.5. All compounds demonstrated a linear decrease in the GTPase activity with an increase in concentration. For instance, the concentration-response curves for compounds **5-316** and **5-387** against *Sa*FtsZ are shown in Figure 4.12. Regarding **5-701**, **5-702**, **5-705** and **5-706**, the concentration-response curves against *Sa*FtsZ and *Ec*FtsZ are displayed in Figures 4.13-14 respectively. As shown in Table 4.5, compounds **5-254**, **5-306**, **5-307**, **5-312** and **5-324** were found to exert a low affinity against both forms of FtsZ, they exhibited IC_{50} values of >500 μg/mL. Other derivatives inhibited the GTPase activity of *Sa*FtsZ with the IC_{50} values between 34.4 and 478.5 μg/mL. These compound **5** derivatives inhibited the GTPase activity of *Ec*FtsZ with IC_{50} values between 40.9 and 302.4 μg/mL. Among these derivatives, **5-706** displayed the greatest inhibitory activity against both *Sa*FtsZ and *Ec*FtsZ with IC_{50} values of 34.4 ± 5.6 μg/mL (72.4 μM) and 40.9 ± 4.6 μg/mL (86.1 μM) respectively; **5-706** showed a 15-fold lower affinity than **5**. **5-387** was less potent than **5-706** with IC_{50} values of 47.7 ± 12.6 and 105.5 ± 16.8 μg/mL against *Sa*FtsZ and *Ec*FtsZ respectively. The other derivatives in Table 4.5 displayed a weak inhibition on *Sa*FtsZ and *Ec*FtsZ GTPase activities (IC_{50} >500 μg/mL). Compound

5-655, bearing a pyrazole-linked quinuclidine, was unable to inhibit the GTPase activity of *Ec*FtsZ and *Sa*FtsZ with IC_{50} >500 μg/mL.

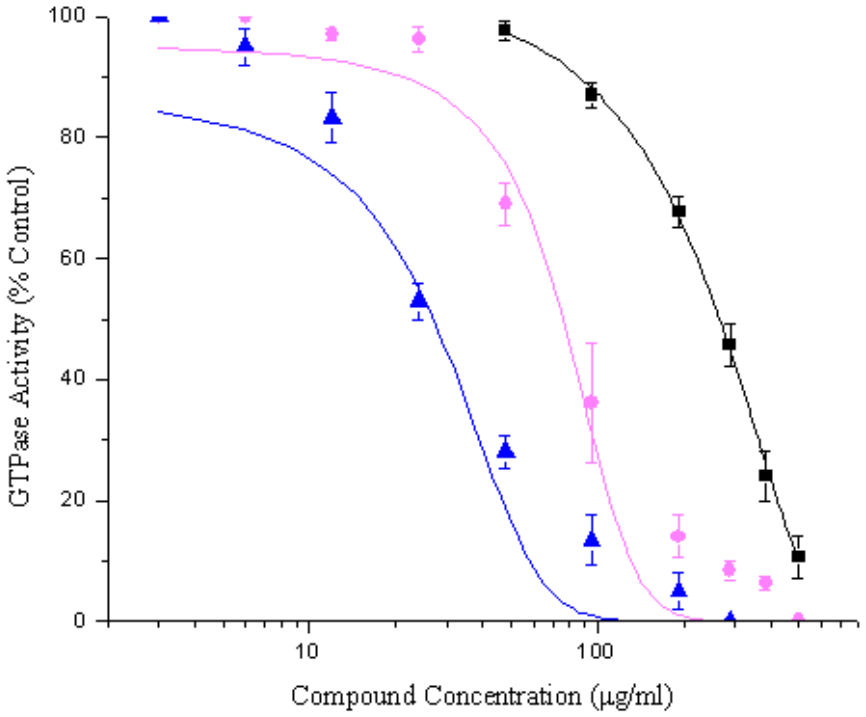

Figure 4.12 Concentration-response curve of **5** (■), **5-316** (●) and **5-387** (▲) tested against *Sa*FtsZ. Each point represents the mean of three independent assays, and the vertical bars show the standard derivation of the mean. The data were plotted and IC_{50} was calculated by nonlinear regression using a sigmoidal concentration-response curve (Origin Software).

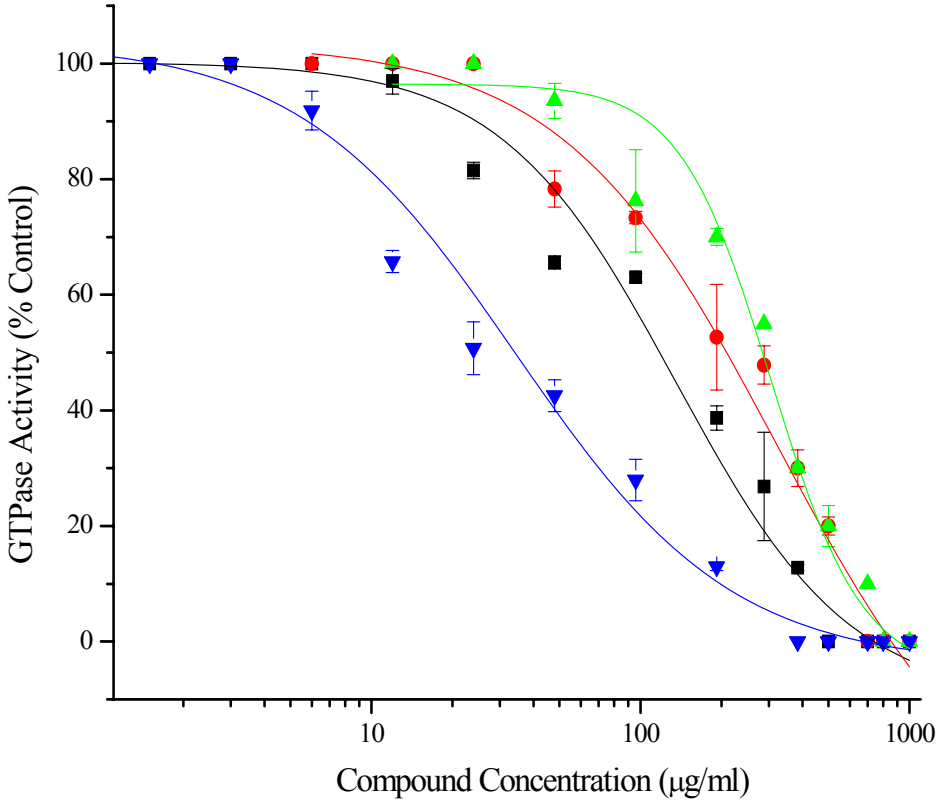

Figure 4.13 Concentration-response curve of **5-701** (■), **5-702** (●), **5-705** (▲) and **5-706** (▼) tested against *Sa*FtsZ. Each point represents the mean of three independent assays, and the vertical bars show the standard derivation of the mean. The data were plotted and IC_{50} was calculated by nonlinear regression using a sigmoidal concentration-response curve (Origin Software).

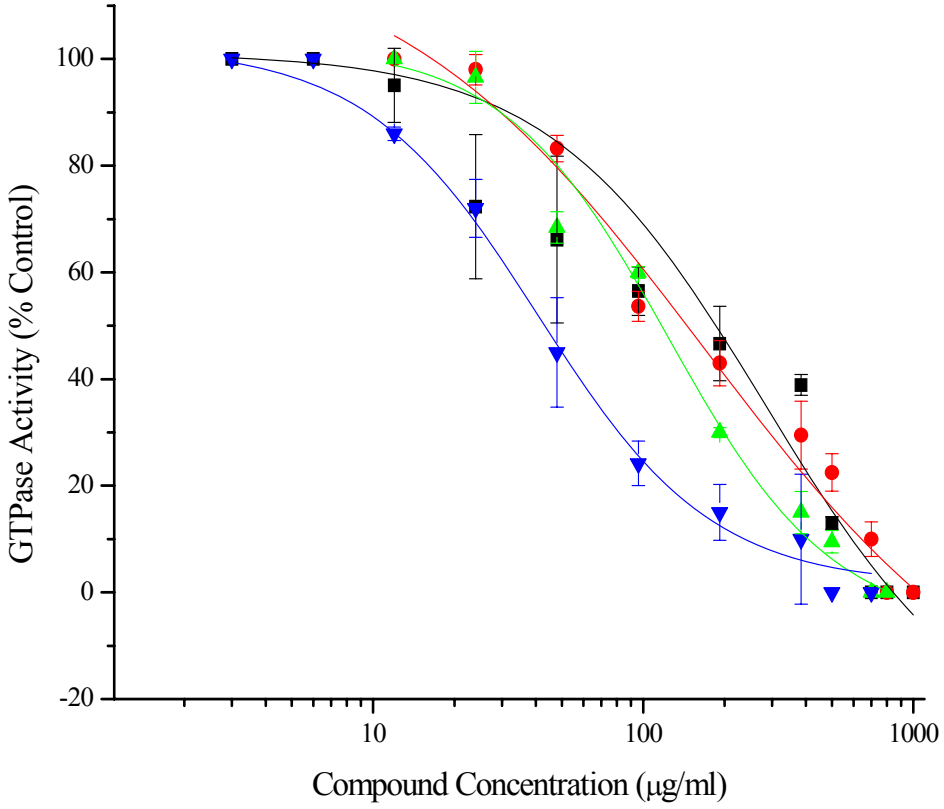

Figure 4.14 Concentration-response curve of **5-701** (■), **5-702** (●), **5-705** (▲) and **5-706** (▼) tested against *Ec*FtsZ. Each point represents the mean of three independent assays, and the vertical bars show the standard derivation of the mean. The data were plotted and IC_{50} was calculated by nonlinear regression using a sigmoidal concentration-response curve (Origin Software).

Table 4.5 IC_{50} values of compound **5** and selected derivatives against *Sa*FtsZ and *Ec*FtsZ

	IC_{50} ± SEM[a] (μg/mL)	
Compound	*S. auerus* FtsZ	*E. coli* FtsZ
5	145.0 ± 37.2	221.5 ± 19.7
5-254	>500	>500
5-256	346.3 ± 38.7	302.4 ± 22.5
5-306	>500	>500
5-307	>500	>500
5-312	>500	>500
5-315	478.5 ± 20.4	258.6 ± 10.4
5-316	180.5 ± 9.8	192.0 ± 20.8
5-320	>500	>500
5-324	>500	>500
5-326	250.2 ± 11.8	192.5 ± 14.5
5-387	47.7 ± 12.6	105.5 ± 16.8
5-701	135.4 ± 14.2	283.5 ± 13.5
5-702	323.1 ± 19.4	166.6 ± 25.6
5-705	305.6 ± 13.2	123.5 ± 19.5
5-706	34.4 ± 5.6	40.9 ± 4.6

[a] SEM: standard error of the mean

4.3.2.3 Transmission electron microscopy

The effect of compounds **5-316**, **5-705** and **5-706** on the assembly of *S. auerus* FtsZ were analysed by transmission electron microscopy (TEM) (Figures 4.15-4.17). Electron microscopic images showed that these three compounds inhibited FtsZ protofilaments in a dose-dependent manner. In the absence of derivatives, a dense network of FtsZ protofilaments was observed (Figures 4.15-4.17A). The three derivatives were found to drastically reduce the size and thickness of FtsZ polymers and the bundling of FtsZ protofilaments with increasing concentrations. Compounds **5-316** (124 μM), **5-705** (99 μM) and **5-706** (50 μM) reduced the thickness of the bundles of FtsZ protofilaments by 50% (Figures 4.15B, 4.16C and 4.17C respectively). For instance, **5-706** (50 μM) reduced the thickness of FtsZ protofilaments from 118 ± 21 to 60 ± 12 nm. Among the three derivatives, **5-706** was found to be the most potent derivative to inhibit the bundling of FtsZ protofilaments (Figure 4.17C). Only a few straight, short and thin FtsZ filaments were observed in the presence of **5-706** (50 μM) (Figure 4.17B). On the contrary, **5-316** (62 μM) and **5-705** (49 μM) were found not to completely inhibit the polymerization and bundling of FtsZ protofilament (Figures 4.15C and 4.16D respectively). These results together suggested that the reduction in bundling and thickness of FtsZ protofilaments were caused by weakening the lateral interaction between FtsZ protofilaments and the interaction between FtsZ monomers.

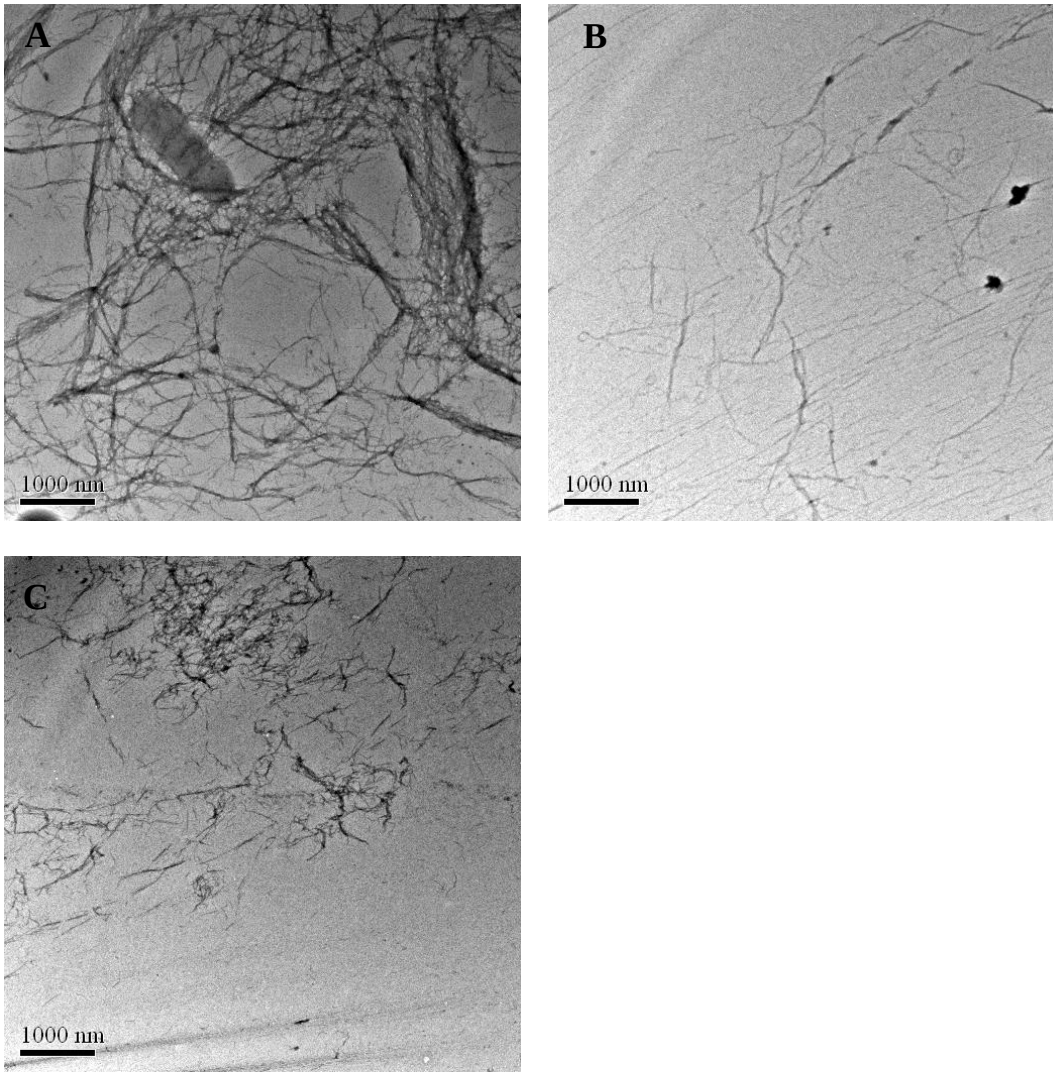

Figure 4.15 Electron micrographs of FtsZ polymers. *Sa*FtsZ (12 μM) was polymerized in 50 mM MOPS buffer, pH 6.5, containing 50 mM KCl, 5 mM $MgCl_2$, and 1 mM GTP in the absence and presence of **5-316** for 15 min at 37 ^{o}C. Shown are the electron micrographs of FtsZ polymers formed in the absence (A) and presence of 124 μM (B) and 31 μM (C) **5-316**. The scale bar = 1000 nm.

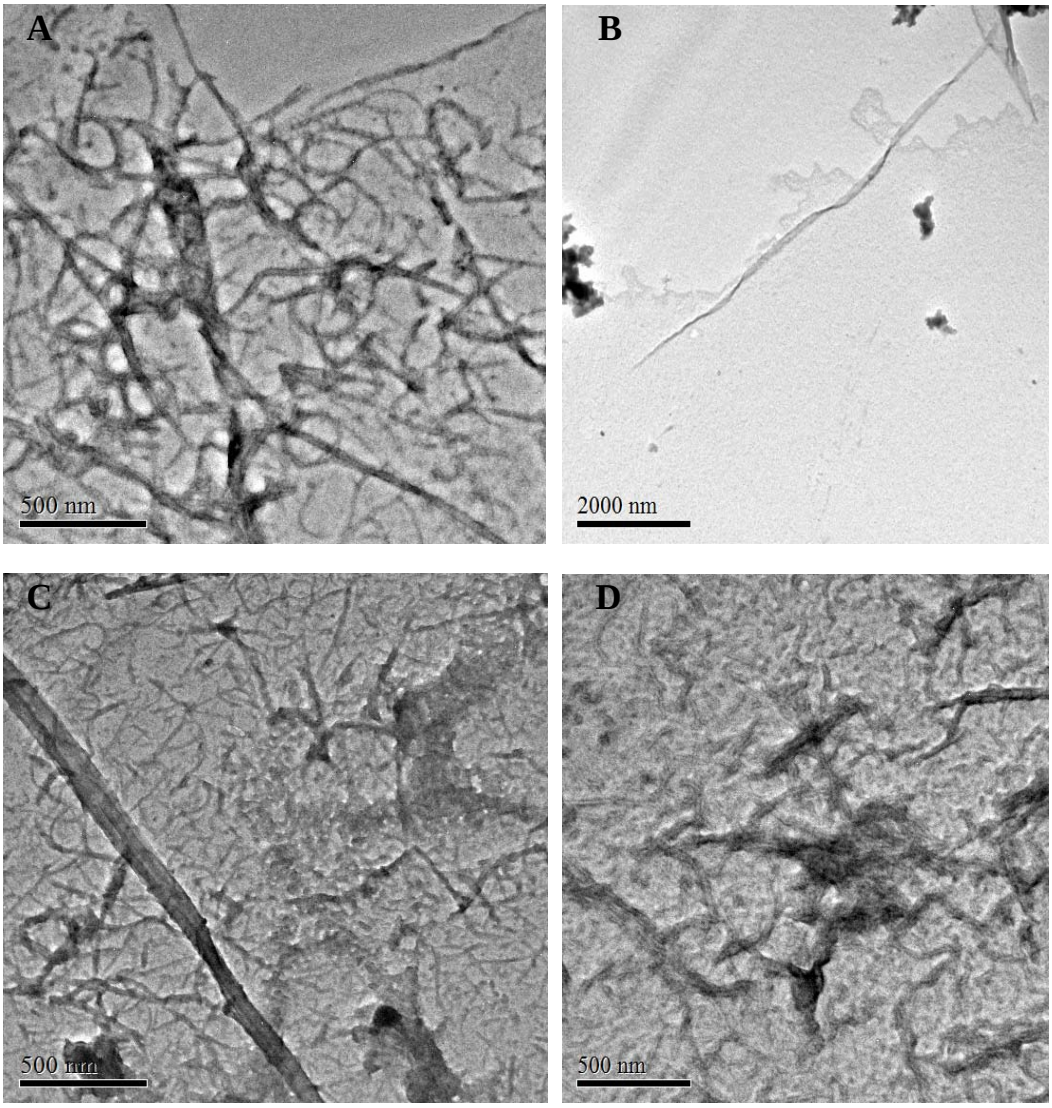

Figure 4.16 Electron micrographs of FtsZ polymers. *Sa*FtsZ (12 μM) was polymerized in 50 mM MOPS buffer, pH 6.5, containing 50 mM KCl, 5 mM $MgCl_2$, and 1 mM GTP in the absence and presence of **5-705** for 15 min at 37 ^{o}C. Shown are the electron micrographs of FtsZ polymers formed in the absence (A) and presence of 100 μM (B), 50 μM (C) and 25 μM (D) **5-705**. The scale bar of A and B = 500 nm. The scale bar of C = 1000 nm.

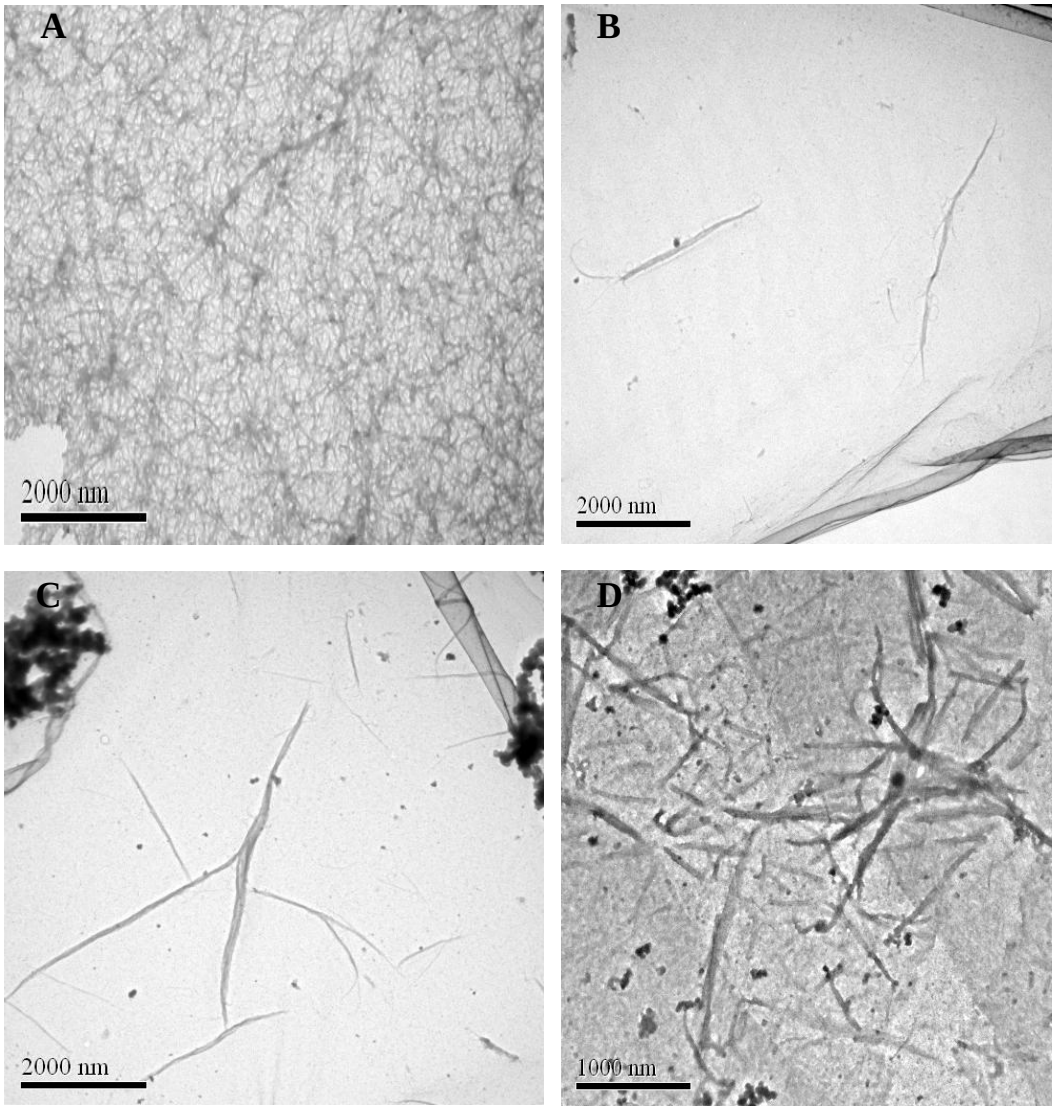

Figure 4.17 Electron micrographs of FtsZ polymers. *Sa*FtsZ (12 μM) was polymerized in 50 mM MOPS buffer, pH 6.5, containing 50 mM KCl, 5 mM $MgCl_2$, and 1 mM GTP in the absence and presence of **5-706** for 15 min at 37 ^{o}C. Shown are the electron micrographs of FtsZ polymers formed in the absence (A) and presence of 100 μM (B), 50 μM (C) and 25 μM (D) **5-706**. The scale bar of A, B and C = 2000 nm. The scale bar of D = 1000 nm.

4.3.2.4 Tubulin polymerization assay

The effects of **5-705** and **5-706** on mammalian tubulin polymerization are summarized in Figure 4.18. Clear-cut polymerization behavior was observed in the presence of 50 μM of compounds **5-705** and **5-706**, indicating that they did not influence the mammalian tubulin polymerization *in vitro*. Same as before, paclitaxel (a tubulin enhancer) and vinblastine (a tubulin inhibitor) were used as the positive and negative controls respectively.

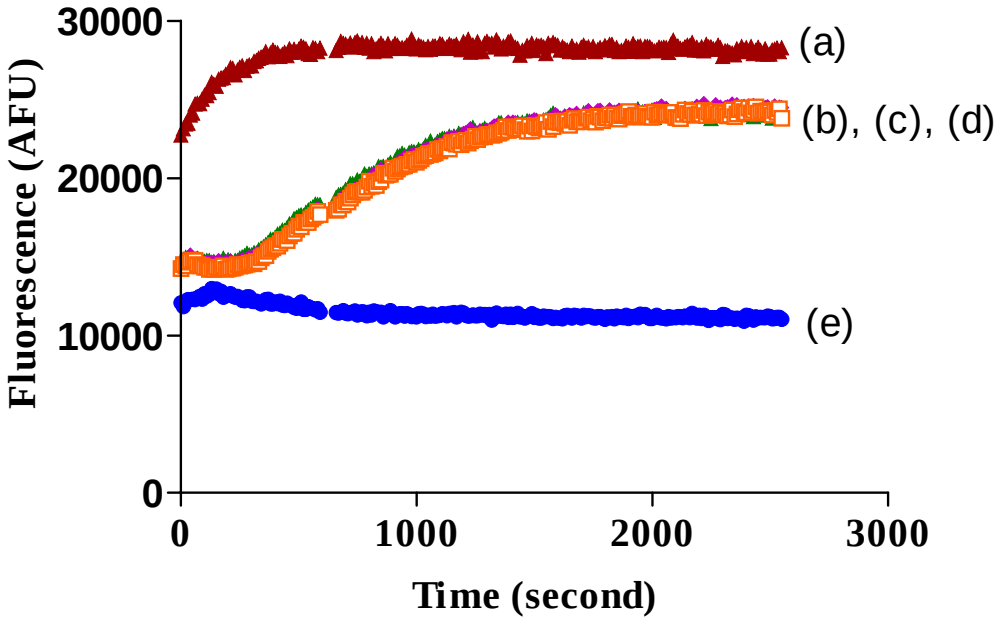

Figure 4.18 Effect of **5-705** and **5-706** on the polymerization of mammalian tubulin. The tubulin polymerization assay was performed under the presence of 20 μM paclitaxel (a tubulin enhancer) (a), 50 μM compound **5-705** (b), 50 μM **5-706** (c), DMSO only (d) and 3 μM vinblastine (a tubulin inhibitor) (e). The polymerization of mammalian tubulin was monitored by the increase in the Absolute Fluorescence Units (AFU) for 40 minutes.

4.3.2.5 Cytotoxicity

A variety of *in vitro* and *in vivo* tests have been carried out on FtsZ to determine the potency of compound **5** derivatives. Here, we also investigated the toxicity effect of the four compounds **5-316**, **5-387**, **5-705** and **5-706** on three cell lines using *in vitro* cytotoxicity assay (Table 4.6). In this assay, tetrazolium salts (MTS) was reduced to intensely coloured formazan dyes by mitochondrial activity that can be used to measure cellular metabolic function. Compounds **5-316**, **5-387**, **5-705** and **5-706** were found to exert toxic effects. They inhibited the proliferation of mouse fibroblast cells (L929 cell line) in a concentration-dependent manner with IC_{50} of 85.2, 116.5, 35.1 and 36.1 μM respectively. Regarding the inhibition of the proliferation of canine kidney cells of MDCKII cell line, the IC_{50}s of compounds **5-316**, **5-387**, **5-705** and **5-706** are 125.8, 99.1, 37.2 and 41.6 μM respectively. The toxicity effect of **5-316**, **5-387**, **5-705** and **5-706** were also examined on the human embryonic kidney cells (HEK293/pcDNA3.1 cell line) with IC_{50}s of 106.9, 161.8, 36.2 and 38.4 μM respectively. In contrast, 50% inhibition of *S. aureus* proliferation (MIC_{50}) occurred in the presence of 164.9 μM **5-316**, 71.6 μM **5-387**, 30.8 μM **5-705** and 19.1 μM **5-706**. These derivatives were found to show cytotoxicity effects on mammalian cell lines. The MIC_{50} of **5-316** on the bacterial inhibition was 2-fold higher than IC_{50} on the proliferation of three cell lines exhibiting a toxic effect. Although the MIC_{50} values of compounds **5-387**, **5-705** and **5-706** are the same or lower than those on the IC_{50} of three mammalian cell lines, they still contributed a significant toxicity effect as the acceptable ratio of MIC_{50} (bacterial inhibition) vs

IC_{50} (cytotoxicity) should be at least 1:10. There are several reasons to cause the toxicity of compounds. One possible reason is toxic metabolites. Some functional groups are more susceptible to chemical and enzymatic degradation than others, which may trigger metabolism-induced toxicity. For example, the methyl group on the pyridimine ring of compounds **5-316**, **5-387** and **5-705** are often oxidized to carboxylic acid. Compounds **5-316** and **5-705** have a thiophene ring whereas compounds **5-387** and **5-706** have a liable furan ring. These two functionalities are easily activated to electrophilic species. The literature reported that the thiophene ring of tienilic acid, a uricosuric diuretic drug used in the treatment of hypertension [204], was shown to be metabolized to the S-oxide by the liver protein cytochrome P450, which cause hepatotoxic effect. Compounds containing the furan ring have been reported to exert a toxic effect to both the lung and liver of the rat by forming convalent bond to protein and nucleic acids in the cell [205].

Table 4.6 IC_{50} determination in the susceptibility test and the cytotoxicity test

Compound	IC_{50} (μM)		Cytotoxicity (IC_{50}, μM)	
	S. aureus ATCC 29213	L929	MDCKII	HEK293/pcDNA3.1
5-316	164.9	85.2	125.8	106.9
5-387	71.6	116.5	99.1	161.8
5-705	30.8	35.1	37.2	36.2
5-706	19.1	36.1	41.6	38.4

L929, MDCKII and HEK293/pcDNA3.1 cells: mouse fibroblast, Madan-Darby Canine Kidney and human embryonic kidney cell containing a pcDNA3.1 vector cell lines, respectively

4.3.3 Molecular docking studies of the binding mode of compound 5 derivatives

4.3.3.1 Correlation between docking poses of derivatives and biochemical results

In order to gain a better understanding of the interactions between derivatives and FtsZ and investigate the SAR study of compound **5** derivatives, a homology model for *S. auerus* FtsZ was built for docking a small library of compound **5** derivatives in chapter 3. The docking results were then used to explain how the substituent groups affect the interaction with the GTP binding site of FtsZ. Figure 3.4 shows that compound **5** consists of three parts including a R_1 group (4-carbamoylbutanoic acid), a quinuclidine core and a R_2 group [2-methyl-4-(thiophen-2-yl)-pyrimidine]. With docking analysis, compound **5** was found to occupy the whole GTP binding site (Figure 4.19A). The pyrimidine moiety of compound **5** deeply bound to the hydrophobic cavity of the GTP binding site by hydrophobic interaction and formation of hydrogen bond with the backbone oxygen atom of Thr129 (2.1 Å). The 3D sequence alignments with other FtsZ proteins whose X-ray structures are available show some residues in contact with **5** in the *S. auerus* model are responsible for GTP binding site. When the thiophene ring of **5** was changed to other ring equivalents (a phenyl ring of compound **5-306** or furan ring compound **5-307**), no significant difference in bioactivity was observed *in vitro*. From the docking results, similar docking poses were observed for these three derivatives, indicating that the thiophene function group of compound **5** may not be

a key factor for the activity. Nevertheless, upon the addition of methoxy group (**5-316**) to the amide moiety, the antibacterial activity (Table 4.2) and binding affinity (Table 4.7) were slightly enhanced. In the docked model, better binding interactions were found between **5-316** and the GTP binding site by forming the hydrogen bond (1.9 Å) between the oxygen atom of carbonyl group of **5-316** and Gly106. The methoxy moiety of **316** established two hydrogen bonds with the side chain of Thr105 (2.0 Å) and the main chain of Thr105 (2 Å) (Figure 4.19A). Interestingly, replacing the butyric acid group of **5** by the methoxy group did not affect the docking pose of R_2 substituent group (Figure 4.20B). But **5-316** exhibited a higher antibacterial activity and inhibitory effect on FtsZ, implying that the longer carbon chain of butyric acid group may affect the strength and orientation of hydrogen bond formation because it has a high degree of freedom. However, it is also possible that the methoxy group of compound **5-316** interacts with two significant residues (Thr105 and Gly106) and hence impairs the GTP substrate binding ability of enzyme. But replacing the methoxy moiety in **5-316** by an anisole group (**5-320**) caused poor antibacterial activity (Table 4.2) and weakened its inhibitory ability toward FtsZ (Table 4.7). From the docking conformation of compound **5-320**, it was observed that the bulky anisole group of **5-320** not only decreases the degree of freedom of R_1 group to hinder the hydrogen bond formation, it also may reduce the electron density of adjacent oxygen atom to form a hydrogen bond with Gly104 (Figure 4.19C). Regarding the substitution of methoxy group by a furan ring (**5-379**), the antibacterial activity (Table 4.2) and inhibitory effect (Table 4.7) were deleterious *in vitro*. The possible reason causing weak binding affinity is

that no hydrogen bond could be formed as shown in the docked model. The antibacterial activity (Table 4.2) and inhibitory effect (Table 4.7) of **5-326** are similar to **5-316**. They exhibited higher antibacterial effect than **5**. On the one hand, thioether is an angular functional group, the C-S-C angle approaching 90°, which causes the R_1 substituent group of **5-326** to become more rigid. Hence, the R_1 group could not freely rotate; the carboxyl group was found to be flipped inward forming three hydrogen bonds with Gly104 (1.9 Å), the side chain (1.6 Å) and the main chain (1.8 Å) of Thr105 (Figure 4.19A). In addition, the bulkiness of sulfur atom caused the carbonyl of amide group to point outward, which is different from that of compound **5** (Figure 4.21B). From the binding mode of **5-379**, the furan ring of this compound would disrupt the binding interaction with important residues of the GTP binding site. The docking results also indicated that substituting non-polar substituents into the butyric acid group of the amide moiety in **5** may not facilitate the fitting of the R_1 group into the GTP binding site. This weak interaction to the binding pocket of FtsZ might be the reason for the weaker activity exhibited by this compound. Two compounds, **5-256** with a para-methyl or **5-360** with a para-dimethyl amine substitution of the benzene ring, retained similar activity to **5**. On the contrary, substituting the phenyl ring with para-trifluoromethyl (**5-705**) was found to exert greater antibacterial activity as shown in Table 4.2. The IC_{50} of **5-705** on both FtsZ proteins were similar to those of compounds **5-256** and **5-360** *in vitro* (Table 4.7). Based on the docking results, compounds **5-256**, **5-360** and **5-705** displayed the same docking pose and the amide moiety at R_1 group and pyrimidine moiety at R_2 group both formed a hydrogen bond with Gly106 (1.5 Å) and Thr129

(2.2 Å) respectively (Figure 4.22A). Interestingly, compound **5-256** was found to be as active as compound **5-705** to inhibit FtsZ GTPase activity *in vitro*, but a dramatic difference was observed between the antibacterial activities of these two compounds *in vivo*. The possible reason is that the para-trifluoromethyl substituent group facilitates cell permeability. Concerning substituting the thiourea group with an amide moiety, the antibacterial activity and inhibitory effect of **5-701** was slightly higher than **5**. But the binding score of **5-701** was poor in the docking simulation (Table 4.7). Replacement of the amide moiety of R_1 group in **5** with the flexible amine moiety (**5-387**) resulted in increasing both the antibacterial activity and inhibitory effect (Tables 4.2 and 4.7). Figure 4.22B shows that the furan ring of furfuryl alcohol group (**5-387**) interacted with residues of the GTP binding site in a totally different manner from the ring of compound **5-379**. The nitrogen atom of amine moiety of **5-387** formed a hydrogen bond with the main chain oxygen atom of Gly100 (2.3 Å). But no hydrogen bond was observed between Gly100 and the amine group of compound **5-379**. **5-387** had a higher antibacterial activity and FtsZ inhibitory activity because it formed a strong hydrogen bond between the furan ring and the important active site residue Gly17 (2 Å). This interaction may seriously disrupt the binding between GTP substrate and FtsZ. (Figure 4.21B). Another possible reason is that the amine group of **5-387** can freely rotate that would alter the relative position of the hydroxyl group of furfuryl alcohol moiety to form a hydrogen bond with the side chain of Asn40 (1.8 Å). The binding pose of compound **5-387** illustrated that the flexible amine functional group of this compound may play a significant role in antibacterial and FtsZ inhibitory activities. When the furfuryl

alcohol moiety of **5-387** was replaced by an imidazole group (**5-702**), the antibacterial activity was still retained. But the inhibitory affect of **5-702** on FtsZ GTPase activity was found to be lower than that of **5-387** *in vitro* (Table 4.7). Only one hydrogen bond was formed between the main chain nitrogen atom of Gly104 and the nitrogen atom of the imidazole group of **5-702** in the docked model (Figure 4.22C). The docking simulation results of compounds **5-387** and **5-702** are consistent with the experimental results. When the 2-methyl-4-(thiophen-2-yl)-pyrimidine moiety of compound **5** was replaced by the hydrophobic substitutent 4-(pentan-3-yl)-2-(pyridin-4-yl)pyrimidine, greater inhibitory activity of **5-706** were achieved *in vivo* and *in vitro*. The docking results showed that **5-706** was the most top-scoring compound in comparison to other derivatives (Table 4.7). The docking pose of **5-706** (Figure 4.23A) is totally different from **5** and other derivatives. A planar thiophene ring and the small size methyl group of pyrimidine moiety in **5** may favor the R_2 substituent side chain to deeply bind to the cavity of the GTP binding site. On the contrary, the bulky pentan-3-yl group prevented the R_2 substituent side chain of **5-706** to deeply enter into the cavity, which may in turn facilitate the formation of π-π and van der Waals interactions between the pyrimidine ring of **5-706** and the phenylalanine side chain of Phe179 (Figure 4.23A-B). The other end of **5-706** exhibited four hydrogen bonds with the side chain of Ala67 (1.9 Å), the side chain (1.8 Å) and main chain (2.4 Å) of Thr105 and the main chain of Gly104 (2.4 Å) (Figure 4.22C). Besides forming strong hydrogen and hydrophobic interactions, the molecular geometry of **5-706** favors its fit into the GTP binding pocket of FtsZ. **5-706** was observed to perfectly occupy the whole region of GTP

binding site (Figures 4.23D and E) Those features are responsible for the great difference in the activity of derivatives (Tables 4.2 and 4.7).

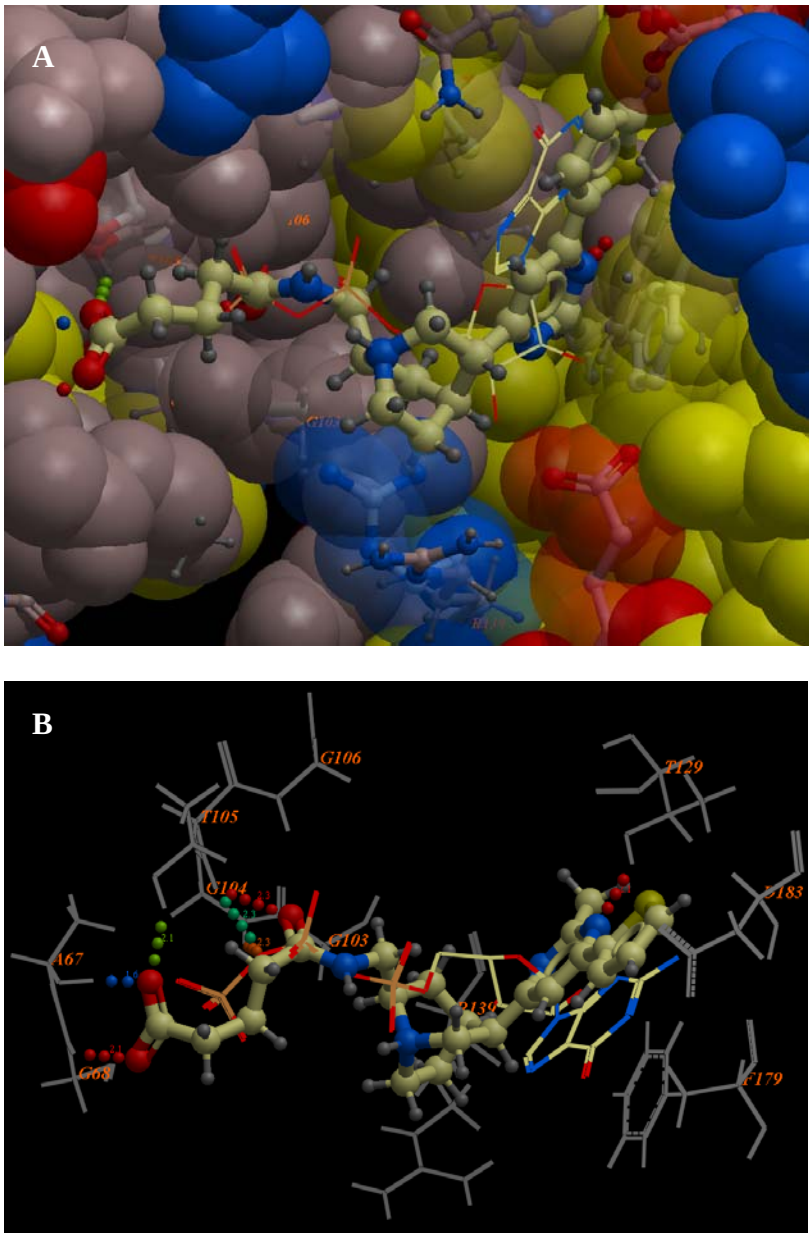

Figure 4.19 (A) Predicted binding mode of **5** and GTP in the GTP binding site of the homology model of *S. auerus* FtsZ. Yellow color represented hydrophobic, red and blue represented polar and grey represented neutral region in the GTP binding site. (B) Interaction of **5** and GTP with residues of the GTP binding site. Grey wire represented the side chain of residues. **5** was depicted as a ball-and-stick model and coloured by atom types. GTP substrate was depicted as a wire model and coloured by atom types.

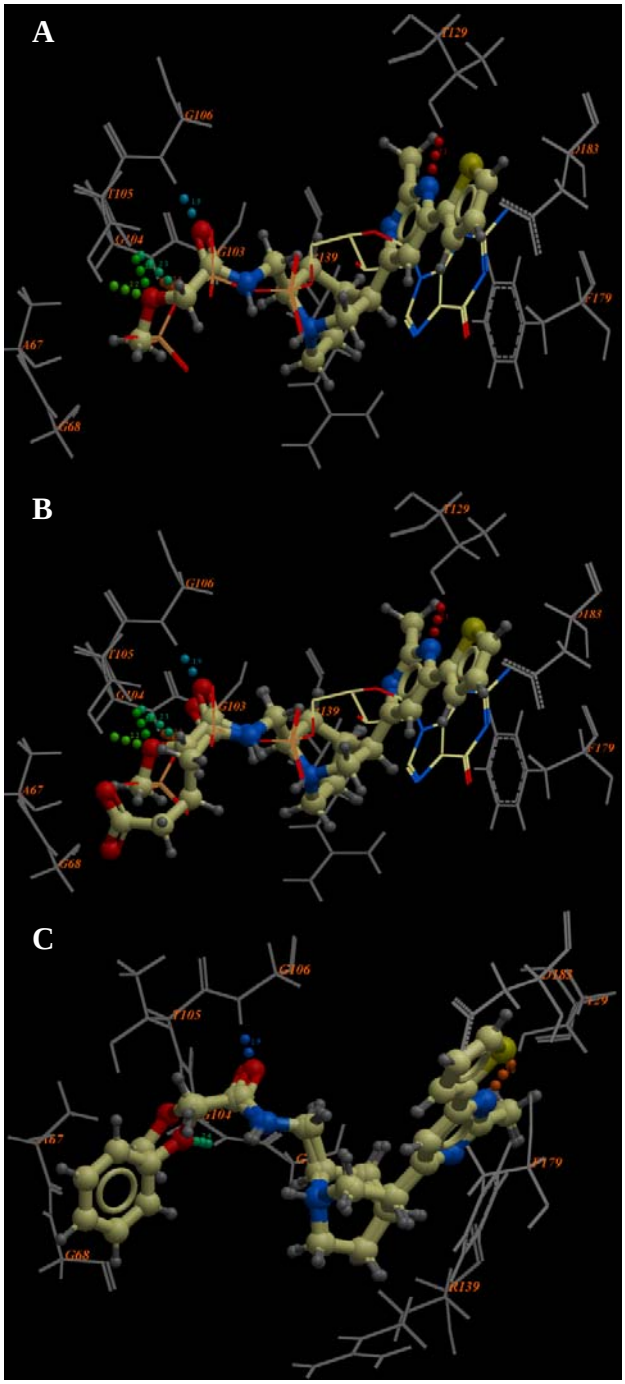

Figure 4.20 (A) Interaction of **5-316** and GTP with residues of the GTP binding site. (B) Interaction of **5**, **5-316** and GTP with residues of the GTP binding site. (C) Interaction of **5-316** and **5-320** with residues of the GTP binding site. **5**, **5-316** and **5-320** were depicted as a ball-and-stick model and coloured by atom types. GTP substrate was depicted as a thin wire model and coloured by atom types. Grey wire represented the side chain of residues.

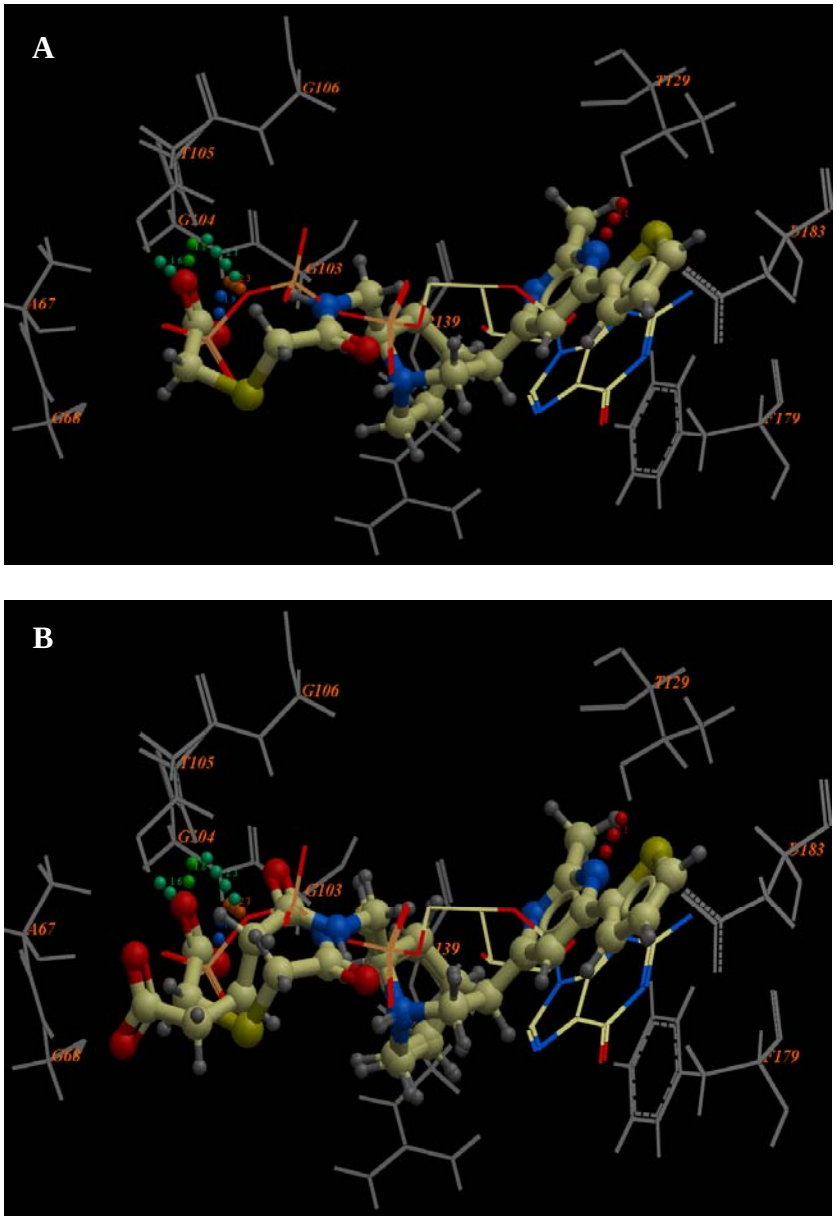

Figure 4.21 (A) Interaction of **5-326** and GTP with residues of the GTP binding site. (B) Interaction of **5**, **5-326** and GTP with residues of the GTP binding site. **5** and **5-326** were depicted as a ball-and-stick model and coloured by atom types. GTP substrate was depicted as a thin wire model and coloured by atom types.

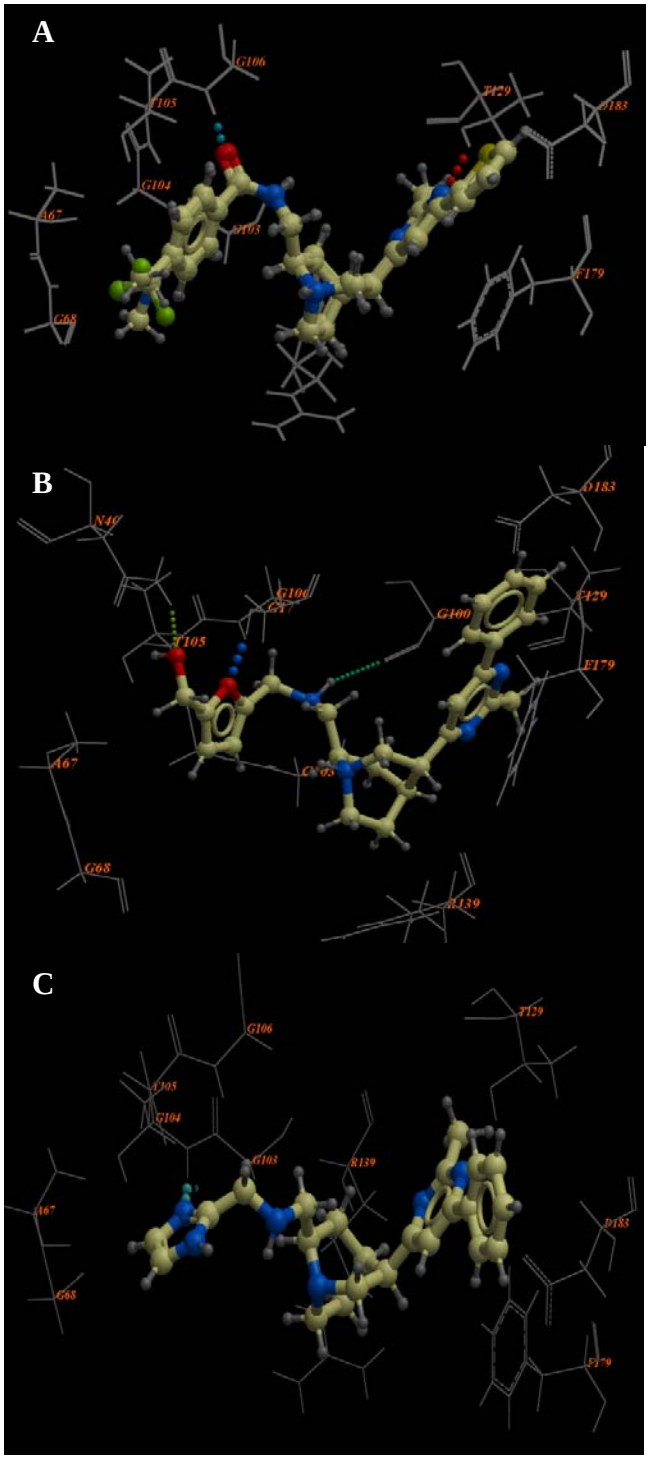

Figure 4.22 (A) Interaction of **5-256**, **5-360** and **5-705** with residues of the GTP binding site. (B) Interaction of **5-387** with residues of the GTP binding site. (C) Interaction of **5-702** with residues of the GTP binding site. All residues were represented by grey wires and compounds were depicted as a ball-and-stick model and coloured by atom types.

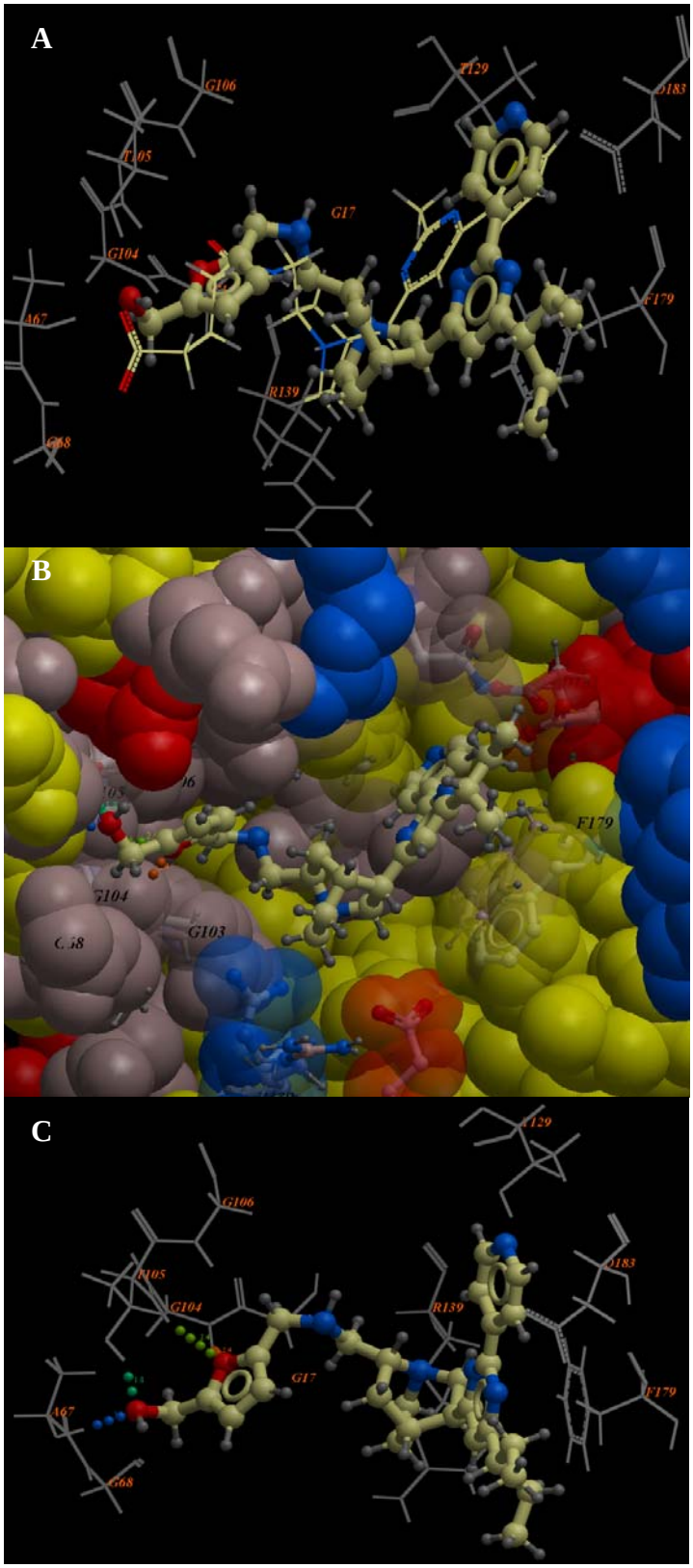

Figure 4.23 (caption on next page)

Continue……

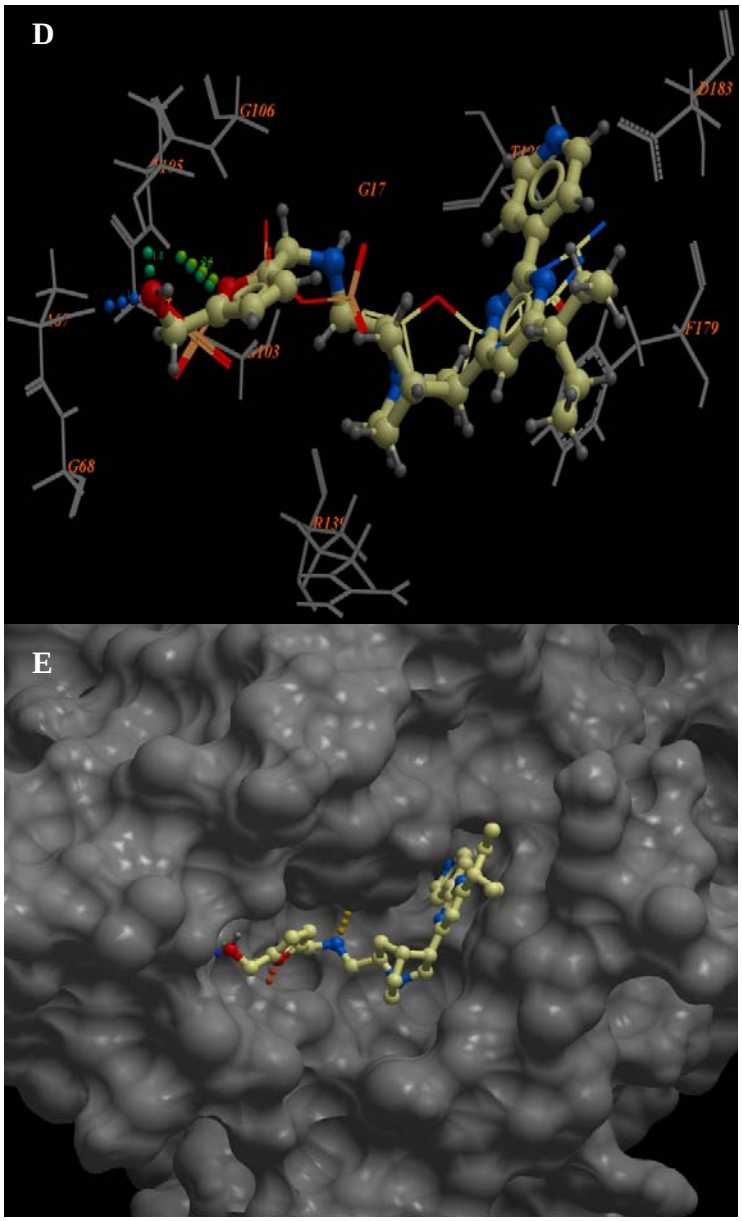

Figure 4.23 (A) Interaction of **5** and **5-706** with residues of the GTP binding site. compound **5** was displayed as a thin wire and colored by atom type and residues represented grey wire. (B) Interaction of **5-706** with residues of the GTP binding site, residues was depicted as a hydrophobic surface. (C) Close-up view of the active site of **5** on FtsZ. (D) Close-up view of the active site of **5** and GTP on FtsZ. (E) Overall view of **5-706** bound in the GTPase binding site. Surface map of FtsZ was represented as grey, **5-706** were depicted as a ball-and-stick model and coloured by atom types.

Table 4.7 Comparison of the calculated score of the five receptor/ligand complexes with the biological activity of the compound **5** derivatives

Compound	Binding score[a]					IC_{50} ± SEM[b] (μg/mL)	
	2R6R	2R75	1RLU	1OFU	Model of *S. auerus* FtsZ	*S. auerus* FtsZ	*E. coli* FtsZ
5	-39	-40.26	-34.88	-36.01	-37.59	145.0 ± 37.2	221.5 ± 19.2
5-31	-24.19	-11.13	-11.82	-19.97	-20.91	>500	>500
5-254	-29.32	-10.56	-13.24	-8.00	-26.26	>500	>500
5-256	-26.3	-8.994	-14.42	-8.08	-25.15	346.3 ± 38.7	302.4 ± 22.5
5-306	-32.43	-30.92	-34.69	-34.75	-28.58	232.4 ± 12.6	400.5 ± 25.5
5-307	-30.11	-30.51	-33.62	-24.99	-30.34	205.4 ± 25.9	375.9 ± 24.5
5-312	-10	-10.93	-20.34	-9.14	-29.43	>500	>500
5-315	-28.34	-22.73	-17.73	-5.01	-31.76	478.5 ± 20.4	258.6 ± 10.4
5-316	-34.72	-31.01	-20.21	-26.51	-32.88	180.5 ± 9.8	192.0 ± 20.8
5-320	-26.92	-27.36	-22.02	-10.07	-25.5	>500	>500
5-324	-28.93	-35.38	-37.95	-22.2	-28.23	>500	>500
5-326	-32.46	-38.41	-35.73	-33.83	-30.66	250.2 ± 11.8	192.5 ± 14.5
5-379	-28.3	-15.86	-18.74	-9.06	-27.64	334.3 ± 26.4	368.7 ± 18.2
5-387	-30.6	-16.02	-18.49	-18.46	-32.57	47.7 ± 12.6	105.5 ± 16.8
5-701	-20.1	-19.48	-10.6	-16.22	-17.11	135.4 ± 14.2	283.5 ± 13.5
5-702	-22.57	-20.58	-17.5	-8.956	-28.66	323.1 ± 19.4	166.6 ± 25.6
5-705	-32.27	-31.08	-19.14	-20.73	-29.46	305.6 ± 13.2	123.5 ± 19.5
5-706	-35.5	-27.97	-26.37	-23.58	-35.86	34.4 ± 5.6	40.9 ± 4.6

[a] Binding score calculated by ICM in chapter 3

[b] SEM: standard error of the mean and IC_{50}s of compound **5** derivatives on GTPase activity of *S. auerus* FtsZ and *E. coli* FtsZ were determined in section 4.3.2.3.

4.3.3.2 Biochemical validation of accuracy of five FtsZ docking templates

In chapter 3, we selected five best docking templates to screen a small database of compound **5** derivatives. Each derivative was assigned a score reflecting its fitness of binding with the receptor. The experimental IC_{50} values and the corresponding scores calculated in a docking simulation are given in Table 4.7. For the five docked templates, an acceptable trend between calculated binding scores and experimental activities for the compound **5** derivatives was observed for *A. aeolicus* FtsZ (PDB codes: 2R6R and 2R75) and the homology model of FtsZ for *S. auerus*. With the docking analysis, we found that two best inhibitors (**5-387** and **5-706**) were among the top four scoring compounds whereas three analogues (**5-316**, **5-326** and **5-705**) with moderate FtsZ inhibition activity were among the top four scoring compounds. Compounds **5-31**, **5-254**, **5-256**, **5-312**, **5-320**, **5-324**, **5-701** and **5-702** with lower activity were found to have the lowest score. Even *S. auerus* FtsZ model built with as little as 44% identity of FtsZ template could identify more potent FtsZ inhibitors via a structural-based virtual screening.

4.3.4 Synergistic effect of compound 5 or its derivatives with 3-MBA or ampicillin

The combination effect of compound **5** or its derivatives with conventional antibiotic (ampicillin) or T7-loop inhibitor of FtsZ (3-MBA) was studied in order to improve the antibacterial activity of compound **5** and its derivatives. The results from the synergy test are summarized in Table 4.8. When tested alone, **5** and **5-316** showed modest antibacterial activities, whereas 3-MBA showed only a weak activity against the Gram-positive strains (Table 4.8). But the combination of **5** or **5-316** with 3-MBA improved the antibacterial activity. The results showed that a combination of compound **5** or **5-316** with 3-MBA displayed partial synergy against the Gram-positive strains with FIC indexes of 0.63-0.82 (Table 4.8). In the case of the combination of **5** or **5-316** with ampicillin, the antibacterial activity of ampicillin was significantly improved against ampicillin-resistant strain *S. auerus* ATCC 29247 with FIC indexes of 0.38-0.5, indicating synergism for both compounds (Table 4.8). On the contrary, the combination of **5-316** with 3-MBA is indifferent against the Gram-negative strain (*E. coli* ATCC 25922) with a FICI of 1.16 (Table 4.8). The possible reason is that the antibacterial activity of 3-MBA was poor against Gram-negative strain *E. coli*. The FICI of the combination of compound **5-706** and 3-MBA for *S. auerus* strains ranged from 0.75-0.97 contributing a synergistic effect (data not shown in Table 4.8). 3-MBA has been reported to target the T7-loop binding site of FtsZ [60]. Although compound **5** or its derivatives and 3-MBA seem to bind different sites of FtsZ, their modes of inhibition on FtsZ are not mutually

exclusive. In the assembly process, GTP binds at one end of the GTP-binding domain of FtsZ monomer, designated the 'plus' end by convention. Addition of C-terminal T7 loop domain of another monomer provides two water-polarizing residues directly in contact with the water molecule for γ-phosphate hydrolysis that forms the GTPase catalytic site [174, 175]. As a result, the combination of **5** or **5-316** and 3-MBA only caused a partial synergy effect. Regarding the combination of **5** or **5-316** and ampicillin, apparent synergistic interactions were found because they act on different mechanisms. Ampicillin has been shown to inhibit the formation of peptidoglycan cross-links in the bacterial cell wall. It is conceivable that the synergy effect of the combination of compound **5** or **5-316** and 3-MBA is less significant than with ampicillin. Despite the relatively small number of strains tested, the results demonstrated that the effect of combining compound **5** or **5-316** with 3-MBA are similar among different species.

Table 4.8 Synergistic effects of compound **5** or its derivatives with 3-MBA or ampicillin against the testing organisms

Bacteria	MICs (μg/mL) of **5**/ **5-316**/3-MBA/AMP[a] Individually	In combination	Combined FIC	Result[b]
Gram-positive bacteria				
S. aureus (drug-sensitive)	384/NT/2500/NT	192/NT/800/NT	0.82	PS
	NT/96/2500/NT	NT/48/312/NT	0.63	PS
S. aureus (AMP-resistant)	384/NT/2500/NT	96/NT/1250/NT	0.75	PS
	384/NT/NT/24	96/NT/NT/6	0.5	S
	NT/96/2500/NT	NT/24/1250/NT	0.75	PS
	NT/96/NT/24	NT/24/NT/3	0.38	S
B. subtilis	192/NT/2500/NT	48/NT/1250/NT	0.75	PS
Gram-negative bacteria				
E. coli (drug-sensitive)	NT/96/5000/NT	NT/96/800/NT	1.16	I

[a] 3-MBA, 3-Methoxybenzamide; AMP, ampicillin; NT, not tested.
[b] S, synergistic; PS, partial synergy; I, indifference.

4.3.5 Comparison the antibacterial activities of compound 5-706 with known FtsZ inhibitors

Although the most potent derivative **5-706** was found to exhibit a slight cytotoxicity against the mouse fibroblast cells of L929 cell line, the canine kidney cells of MDCKII cell line and the human embryonic kidney cells of HEK293/pcDNA3.1 cell line, **5-706** did not show any effect on the polymerization of mammalian cytoskeleton protein tubulin. On the contrary, some FtsZ inhibitors such as sanguinarine [66] and curcumin [64] have been shown to inhibit the tubulin assembly into microtubules. Hence, compound **5-706** has the potential to be developed as a lead compound because it exhibits broader spectrum of activities than most natural product and synthetic FtsZ inhibitors that were shown only to inhibit Gram-positive bacteria. For examples, berberine, cinnamaldehyde, curcumin, totarol, viriditoxin, A-189, PC 170942 and PC 190723 have been found to inhibit the proliferation of Gram-negative *E. coli* cells with MICs of > 400 μg/mL [181], 1000 μg/mL [63], > 64 μg/mL [64], > 400 μg/mL [67], > 64 μg/mL [62], > 128 μg/mL [78], > 256 μg/mL [81] and > 64 μg/mL [60] respectively. Compound **5-706** was found to effectively inhibit *E. coli* with a MIC of 36 μg/mL. Dicharnanetin [68] and OTBA [85] showed a weaker inhibitory effect on the proliferation of Gram-negative *E. coli* cells as compared with compound **5-706**. The antibacterial activity of **5-706** against *E. coli* is comparable to sanguinarine [66]. Zantrins were shown to inhibit *E. coli* with MIC values from 20 to 80 μM, and only zantrin Z5 induced filamentation in *E. coli* [80]. But **5-706** (12 μg/mL) was found to effectively cause the cell elongation of *E. coli*. Besides, **5-706** also showed higher antibacterial activity

against the Gram-positive strains than most known FtsZ inhibitors such as berberine [181], curcumin [64], A-189 [78] and PC170942 [81]. Although chrysohaentins A was shown to exert higher potency than compound **5-706** against Gram-positive bacterial strains such as *S. auerus* and *E. faecium*, the antibacterial activity of chrysohaentins A were not validated against Gram-negative bacteria. Indeed, discovery of new antibacterials against Gram-negative bacteria is very crucial to the treatment of bacterial infections because most clinical pathogenic bacteria are Gram-negative. *In vitro*, compound **5-706** showed higher inhibitory activity on FtsZ GTPase activity than most FtsZ inhibitors. The IC_{50} value of compound **5-706** on the GTPase activity is 34.4 μg/mL (72.4 μM), while compound 534F6 (100 μM) [82], A-189 (80 μg/mL) [78], PC170942 (24 μg/mL) [81] and SRI-3072 (100 μM) [75] inhibited the GTPase activity by 20, 67, 50, 50 and 20% respectively. Though many compounds such as dicharnanetin [68], sanguinarine [66], totarol [67], viriditoxin [62], OTBA [85] and zantrin [80] have experimentally been shown to inhibit the GTPase activity and FtsZ polymerization, the binding modes of these compounds are unknown. As a result, it is difficult to design more potent derivatives based on the scaffold of these compounds. On the contrary, the possible binding mode of compound **5-706** has been investigated using computational docking, which also facilitates the future design of more potent derivatives *in silico*. In addition, **5-706** binds to the highly conserved GTP binding site rather than other binding sites such as the T7-loop at the C-terminus of FtsZ. This is the possible reason why compound **5-706** showed broader spectrum activity than other T7-loop binding FtsZ inhibitors such as cinnamaldehyde[63], curcumin [64] and PC190723 [60].

4.4 Conclusing remarks

After testing the 69 derivatives, several compounds were found to significantly improve the potency of compound **5**. The results from *in vivo* assays indicated that compounds **5-316**, **5-387**, **5-705** and **5-706** possessed higher antibacterial activities and spectrum of activity. These compounds were also found to cause the cell elongation of *E. coli* and *B. subtilis*. Among them, **5-706** showed the largest increase in cell elongation of *B. subtilis* and *E. coli* by 4-fold and 8-fold respectively. These more potent derivatives effectively disrupted dynamic Z-ring formation with no influence on nucleoid segregation and DNA replication, and did not perturb the structure of bacterial cell membrane. Although some compounds were found to exert higher potencies against bacterial strains *in vivo*, the inhibitory effect of **5-701**, **5-702** and **5-705** on the GTPase activities of both FtsZ proteins *in vitro* were weak. Based on the results from docking simulations and biochemical assays, **5-706** is the most potent derivative targeting FtsZ protein. The highest scoring pose of **5-706** can fit very well in the GTP binding site to form several strong hydrogen bonding and hydrophobic interactions. The docking results also demonstrated that three models from *A. aeolicus* FtsZ (PDB codes: 2R6R and 2R75) and a homology model of FtsZ for *S. auerus* were found to directly correlate with the experimental results. However, the most potent derivative **5-706** exerted a toxic effect on mammalian cell lines. In the study of synergy effect, the combination of **5** or **5-316** with 3-MBA or ampicillin were found to show a partial synergy or synergy effect respectively on antibiotic -sensitive and -resistant bacterial strains.

Chapter 5

Conclusions

Natural product and semisynthetic natural product compounds provide a rich source of potent and highly diverse structures for the development of new drugs. Nowadays, many clinical used antibiotics are derived from semisynthetic modification of natural products. This approach can improve the pharmacokinetics and pharmacodynamics of a drug. In this study, a moderate FtsZ inhibitor, compound **5**, was firstly identified using a high-throughput virtual screening of the natural product databases. In the biological and biochemical studies, compound **5** was shown to inhibit FtsZ assembly that interfered with the formation and functioning of the Z-ring ultimately leading to bacterial cell death. In order to identify more potent compound **5** derivatives *in silico*, Scan Alanines and REfine (SCARE) and homology modeling techniques were utilized. In these docking studies, several optimal docked models were successfully determined to predict the optimal binding modes of **5**. Thus, the most potent derivative **5-706** was identified by *in silico* screening a series of compound **5** derivatives. The synergy study of compound **5** or its derivatives with 3-MBA or ampicillin were also investigated in this study. Compounds **5** and **5-316** were found to show partial synergy effect in combination with 3-MBA on the tested bacterial strains. Interestingly, the combination of weak compound **5** derivatives with ampicillin showed a strong synergy effect.

Although the findings reported in this thesis are encouraging, compound **5-706** requires further optimization to enhance the binding affinity to FtsZ and reduce the cytotoxicity and the dose necessary for bacterial inhibition. In subsequent hit-lead optimization, docking simulations could be employed to screen newly designed derivatives based on the scaffold of compound **5-706**. For example, the bulky and

hydrophobic functional groups of the pyrimidine moiety of R_2 group in compound **5-706** could be kept because these functional groups were found to be essential to anti-FtsZ activity by forming hydrophobic interaction with crucial active site residues. Then the furan ring of the amine moiety of R_1 group could be replaced by different function groups such as a tetrazole ring or a triazole ring. These functional groups are planar in structure, which is similar to that furan ring of compound **5-706**. These functional groups may improve target interactions and eliminate the toxicity effect. On the other hand, the furan ring could not be replaced by an imidazole ring because this ring was found to be susceptible to metabolic degradation leading to toxic species. Through an iteration of *in silico* screening, chemical synthesis and bioassays, lead compounds with improved potency, reduced off-target activities and appropriate physiochemical or metabolic properties will be identified.

References

1. Projan, S. J.; Youngman, P. J. *Current Opinion in Microbiology*, 2002, 5(5), 463-465.
2. Walsh, C. *Antibiotics: Actions, Origins, Resistance*, Washington, D. C.: ASM 2003.
3. Errington, J.; Daniel, R. A.; Scheffers, D. J. *Microbiology and Molecular Biology Reviews*, 2003, 67(1), 52-65.
4. Goehring, N. W.; Beckwith, J. *Current Biology*, 2005, 15(13), R514-R526.
5. Harry, E.; Monahan, L.; Thompson, L. *International Review of Cytology*, 2006, 253, 27-94.
6. Vicente, M.; Rico, A. I.; Martinez-Arteaga, R.; Mingorance, J. *Journal of Bacteriology*, 2006, 188(1), 19-27.
7. Rothfield, L. I.; Justice, S. S. *Cell*, 1997, 88(5), 581-584.
8. Donachie, W. D. *Annual Review of Microbiology*, 1993, 47, 199-203.
9. Lutkenhaus, J.; Addinall, S. G. *Annual Review of Biochemistry*, 1997, 66, 93-116.
10. Margolin, W. *FEMS Microbiology Reviews*, 2000, 24(4), 531-548.
11. Adams, D. W.; Errington, J. *Nature Reviews Microbiology*, 2009, 7(9), 642-653.
12. Begg, K. J.; Donachie, W. D. *Journal of Bacteriology*, 1985, 163(2), 615-622.
13. Taschner, P. E. M.; Huls, P. G.; Pas, E.; Woldringh, C. L. *Journal of Bacteriology*, 1988, 170(4), 1533-1540.
14. Bi, E.; Lutkenhaus, J. *Nature*, 1991, 354(6349), 161-164.
15. Levin, P. A.; Losick, R. *Genes and Development*, 1996, 10(4), 478-488.
16. Ma, X. L.; Ehrhardt, D. W.; Margolin, W. *Proceedings of the National Academy of Sciences of the United States of America*, 1996, 93(23), 12998-13003.

17. RayChaudhuri, D.; Gordon, G. S.; Wright, A. *Nature Structural Biology*, 2000, 7(11), 997-999.

18. Fu, X. L.; Shih, Y. L.; Zhang, Y.; Rothfield, L. I. *Proceedings of the National Academy of Sciences of the United States of America*, 2001, 98(3), 980-985.

19. Raskin, D. M.; deBoer, P. A. J. *Cell*, 1997, 91(5), 685-694.

20. Hu, Z. L.; Mukherjee, A.; Pichoff, S.; Lutkenhaus, J. *Proceedings of the National Academy of Sciences of the United States of America*, 1999, 96(26), 14819-14824.

21. Woldringh, C. L.; Mulder, E.; Huls, P. G.; Vischer, N. *Research in Microbiology*, 1991, 142(2-3), 309-320.

22. Hale, C. A.; deBoer, P. A. J. *Cell*, 1997, 88(2), 175-185.

23. Wang, X. D.; Huang, J. A.; Mukherjee, A.; Cao, C.; Lutkenhaus, J. *Journal of Bacteriology*, 1997, 179(17), 5551-5559.

24. Gueiros, F. J.; Losick, R. *Genes and Development*, 2002, 16(19), 2544-2556.

25. Osawa, M.; Anderson, D. E.; Erickson, H. P. *Science*, 2008, 320(5877), 792-794.

26. Löwe, J.; Amos, L. A. *Nature*, 1998, 391(6663), 203-206.

27. Vaughan, S.; Wickstead, B.; Gull, K.; Addinall, S. G. *Journal of Molecular Evolution*, 2004, 58(1), 19-29.

28. Erickson, H. P. *Cell*, 1995, 80(3), 367-370.

29. Nogales, E.; Downing, K. H.; Amos, L. A.; Lowe, J. *Nature Structural Biology*, 1998, 5(6), 451-458.

30. Nogales, E.; Wolf, S. G.; Downing, K. H. *Nature*, 1998, 391, 199-203.

31. Erickson, H. P. *Trends in Cell Biology*, 1998, 8(4), 133-137.

32. dePereda, J. M.; Leynadier, D.; Evangelio, J. A.; Chacon, P.; Andreu, J. M.

Biochemistry, 1996, 35(45), 14203-14215.

33. Scheffers, D. J.; de Wit, J. G.; den Blaauwen, T.; Driessen, A. J. M. *FEBS Letters*, 2001, 494(1-2), 34-37.

34. Abagyan, R.; Orry, A.; Raush, E. B. L.; Totrov, M. *Icm Manual 3.6*. La Jolla, CA: Molsoft LCC. 2008.

35. Romberg, L.; Levin, P. A. *Annual Review of Microbiology*, 2003, 57, 125-154.

36. Bi, E.; Dai, K.; Subbarao, S.; Beall, B.; Lutkenhaus, J. *Research in Microbiology*, 1991, 142(2-3), 249-252.

37. Lu, C. L.; Stricker, J.; Erickson, H. P. *Cell Motility and the Cytoskeleton*, 1998, 40(1), 71-86.

38. Rueda, S.; Vicente, M.; Mingorance, J. *Journal of Bacteriology*, 2003, 185(11), 3344-3351.

39. Den Blaauwen, T.; Buddelmeijer, N.; Aarsman, M. E. G.; Hameete, C. M.; Nanninga, N. *Journal of Bacteriology*, 1999, 181(17), 5167-5175.

40. Stricker, J.; Maddox, P. S.; Salmon, E. D.; Erickson, H. P. *Molecular Biology of the Cell*, 2001, 12, 429a-430a.

41. Stricker, J.; Maddox, P.; Salmon, E. D.; Erickson, H. P. *Proceedings of the National Academy of Sciences of the United States of America*, 2002, 99(5), 3171-3175.

42. Popp, D.; Iwasa, M.; Narita, A.; Erickson, H. P.; Maeda, Y. *Biopolymers*, 2009, 91(5), 340-350.

43. Anderson, D. E.; Gueiros-Filho, F. J.; Erickson, H. P. *Journal of Bacteriology*, 2004, 186(17), 5775-5781.

44. Lutkenhaus, J. *Molecular Microbiology*, 1993, 9(3), 403-409.

45. Deboer, P.; Crossley, R.; Rothfield, L. *Nature*, 1992, 359(6392), 254-256.

46. Sossong, T. M.; Brigham-Burke, M. R.; Hensley, P.; Pearce, K. H. *Biochemistry*, 1999, 38(45), 14843-14850.

47. Mukherjee, A.; Lutkenhaus, J. *Journal of Bacteriology*, 1994, 176(9), 2754-2758.

48. Erickson, H. P.; Taylor, D. W.; Taylor, K. A.; Bramhill, D. *Proceedings of the National Academy of Sciences of the United States of America*, 1996, 93(1), 519-523.

49. Yu, X. C.; Margolin, W. *EMBO Journal*, 1997, 16(17), 5455-5463.

50. Kuchibhatla, A.; Rasheed, A. S. A.; Narayanan, J.; Bellare, J.; Panda, D. *Langmuir*, 2009, 25(6), 3775-3785.

51. Beuria, T. K.; Krishnakumar, S. S.; Sahar, S.; Singh, N.; Gupta, K.; Meshram, M.; Panda, D. *Journal of Biological Chemistry*, 2003, 278(6), 3735-3741.

52. Beuria, T. K.; Shah, J. H.; Santra, M. K.; Kumar, V.; Panda, D. *International Journal of Biological Macromolecules*, 2006, 40(1), 30-39.

53. Singh, J. K.; Makde, R. D.; Kumar, V.; Panda, D. *Journal of Biological Chemistry*, 2008, 283(45), 31116-31124.

54. RayChaudhuri, D. *Embo Journal*, 1999, 18(9), 2372-2383.

55. Chen, Y. D.; Erickson, H. P. *Biochemistry*, 2009, 48(28), 6664-6673.

56. Huecas, S.; Schaffner-Barbero, C.; Garcia, W.; Yebenes, H.; Palacios, J. M.; Diaz, J. F.; Menendez, M.; Andreu, J. M. *Journal of Biological Chemistry*, 2007, 282(52), 37515-37528.

57. Mingorance, J.; Rueda, S.; Gomez-Puertas, P.; Valencia, A.; Vicente, M.

Molecular Microbiology, 2001, 41(1), 83-91.

58. Lu, C. L.; Reedy, M.; Erickson, H. P. *Journal of Bacteriology*, 2000, 182(1), 164-170.

59. Bramhill, D. *Annual Review of Cell and Developmental Biology*, 1997, 13, 395-424.

60. Haydon, D. J.; Stokes, N. R.; Ure, R.; Galbraith, G.; Bennett, J. M.; Brown, D. R.; Baker, P. J.; Barynin, V. V.; Rice, D. W.; Sedelnikova, S. E.; Heal, J. R.; Sheridan, J. M.; Aiwale, S. T.; Chauhan, P. K.; Srivastava, A.; Taneja, A.; Collins, I.; Errington, J.; Czaplewski, L. G. *Science*, 2008, 321(5896), 1673-1675.

61. Plaza, A. K.; Jessica, L.; Bifulco, G.; Lloyd, J. R.; Bewley, C. A. *Journal of the American Chemical Society*, 2010, 132(26), 9069-9077.

62. Wang, J.; Galgoci, A.; Kodali, S.; Herath, K. B.; Jayasuriya, H.; Dorso, K.; Vicente, F.; Gonzalez, A.; Cully, D.; Bramhill, D.; Singh, S. *Journal of Biological Chemistry*, 2003, 278(45), 44424-44428.

63. Domadia, P.; Swarup, S.; Bhunia, A.; Sivaraman, J.; Dasgupta, D. *Biochemical Pharmacology*, 2007, 74(6), 831-840.

64. Rai, D.; Singh, J. K.; Roy, N.; Panda, D. *Biochemical Journal*, 2008, 410(1), 147-155.

65. Hemaiswarya, S.; Kruthiventi, A. K.; Doble, M. *Phytomedicine*, 2008, 15(8), 639-652.

66. Beuria, T. K.; Santra, M. K.; Panda, D. *Biochemistry*, 2005, 44(50), 16584-16593.

67. Jaiswal, R.; Beuria, T. K.; Mohan, R.; Mahajan, S. K.; Panda, D. *Biochemistry*, 2007, 46(14), 4211-4220.

68. Urgaonkar, S.; La Pierre, H. S.; Meir, I.; Lund, H.; RayChaudhuri, D.; Shaw, J. T. *Organic Letters*, 2005, 7(25), 5609-5612.

69. Domadia, P. N.; Bhunia, A.; Sivaraman, J.; Swarup, S.; Dasgupta, D. *Biochemistry*, 2008, 47(10), 3225-3234.

70. Rai, D.; Singh, J. K.; Roy, N.; Panda, D. *Biochemical Journal*, 2008, 410, 147-155.

71. Ohashi, Y.; Chijiiwa, Y.; Suzuki, K.; Takahashi, K.; Nanamiya, H.; Sato, T.; Hosoya, Y.; Ochi, K.; Kawamura, F. *Journal of Bacteriology*, 1999, 181(4), 1348-1351.

72. Czaplewski, L. G.; Collins, I.; Boyd, E. A.; Brown, D.; East, S. P.; Gardiner, M.; Fletcher, R.; Haydon, D. J.; Henstock, V.; Ingram, P.; Jones, C.; Noula, C.; Kennison, L.; Rockley, C.; Rose, V.; Thomaides-Brears, H. B.; Ure, R.; Whittaker, M.; Stokes, N. R. *Bioorganic & Medicinal Chemistry Letters*, 2009, 19(2), 524-527.

73. Andreu, J. M.; Schaffner-Barber, C.; Huecas, S.; Alonso, D.; Lopez-Rodriguez, M. L.; Ruiz-Avila, L. B.; Nunez-Ramirez, R.; Llorca, O.; Martin-Galiano, A. J. *Journal of Biological Chemistry*, 2010, 285(19), 14239-14246.

74. Reynolds, R. C.; Srivastava, S.; Ross, L. J.; Suling, W. J.; White, E. L. *Bioorganic & Medicinal Chemistry Letters*, 2004, 14(12), 3161-3164.

75. White, E. L.; Suling, W. J.; Ross, L. J.; Seitz, L. E.; Reynolds, R. C. *Journal of Antimicrobial Chemotherapy*, 2000, 50, 111-114.

76. Lappchen, T.; Hartog, A. F.; Pinas, V. A.; Koomen, G. J.; den Blaauwen, T. *Biochemistry*, 2005, 44(21), 7879-7884.

77. Lappchen, T.; Pinas, V. A.; Hartog, A. F.; Koomen, G. J.; Schaffner-Barbero, C.; Andreu, J. M.; Trambaiolo, D.; Lowe, J.; Juhem, A.; Popov, A. V.; den Blaauwen, T. *Chemistry & Biology*, 2008, 15(2), 189-199.

78. Ito, H.; Ura, A.; Oyamada, Y.; Tanitame, A.; Yoshida, H.; Yamada, S.; Wachi, M.; Yamagishi, J. *Microbiology and Immunology*, 2006, 50(10), 759-764.

79. Paradis-Bleau, C.; Beaumont, M.; Sanschagrin, F.; Voyer, N.; Levesque, R. C. *Bioorganic and Medicinal Chemistry*, 2007, 15(3), 1330-1340.

80. Margalit, D. N.; Romberg, L.; Mets, R. B.; Hebert, A. M.; Mitchison, T. J.; Kirschner, M. W.; RayChaudhuri, D. *Proceedings of the National Academy of Sciences of the United States of America*, 2004, 101(38), 13969-13969.

81. Stokes, N. R.; Sievers, J.; Barker, S.; Bennett, J. M.; Brown, D. R.; Collins, I.; Errington, V. M.; Foulger, D.; Hall, M.; Halsey, R.; Johnson, H.; Rose, V.; Thomaides, H. B.; Haydon, D. J.; Czaplewski, L. G.; Errington, J. *Journal of Biological Chemistry*, 2005, 280(48), 39709-39715.

82. Mukherjee, S.; Robinson, C. A.; Howe, A. G.; Mazor, T.; Wood, P. A.; Urgaonkar, S.; Hebert, A. M.; RayChaudhuri, D.; Shaw, J. T. *Bioorganic & Medicinal Chemistry Letters*, 2007, 17(23), 6651-6655.

83. Huang, Q.; Kirikae, F.; Kirikae, T.; Pepe, A.; Amin, A.; Respicio, L.; Slayden, R. A.; Tonge, P. J.; Ojima, I. *Journal of Medicinal Chemistry*, 2006, 49(2), 463-466.

84. Possoz, C.; Newmark, J.; Sorto, N.; Sherratt, D. J.; Tolmasky, M. E. *Antimicrobial Agents and Chemotherapy*, 2007, 51(1), 252-256.

85. Beuria, T. K.; Singh, P.; Surolia, A.; Panda, D. *Biochemical Journal*, 2009, 423(1), 61-69.

86. DiMasi, J. A.; Hansen, R. W.; Grabowski, H. G. *Journal of Health Economics*, 2003, 22(2), 151-185.

87. Rawlins, M. D. *Nature Reviews Drug Discovery*, 2004, 3(4), 360-364A.

88. Kola, I.; Landis, J. *Nature Reviews Drug Discovery*, 2004, 3(8), 711-715.

89. Bajorath, F. *Nature Reviews Drug Discovery*, 2002, 1(11), 882-894.

90. Bleicher, K. H.; Bohm, H. J.; Muller, K.; Alanine, A. I. *Nature Reviews Drug Discovery*, 2003, 2(5), 369-378.

91. Van de Waterbeemd, H.; Gifford, E. *Nature Reviews Drug Discovery*, 2003, 2(3), 192-204.

92. Greer, J.; Erickson, J. W.; Baldwin, J. J.; Varney, M. D. *Journal of Medicinal Chemistry*, 1994, 37(8), 1035-1054.

93. Vonitzstein, M.; Wu, W. Y.; Kok, G. B.; Pegg, M. S.; Dyason, J. C.; Jin, B.; Phan, T. V.; Smythe, M. L.; White, H. F.; Oliver, S. W.; Colman, P. M.; Varghese, J. N.; Ryan, D. M.; Woods, J. M.; Bethell, R. C.; Hotham, V. J.; Cameron, J. M.; Penn, C. R. *Nature*, 1993, 363(6428), 418-423.

94. Wlodawer, A.; Vondrasek, J. *Annual Review of Biophysics and Biomolecular Structure*, 1998, 27, 249-284.

95. Williams, D. H.; Mitchell, T. *Current Opinion in Pharmacology*, 2002, 2(5), 567-573.

96. Leach, A. R. *Empirical Force Field Methods: Molecular Mechanics. In Molecular Modelling: Principles and Applications.* 2nd ed: Pearson Education, Dorchester, 165-252. 2001.

97. Leach, A. R. *Energy Minimisation and Related Methods for Exploring the Energy*

Surface. In Molecular Modelling: Principles and Applications. 2nd ed: Pearson Education, Dorchester, 253-302. 2001.

98. Karplus, M. *Accounts of Chemical Research*, 2002, 35(6), 321-323.

99. Hansson, T.; Oostenbrink, C.; van Gunsteren, W. F. *Current Opinion in Structural Biology*, 2002, 12(2), 190-196.

100. Case, D. A.; Cheatham, T. E.; Darden, T.; Gohlke, H.; Luo, R.; Merz, K. M.; Onufriev, A.; Simmerling, C.; Wang, B.; Woods, R. J. *Journal of Computational Chemistry*, 2005, 26(16), 1668-1688.

101. Van der Spoel, D.; Lindahl, E.; Hess, B.; Groenhof, G.; Mark, A. E.; Berendsen, H. J. C. *Journal of Computational Chemistry*, 2005, 26(16), 1701-1718.

102. MacKerell, A. D.; Bashford, D.; Bellott, M.; Dunbrack, R. L.; Evanseck, J. D.; Field, M. J.; Fischer, S.; Gao, J.; Guo, H.; Ha, S.; Joseph-McCarthy, D.; Kuchnir, L.; Kuczera, K.; Lau, F. T. K.; Mattos, C.; Michnick, S.; Ngo, T.; Nguyen, D. T.; Prodhom, B.; Reiher, W. E.; Roux, B.; Schlenkrich, M.; Smith, J. C.; Stote, R.; Straub, J.; Watanabe, M.; Wiorkiewicz-Kuczera, J.; Yin, D.; Karplus, M. *Journal of Physical Chemistry B*, 1998, 102(18), 3586-3616.

103. Halgren, T. A. *Journal of Computational Chemistry*, 1996, 17(5-6), 490-519.

104. Kubli-Garfias, C. *Theochem-Journal of Molecular Structure*, 1998, 422, 167-177.

105. Leach, A. R. *An Introduction to Computational Quantum Mechanics. In Molecular Modelling: Principles and Applications.* 2nd ed: Pearson Education, Dorchester, 26-107. 2001.

106. Laskowski, R. A. *Structural Quality Assurance. In Structural Bioinformatics.*: John Wiley & Sons, Hoboken, NJ, 273-303. 2003.

107. Sali, A. *Current Opinion in Biotechnology*, 1995, 6(4), 437-451.

108. Krieger, E.; Nabuurs, S. B.; Vriend, G. *Homology Modeling. In Structural Bioinformatics.*: John Wiley & Sons, Hoboken, NJ, 509-523. 2003.

109. Bajorath, J. *Journal of Chemical Information and Computer Sciences*, 2001, 41(2), 233-245.

110. Hou, T. J.; Xu, X. J. *Current Pharmaceutical Design*, 2004, 10(9), 1011-1033.

111. Barril, X.; Hubbard, R. E.; Morley, S. D. *Mini-Reviews in Medicinal Chemistry*, 2004, 4(7), 779-791.

112. Good, A. C.; Krystek, S. R.; Mason, J. S. *Drug Discovery Today*, 2000, 5(12), S61-S69.

113. Schapira, M.; Raaka, B. M.; Samuels, H. H.; Abagyan, R. *Proceedings of the National Academy of Sciences of the United States of America*, 2000, 97(3), 1008-1013.

114. Powers, R. A.; Morandi, F.; Shoichet, B. K. *Structure*, 2002, 10(7), 1013-1023.

115. Abagyan. RA, T. M., and Kuznetsov, D. *Journal of Computational Chemistry*, 1994, 15, 488-506.

116. Abagyan, R. A.; Totrov, M. M. *Abstracts of Papers of the American Chemical Society*, 1996, 211, 35-Comp.

117. Argos, P.; Abagyan, R. *Computers & Chemistry*, 1994, 18(3), 225-231.

118. Abagyan, R.; Totrov, M. *Journal of Molecular Biology*, 1994, 235(3), 983-1002.

119. Taylor, R. D.; Jewsbury, P. J.; Essex, J. W. *Journal of Computer-Aided Molecular Design*, 2002, 16(3), 151-166.

120. Ewing, T. J. A.; Makino, S.; Skillman, A. G.; Kuntz, I. D. *Journal of*

Computer-Aided Molecular Design, 2001, 15(5), 411-428.

121. Jones, G.; Willett, P.; Glen, R. C.; Leach, A. R.; Taylor, R. *Journal of Molecular Biology*, 1997, 267(3), 727-748.

122. Rarey, M.; Kramer, B.; Lengauer, T.; Klebe, G. *Journal of Molecular Biology*, 1996, 261(3), 470-489.

123. *Icm Is Available From*: MolSoft LLC, 3366 North Torrey Pines Court Suite 300 La Jolla, CA 92037, USA.

124. Bohm, H. J. *Journal of Computer-Aided Molecular Design*, 1998, 12(4), 309-323.

125. Velec, H. F. G.; Gohlke, H.; Klebe, G. *Journal of Medicinal Chemistry*, 2005, 48(20), 6296-6303.

126. Pang, Y. P.; Perola, E.; Xu, K.; Prendergast, F. G. *Journal of Computational Chemistry*, 2001, 22(15), 1750-1771.

127. Venkatachalam, C. M.; Jiang, X.; Oldfield, T.; Waldman, M. *Journal of Molecular Graphics & Modelling*, 2003, 21(4), 289-307.

128. *Fred Is Available from Openeye Inc*: 3600 Cerrillos Rd, Suite 1107.

129. Schnecke, V.; Kuhn, L. A. *Perspectives in Drug Discovery and Design*, 2000, 20(1), 171-190.

130. *Affinity Is Available from Accelrys*: 9685 Scranton Road, San Diego, CA 92121, USA.

131. Morris, G. M.; Goodsell, D. S.; Huey, R.; Olson, A. J. *Journal of Computer-Aided Molecular Design*, 1996, 10(4), 293-304.

132. *Glide Is Available from Schrödinger*: 1500 SW First Avenue, Suite 1180, Portland.

133. Rastelli, G.; Ferrari, A. M.; Costantino, L.; Gamberini, M. C. *Bioorganic &*

Medicinal Chemistry, 2002, 10(5), 1437-1450.

134. Gruneberg, S.; Stubbs, M. T.; Klebe, G. *Journal of Medicinal Chemistry*, 2002, 45(17), 3588-3602.

135. Brenk, R.; Naerum, L.; Gradler, U.; Gerber, H. D.; Garcia, G. A.; Reuter, K.; Stubbs, M. T.; Klebe, G. *Journal of Medicinal Chemistry*, 2003, 46(7), 1133-1143.

136. Filikov, A. V.; Mohan, V.; Vickers, T. A.; Griffey, R. H.; Cook, P. D.; Abagyan, R. A.; James, T. L. *Journal of Computer-Aided Molecular Design*, 2000, 14(6), 593-610.

137. Perola, E.; Xu, K.; Kollmeyer, T. M.; Kaufmann, S. H.; Prendergast, F. G.; Pang, Y. P. *Journal of Medicinal Chemistry*, 2000, 43(3), 401-408.

138. Wermuth, G.; Ganellin, C. R.; Lindberg, P.; Mitscher, L. A. *Pure and Applied Chemistry*, 1998, 70(5), 1129-1143.

139. VanDrie, J. H. *Journal of Computer-Aided Molecular Design*, 1997, 11(1), 39-52.

140. Berenbaum, M. C. *Clinical and Experimental Immunology*, 1977, 28(1), 1-18.

141. Ulrich-Merzenich, G.; Panek, D.; Zeitler, H.; Vetter, H.; Wagner, H. *Indian Journal of Experimental Biology*, 2010, 48(3), 208-219.

142. Wagner, H.; Ulrich-Merzenich, G. *Phytomedicine*, 2009, 16(2-3), 97-110.

143. Chou, T. C. *Pharmacological Reviews*, 2006, 58(3), 621-681.

144. Desbois, A. P.; Lang, S.; Gemmell, C. G.; Coote, P. J. *Journal of Applied Microbiology*, 2010, 108(2), 723-730.

145. Hall, M. J.; Middleton, R. F.; Westmacott, D. *Journal of Antimicrobial Chemotherapy*, 1983, 11(5), 427-433.

146. Doman, T. N.; McGovern, S. L.; Witherbee, B. J.; Kasten, T. P.; Kurumbail, R.;

Stallings, W. C.; Connolly, D. T.; Shoichet, B. K. *Journal of Medicinal Chemistry*, 2002, 45(11), 2213-2221.

147. Paiva, A. M.; Vanderwall, D. E.; Blanchard, J. S.; Kozarich, J. W.; Williamson, J. M.; Kelly, T. M. *Biochimica Et Biophysica Acta-Protein Structure and Molecular Enzymology*, 2001, 1545(1-2), 67-77.

148. Oshiro, C.; Bradley, E. K.; Eksterowicz, J.; Evensen, E.; Lamb, M. L.; Lanctot, J. K.; Putta, S.; Stanton, R.; Grootenhuis, P. D. J. *Journal of Medicinal Chemistry*, 2004, 47(3), 764-767.

149. Polgar, T.; Baki, A.; Szendrei, G. I.; Keseru, G. M. *Journal of Medicinal Chemistry*, 2005, 48(25), 7946-7959.

150. Waszkowycz, B.; Perkins, T. D. J.; Sykes, R. A.; Li, J. *Ibm Systems Journal*, 2001, 40(2), 360-376.

151. Enyedy, I. J.; Egan, W. J. *Journal of Computer-Aided Molecular Design*, 2008, 22(3-4), 161-168.

152. Kolb, P.; Ferreira, R. S.; Irwin, J. J.; Shoichet, B. K. *Current Opinion in Biotechnology*, 2009, 20(4), 429-436.

153. Yoon, S.; Smellie, A.; Hartsough, D.; Filikov, A. *Journal of Computer-Aided Molecular Design*, 2005, 19(7), 483-497.

154. Oprea, T. I.; Matter, H. *Current Opinion in Chemical Biology*, 2004, 8(4), 349-358.

155. Oliva, M. A.; Trambaiolo, D.; Lowe, J. *Journal of Molecular Biology*, 2007, 373(5), 1229-1242.

156. Leung, A. K. W.; White, E. L.; Ross, L. J.; Reynolds, R. C.; DeVito, J. A.;

Borhani, D. W. *Journal of Molecular Biology*, 2004, 342(3), 953-970.

157. Oliva, M. A.; Cordell, S. C.; Lowe, J. *Nature Structural & Molecular Biology*, 2004, 11(12), 1243-1250.

158. Cordell, S. C.; Robinson, E. J. H.; Lowe, J. *Proceedings of the National Academy of Sciences of the United States of America*, 2003, 100(13), 7889-7894.

159. Newman, D. J.; Cragg, G. M. *Journal of Natural Products*, 2007, 70(3), 461-477.

160. Ertl, P.; Roggo, S.; Schuffenhauer, A. *Journal of Chemical Information and Modeling*, 2008, 48(1), 68-74.

161. Breinbauer, R.; Vetter, I. R.; Waldmann, H. *Angewandte Chemie-International Edition*, 2002, 41(16), 2879-2890.

162. Bairoch, A.; Bougueleret, L.; Altairac, S.; Amendolia, V.; Auchincloss, A.; Puy, G. A.; Axelsen, K.; Baratin, D.; Blatter, M. C.; Boeckmann, B.; Bollondi, L.; Boutet, E.; Quintaje, S. B.; Breuza, L.; Bridge, A.; deCastro, E.; Coral, D.; Coudert, E.; Cusin, I.; Dobrokhotov, P.; Dornevil, D.; Duvaud, S.; Estreicher, A.; Famiglietti, L.; Feuermann, M.; Gehant, S.; Farriol-Mathis, N.; Ferro, S.; Gasteiger, E.; Gateau, A.; Gerritsen, V.; Gos, A.; Gruaz-Gumowski, N.; Hinz, U.; Hulo, C.; Hulo, N.; Ioannidis, V.; Ivanyi, I.; James, J.; Jain, E.; Jimenez, S.; Jungo, F.; Junker, V.; Keller, G.; Lachaize, C.; Lane-Guermonprez, L.; Langendijk-Genevaux, P.; Lara, V.; Lemercier, P.; Le Saux, V.; Lieberherr, D.; Lima, T. D.; Mangold, V.; Martin, X.; Michoud, K.; Moinat, M.; Moreira, C.; Morgat, A.; Nicolas, M.; Ohji, S.; Paesano, S.; Pedruzzi, I.; Perret, D.; Phan, I.; Pilbout, S.; Pillet, V.; Poux, S.; Redaschi, N.; Reynaud, S.; Rivoire, C.; Roechert, B.; Sapsezian, C.; Schneider, M.; Sigrist, C.; da Silva, M.; Sonesson, K.; Stutz, A.; Sundaram, S.; Tognolli, M.;

Verbregue, L.; Veuthey, A. L.; Vitorello, C.; Yip, L.; Apweiler, R.; Alam-Faruque, Y.; Barrell, D.; Bower, L.; Browne, P.; Chan, W. M.; Daugherty, L.; Donate, E. S.; Eberhardt, R.; Fedotov, A.; Foulger, R.; Fraser, G.; Frigerio, G.; Garavelli, J.; Golin, R.; Horne, A.; Jacobsen, J.; Kleen, M.; Kersey, P.; Kretschmann, E.; Laiho, K.; Leinonen, R.; Legge, D.; Magrane, M.; Martin, M. J.; Monteiro, P.; O'Donovan, C.; Orchard, S.; O'Rourke, J.; Patient, S.; Pruess, M.; Sitnov, A.; Sklyar, N.; Whitfield, E.; Wieser, D.; Lin, Q.; Rynbeek, M.; di Martino, G.; Donnelly, M.; van Rensburg, P.; Wu, C.; Arighi, C.; Arminski, L.; Barker, W.; Chen, Y. X.; Chung, S. H.; Fang, C.; Hermoso, V.; Hu, Z. Z.; Hua, H. K.; Huang, H. Z.; Kahsay, R.; Mazumder, R.; McGarvey, P.; Natale, D.; Nikolskaya, A.; Petrova, N.; Suzek, B.; Vasudevan, S.; Vinayaka, C. R.; Yeh, L. S.; Yuan, X.; Zhang, J.; Consortium, U. *Nucleic Acids Research*, 2007, 35, D193-D197.

163. An, J. H.; Totrov, M.; Abagyan, R. *Proteomics*, 2005, 4, 752-761.

164. Totrov, M.; Abagyan, R. *Proteins*, 1997, Supp 1, 215-220.

165. *Natural Product and Semi-Synthetic Natural Product Libraries*, AnalytiCon Discovery

166. Nemethy, G.; Gibson, K. D.; Palmer, K. A.; Yoon, C. N.; Paterlini, G.; Zagari, A.; Rumsey, S.; Scheraga, H. A. *Journal of Physical Chemistry*, 1992, 96(15), 6472-6484.

167. Jorgensen, W. L. *Theoretical Chemistry Accounts*, 2000, 103(3-4), 225-227.

168. Schapira, M.; Abagyan, R.; Totrov, M. *Journal of Medicinal Chemistry*, 2003, 46(14), 3045-3059.

169. Wayne, P. *Methods for Dilution Antimicrobial Susceptibility Tests for Bacteria*

That Grow Aerobically. Clsi Document M7-A7, ed. edition, A.s.-s.: Clinical and Laboratory Standards Institute. 2006.

170. Addinall, S. G.; Cao, C.; Lutkenhaus, J. *Journal of Bacteriology*, 1997, 179(13), 4277-4284.

171. Addinall, S. G.; Bi, E. F.; Lutkenhaus, J. *Journal of Bacteriology*, 1996, 178(13), 3877-3884.

172. Dai, K.; Lutkenhaus, J. *Journal of Bacteriology*, 1991, 173(11), 3500-3506.

173. Mukherjee, A.; Lutkenhaus, J. *Journal of Bacteriology*, 1999, 181(3), 823-832.

174. Scheffers, D. J.; de Wit, J. G.; den Blaauwen, T.; Driessen, A. J. M. *Biochemistry*, 2002, 41(2), 521-529.

175. Mukherjee, A.; Lutkenhaus, J. *EMBO Journal*, 1998, 17(2), 462-469.

176. Mukherjee, A.; Dai, K.; Lutkenhaus, J. *Proceedings of the National Academy of Sciences of the United States of America*, 1993, 90(3), 1053-1057.

177. Teague, S. J. *Nature Reviews Drug Discovery*, 2003, 2(7), 527-541.

178. Teodoro, M. L.; Kavraki, L. E. *Current Pharmaceutical Design*, 2003, 9(20), 1635-1648.

179. Taylor, R. D.; Jewsbury, P. J.; Essex, J. W. *Journal of Computational Chemistry*, 2003, 24(13), 1637-1656.

180. Carlson, H. A. *Current Pharmaceutical Design*, 2002, 8(17), 1571-1578.

181. Prerna N. Domadia, A. B., J. Sivaraman, Sanjay Swarup and Debjani Dasgupta *Biochemistry*, 2008, 47, 3225-3234.

182. Berman, H. M.; Westbrook, J.; Feng, Z.; Gilliland, G.; Bhat, T. N.; Weissig, H.; Shindyalov, I. N.; Bourne, P. E. *Nucleic Acids Research*, 2000, 28(1), 235-242.

183. Bottegoni, G.; Kufareva, I.; Totrov, M.; Abagyan, R. *Journal of Computer-Aided Molecular Design*, 2008, 22(5), 311-325.

184. Abagyan, R.; Batalov, S.; Cardozo, T.; Totrov, M.; Webber, J.; Zhou, Y. Y. *Proteins-Structure Function and Genetics*, 1997, 29-37.

185. Schapira, M.; Raaka, B. M.; Das, S.; Fan, L.; Totrov, M.; Zhou, Z. U.; Wilson, S. R.; Abagyan, R.; Samuels, H. H. *Proceedings of the National Academy of Sciences of the United States of America*, 2003, 100(12), 7354-7359.

186. Abagyan, R.; Totrov, M. *Current Opinion in Chemical Biology*, 2001, 5(4), 375-382.

187. Klebe, G. *Drug Discovery Today*, 2006, 11(13-14), 580-594.

188. Freire, E. *Proceedings of the National Academy of Sciences of the United States of America*, 1999, 96(18), 10118-10122.

189. Pazos, F.; Bang, J. W. *Current Bioinformatics*, 2006, 1(1), 15-23.

190. Yoon, S.; Welsh, W. J. *Journal of Chemical Information and Computer Sciences*, 2004, 44(1), 88-96.

191. Huang, S. Y.; Zou, X. Q. *Proteins-Structure Function and Bioinformatics*, 2007, 66(2), 399-421.

192. Ponder, J. W.; Richards, F. M. *Journal of Molecular Biology*, 1987, 193(4), 775-791.

193. Leach, A. R. *Journal of Molecular Biology*, 1994, 235(1), 345-356.

194. Zavodszky, M. I.; Kuhn, L. A. *Protein Science*, 2005, 14(4), 1104-1114.

195. Giovanni Bottegoni, I. K., Maxim Totrov, Ruben Abagyan *Journal of Computer-Aided Molecular Design*, 2008, 22, 311-325.

196. Lin, J. H.; Perryman, A. L.; Schames, J. R.; McCammon, J. A. *Journal of the American Chemical Society*, 2002, 124(20), 5632-5633.

197. Gervasio, F. L.; Laio, A.; Parrinello, M. *Journal of the American Chemical Society*, 2005, 127(8), 2600-2607.

198. Smith, D. A. W.; Walker, D. K. *Methods and Principles in Medicinal Chemistry.* 2 nd ed. Pharmacokinetics and Metabolism in Drug Design. Vol. 31: Wiley-VCH Verlag GmbH & Co. KGaA. 2006.

199. Falik, R.; Flores, B. T.; Shaw, L.; Gibson, G. A.; Josephson, M. E.; Marchlinski, F. E. *American Journal of Medicine*, 1987, 82(6), 1102-1108.

200. Harris, L.; Mckenna, W. J.; Rowland, E.; Holt, D. W.; Storey, G. C. A.; Krikler, D. M. *Circulation*, 1983, 67(1), 45-51.

201. Yoshiaki, O.; Yoshie, C.; Koichiro, S.; Kouki, T.; Hideaki, N.; Tsutomu, S.; Yoshiko, H.; Kozo, O.; Fujio, K. *Journal of Bacteriology*, 1999, 181(4), 1348-1351.

202. Sung, W. S.; Lee, D. G. *Biological & Pharmaceutical Bulletin*, 2008, 31(9), 1798-1801.

203. White, E. L.; Suling, W. J.; Ross, L. J.; Seitz, L. E.; Reynolds, R. C. *Journal of Antimicrobial Chemotherapy*, 2002, 50(1), 111-114.

204. Mansuy, D. *Journal of Hepatology*, 1997, 26, 22-25.

205. Guengerich, F. P. *Biochemical Pharmacology*, 1977, 26(20), 1909-1915.